DISSERTATION

ELECTROMECHANICAL AND CURVATURE-DRIVEN MOLECULAR FLOWS FOR LIPID MEMBRANES

Submitted by
Michael Mikucki
Department of Mathematics

In partial fulfillment of the requirements
For the Degree of Doctor of Philosophy
Colorado State University
Fort Collins, Colorado
Summer 2015

Doctoral Committee:

Advisor: Yongcheng Zhou

Simon Tavener
Jiangguo (James) Liu
Ashok Prasad

ABSTRACT

ELECTROMECHANICAL AND CURVATURE-DRIVEN MOLECULAR FLOWS FOR LIPID MEMBRANES

Lipid membranes play a crucial role in sustaining life, appearing ubiquitously in biology. Gaining a quantitative understanding of the flows of lipid membranes is critical to understanding how living systems operate. Additionally, the mechanical properties of lipid membranes make them ideal material for nanotechnology, further motivating a need for accurate computational models. This thesis is organized in three projects that model important features of lipid membranes.

First, we define the mechanical energy of vesicle lipid membranes and propose a fast numerical algorithm for minimizing this energy. The mechanical energy is well known, and existing computational techniques for minimizing this energy include solving the Euler-Lagrange equations for axisymmetric shapes [91] or approximating the minimization problem by minimizing over a subspace of membrane configurations. We choose the latter approach, making no restrictive symmetry assumptions. Specifically, we use surface harmonic functions to parameterize the membrane surface, drastically reducing the degrees of freedom compared to similar existing approaches. Numerical equilibrium shapes are presented, including conformations exhibited by red blood cells. The numerical results are verified against analytical values of axisymmetric shapes.

Second, we develop the electrostatic potential energy for lipid bilayer membranes in the context of lipid-protein interactions. We extend the electrostatic potential energy of a protein-solvent system in [62] to include charged lipids in a protein-membrane-solvent system. Here, we model the bilayer membrane as a continuum with general continuous distributions of lipids charges on membrane surfaces. Key geometrical properties of the membrane surfaces under a smooth velocity field allow us to apply the Hadamard-Zolésio structure theorem of shape calculus, and we compute the electrostatic force on membrane surfaces as the shape derivative of the electrostatic energy functional.

Third and finally, we develop the mathematical theory and the computational tools for curvature-driven flow of proteins within lipid membranes. Recently, much attention has been devoted to understanding curvature generating and curvature sensing properties of proteins in vesicle membranes. That is, certain proteins prefer regions of specific curvature and naturally flow to these regions. We develop the mathematical theory for curvature-driven diffusion along these membranes, which involves a variable diffusion coefficient. Finite element and finite difference methods have been used to solve diffusion equations on surfaces, but these methods require costly spatial resolution and adaptive mesh refinements for dynamic membrane surfaces. Instead, we use a phase field model with Fourier spectral methods so that no explicit tracking of the surface is required. Furthermore, the spectral accuracy allows for uniform mesh with no refinement near the boundary. The numerical solution of the diffusion equation and the numerical solution of the membrane shape equation is performed in a consistent framework to allow for the coupling of membrane shape with the curvature-driven surface diffusion. Results which capture the curvature preference are presented.

ACKNOWLEDGEMENTS

I am sincerely grateful for the many people who made this dissertation possible. First and foremost, I thank God as the author of my life and the author of my salvation. Every good and perfect gift comes from Him, including the ability to conduct research in a created world full of order and beauty. I also thank my wife Mary, whose love and support enabled me to persevere through the long hours and late nights. Your encouragement is inspiring. I love you. Thanks also to my parents Barry and Leslee, who raised me and provided me with every opportunity to pursue my education.

Academically, I first thank my advisor, Yongcheng. I have learned so much from your teaching and mentoring in the last three years. You have made a tremendous impact in my ability to ask the right questions and conduct mathematical research. Thank you for your patience with me and for your commitment to my success. You have made an impact that will last a lifetime. While I could never pay you back, I hope to pay it forward to future students. I also thank my Master's thesis advisor and committee member, Simon. Without you, I don't know if I would be in graduate school. Thank you for getting me started and teaching me how to break up a seemingly insurmountable problem into manageable pieces. Your support and mentorship throughout the last five years has been consistent and invaluable.

I also want to thank all of the great teachers who have enabled me to complete this work. James, your finite elements course was awesome, and thanks for serving on my committee. Ashok, thanks for serving on my committee and training an applied mathematician on some interesting biology. Thanks also to Patrick Shipman, Jennifer Mueller, and Dan Bates for being excellent teachers and resources. Thank you Mary Pilgrim and Jess Ellis for helping

me become a better teacher. Much thanks to Bryan Elder for taking care of all of my paperwork, fixing the temperature in my office a few hundred times, and many helpful and uplifting conversations at lunch.

Finally, I want to thank my friends and colleagues who supported me academically and personally throughout this process: my sister Krista, my in-laws Steve and Jeannie Taylor, Professor Tim Gates, David Hopkins, Gerrek Zwickle, Eric Hanson, Melissa Adkins, Melody Alsaker, Cory Previte-Joshnson, Andy and Laura Abbott, Ross and Sheri Ridgeway, and Tyler and Hanke.

TABLE OF CONTENTS

LIST OF FIGURES

CHAPTER 1

Introduction

1.1. Mathematics Preliminaries

Before reading this thesis, the reader should be familiar with some basic calculus formulas. Recall the formula for integration by parts:

$$\int_\Omega \nabla u \cdot \mathbf{v} \, dX = \int_{\partial\Omega} (u\,\mathbf{v}) \cdot n \, dS - \int_\Omega u \, \nabla \cdot \mathbf{v} \, dX. \tag{1}$$

The divergence theorem is a realization of integration by parts with $u = 1$,

$$\int_{\partial\Omega} \mathbf{v} \cdot n \, dS = \int_\Omega \nabla \cdot \mathbf{v} \, dX. \tag{2}$$

For a scalar-valued function $f : \mathbb{R}^n \to \mathbb{R}$ and a vector valued function $V : \mathbb{R}^n \to \mathbb{R}^n$, the divergence operator satisfies the product rule,

$$\nabla \cdot (fV) = f(\nabla \cdot V) + V \cdot (\nabla f). \tag{3}$$

On a two dimensional surface, the surface gradient and surface divergence can be defined by subtracting off the normal components from the usual gradient and divergence. For a scalar valued function $g : \mathbb{R}^2 \to \mathbb{R}$, the surface gradient is

$$\nabla_s g = \nabla g - (\nabla g \cdot n)n. \tag{4}$$

Also, for any vector-valued function $W : \mathbb{R}^2 \to \mathbb{R}^2$, the surface divergence is defined as

$$\nabla_s \cdot W = \nabla \cdot W - n \cdot (\nabla W)n. \tag{5}$$

The reader should also be familiar with the calculus of variations. As a refresher, we provide a simple computational formula. Given a functional $F[\phi] : M \to \mathbb{R}$, where M is a manifold, the functional derivative of $F[\phi]$ with respect to ϕ is defined by

$$\begin{aligned} \delta F &= \int \frac{\delta F}{\delta \phi} \psi \, dx \\ &= \lim_{\tau \to 0} \frac{F[\phi + \tau\psi] - F[\phi]}{\tau} \\ &= \frac{d}{d\tau} F[\phi + \tau\psi] \bigg|_{\tau=0} . \end{aligned} \tag{6}$$

The functional derivative is the quantity $\frac{\delta F}{\delta \phi}$ and it can be computed by the formula (6). The quantity δF is called the first variation of F.

Now we are ready to begin.

1.2. WHAT ARE LIPID VESICLES?

Lipid bilayers play a crucial role in sustaining life. They serve as boundaries of cells and cell organelles such as the endoplasmic reticulum, Golgi apparatus, mitochondria, and transport vesicles. Primarily, lipid bilayers act as interfaces between the enclosed structure and the surrounding aqueous environment and serve as smart controls for the transport of specific ions, sugars, amino acids, and vitamins in and out of the enclosed structures [66]. The membrane is flexible and permits the flow of these metabolic products by stretching, bending, merging and separating in specific locations. The control of flow through the membrane is precisely regulated by different proteins and other macromolecules, each with its own specific function.

Lipids are amphiphilic molecules. They are composed of two structured groups, a hydrophilic “head” and a hydrophobic “tail.” Therefore, when placed in aqueous solution, the head groups of the lipids aggregate in such a way to protect the tail groups from the water, forming a bilayer membrane automatically, as shown in Figure 1.1. Each layer of the membrane is called a leaflet. A cell vesicle is an example of an organelle formed by a lipid bilayer structure. Vesicles primarily serve as transport vehicles, carrying cellular products and wastes to specific locations. Like any organelle, the membrane includes more than just the lipid bilayer. Numerous proteins and cholesterols may be attached or embedded in the lipid membrane. A cell vesicle with its numerous attachments is shown in Figure 1.1, alongside a depiction of a vesicle without any attachments.

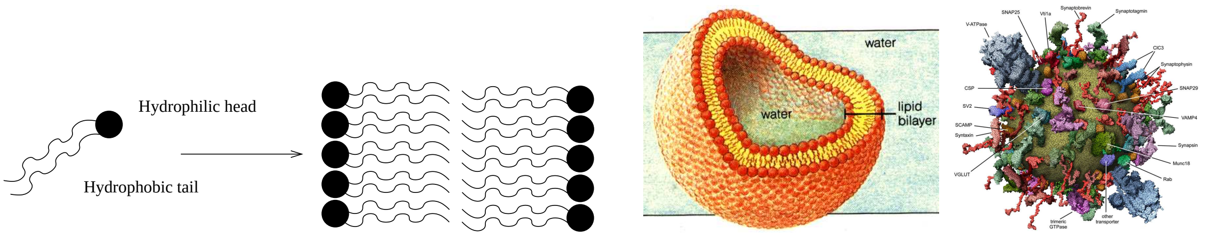

Figure 1.1: Left: Self assembly of lipid bilayer. Middle: Lipid bilayer forming a liposome vesicle with no protein attachments [77]. Right: Cell vesicle with attachments [99].

In principle, the flow through the lipid bilayer membrane is regulated by two major types of membrane deformations. One type of deformation occurs directly at the location of transport. Two examples are endocytosis and exocytosis. In endocytosis, the membrane bubbles inwardly, creating a vesicle that engulfs certain substances. In exocytosis, the membrane bubbles outwardly, creating a vesicle that excretes certain substances. Another type of flow is caused by indirect membrane deformations through mechanosensitive channels. A stimulus away from the transport site may induce membrane deformations, signaling proteins embedded in the membrane to open or close, in turn allowing or disallowing certain products to pass through. Both of these major types of transport are illustrated in Figure 1.2.

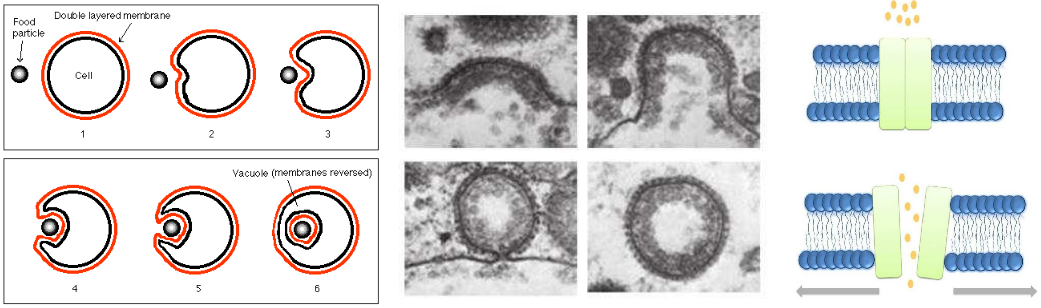

Figure 1.2: Left: Illustration of transport through endocytosis [40]. Middle: Transport through of exocytosis [70]. Right: Transport through a mechanosensitive ion channel opening in response to membrane tension.

Investigating the forces on lipid membranes is essential to study membrane deformations and flows, and ultimately understand the complex activities of cells and organelles. In addition, the mechanics of lipid membranes is critically important for drug encapsulation and delivery [84].

1.3. Mathematical models: an overview

The underlying theme for these problems in mathematical biology is energy minimization. The geometric structure to which a molecule, ion, phase, membrane, etc. assumes often corresponds to a configuration with minimum energy. This is due to a fundamental concept in physics, chemistry, and biology: the second law of thermodynamics. That is, the entropy of a closed system always decreases and is maximized at equilibrium. As a simple example, a ball placed on the side of a hill will roll to the bottom without being pushed, minimizing its gravitational potential energy.

In relation to lipid membranes, the bending, stretching, merging, and separating of the lipid membrane incurs some associated energy cost. The equilibrium membrane shapes should appear in configurations which minimize these energies. Defining the energy of a membrane with no external forces is discussed in Chapter 2. Later, in Chapter 5, we investigate the total energy when the the lipid membrane is placed under an external field, e.g., electrostatic field generated by protein-membrane interactions.

1.3.1. Atomistic models.

There are many methods one can choose to model the dynamics and equilibrium configurations of lipid membranes. Probably the most straightforward is molecular dynamics simulations (MD). In MD, each atom is explicitly defined in space, and all the bonded and nonbonded interactions are calculated at each time step. These interactions produce forces, causing the atoms to move, and new forces for the new positions must be computed on each atom. The process continues, simulating the dynamics until equilibrium. While this method is conceptually precise, it certainly has its setbacks. If a large deformation is sought, in either length or time, MD simulation is too computationally expensive. Moreover, we're really only interested in the movement of the lipids, but

MD requires computations on every atom in the simulation, including the water molecules in the solvent. Much computation time is spent on simulating the movement of the water molecules, which isn't really the problem of interest. Other methods of membrane simulation include Monte Carlo (MC) and Brownian dynamics (BD), but these methods also have similar drawbacks.

1.3.2. CONTINUUM MODELS. In this thesis, a continuum model describing large and meso-scale deformations of lipid bilayer membranes is established, specifically for vesicle membranes. Lipid vesicles are typically 50nm in diameter, while other membranes (e.g. cell membranes) can be 100μm in diameter. The lipid constituents have heads that are 0.8-0.9nm in diameter with tails that are 2-2.5nm long [76, Ch. 2]. The size discrepancy between the vesicle configuration and the individual lipids justifies the continuum assumption. Continuum mechanical properties of the membrane, including the bending modulus, have been measured under sufficiently long time scales (for example 10-60ns for a system with 1024 lipids) and agree nicely with experiment [65]. Moreover, lipid membranes modeled in continuum electrostatic contexts are in agreement with atomic simulation [16]. However, this treatment cannot capture some short time and specific local interactions, and in some applications hybrid implicit-explicit approaches may be necessary [64].

1.4. OUTLINE AND CONTRIBUTION OF THESIS

The rest of the thesis is organized in three major sections. The specific contributions are highlighted for each section.

We begin in the next chapter by defining the mechanical forces on a vesicle. In fact, a very common vesicle serves as a good test against a model with only mechanical forces: red blood cells. We review the derivation for the total mechanical energy of vesicles with its rich history. This mechanical energy includes curvature terms, and some differential geometry will be discussed. In Chapter 3, we propose a variational problem to minimize the mechanical energy over membrane configurations which are physically relevant. We use surface harmonic functions to parameterize the membrane and solve the variational problem in an efficient way. This is novel work and is a simplification from the use of spherical harmonic functions as in [52]. Chapter 4 gives the numerical results of the parameterized problem, comparing the results against analytical solutions.

In Chapter 5, we define the electrostatic forces on a vesicle, induced by a charged protein located outside of the membrane. The chapter culminates in an expression for the electrostatic potential energy for the protein-membrane-solvent system. The novelty of this chapter is the introduction of charged lipids on the membrane, extending the functional in [62] for protein-solvent systems. Chapter 6 defines the dielectric boundary force on the vesicle membrane using the electrostatic potential energy from Chapter 5. The calculation is rigorously justified through techniques of shape calculus and is physically verified by the use of the Maxwell Stress Tensor.

The third and final section models topological vesicle deformations. In Chapter 7, the mechanical energy defined in Chapter 2 is cast in an Eulerian framework. Rather than tracking the position of the membrane explicitly, we track the membrane implicitly as a level set of a 3D function called a phase field function. A new energy minimizing procedure is proposed and solved, which minimizes the curvature energy (mechanical energy) of the membrane(s). Chapter 8 uses this framework to model curvature-driven protein localization within a multicomponent vesicle membrane, which is novel work. Proteins, this time embedded in the membrane itself, may diffuse laterally along the membrane, just as the lipids do. However, the protein may prefer a region of specific curvature. Numerical results of this model are presented in Chapter 9.

A concluding chapter summarizing the results and proposing extensions from these works is presented in Chapter 10.

CHAPTER 2

BIOMOLECULAR MECHANICS

Red blood cells (RBCs) are highly deformable in flow conditions, but at rest, they are biconcave discocytes. Understanding why RBCs take their biconcave shape has been a very active problem in the last century. Since RBCs have no nucleus, their shape must be regulated by a balance of forces on the cell membrane. Figure 2.1 shows a photograph of a red blood cell using an electron microscope. We wish to model the membrane of a red blood cell in a physically justifiable way. Some clues to this model are attained from experiment. In blood flow, the RBC passes through narrow blood vessels and can deform into long finger-like cylinders, all the while maintaining constant thickness. For example, an 8 μm diameter RBC has been observed to squeeze through inter-endothelia slits that are 0.2-0.5 μm in width [8]. Yet, after these deformations, the RBC can return to its original discoidal shape. Therefore, the RBC membrane possesses elastic deformation properties.

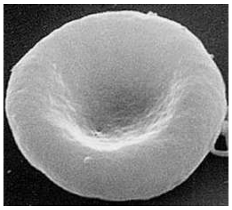

Figure 2.1: Red blood cells have biconcave discoidal shape in the absence of external force.

Some attempts have been made in the 1900s to attribute an accurate model to the RBC shape. In 1965, Murphy suggested that the RBC shape was related to variations in the distribution of cholesterol in the membrane [74]. However, this is not supported by experiment [89]. In 1968, Fung and Tong treated the RBC as a fluid-like shell, where the thickness of the membrane varied to regulate the biconcave shape [39]. This contradicts the experiments mentioned above. In the same year, Loepz et. al. suggested the charge distribution on the membrane could influence the shape [67]. But a uniform charge distribution was shown on the surface of RBCs by Greer and Baker [44]. By and large, the failure of these theories is that they did not recognize the liquid crystal state of the membrane.

In 1970, Canham suggested that the RBC shape was determined completely by the bending elasticity of the membrane [13]. This was a major breakthrough in the research. However, the model leads to other shapes not observed in RBCs. Refining this model, in 1973, Helfrich proposed that the lipid membrane acts like a homeotropic nematic liquid crystal, where the normal to the surface is the preferred orientation [47]. He based the expression of the energy density of a lipid membrane on the derivation for uniaxial liquid crystals developed by Frank in 1958 [38]. A heuristic derivation for the total mechanical energy of a lipid membrane is given in the following sections, culminating in Section 2.3. A more in depth approach, following the work of Frank [38] is given in Section 2.5.

2.1. Stretching and shearing

The energy cost due to stretching/compressing the membrane from area A_0 to a new area A is given by

$$E_{\text{stretch}} = \frac{1}{2}\mathscr{K}_{\text{stretch}}\frac{(A-A_0)^2}{A_0}, \tag{7}$$

where $\mathscr{K}_{\text{stretch}}$ is the stretching/compression modulus of elasticity. The lateral stress (or tensile stress, or tension), i.e. force per unit area, is calculated by the derivative of the energy,

$$\sigma = \frac{\partial E_{\text{stretch}}}{\partial A} = \mathscr{K}_{\text{stretch}}\frac{A-A_0}{A_0} = \mathscr{K}_{\text{stretch}}\,\varepsilon, \tag{8}$$

where ε is the normalized displacement, or the strain,

$$\varepsilon = \frac{A-A_0}{A_0}. \tag{9}$$

This formula (8) is well known as Hooke's Law. The value of $\mathscr{K}_{\text{stretch}}$ can be calculated for large unilamellar vesicles (e.g. soap bubbles), and the value is approximately 250 erg/cm^2 [86]. Under experiments, the membrane ruptures at only a few millinewtons per meter. Since

$\mathscr{K}_{\text{stretch}}$ is so large, this means the change in area $A - A_0$ must be small to avoid rupture. In other words, the membrane cannot sustain much stretching force.

To understand why this is the case, let's consider the molecular nature of the lipids, specifically the hydrophobicity of the lipid tail (hydrocarbon chain). The concentration of free lipid molecules in aqueous solution is typically 1-100 molecules per cubic micron [69]. In other words, for bilayers, the solubility of lipids is low. Therefore, the total number of lipids in the membrane is by-and-large constant. The flip-flop of lipids from one leaflet to another is rare compared to lateral diffusion, since the polar head group must pass through the inner hydrophobic region. Since the number of molecules within the membrane leaflets are fixed, the area must also be fixed. Therefore, it is the constant composition of lipids in the bilayer which provides the area constraint.

The energy due to the area stretching and compression is on the order of $\mathscr{K}_{\text{stretch}} A_0$. Using the typical values for large vesicles, where $A_0 = 1000\ \mu\text{m}^2$, the energy is of the order

$$E_{\text{stretch}} \simeq \mathscr{K}_{\text{stretch}} A_0 = 250 \frac{\text{erg}}{\text{cm}^2} \left(\frac{100\,\text{cm}}{1\text{m}} \right)^2 \cdot 1000\,\mu\text{m}^2 \left(\frac{\text{m}}{10^6\,\mu\text{m}} \right)^2 \simeq 10^{-3}\,\text{erg} = 10^{-10} J.$$

The energy from bending the membrane (to be discussed in Section 2.3) is on the order of the bending modulus $\mathscr{K}_C$, which takes values $\mathscr{K}_C \simeq 10^{-12}$ erg $= 10^{-19}$ J [33]. Comparing the bending energy to the stretching energy above, we see that the energy from stretching is on the order of $\simeq 10^9 \mathscr{K}_C$. The stretching energy is nine orders of magnitude larger, and therefore we can treat the surface area of the membrane as constant, effectively keeping the area difference of equation (9) fixed. Following equation (7), we use the tensile stress σ as a Lagrange multiplier to write an effective area constraint,

$$E_{\text{area}} = \sigma \int_{\Gamma} dS, \tag{10}$$

where Γ is the membrane surface and dS is a differential surface area element.

While the membrane cannot withstand large stretching force, it cannot sustain *any* shearing force. The lipids are free to diffuse laterally throughout the membrane, and therefore any shear will be absorbed by the fluidity of the membrane.

2.2. Osmotic pressure

Another constraint comes from the fact that lipid membranes are relatively impermeable by ions. This means that the volume of a vesicle is relatively constant, regulated by osmotic pressure. Osmotic pressure is the pressure required to resist osmosis and maintain equilibrium volume. Osmosis is the flow of solvent molecules through semi-permeable membranes to a region of higher solute concentration in efforts to equalize the concentrations on either side of the membrane. The low permeability of the membrane (and corresponding high resistance to osmosis) serves as a volume constraint. If we let R_g be the gas constant, $R_g \approx 8.31$ J/(mol·K), and assume an ideal solution, then the pressure difference of the inside to outside volume $p = p_{\text{in}} - p_{\text{out}}$ is given by

$$p = R_g T(n/V - c),$$

where the quantity $n/V - c$ represents the concentration of impermeable molecules inside the vesicle (n/V) minus the concentration of impermeable molecules (e.g. sugar) outside the vesicle (c) in moles per unit volume. A typical value for the sugar concentration is 10^{-4} mol/m^3. The energy corresponding to this pressure is found by integrating the pressure over the volume from the initial volume V_0 to the final volume after the pressure is exerted V,

$$\begin{aligned} E_o &= \int_{V_0}^{V} p(v)\, dv = \int_{V_0}^{V} R_g T(n/v - c)\, dv \\ &= R_g T \left(n \ln(V/V_0) - c(V - V_0)\right). \end{aligned}$$

Since we assume the volume difference is small, $V \approx V_0$, we have $V/V_0 - 1 \ll 1$, which allows for the Taylor approximation to $\ln(x) \approx (x - 1)$. This gives

$$\begin{aligned} E_o &\approx R_g T(n(V/V_0 - 1) - c(V - V_0) \\ &= R_g T(n - cV_0)(V/V_0 - 1) \\ &\approx R_g T c V_0/2, \end{aligned}$$

where the last equality was obtained by using the number of molecules as an average of the number of molecules of the initial volume and the final volume, $n \approx cV/2 + cV_0/2$, which is valid since $V \approx V_0$. The energy here is calculated using typical values for a sphere-like vesicle of radius 10 μm, at room temperature 295 K,

$$\frac{R_g T c V_0}{2} \simeq \frac{4}{3}\pi(10 \times 10^{-6}\mathrm{m})^3(295\,\mathrm{K})(10^{-4}\frac{\mathrm{mol}}{\mathrm{m}^3})(8.31\frac{\mathrm{J}}{\mathrm{mol}\cdot\mathrm{K}})/2 \simeq 10^{-16}\mathrm{J}.$$

Compared to the bending energy, this energy is three orders of magnitude larger. That is, using the same bending modulus of $\mathscr{K}_C \simeq 10^{-19}J$, the osmotic energy is of the order $\simeq 10^3\mathscr{K}_C$. This means that the bending energy cannot account for the osmotic pressure from the presence of insoluble sugar molecules in the exterior solution. Because of this, the enclosed volume of the vesicle is controlled by the condition that no osmotic pressure builds up. We use the pressure difference as a Lagrange multiplier to write an effective volume constraint,

$$E_{\text{volume}} = p\int dV, \tag{11}$$

where the integral is computed over the 3D domain of the enclosed membrane. Note that since a surface can be parameterized in two variables, this integral can be reduced to two dimensions after a proper parameterization.

2.3. BENDING

In this section, we provide a formula for the energy due to bending the membrane. Since the energy of membranes does not depend on the frame of reference, it must arise from the invariants of the shape operator only. These invariants are the mean and Gaussian curvatures. We must express these quantities as dimensionless strains to be consistent with the elasticity theory. The bending energy of the membrane up to quadratic order is given by

$$E_{\text{bend}}[\Gamma] = \frac{\mathscr{K}_C}{2}\int_\Gamma (2H)^2\, dS + \frac{\mathscr{K}_G}{2}\int_\Gamma K\, dS, \tag{12}$$

where $\mathscr{K}_C$ is the bending modulus (or bending/flexural rigidity) and $\mathscr{K}_G$ is the Gaussian saddle-splay modulus (or Gaussian rigidity). A derivation of this equation is provided in Section 2.5. Notice that the integral of the square mean curvature and the Gaussian curvature with respect to the surface area are dimensionless quantities ($[H] = 1/L, [K] = 1/L^2, [dS] = L^2$), so we can think of the curvatures as a measure of strain due to bending.

The bending energy equation (12) holds for membranes with symmetric lipid distributions on each leaflet. However, in most bilayer membranes, this is not the case. A modification needs to be made to account for naturally arising asymmetry. Based on the chemical bonds in the hydrocarbon chains, lipids have an intrinsic curvature, illustrated in Figure 2.2 [83]. If the lipid composition in each leaflet is symmetric, the overall curvature of the membrane will not be affected by the lipids themselves, since the curvatures will cancel each other out. However, if the lipid composition in each leaflet is different, the membrane might be spontaneously curved in one direction. Equation (12) is modified to account for this spontaneous curvature resulting from asymmetric lipid compositions, which occurs often in real biological systems. The spontaneous curvature C_0 depends on the lipid species present, but it is difficult to measure. Note that the spontaneous curvature may be different at different positions along the membrane. The result is the spontaneous curvature model, developed by Canham [13], Helfrich [47], and Evans [31]:

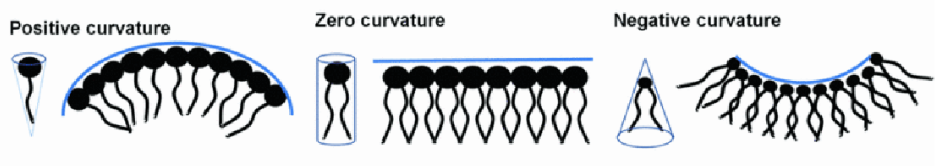

Figure 2.2: Different lipid species have different intrinsic curvature. Photo from [83].

$$E[\Gamma] = \frac{\mathscr{K}_C}{2} \int_\Gamma (2H - C_0)^2 \, dS + \frac{\mathscr{K}_G}{2} \int_\Gamma K \, dS. \tag{13}$$

We now have a minimization problem subject to area and volume constraints. Note that the second term in (13) is constant for surfaces with the same topology according to the

Gauss-Bonet formula, so the variation is zero and it has no effect on the minimization of the mechanical energy (see [25] for the Gauss-Bonet theorem).

2.4. Lipids: material for nanotechnology

Before deriving the bending energy formula, we pause to examine the relationship between the bending modulus and the stretching modulus for a single elastic sheet, given by

$$\mathscr{K}_C = \frac{Yh^3}{12(1-\nu^2)} \qquad \text{(single elastic sheet)}, \tag{14}$$

where Y is the (3D) Young's modulus, h is the thickness of the membrane, and ν is Poisson's ratio. The Young's modulus can be expressed in terms of the stretch modulus by

$$Y = \mathscr{K}_{\text{stretch}}/h. \tag{15}$$

If you stretch an elastic material in one direction, the other two directions will experience some compression. Poisson's ratio is used to transfer the axial strain in one dimension to the other two dimensions. We assume the vesicle structure is incompressible, and so we simplify by setting $\nu = 0.5$. Therefore, in terms of the stretching modulus, the bending modulus is

$$\mathscr{K}_C = \frac{\mathscr{K}_{\text{stretch}} h^2}{9} \qquad \text{(single elastic sheet)}. \tag{16}$$

It should be emphasized that the equation for the bending modulus (14) is valid for a single elastic sheet only. However, we have a lipid *bi*layer, so there are really two elastic sheets involved. Assuming the thickness of the full bilayer is the same (h), we should modify (14) by considering two sheets of thickness $h/2$ each. Since we are bending two sheets, we multiply the right-hand side by 2. Furthermore, we replace h with $h/2$ and use (15) with the assumption that $\nu = 0.5$ to get

$$\mathscr{K}_C = 2\frac{Y(h/2)^3}{12(1-\nu^2)} = \frac{Yh^3}{48(1-(0.5)^2)} = \frac{\mathscr{K}_{\text{stretch}} h^2}{36} \qquad \text{(bilayer)}. \tag{17}$$

One important question in deriving the model is which value of h we should use to calculate $\mathscr{K}_C$ in (17). Is it the distance between headgroups of lipids, or just the hydrophobic core?

This difference may be small, but since h is squared, it may be important. Therefore, (17) should not be taken to be absolutely reliable in this context, but it does serve as a reasonable estimate. Using a stretching modulus of 0.25 N/m as before and a bilayer thickness of $h = 5$nm, we obtain

$$\mathscr{K}_C \approx \frac{1}{36} 0.25 \frac{\mathrm{N}}{\mathrm{m}} \cdot (5 \times 10^{-9}\mathrm{m})^2 \approx 1.7 \times 10^{-19} J \approx 42\ k_B T,$$

where $k_B \approx 1.38 \times 10^{-23}$J/K is the Boltzmann constant and T is the temperature in Kelvin (experiments taken at normal room temperature, $\approx$ 295K). The product $k_B T$ is called the thermal energy and is used as a standard scaling factor for energies on the molecular scale. This estimate is quite accurate compared to experimental values (see for instance, Table 7.3 in [9]), including the estimate we have been using since Section 2.1 from [33]. This energy is large enough to withstand thermal fluctuations without rupturing the membrane, but is not too much bigger than the thermal energy, so it is small enough to be deformed by nanoscopic sources of energy. Therefore, lipid bilayers are ideal material for nanotechnology [24].

2.5. Derivation of mechanical energy

In this section, we derive the bending energy (12) using elasticity theory. The mathematical elasticity of solids is based on the analysis of a differential element of the solid. The element is deformed, and restoring forces, including forces that oppose displacement of neighboring points in the material, are considered. Constitutive relations between stress and strain, such as Hooke's law, are applied to determine the strain. Assuming a linear stress-strain relation, the energy is a quadratic function of the strain.

We begin by following Frank's seminal work [38]. In the elasticity theory of liquid crystals, there are no forces that oppose the displacement of neighboring points in the material. Therefore, for a differential element of the liquid crystal, restoring torques are considered, which oppose changes in the curvature. An analog of Hooke's law is applied to these curvature-strains using a linear constitutive relation, resulting in an energy that is quadratic in the curvature-strain. The elastic moduli are the linear constants of proportionality.

Take a differential (surface) element of the lipid membrane, considered as a liquid crystal with orientation in the normal direction. We define a local coordinate system on the surface patch, where the z-axis is parallel to the normal at the center of the patch. Of course, away from the center, the normal direction may change, but if the size of the patch is small enough, this discrepancy becomes negligible. We define six components of curvature-strain, based on this local coordinate system: two splays, two twists, and two bends.

$$\text{Splays}: s_1 = \frac{\partial n_x}{\partial x}, \quad s_2 = \frac{\partial n_y}{\partial y}, \tag{18}$$

$$\text{Twists}: t_1 = -\frac{\partial n_y}{\partial x}, \quad t_2 = \frac{\partial n_x}{\partial y}, \tag{19}$$

$$\text{Bends}: b_1 = \frac{\partial n_x}{\partial z}, \quad b_2 = \frac{\partial n_y}{\partial z}. \tag{20}$$

From the equations, a splay (short for the word “display”) is a deformation parallel to the axis; a twist is an deformation orthogonal to the axis *on* the surface, and a bend is a deformation orthogonal *to* the surface. These deformations are illustrated in Figure 2.3.

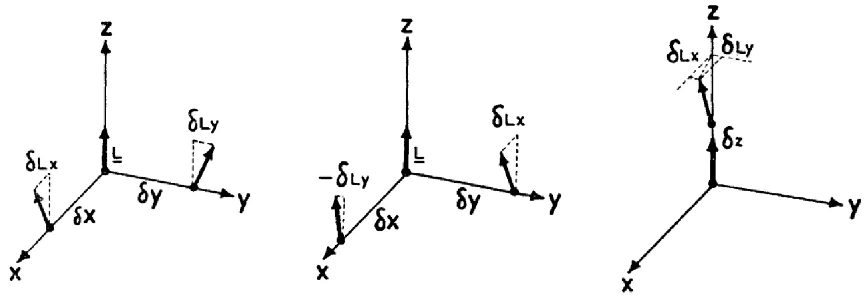

1. Splays 2. Twists 3. Bends

Figure 2.3: The three curvature-strain deformations from [38].

The expression for the (unit) normal vector to the surface at any point on the patch is given as a linear expansion of the curvature strains in each coordinate direction,

$$\begin{cases} n_x = a_1 x + a_2 y + a_3 z + \mathcal{O}(r^2), \\ n_y = a_4 x + a_5 y + a_6 z + \mathcal{O}(r^2), \\ n_z = 1 + \mathcal{O}(r^2). \end{cases} \tag{21}$$

This approximation is on the order of $r^2 = x^2 + y^2 + z^2$ for points within some radius r of the center of the patch. Notice that the director n is still a unit vector, since we assume that the patch size is very small, so that the normal does not change very much under the deformation and hence $n \approx \langle 0, 0, 1 \rangle$. The coefficients a_i are just the splays, twists, and bends. By (18), (19), and (20), we can see that

$$\begin{aligned} a_1 &= \frac{\partial n_x}{\partial x} = s_1, & a_2 &= \frac{\partial n_x}{\partial y} = t_2, \\ a_3 &= \frac{\partial n_x}{\partial z} = b_1, & a_4 &= \frac{\partial n_y}{\partial x} = -t_1, \\ a_5 &= \frac{\partial n_y}{\partial y} = s_2, & a_6 &= \frac{\partial n_y}{\partial z} = b_2. \end{aligned} \tag{22}$$

Next, assume an analog of Hooke's Law, that the "torque-stress" is linearly proportional to the curvature-strain, yielding an energy which is a quadratic function of the curvature-strain. We will take this as our assumption, that the energy density e is a quadratic function of the curvature coefficients a_i, $i = 1, \cdots, 6$.

$$e = k_i a_i + \frac{1}{2} k_{ij} a_i a_j, \tag{23}$$

where summation is implied over matching indicies (Einstein summation convention). This gives a system of 6 linear coefficients a_i and 36 quadratic coefficients a_{ij}. However, not all of these coefficients are nonzero, and not all of them are unique. Next, we make simplifications to the system based on symmetry requirements.

The first simplification comes from expanding the quadratic terms. In the expansion, there will be two terms corresponding to $a_i a_j$ when $i \neq j$. The coefficients k_{ij} and k_{ji} must be equal, since $a_i a_j$ is the same term as $a_j a_i$ physically. This simplification is known as minor symmetry.

The next simplifications are made based on the fact that different coordinate systems should give the same energy, provided the normal axis (preferred orientation of the bilayer) is maintained. Any rotation of the coordinate system about the z-axis should give the same energy. Furthermore, since the normal vector to a bilayer of lipids can point in either direction, it is permissible to transform $n' = -n$. Following Frank [38], we choose $x' = x$ and $y' = -y$, and $z' = -z$ in addition to $n' = -n$ to maintain a right-handed coordinate system. Then, the linear expansion for (21), keeping the coefficients a_i the same, is

$$\begin{cases} n'_{x'} = -n_{x'} = -n_x = -\left(a_1 x + a_2 y + a_3 z\right) = -\left(a_1 x' - a_2 y' - a_3 z'\right) = -a_1 x' + a_2 y' + a_3 z', \\ n'_{y'} = -n_{y'} = n_y = a_4 x + a_5 y + a_6 z = a_4 x' - a_5 y' - a_6 z'. \end{cases} \tag{24}$$

The new expression for the energy (23) will have different coefficients, but must be equivalent to the original expression due to the invariance of the energy under this transformation. Looking at the linear terms, the old and new linear parts of the energy are

$$e_{\text{lin}} = k_1 a_1 + k_2 a_2 + k_3 a_3 + k_4 a_4 + k_5 a_5 + k_6 a_6, \tag{25}$$

$$e'_{\text{lin}} = -k_1 a_1 + k_2 a_2 + k_3 a_3 + k_4 a_4 - k_5 a_5 - k_6 a_6. \tag{26}$$

Equating $\dfrac{\partial e_{\text{lin}}}{\partial a_i}$ with $\dfrac{\partial e'_{\text{lin}}}{\partial a_i}$ gives the following relations,

$$\begin{aligned} k_1 &= \pm k_1, \\ k_5 &= \pm k_5, \\ k_6 &= \pm k_6. \end{aligned} \tag{27}$$

From these relations, we can see that

$$k_1 = k_5 = k_6 = 0. \tag{28}$$

For the quadratic part of the energy, one can expand all 36 terms of g_{nlin} and g'_{nlin} and take $\dfrac{\partial^2 e_{\text{lin}}}{\partial a_i \partial a_j}$ for each $i, j = 1, \ldots, 6$, but since the quadratic coefficients are just the linear coefficients multiplied, we can just multiply the linear equations (28) to find the quadratic relations. For example, k_{12} is the coefficient of $a_1 a_2$. The coefficient of a_1 is k_1, which must satisfy the sign change according to (27), but the coefficient of a_2 does not have a sign change; therefore, we have $k_{12} = k_1 k_2 = -k_1 k_2 = 0$ (as is $k_{21} = 0$ by minor symmetry). On the other hand, the coefficient of a_{11} is not zero, since $k_{11} = k_1 k_1 = (-k_1)(-k_1) = k_1 k_1$. In the end, we have the following zero terms,

$$k_{12} = k_{13} = k_{14} = k_{25} = k_{26} = k_{35} = k_{36} = k_{45} = k_{46} = 0 \tag{29}$$

After these simplifications, the system is characterized by 3 independent linear components and 12 independent quadratic components,

$$k_i = \begin{pmatrix} 0 \\ k_2 \\ k_3 \\ k_4 \\ 0 \\ 0 \end{pmatrix}, \quad k_{ij} = \begin{bmatrix} k_{11} & 0 & 0 & 0 & k_{15} & k_{16} \\ 0 & k_{22} & k_{23} & k_{24} & 0 & 0 \\ 0 & k_{23} & k_{33} & k_{34} & 0 & 0 \\ 0 & k_{24} & k_{34} & k_{44} & 0 & 0 \\ k_{15} & 0 & 0 & 0 & k_{55} & k_{56} \\ k_{16} & 0 & 0 & 0 & k_{56} & k_{66} \end{bmatrix}. \tag{30}$$

The system can further be simplified by assuming the absence of enantiomorphy. That is, the lipids themselves possess reflection symmetry, so our choice of a right-handed coordinate system was not necessary. If we transform the coordinates to $x' = x, y' = -y, z' = z$, and keep the normal vector the same, the curvature-strains are now

$$\begin{cases} n_{x'} = n_x = a_1 x + a_2 y + a_3 z = \ a_1 x' - a_2 y' + a_3 z', \\ n_{y'} = -n_y = -\left(a_4 x + a_5 y + a_6 z\right) = -a_4 x' + a_5 y' - a_6 z'. \end{cases} \tag{31}$$

Following the energy invariance argument as before, the linear coefficients which change sign must be zero, Removing the redundant constraints, we have additionally that

$$k_2 = k_4 = 0. \tag{32}$$

In the quadratic terms, we have

$$k_{16} = k_{23} = k_{34} = k_{56} = 0. \tag{33}$$

Now, there is only 1 linear coefficient and 8 quadratic coefficients.

$$k_i = \begin{pmatrix} 0 \\ 0 \\ k_3 \\ 0 \\ 0 \\ 0 \end{pmatrix}, \quad k_{ij} = \begin{bmatrix} k_{11} & 0 & 0 & 0 & k_{15} & 0 \\ 0 & k_{22} & 0 & k_{24} & 0 & 0 \\ 0 & 0 & k_{33} & 0 & 0 & 0 \\ 0 & k_{24} & 0 & k_{44} & 0 & 0 \\ k_{15} & 0 & 0 & 0 & k_{55} & 0 \\ 0 & 0 & 0 & 0 & 0 & k_{66} \end{bmatrix}. \tag{34}$$

Next, we rotate the coordinates about the z-axis by 90° clockwise, giving $x' = y, y' = -x, z' = z$. Then, the curvature-strain relations are

$$\begin{cases} n_{x'} = n_y = a_4 x + a_5 y + a_6 z = a_5 x' - a_4 y' + a_6 z', \\ n_{y'} = -n_x = -\left(a_1 x + a_2 y + a_3 z\right) = -a_2 x' + a_1 y' - a_3 z'. \end{cases} \tag{35}$$

Again, by the energy invariance, we have

$$\begin{aligned} k_1 &= k_5, \\ k_2 &= -k_4, \\ k_3 &= \pm k_6. \end{aligned} \tag{36}$$

From the last relation in (36) and (28), we can conclude that

$$k_3 = k_6 = 0. \tag{37}$$

For the quadratic terms, we have the additional constraints

$$k_{11} = k_{55}, \quad k_{22} = k_{44}, \quad k_{33} = k_{66}. \tag{38}$$

At this point, we have removed all the linear coefficients, and have only 5 remaining quadratic coefficients,

$$k_i = \begin{pmatrix} 0 \\ 0 \\ 0 \\ 0 \\ 0 \\ 0 \end{pmatrix}, \quad k_{ij} = \begin{bmatrix} k_{11} & 0 & 0 & 0 & k_{15} & 0 \\ 0 & k_{22} & 0 & k_{24} & 0 & 0 \\ 0 & 0 & k_{33} & 0 & 0 & 0 \\ 0 & k_{24} & 0 & k_{22} & 0 & 0 \\ k_{15} & 0 & 0 & 0 & k_{11} & 0 \\ 0 & 0 & 0 & 0 & 0 & k_{33} \end{bmatrix}. \tag{39}$$

Finally, we rotate the coordinates about the z-axis by 45° clockwise so that $x' = (\sqrt{2}/2)x + (\sqrt{2}/2)y,\ y' = -(\sqrt{2}/2)x + (\sqrt{2}/2)y,\ z' = z$, or equivalently, $x = (\sqrt{2}/2)x' - (\sqrt{2}/2)y',\ y = (\sqrt{2}/2)x' + (\sqrt{2}/2)y',\ z = z'$. The work is a bit more tedious in this case. The curvature-strain relations are

$$\begin{cases} n_{x'} = \dfrac{\sqrt{2}}{2}\left(a_1x + a_2y + a_3z\right) + \dfrac{\sqrt{2}}{2}\left(a_4x + a_5y + a_6z\right) \\ \quad = \dfrac{\sqrt{2}}{2}\left(a_1\left(\dfrac{\sqrt{2}}{2}x' - \dfrac{\sqrt{2}}{2}y'\right) + a_2\left(\dfrac{\sqrt{2}}{2}x' + \dfrac{\sqrt{2}}{2}y'\right) + a_3z'\right) \\ \qquad + \dfrac{\sqrt{2}}{2}\left(a_4\left(\dfrac{\sqrt{2}}{2}x' - \dfrac{\sqrt{2}}{2}y'\right) + a_5\left(\dfrac{\sqrt{2}}{2}x' + \dfrac{\sqrt{2}}{2}y'\right) + a_6z'\right) \\ \quad = \dfrac{1}{2}(a_1 + a_2 + a_4 + a_5)x' + \dfrac{1}{2}(-a_1 + a_2 - a_4 + a_5)y' + \dfrac{\sqrt{2}}{2}(a_3 + a_6)z', \\ n_{y'} = -\dfrac{\sqrt{2}}{2}\left(a_1x + a_2y + a_3z\right) + \dfrac{\sqrt{2}}{2}\left(a_4x + a_5y + a_6z\right) \\ \quad = -\dfrac{\sqrt{2}}{2}\left(a_1\left(\dfrac{\sqrt{2}}{2}x' - \dfrac{\sqrt{2}}{2}y'\right) + a_2\left(\dfrac{\sqrt{2}}{2}x' + \dfrac{\sqrt{2}}{2}y'\right) + a_3z'\right) \\ \qquad + \dfrac{\sqrt{2}}{2}\left(a_4\left(\dfrac{\sqrt{2}}{2}x' - \dfrac{\sqrt{2}}{2}y'\right) + a_5\left(\dfrac{\sqrt{2}}{2}x' + \dfrac{\sqrt{2}}{2}y'\right) + a_6z'\right) \\ \quad = \dfrac{1}{2}(-a_1 - a_2 + a_4 + a_5)x' + \dfrac{1}{2}(a_1 - a_2 - a_4 + a_5)y' + \dfrac{\sqrt{2}}{2}(-a_3 + a_6)z'. \end{cases} \tag{40}$$

The linear part of the energy is expanded by

$$
\begin{aligned}
g'_{\text{lin}} &= \frac{1}{2}(a_1+a_2+a_4+a_5)k_1 + \frac{1}{2}(-a_1+a_2-a_4+a_5)k_2 + \frac{\sqrt{2}}{2}(a_3+a_6)k_3 \\
&\quad + \frac{1}{2}(-a_1-a_2+a_4+a_5)k_4 + \frac{1}{2}(a_1-a_2-a_4+a_5)k_5 + \frac{\sqrt{2}}{2}(-a_3+a_6)k_6.
\end{aligned} \tag{41}
$$

Differentiating (41) with respect to certain a_i gives

$$
\begin{aligned}
\frac{1}{2}\left(k_1-k_2-k_4+k_5\right) &= k_1, \\
\frac{1}{2}\left(k_1+k_2-k_4-k_5\right) &= k_2, \\
\frac{1}{2}\left(k_1-k_2+k_4-k_5\right) &= k_4, \\
\frac{1}{2}\left(k_1+k_2+k_4+k_5\right) &= k_5.
\end{aligned}
$$

Using this, we have

$$
\begin{aligned}
&4(k_{11}-k_{15}-k_{22}-k_{24}) \\
&\quad = (k_1-k_2-k_4+k_5)(k_1-k_2-k_4+k_5) - (k_1-k_2-k_4+k_5)(k_1+k_2+k_4+k_5) \\
&\qquad - (k_1+k_2-k_4-k_5)(k_1+k_2-k_4-k_5) - (k_1+k_2-k_4-k_5)(k_1-k_2+k_4-k_5) \\
&\quad = -2(k_1-k_2-k_4+k_5)(k_2+k_4) - 2(k_1+k_2-k_4-k_5)(k_1-k_5) \\
&\quad = -2k_{11}-4k_{12}+4k_{15}+2k_{22}+4k_{24}+2k_{44}-4k_{45}-2k_{55}.
\end{aligned}
$$

But, from (38), we have $k_{11}=k_{55}$, $k_{12}=0$, $k_{22}=k_{44}$, and $k_{45}=0$. So the equality above simplifies to

$$
4(k_{11}-k_{15}-k_{22}-k_{24}) = -4(k_{11}-k_{15}-k_{22}-k_{24}) = 0.
$$

The final relation we have follows immediately:

$$
k_{15} = k_{11}-k_{22}-k_{24}. \tag{42}
$$

After all these simplifications, we have 0 linear terms, and only 4 independent quadratic terms.

$$k_i = \begin{pmatrix} 0 \\ 0 \\ 0 \\ 0 \\ 0 \\ 0 \end{pmatrix}, \quad k_{ij} = \begin{bmatrix} k_{11} & 0 & 0 & 0 & k_{11}-k_{22}-k_{24} & 0 \\ 0 & k_{22} & 0 & k_{24} & 0 & 0 \\ 0 & 0 & k_{33} & 0 & 0 & 0 \\ 0 & k_{24} & 0 & k_{22} & 0 & 0 \\ k_{11}-k_{22}-k_{24} & 0 & 0 & 0 & k_{11} & 0 \\ 0 & 0 & 0 & 0 & 0 & k_{33} \end{bmatrix}. \tag{43}$$

Now, the matrix notation is superfluous, so we write the energy density term-by-term using (23) and (43),

$$e = \frac{1}{2}\Big[k_{11}(a_1^2 + a_5^2) + k_{22}(a_2^2 + a_4^2) + k_{33}(a_3^2 + a_6^2)\Big] + (k_{11} - k_{22} - k_{24})a_1a_5 + k_{24}a_2a_4. \tag{44}$$

In terms of the splays, twists, and bends in (22), the energy density (44) becomes

$$\begin{aligned} e &= \frac{1}{2}\Big[k_{11}(s_1^2 + s_2^2) + k_{22}(t_2^2 + t_1^2) + k_{33}(b_1^2 + b_2^2)\Big] + (k_{11} - k_{22} - k_{24})s_1s_2 - k_{24}t_2t_1 \\ &= \frac{1}{2}k_{11}(s_1 + s_2)^2 + \frac{1}{2}k_{22}(t_1 + t_2)^2 + \frac{1}{2}k_{33}(b_1^2 + b_2^2) - (k_{22} + k_{24})(s_1s_2 + t_1t_2). \end{aligned} \tag{45}$$

The total energy is given by

$$E[\Gamma] = \int_\Gamma \frac{1}{2}k_{11}(s_1 + s_2)^2 + \frac{1}{2}k_{22}(t_1 + t_2)^2 + \frac{1}{2}k_{33}(b_1^2 + b_2^2) - (k_{22} + k_{24})(s_1s_2 + t_1t_2)\, dS. \tag{46}$$

We proceed from here following Helfrich's work in [47]. Since n is the unit normal vector, the quantities s_1, s_2, t_1, and t_2 are related to the principle curvatures c_1 and c_2. Specifically,

$$\begin{aligned} s_1 + s_2 &= \frac{\partial n_x}{\partial x} + \frac{\partial n_y}{\partial y} = c_1 + c_2 \\ s_1s_2 + t_1t_2 &= \frac{\partial n_x}{\partial x}\frac{\partial n_y}{\partial y} - \frac{\partial n_x}{\partial y}\frac{\partial n_y}{\partial x} = c_1c_2 \end{aligned} \tag{47}$$

Now consider the surface of the vesicle membrane $z = f(x, y)$ as the zero-level set of $h(x, y, z) = z - f(x, y)$. Then the normal vector to the surface is given by $n = \nabla h$. The curl of the gradient is always zero, hence,

$$\nabla \times n = 0. \tag{48}$$

The above equation (48) in component form is

$$\frac{\partial n_z}{\partial y} - \frac{\partial n_y}{\partial z} = 0, \quad \frac{\partial n_x}{\partial z} - \frac{\partial n_z}{\partial x} = 0, \quad \frac{\partial n_y}{\partial x} - \frac{\partial n_x}{\partial y} = 0. \tag{49}$$

The z-component of (49) can be written in terms of the twists,

$$t_2 + t_1 = 0. \tag{50}$$

The x and y-components of (49) can be simplified, since $z = 1$ is constant in both n_x and n_y. Hence,

$$\frac{\partial n_y}{\partial z} = 0, \quad \frac{\partial n_x}{\partial z} = 0. \tag{51}$$

But these are the exact expression for the bends, so we have

$$b_1 = b_2 = 0. \tag{52}$$

Using (47), (50), (52), the total energy (46) is simplified to

$$E[\Gamma] = \int_\Gamma \frac{1}{2}\mathscr{K}_C(c_1 + c_2)^2 + \frac{1}{2}\mathscr{K}_G(c_1c_2)\, dS, \tag{53}$$

where $\mathscr{K}_C = k_{11}$ and $\mathscr{K}_G = -2(k_{22} + k_{24})$. This matches the form of the bending energy (12) exactly, since the mean curvature $H = \frac{1}{2}(c_1 + c_2)$ and the Gaussian curvature $K = c_1c_2$.

2.5.1. NOTE ON THE TERM BENDING ENERGY.

The energy given by equations (12) and (53) is called the bending energy, and in the derivation, it was discovered that the bends $b_1 = b_2 = 0$ per equation (52). When we say in English *bending energy*, we mean that it is the energy caused by any change in the curvature of the shape. It is not equivalent to the mathematically defined bends b_1 and b_2 used in the derivation.

2.6. Total mechanical energy

Now we have all of the pieces of the total mechanical energy of the membrane. The total energy includes bending energy modified by the spontaneous curvature (13) with added energy constraints for the surface area (10) and volume (11),

$$E[\Gamma] = \frac{\mathscr{K}_C}{2}\int_\Gamma (2H - C_0)^2 \, dS + \frac{\mathscr{K}_G}{2}\int_\Gamma K \, dS + p\int_\Omega dV + \sigma \int_\Gamma dS. \tag{54}$$

To determine how the membrane takes its shape, we minimize the energy by setting to zero the variation with respect to any membrane position. The form of this equation, known as the shape equation, depends upon the parameterization of the membrane surface. For surface parameterizations, we will need to establish some basic concepts from differential geometry.

2.7. Some differential geometry

In its most general form, the membrane is treated as a 2D sheet in a Monge parameterization, $\mathbf{x}(u,v) = (u, v, f(u,v))$. Using this parameterization, one can obtain formulas for the mean and Gaussian curvatures and express the mechanical energy (54) in terms of $f(u,v)$. To compute the total area of this surface, we consider breaking the surface into infinitesimal parallelograms with lengths of the tangent vectors $\mathbf{x}_u \, du$ and $\mathbf{x}_v \, dv$, where the subscripts denote partial differentiation. The area of a parallelogram is given by the length of the cross product of the vectors, $\|\mathbf{x}_u \times \mathbf{x}_v\| \, du \, dv$. Conveniently, in a Monge parameterization, a lot of simplification occurs:

$$\mathbf{x}_u = (1, 0, f_u), \qquad \mathbf{x}_v = (0, 1, f_v),$$

so the cross product is $\mathbf{x}_u \times \mathbf{x}_v = (-f_u, -f_v, 1)$ and hence $\|\mathbf{x}_u \times \mathbf{x}_v\| = (1 + f_u^2 + f_v^2)^{1/2}$. The differential area element is then

$$dS = \sqrt{1 + (\nabla f)^2} \, du \, dv. \tag{55}$$

Integrating over the entire surface gives the total surface area,

$$A(f) = \int_{\Gamma} \sqrt{1 + f_u^2 + f_v^2}\, du\, dv. \tag{56}$$

Before going too far with a Monge parameterization, what we really want to do is construct an equation for the mean curvature H in terms of *any* parameterization. We begin with two vectors $\mathbf{x}_u$ and $\mathbf{x}_v$ that lie on the tangent plane to the surface. Since the cross product of two vectors is always perpendicular to the vectors themselves, the unit normal to the surface is given by

$$U = \frac{\mathbf{x}_u \times \mathbf{x}_v}{||\mathbf{x}_u \times \mathbf{x}_v||}. \tag{57}$$

Define E, F, G, by

$$E = \mathbf{x}_u \cdot \mathbf{x}_u, \qquad F = \mathbf{x}_u \cdot \mathbf{x}_v, \qquad G = \mathbf{x}_v \cdot \mathbf{x}_v.$$

We note that this E should not be confused with the energy functional $E[\Gamma]$ in (54). It should be clear from context whether we are using E for geometry purposes or the total mechanical energy $E[\Gamma]$, but to remove any doubt, when we refer to the total mechanical energy, we will always write it as $E[\Gamma]$ rather than just E. Let $\alpha(t) = \mathbf{x}_u(t) + \mathbf{x}_v(t)$ be a curve parameterized by t such that α is has unit speed. That is, if α' is the vector tangent to the curve, it has magnitude 1. Then,

$$\begin{aligned} 1 &= |\alpha'| \\ &= (\mathbf{x}_u u' + \mathbf{x}_v v') \cdot (\mathbf{x}_u u' + \mathbf{x}_v v') \\ &= \mathbf{x}_u \cdot \mathbf{x}_u u'^{\,2} + (\mathbf{x}_v \cdot \mathbf{x}_u + \mathbf{x}_u \cdot \mathbf{x}_v) u'v' + \mathbf{x}_v \cdot \mathbf{x}_v v'^{\,2} \\ &= Eu'^{\,2} + 2Fu'v' + Gv'^{\,2}, \end{aligned} \tag{58}$$

and so E, F, and G are named the coefficients of the first fundamental form. (The first fundamental form is the inner product of two vectors in the tangent space of a surface.) The first fundamental form is the following linear operator with these coefficients,

$$I = \begin{pmatrix} E & F \\ F & G \end{pmatrix}. \tag{59}$$

Because of (58), we can define an arc length element ds to be

$$ds^2 = E\,du^2 + 2F\,du\,dv + G\,dv^2. \tag{60}$$

As the equation (60) shows, the first fundamental form describes how a surface distorts the length of a vector in $\mathbb{R}^3$. One can write equations (55) and (56) in terms of the first fundamental form as well,

$$dS = \sqrt{EG - F^2}\;du\;dv. \tag{61}$$

Often, the elements of the first fundamental form is given in tensor notation. Let the matrix $I = I_{ij}$ in (59) be defined by

$$I_{11} = E, \quad I_{12} = I_{21} = F, \quad I_{22} = G. \tag{62}$$

Denote the determinant of the 2 by 2 matrix I by ω,

$$\omega = \det \begin{pmatrix} I_{11} & I_{12} \\ I_{21} & I_{22} \end{pmatrix} = \det(I) = \sqrt{EG - F^2}. \tag{63}$$

One may also rewrite the unit normal vector (57) in terms of ω, by

$$U = \frac{\mathbf{x}_u \times \mathbf{x}_v}{\omega}. \tag{64}$$

Similarly, we can define the coefficients of the second fundamental form by

$$L = -\mathbf{x}_u \cdot U_u, \qquad 2M = -(\mathbf{x}_v \cdot U_u + \mathbf{x}_u \cdot U_v), \qquad N = -\mathbf{x}_v \cdot U_v.$$

The second fundamental form is

$$II = \begin{pmatrix} L & M \\ M & N \end{pmatrix}. \tag{65}$$

Now let α be a curve parameterized by t (of any speed). Since α' is tangent to the surface, it is perpendicular to the normal U. Thus, $(\alpha' \cdot U) = 0$. But,

$$\begin{aligned} 0 &= (\alpha' \cdot U)' \\ &= \alpha'' \cdot U + \alpha' \cdot U'. \end{aligned}$$

Therefore, the component of the acceleration α'' that is normal to the surface, $\alpha'' \cdot U = -\alpha' \cdot U'$. Since this is true for any curve with velocity α', the normal curvature is determined completely by the bending of the surface. This gives a natural definition for the normal curvature in the $\mathbf{w}$ direction,

$$k(\mathbf{w}) = \alpha'' \cdot U.$$

Using this definition and taking a curve α with unit speed,

$$\begin{aligned} k(\mathbf{w}) &= \alpha'' \cdot U \\ &= -\alpha' \cdot U' \\ &= -(\mathbf{x}_u u' + \mathbf{x}_v v') \cdot (U_u u' + U_v v') \\ &= -\mathbf{x}_u \cdot U_u u'^{\,2} - (\mathbf{x}_v \cdot U_u + \mathbf{x}_u \cdot U_v) u'v' - \mathbf{x}_v \cdot U_v v'^{\,2} \\ &= L u'^{\,2} + 2M u'v' + N v'^{\,2}. \end{aligned}$$

In tensor notation, we can write define $II = II_{ij}$ in equation (65) by

$$II_{11} = L, \quad II_{12} = II_{21} = M, \quad II_{22} = N. \tag{66}$$

Again, let $\mathbf{w}_1$ and $\mathbf{w}_2$ be any two perpendicular unit vectors with normal curvatures $k_1 = k(\mathbf{w}_1)$ and $k_2 = k(\mathbf{w}_2)$, respectively. The local mean curvature of the surface is defined by to be the average of these normal curvatures k_1 and k_2. The local mean curvature can be expressed in terms of the coefficients of the fundamental forms as follows:

$$H = \frac{1}{2}\,(k_1 + k_2) = \frac{EN + GL - 2FM}{2(EG - F^2)}. \tag{67}$$

The derivation of (67) is straightforward but very standard, so we refer the reader to find it in any (good) differential geometry text (see [25, 80, 57] for example). An important fact about (67) is that it shows that the mean curvature does not depend on the choices of the vectors $\mathbf{w}_1$ and $\mathbf{w}_2$, and therefore does not depend on the choice of normal curvatures k_1 and k_2. This means we can take the curvatures k_1 and k_2 to be the principal curvatures of the surface, which are defined to be the maximum normal curvature and the minimum normal curvature. The principal curvatures are also the eigenvalues of the second fundamental form (65). The Gaussian curvature is defined as the product of the principle curvatures,

$$K = k_1\, k_2 = \frac{LN - M^2}{EG - F^2}. \tag{68}$$

For completeness, we note that one can obtain the two curvatures as the trace and determinant of the two fundamental forms,

$$H = \frac{\mathrm{Tr}(I \cdot \mathrm{adj}(II))}{2\,\det(I)}, \tag{69}$$

$$K = \frac{\det(II)}{\det(I)}, \tag{70}$$

where the adjoint of II is defined as the transpose of the cofactor matrix,

$$\mathrm{adj}(II) = \begin{pmatrix} N & -M \\ -M & L \end{pmatrix}.$$

We now have the tools necessary to compute the shape equation for the mechanical energy (54).

2.8. The shape equation

Recall that the shape equation is $\delta_\Gamma E[\Gamma] = 0$. The second term in (54) is constant for surfaces with the same topology according to the Gauss-Bonet formula, so the variation is zero and it has no effect on the minimization (see [25] for the Gauss-Bonet theorem). However, we must ensure invariant topology to avoid any discontinuities in the energy equation. The variation will include the first term of (54) and the constraint terms. The form of the variation depends on the parameterization used for Γ. Zhong-can and Helfrich have done this using a Monge parameterization $\Gamma = \mathbf{x}(u, v) = (u, v, f(u, v))$ and expressed $\delta_\Gamma E[\Gamma]$ back in terms of the curvatures in [107]. They obtained the following equation:

$$p - 2\sigma H + \mathscr{K}_C(2H + C_0)(2H^2 - 2K - C_0 H) + 2\mathscr{K}_C \Delta H = 0. \tag{71}$$

The derivation is complicated and will not be repeated here; a full treatment is found in [107].

Even after obtaining the shape equations, solving it for the general shape Γ is an extremely challenging problem. To attack it, various approaches have been made. One approach, requiring a simplification which may be assumed in certain applications, is to require the surface have symmetry about an axis [90, 91]. This reduces the complexity of the shape equation to a system of ordinary differential equations. The analysis is done by Seifert et. al. in [91]. Another approach that does not restrict to axisymmetric surfaces is to minimize the energy over a smaller subspace of membrane configurations. For example, the vesicle surface can be approximated by a linear combination of basis functions, and the coefficients are adjusted to minimize the energy. This can be accomplished either by Rayleigh-Ritz procedures [13, 45, 46], or finite element methods [37, 68], for example. These methods also have their restrictions. If the curvature is large in a given area of the surface, mesh refinement may result in a large number of basis functions, increasing the computational cost.

The approach we will take in the next chapter follows the subspace idea. However, instead of a Cartesian triangulation or Monge parameterization of the surface, we exploit the vesicle structure by using surface harmonic functions as the choice of basis functions.

These functions are a special case of spherical harmonic functions, and provide a natural basis for vesicle-like shapes, which can greatly reduce the number of degrees of freedom required to solve the shape equation. For this approach, we will recast the energy functional (54) by treating the surface area and volume terms as fixed quantities. This is justified by the separable energy scales, as explained in Section 2.3. Therefore, our goal is to minimize the total mechanical energy (13) over membrane configurations which have continuous curvature and preserve the total surface area and volume. In the next chapter, we state this variational problem precisely.

CHAPTER 3

SURFACE HARMONIC PARAMETERIZATION

In this chapter, we introduce the surface harmonic parameterization for vesicles, and provide formulas for the total mechanical energy (54) according to this parameterization. This is done in efforts to solve the following variational problem motivated by the previous chapter.

3.1. VARIATIONAL PROBLEM

Our goal is to minimize the bending energy of a membrane (13) over membrane configurations which have continuous curvature and preserve the total surface area and volume. The space of admissible membrane configurations is therefore

$$H^2_{S_A V}(\Gamma) = \{x : x \in H^2(\Gamma), S_A(x) = \bar{S}, V[x] = \bar{V}\}, \tag{72}$$

where $H^2 = W^{2,2}$ is the standard Sobolev space of square integrable functions with square integrable partial derivatives through second order. The functionals $S_A[x]$ and $V[x]$ are the surface area and volume of the membrane, respectively, and $\bar{S}$ and $\bar{V}$ are the prescribed surface area and volume, respectively. The variational problem to be solved is

$$\min_{x \in H^2_{S_A V}(\Gamma)} E[\Gamma]. \tag{73}$$

To be clear, the membrane position is denoted $\Gamma = \Gamma(x)$. To compute the total energy and account for the area expansion/contraction and osmotic pressure, the constraints for the conservation of the surface area of the membrane and the total volume enclosed are enforced as penalty terms. The minimization problem (neglecting any other sources of energy for now) with the penalty functions is given by

$$\min_{x \in H^2(\Gamma)} I[\Gamma], \tag{74}$$

$$I[\Gamma] = E[\Gamma] + \frac{k_S}{2}(S_A - \bar{S})^2 + \frac{k_V}{2}(V - \bar{V})^2, \tag{75}$$

where k_S and k_V are large constants to enforce the constraints to a chosen degree of precision.

3.2. Choice of parameterization

The computation of the terms in the total energy (75) and the terms in its variation depends on the choice of parameterization of the membrane surface. A convenient consequence of the bending energy of lipid bilayers is that the energy functionals are independent of the surface parameterization [14]. Therefore, we choose to parameterize the surface not by brute force using local Cartesian coordinates, but rather by using a global basis of surface harmonic functions. Since lipid vesicles are sphere-like structures, the choice of surface harmonics to represent the surface is natural, and this choice reduces the number of terms necessary for the computation.

We find an approximate solution to the original problem (74) by minimizing the total energy over membrane configurations determined by a linear combination of surface harmonic functions. That is, the exact membrane $\Gamma(\vec{x})$ is approximated by $\Gamma(\vec{a})$, where the real-valued coefficients $\vec{a}$ are chosen such that the bending energy $I[\Gamma]$ is minimized. The surface harmonics functions are an infinite dimensional basis; however, for the numerical implementation, we only use a finite number $(N+1)^2$ of surface harmonic functions. Stated mathematically, the new minimization problem is

$$\min_{\vec{a}\in\mathbb{R}^{(N+1)^2}} I[\Gamma(\vec{a})], \tag{76}$$

$$I[\Gamma(\vec{a})] = E[\Gamma(\vec{a})] + \frac{k_S}{2}(S_A[\vec{a}] - \bar{S})^2 + \frac{k_V}{2}(V[\vec{a}] - \bar{V})^2. \tag{77}$$

Equation (76) is the problem we solve here. The minimization of (77) leads to the shape equation,

$$\delta_\Gamma I[\Gamma] = \delta_\Gamma E[\Gamma] + k_S(S_A - \bar{S})\delta S_A + k_V(V - \bar{V})\delta V = 0. \tag{78}$$

Next, we introduce the surface harmonic parameterization, and provide formulas for the terms in (77). Surface harmonic functions are a real-valued version of spherical harmonic functions. In the following section, we briefly review *spherical* harmonics first.

3.3. Spherical harmonic functions

Spherical harmonics are solutions to Laplace's Equation in spherical coordinates. The solution can be obtained through separation of the variables θ and ϕ; however, a more convenient way to construct spherical harmonics is to use a generalization of Legendre polynomials. Legendre polynomials, also called Legendre functions of the first kind, Legendre coefficients, or zonal harmonics, are solutions to the Legendre differential equation. The Legendre polynomial can be defined by the contour integral

$$P_n(z) = \frac{1}{2\pi i} \oint (1 - 2tz + t^2)^{-1/2} t^{-n-1}\, dt. \tag{79}$$

Another useful representation utilizes Rodrigues respresentation,

$$P_n(x) = \frac{1}{2^n n!} \frac{d^n}{dx^n} (x^2 - 1)^n. \tag{80}$$

The associated Legendre polynomials generalize Legendre polynomials, provided $m \neq 0$, are defined by

$$P_n^m(x) = (-1)^m (1 - x^2)^{m/2} \frac{d^m}{dx^m} P_n(x), \qquad m \neq 0. \tag{81}$$

If $m = 0$, the associated Legendre polynomial is just the Legendre polynomial. By Rodrigues' formula,

$$P_n^m(x) = (-1)^m (1 - x^2)^{m/2} \frac{d^m}{dx^m} \left(\frac{1}{2^n n!} \frac{d^n}{dx^n} (x^2 - 1)^n \right), \qquad m \neq 0. \tag{82}$$

It is convenient to introduce the change of variables $\mu = \cos(\theta)$. In this way, the partial derivatives with respect to the polar angle $\theta \in [0, \pi]$ may be computed. Here, we use the physics notation for the angles, where $\theta \in [0, \pi]$ is the polar or zenith angle extending from the positive z axis, and $\phi \in [0, 2\pi]$ is the azimuthal angle in the xy-plane extending from the positive x-axis. Using this notation, normalized spherical harmonic functions are defined by

$$Y_n^m(\theta, \phi) = \sqrt{\left(\frac{(2n + 1)(n - m)!}{4\pi (n + m)!} \right)} P_n^m(\mu) e^{im\phi}, \tag{83}$$

where $P_n^m(\mu)$ is the associated Legendre polynomial evaluated at $\mu = \cos(\theta)$.

Since spherical harmonics form an orthonormal basis for $L^2(\mathbb{R}^2)$, we can use linear combinations to parameterize vesicle surfaces. We parameterize the surface in spherical coordinates $(\theta, \phi, r(\theta, \phi))$, where the radius r is expressed in terms of spherical harmonics,

$$r(\theta, \phi) = \sum_{n=0}^{\infty} \sum_{m=-n}^{n} a_n^m Y_n^m(\theta, \phi). \tag{84}$$

The a_n^m are the coefficients of the linear representation. These coefficients can be determined by the following formula:

$$a_n^m = \int_0^{2\pi} \int_0^{\pi} r(\theta, \phi) \overline{Y_n^m(\theta, \phi)} \sin(\theta)\, d\theta\, d\phi \tag{85}$$

where $\overline{Y_n^m(\theta, \phi)}$ is the complex conjugate of $Y_n^m(\theta, \phi)$. Since a real surface is desired, r must be a real number. Clearly the spherical harmonic function $Y_n^m(\theta, \phi)$ at fixed θ and ϕ is complex, thus every coefficient a_{nm} must also be complex, provided $m \neq 0$. In fact, since a_{nm} is defined through the complex conjugate of Y_n^m in formula (85), the complex part of a_{nm} will cancel with the complex part of Y_n^m, yielding $r \in \mathbb{R}$ if $m \neq 0$. When $m = 0$, both Y_n^0 and a_{n0} are real, so $r \in \mathbb{R}$ for every n and m.

3.4. Surface harmonic functions

The coefficients defined by (85) guarantee a real-valued surface. However, if the coefficients a_n^m are poorly chosen so that the complex parts of a_n^m and Y_n^m do not cancel, the radius parameterizing the object (84) will be complex. In an optimization routine, the coefficients are perturbed numerically, so any nonzero perturbation in the complex part will result in a complex surface. Since we seek a real-valued surface that minimizes the potential energy (77), we use only the real parts of the spherical harmonics to ensure that the surface under the energy minimization is real. These are surface harmonics.

Since spherical harmonics are just the angular portion of the solution to Laplace's equation, the real and complex parts of the spherical harmonics are also solutions to Laplace's equation. We will state this as a lemma.

LEMMA 3.4.1. *Let $z = x + iy$ be a solution to Laplace's equation in spherical coordinates ($\nabla^2 f = 0$). Then, x and y are also solutions.*

PROOF. Write Laplace's equation in spherical coordinates as

$$\nabla^2 f(\theta, \phi) = \frac{1}{r^2}\frac{\partial}{\partial r}\left(r^2 \frac{\partial f}{\partial r}\right) + \frac{1}{r^2 \sin\theta}\frac{\partial}{\partial \theta}\left(\sin\theta \frac{\partial f}{\partial \theta}\right) + \frac{1}{r^2 \sin^2\theta}\frac{\partial^2 f}{\partial \phi^2} = 0.$$

Since $\nabla^2(\bar{z}) = \overline{\nabla^2(z))} = \bar{0} = 0$, the complex conjugate $\bar{z}$ is also a solution. The real part of z is $x = (z + \bar{z})/2$ and the imaginary part is $y = (z + \bar{z})/(2i)$. Each are linear combinations of solutions z and $\bar{z}$, and hence are also solutions by the linearity of $\nabla^2(\cdot)$. □

By Euler's formula, each spherical harmonic function can be rewritten as

$$Y_n^m(\theta, \phi) = f_n^m P_n^m(\mu)(\cos(m\phi) + i\sin(m\phi)). \tag{86}$$

where f_n^m is the normalization factor

$$f_n^m = \sqrt{\left(\frac{(2n+1)(n-m)!}{4\pi(n+m)!}\right)}. \tag{87}$$

By Lemma 3.4.1, we define the surface harmonics as

$$S_n^m(\theta, \phi) = \begin{cases} f_n^m P_n^m(\mu)\cos(m\phi), & \text{if } m \geq 0, \\ f_n^{|m|} P_n^{|m|}(\mu)\sin(|m|\phi), & \text{if } m < 0. \end{cases} \tag{88}$$

We now parameterize the radius of a smooth surface by a linear combination of the surface harmonics $S_n^m(\theta, \phi)$,

$$r(a_n^m; \theta, \phi) = \sum_{n=0}^{\infty} \sum_{m=-n}^{n} a_n^m S_n^m(\theta, \phi). \tag{89}$$

The current form matches the form of (84). Another representation of the radius of a surface that avoids the sign changes in m is

$$r(A_n^m, B_n^m; \theta, \phi) = \sum_{n=0}^{\infty} \sum_{m=0}^{n} \Big(A_n^m \cos(m\phi) + B_n^m \sin(m\phi)\Big) f_n^m P_n^m(\mu),$$

where

$$a_n^m = \begin{cases} A_n^m, & \text{if } m \geq 0, \\ B_n^m, & \text{if } m < 0. \end{cases}$$

Now the radius $r(\theta, \phi)$ may be defined by summing m over nonnegative values. If the series is truncated at some N, there are up to $\left(\sum_{n=0}^{N}\sum_{m=0}^{n} 1\right)$ nonzero coefficients of A_n^m. By straightforward calculations,

$$\begin{aligned}\sum_{n=0}^{N}\sum_{m=0}^{n} 1 &= \sum_{n=0}^{N}(n+1) = 1 + \sum_{n=1}^{N}(n+1) = N + 1 + \sum_{n=1}^{N} n = N + 1 + \frac{N(N+1)}{2} \\ &= \frac{(N+2)(N+1)}{2}.\end{aligned}$$

For the B_n^m coefficients, notice that if $m = 0$, $\sin(m\phi) = 0$ for any angle ϕ. Therefore, the coefficients B_n^0 are irrelevant. Then, the maximum number of nonzero coefficients B_n^m is given by

$$\sum_{n=0}^{N}\sum_{m=1}^{n} 1 = \sum_{n=0}^{N} n = \frac{N(N+1)}{2}.$$

The total number of coefficients in a truncation is therefore $\frac{(N+2)(N+1)}{2} + \frac{N(N+1)}{2} = (N+1)^2$.

3.5. DISCRETIZING THE SURFACE

We now need to discretize the surface. Each surface point $\vec{x} = (x, y, z) \in \mathbb{R}^3$ is expressed in terms of spherical coordinates $\vec{x} = (r\sin(\theta)\cos(\phi), r\sin(\theta)\sin(\phi), r\cos(\theta))$. The value of r is determined by the surface harmonic coefficients a_n^m. Thus, for fixed values of θ and ϕ on the surface mesh, a surface point $\vec{x}$ is uniquely determined by the surface harmonic coefficients.

We begin with n_t values of θ and n_p values of ϕ for a total of $\mathcal{N} = n_t \cdot n_p$ points. Since $\mathcal{N}$ can be a very large number, performing pointwise calculations on the mesh can be computationally costly. Under the surface harmonics parameterization, the surface is approximated by truncating the infinite sum in (89) at some number N. This reduces the computation cost since there are far fewer surface harmonic functions required to approximate a surface than a curvilinear Cartesian grid of mesh points due to the uniform convergence property of surface harmonic approximations. Our numerical results confirm that $(N+1)^2 << \mathcal{N}$. This truncation also allows us to represent the radius (89) through a single index i, rather than two indicies n and m.

Let $\vec{a}$ be a vector of all of the surface harmonic coefficients,

$$\vec{a} = [A_0^0,\ A_1^0,\ A_1^1,\ B_1^1,\ A_2^0,\ A_2^1,\ A_2^2,\ B_2^1,\ B_2^2,\ \cdots,\ A_N^0,\ \cdots,\ A_N^N,\ B_N^1,\ \cdots,\ B_N^N]^T. \tag{90}$$

The size of $\vec{a}$ is $(N+1)^2 \times 1$, as discovered in the previous section. There is a convenient way to convert between the index i and the indicies n and m. For the surface harmonic mode $a_i \in \vec{a}$, $i = 0, 1, 2, \cdots (N+1)^2 - 1$, the corresponding n and m is given by

$$n(i) = \lfloor \sqrt{i} \rfloor \tag{91}$$

$$m(i) = \begin{cases} i - n^2, & \text{if } (i - n^2) \leq n, \\ n^2 + n - i, & \text{otherwise.} \end{cases} \tag{92}$$

With this organization, we can write

$$r(a_i; \theta, \phi) = \sum_{i=0}^{(N+1)^2-1} a_i S_i(\theta, \phi). \tag{93}$$

In terms of the surface harmonic coefficients, a fixed point on the surface can be expressed in Cartesian coordinates by

$$\vec{x}_{kl} = \vec{x}(\theta_k, \phi_l) = \begin{pmatrix} r_{kl}(a_i; \theta_k, \phi_l) \sin(\theta_k) \cos(\phi_l) \\ r_{kl}(a_i) \sin(\theta_k) \sin(\phi_l) \\ r_{kl}(a_i) \cos(\theta_k) \end{pmatrix}. \tag{94}$$

Let $\vec{X}$ be the vector of all of $\mathcal{N}$ points on the surface mesh, each expressed as a Cartesian triple. The size of $\vec{X}$ is $3\mathcal{N} \times 1$.

$$\vec{X} = [\vec{x}_{00}^T, \vec{x}_{01}^T, \cdots, \vec{x}_{0,n_p-1}^T, \vec{x}_{10}^T, \cdots, \vec{x}_{1,n_p-1}^T, \cdots, \vec{x}_{nt-1,0}^T, \cdots, \vec{x}_{nt-1,n_p-1}^T]^T. \tag{95}$$

3.6. Energy formulation in terms of surface harmonic parameterization

In this section, we will finish the parameterization of the mechanical energy (77). To accomplish this, we will need expressions for dS, S_A, V, H, K, and their variations in terms of the surface harmonic mode coefficients through $r(a_i)$. We will do this in several steps.

3.6.1. Derivatives of $r(a_i;\theta,\phi)$. First, we need to compute the derivatives of $r(a_i;\theta,\phi)$ with respect to the independent variables θ and ϕ. The derivatives with respect to ϕ are straightforward, since the dependence of the surface harmonic function $S_n^m(\theta,\phi)$ appears directly. The subscripts in the following formulas denote partial derivatives and should not be confused with mesh positions k and l.

$$\begin{aligned} r_\phi &= \sum_{n=0}^{N}\sum_{m=0}^{n}\Big(-m\,A_n^m\sin(m\phi) + m\,B_n^m\cos(m\phi)\Big) f_n^m P_n^m(\mu) \\ &= \sum_{n=0}^{N}\sum_{m=-n}^{n} -m\,a_n^m S_n^{-m}, \end{aligned} \tag{96}$$

$$\begin{aligned} r_{\phi\phi} &= \sum_{n=0}^{N}\sum_{m=0}^{n}\Big(-m^2 A_n^m\cos(m\phi) + -m^2 B_n^m\sin(m\phi)\Big) f_n^m P_n^m(\mu) \\ &= -m^2 r. \end{aligned} \tag{97}$$

The derivatives with respect to θ are

$$r_\theta = \sum_{n=0}^{N}\sum_{m=0}^{n}\Big(A_n^m\cos(m\phi) + B_n^m\sin(m\phi)\Big) f_n^m \partial_\theta P_n^m(\mu), \tag{98}$$

$$r_{\theta\theta} = \sum_{n=0}^{N}\sum_{m=0}^{n}\Big(A_n^m\cos(m\phi) + B_n^m\sin(m\phi)\Big) f_n^m \partial_\theta^2 P_n^m(\mu), \tag{99}$$

$$r_{\phi\theta} = r_{\theta\phi} = \sum_{n=0}^{N}\sum_{m=0}^{n}\Big(- m\,A_n^m \sin(m\phi) + m\,B_n^m \cos(m\phi)\Big) f_n^m \partial_\theta P_n^m(\mu) \tag{100}$$

$$= \sum_{n=0}^{N}\sum_{m=-n}^{n} -m\,a_n^m \frac{\partial S_n^{-m}}{\partial\theta},$$

where $\partial_\theta P_n^m(\mu)$ is given by the recurrence relation for the derivative of the associated Legendre polynomial $P_n^m(\mu)$,

$$\partial_\theta P_n^m(\mu) = \frac{-1}{sin(\theta)}\left((n+1)\cos(\theta)P_n^m(\mu) - (n-m+1)P_{n+1}^m(\mu)\right), \tag{101}$$

and $\partial_\theta^2 P_n^m(\mu)$ is computed directly from (101) as

$$\partial_\theta^2 P_n^m(\mu) = \Big((n+1+(n+1)^2\cos^2\theta)P_n^m(\mu) - 2\cos\theta(n-m+1)(n+2)P_{n+1}^m(\mu) \tag{102}$$

$$+ (n-m+1)(n-m+2)P_{n+2}^m(\mu)\Big)\frac{1}{\sin^2\theta}.$$

3.6.2. Fundamental form coefficients. Now we compute the coefficients of the first fundamental form in terms of the surface harmonic parameterization.

$$E = r_\theta^2 + r^2, \tag{103}$$

$$F = r_\theta r_\phi, \tag{104}$$

$$G = r_\phi^2 + r^2\sin^2(\theta), \tag{105}$$

$$L = -\vec{x}_\theta \cdot U_\theta, \tag{106}$$

$$M = \frac{1}{2}\left(\vec{x}_\theta \cdot U_\phi + \vec{x}_\phi \cdot U_\theta\right), \tag{107}$$

$$N = -\vec{x}_\phi \cdot U_\phi, \tag{108}$$

where $\vec{x}$ is a surface vector in spherical coordinates, and U is the unit normal to the surface at $\vec{x}$, given by (57) with independent variables $u = \theta$ and $v = \phi$. We define

$$R = |\vec{x}_\theta \times \vec{x}_\phi| \tag{109}$$

for notational convenience.

The derivatives of the surface vector $\vec{x}$ are

$$\vec{x}_\phi = [r_\phi \sin\theta\cos\phi - r\sin\theta\sin\phi, r_\phi\sin\theta\sin\phi + r\sin\theta\cos\phi, r_\phi\cos\theta], \tag{110}$$

$$\vec{x}_\theta = [r\cos\theta\cos\phi + r_\theta\sin\theta\cos\phi, r\cos(\theta)\sin(\phi) + r_\theta\sin(\theta)\sin(\phi), r_\theta\cos\theta - r\sin\theta]. \tag{111}$$

The components of the unit normal vector are given by

$$\begin{cases} U_x = R^{-1}\left[rr_\phi\sin\phi - rr_\theta\sin\theta\cos\theta\cos\phi + r^2\sin^2\theta\cos\phi\right], \\ U_y = R^{-1}\left[-rr_\phi\cos\phi - rr_\theta\sin\theta\cos\theta\sin\phi + r^2\sin^2\theta\sin\phi\right], \\ U_z = R^{-1}\left[rr_\theta\sin^2\theta + r^2\cos\theta\sin\theta\right]. \end{cases} \tag{112}$$

(Note that the subscripts in (112) represent coordinate components and not partial derivatives!) The coefficients (106), (107), and (108) can be expressed in terms of r through (110) and (111) and through differentiating (112). The derivatives of (112) are given in components by

$$\begin{cases} \dfrac{\partial U_x}{\partial\theta} = R^{-1}\big(-r_\theta^2\cos(\theta)\sin(\theta)\cos(\phi) + r_\theta r_\phi\sin(\phi) + 3r_\theta r\cos(\phi) - 4r_\theta r\cos(\phi)\cos^2(\theta) \\ \qquad\qquad -rr_{\theta\theta}\cos(\theta)\sin(\theta)\cos(\phi) + rr_{\theta\phi}\sin(\phi) + 2\cos(\theta)r^2\sin(\theta)\cos(\phi)\big), \\ \dfrac{\partial U_y}{\partial\theta} = R^{-1}\big(-r_\theta^2\cos(\theta)\sin(\theta)\sin(\phi) - r_\theta r_\phi\cos(\phi) + 3r_\theta r\sin(\phi) - 4r_\theta r\sin(\phi)\cos^2(\theta) \\ \qquad\qquad -rr_{\theta\theta}\cos(\theta)\sin(\theta)\sin(\phi) - rr_{\theta\phi}\cos(\phi) + 2\cos(\theta)r^2\sin(\theta)\sin(\phi)\big), \\ \dfrac{\partial U_z}{\partial\theta} = R^{-1}\left(4r_\theta r\sin(\theta)\cos(\theta) + 2r^2\cos^2(\theta) + r_\theta^2\sin^2(\theta) - rr_{\theta\theta}\sin^2(\theta) - r^2\right), \end{cases} \tag{113}$$

and

$$
\begin{cases}
\dfrac{\partial U_x}{\partial \phi} = R^{-1}\big(-r_\theta r_\phi \cos(\theta)\sin(\theta)\cos(\phi) + r_\phi^2 \sin(\phi) + 3 r r_\phi \cos(\phi) \\
\qquad - 2 r_\phi r \cos^2(\theta)\cos(\phi) - r r_{\theta\phi}\cos(\theta)\sin(\theta)\cos(\phi) + r_\theta r \cos(\theta)\sin(\theta)\sin(\phi) \\
\qquad + r r_{\phi\phi}\sin(\phi) - r^2 \sin(\phi)\sin^2(\theta)\big)\,, \\
\dfrac{\partial U_y}{\partial \phi} = R^{-1}\big(-r_\theta r_\phi \cos(\theta)\sin(\theta)\sin(\phi) - r_\phi^2 \cos(\phi) + 3 r r_\phi \sin(\phi) \\
\qquad - 2 r_\phi r \cos^2(\theta)\sin(\phi) - r r_{\theta\phi}\cos(\theta)\sin(\theta)\sin(\phi) - r_\theta r \cos(\theta)\sin(\theta)\cos(\phi) \\
\qquad - r r_{\phi\phi}\cos(\phi) + r^2 \cos(\phi)\sin^2(\theta)\big)\,, \\
\dfrac{\partial U_z}{\partial \phi} = R^{-1}\big(r_\theta r_\phi \sin^2(\theta) + 2 r_\phi r \sin(\theta)\cos(\theta) + r r_{\theta\phi}\sin^2(\theta)\big)\,.
\end{cases}
\tag{114}
$$

Remarkably, despite the complexity of the normal derivatives in (113) and (114), the expressions simplify nicely to

$$L = R^{-1}(-2 r r_\theta^2 \sin(\theta) + r^2 r_{\theta\theta}\sin(\theta) - r^3 \sin(\theta)), \tag{115}$$

$$M = R^{-1}(2 r r_\phi r_\theta \sin(\theta) - r^2 r_{\theta\phi}\sin(\theta) + r^2 r_\phi \cos(\theta)), \tag{116}$$

$$N = R^{-1}(-r^3 \sin^3(\theta) + r^2 r_{\phi\phi}\sin(\theta) + r^2 r_\theta \cos(\theta)\sin^2(\theta) - 2 r r_\phi^2 \sin(\theta)). \tag{117}$$

3.6.3. Surface area, volume, and mean curvature. We can now easily obtain a formula for the differential surface area element (61) using (103), (104), and (105):

$$
\begin{aligned}
dS &= \sqrt{EG - F^2}\; d\theta\, d\phi \\
&= \sqrt{(r_\theta^2 + r^2)(r_\phi^2 + r^2\sin^2(\theta) - r_\theta r_\phi^2}\; d\theta\, d\phi \\
&= r[r_\phi^2 + r_\theta^2 \sin^2(\theta) + r^2 \sin^2(\theta)]^{1/2}\; d\theta\, d\phi.
\end{aligned}
\tag{118}
$$

From this, the surface area of Γ is

$$S_A = \int_0^{2\pi}\int_0^{\pi} r[r_\phi^2 + r_\theta^2 \sin^2(\theta) + r^2 \sin^2(\theta)]^{1/2} d\theta d\phi.$$

For simplicity in later calculations, we define the determinant of the covariant metric tensor as in (63) to be

$$\omega = r[r_\phi^2 + r_\theta^2 \sin^2(\theta) + r^2 \sin^2(\theta)]^{1/2}, \tag{119}$$

so that $dS = \omega \, d\theta d\phi$, and

$$S_A = \int_0^{2\pi} \int_0^{\pi} \omega \; d\theta d\phi. \tag{120}$$

The volume enclosed by the membrane is given by

$$V = \int_0^{2\pi} \int_0^{\pi} \int_0^{r(\theta,\phi)} dV = \int_0^{2\pi} \int_0^{\pi} \int_0^{r(\theta,\phi)} \rho^2 \sin(\theta) \; d\rho \; d\theta \; d\phi,$$

which can be evaluated in its first integral to obtain

$$V = \frac{1}{3} \int_0^{2\pi} \int_0^{\pi} r^3 \sin(\theta) \; d\theta \; d\phi. \tag{121}$$

Next, we obtain the local mean curvature and the Gaussian curvature from (67). In terms of r,

$$\begin{aligned} H(\theta,\phi) = \frac{1}{2} R^{-1} \big[& 3r_\theta^2 r^2 \sin^3(\theta) - r_\theta^2 r r_{\phi\phi} \sin(\theta) - r_\theta^3 r \cos(\theta) \sin^2(\theta) + 8 r_\theta^2 r_\phi^2 \sin(\theta) \\ & + 2r^4 \sin^3(\theta) - r^3 r_{\phi\phi} \sin(\theta) - r^3 r_\theta \cos(\theta) \sin^2(\theta) + 3r^2 r_\phi^2 \sin(\theta) \\ & - r_\phi^2 r r_{\theta\theta} \sin(\theta) - r^3 r_{\theta\theta} \sin^3(\theta) - 2 r_\phi r_\theta r r_{\theta\phi} \sin(\theta) + 2 r_\phi^2 r_\theta r \cos(\theta) \big] \\ & / \left[-r^3 \sin^2(\theta) - r r_\theta^2 \sin^2(\theta) - r r_\phi^2 \right]. \end{aligned} \tag{122}$$

The Gaussian curvature is equally messy, but equally straightforward, so its computation is left out.

3.6.4. VARIATION OF THE DERIVATIVES OF $r(a_i; \theta, \phi)$. Now we need to compute the variations of the surface area, volume, and curvature. We will first need the variations of

$r(a_i;\theta,\phi)$ and all of its partial derivatives. The variation of r is given by

$$\frac{\delta r}{\delta a_i} = S_i. \tag{123}$$

From (96) and (97), we obtain

$$\frac{\delta r_\phi}{\delta a_i} = -mS_n^{-m}, \tag{124}$$

$$\frac{\delta r_{\phi\phi}}{\delta a_i} = -m^2\frac{\delta S}{\delta a_i}. \tag{125}$$

The variations of r_θ, $r_{\theta\theta}$, and $r_{\theta\phi}$ are

$$\frac{\delta r_\theta}{\delta a_i} = \begin{cases} \dfrac{\delta r_\theta}{\delta A_n^m} = \cos(m\phi) f_n^m \partial_\theta P_n^m(\mu), & m \geq 0, \\ \dfrac{\delta r_\theta}{\delta B_n^m} = \sin(|m|\phi) f_n^{|m|} \partial_\theta P_n^{|m|}(\mu), & m < 0, \end{cases} \tag{126}$$

$$\frac{\delta r_{\theta\theta}}{\delta a_i} = \begin{cases} \dfrac{\delta r_{\theta\theta}}{\delta A_n^m} = \cos(m\phi) f_n^m \partial_\theta^2 P_n^m(\mu), & m \geq 0, \\ \dfrac{\delta r_{\theta\theta}}{\delta B_n^m} = \sin(|m|\phi) f_n^{|m|} \partial_\theta^2 P_n^{|m|}(\mu), & m < 0, \end{cases} \tag{127}$$

$$\frac{\delta r_{\theta\phi}}{\delta a_i} = \begin{cases} \dfrac{\delta r_{\theta\phi}}{\delta A_n^m} = \dfrac{\delta r_{\phi\theta}}{\delta A_n^m} = -m\sin(m\phi) f_n^m \partial_\theta P_n^m(\mu), & m \geq 0, \\ \dfrac{\delta r_{\theta\phi}}{\delta B_n^m} = \dfrac{\delta r_{\phi\theta}}{\delta B_n^m} = -m\cos(|m|\phi) f_n^{|m|} \partial_\theta P_n^{|m|}(\mu), & m < 0. \end{cases} \tag{128}$$

3.6.5. Variation of the fundamental form coefficients. Now we compute the variation of the coefficients of the first and second fundamental forms. The first set are seen directly from the variations of r and its derivatives,

$$\frac{\delta E}{\delta a_i} = 2r_\theta \frac{\delta r_\theta}{\delta a_i} + 2r\frac{\delta r}{\delta a_i}, \tag{129}$$

$$\frac{\delta F}{\delta a_i} = r_\theta \frac{\delta r_\phi}{\delta a_i} + \frac{\delta r_\theta}{\delta a_i} r_\phi, \tag{130}$$

$$\frac{\delta G}{\delta a_i} = 2r_\phi \frac{\delta r_\phi}{\delta a_i} + 2r\frac{\delta r}{\delta a_i}\sin^2(\theta). \tag{131}$$

Next we compute the variations of L, M, and N. To perform these calculations, we will need the variation of R as defined in (109). Since R is defined in terms of a norm, we first compute the derivative of a norm in general.

$$\begin{aligned}\frac{d|\vec{f}|}{d\vec{x}} &= \frac{d}{d\vec{x}}\sqrt{f_i^2 + f_j^2 + f_k^2}\\ &= \frac{1}{2}\left(f_i^2 + f_j^2 + f_k^2\right)^{-1/2}\left(2f_i\frac{df_i}{d\vec{x}} + 2f_j\frac{df_j}{d\vec{x}} + 2f_k\frac{df_k}{d\vec{x}}\right)\\ &= \frac{1}{|\vec{f}|}\left(\vec{f}\cdot\frac{d\vec{f}}{d\vec{x}}\right).\end{aligned}$$

Using this result and the derivative of a cross product,

$$\begin{aligned}\frac{\delta R}{\delta a_i} &= \frac{\delta}{\delta a_i}|\vec{x}_\theta \times \vec{x}_\phi|\\ &= \frac{1}{|\vec{x}_\theta \times \vec{x}_\phi|}\left(\vec{x}_\theta \times \vec{x}_\phi\right)\cdot\frac{\delta}{\delta a_i}\left(\vec{x}_\theta \times \vec{x}_\phi\right)\\ &= \frac{1}{R}\left(\vec{x}_\theta \times \vec{x}_\phi\right)\cdot\left(\frac{\delta \vec{x}_\theta}{\delta a_i}\times\vec{x}_\phi + \vec{x}_\theta \times \frac{\delta \vec{x}_\phi}{\delta a_i}\right).\end{aligned} \tag{132}$$

If one prefers, we may write (132) in terms of dot products using the Cauchy-Binet identity, which states that $(\vec{a}\times\vec{b})\cdot(\vec{c}\times\vec{d}) = (\vec{a}\cdot\vec{c})(\vec{b}\cdot\vec{d}) - (\vec{a}\cdot\vec{d})(\vec{b}\cdot\vec{c})$. Applying this, (132) becomes

$$\begin{aligned}\frac{\delta R}{\delta a_i} = \frac{1}{R}\Bigg(&\left(\vec{x}_\theta\cdot\frac{\delta\vec{x}_\theta}{\delta a_i}\right)(\vec{x}_\phi\cdot\vec{x}_\phi) - (\vec{x}_\theta\cdot\vec{x}_\phi)\left(\vec{x}_\phi\cdot\frac{\delta\vec{x}_\theta}{\delta a_i}\right)\\ &+ (\vec{x}_\theta\cdot\vec{x}_\theta)\left(\vec{x}_\phi\cdot\frac{\delta\vec{x}_\phi}{\delta a_i}\right) - \left(\vec{x}_\theta\cdot\frac{\delta\vec{x}_\phi}{\delta a_i}\right)(\vec{x}_\phi\cdot\vec{x}_\theta)\Bigg).\end{aligned} \tag{133}$$

The variations of $\vec{x}_\phi$ and $\vec{x}_\theta$ are computed directly from (110) and (111).

$$\frac{\delta x_\phi}{\delta a_i} = \left[\frac{\delta r_\phi}{\delta a_i}\sin\theta\cos\phi - \frac{\delta r}{\delta a_i}\sin\theta\sin\phi, \frac{\delta r_\phi}{\delta a_i}\sin\theta\sin\phi + \frac{\delta r}{\delta a_i}\sin\theta\cos\phi, \frac{\delta r_\phi}{\delta a_i}\cos\theta\right]. \tag{134}$$

$$\begin{aligned}\frac{\delta x_\theta}{\delta a_i} = \Bigg[&\frac{\delta r}{\delta a_i}\cos\theta\cos\phi + \frac{\delta r_\theta}{\delta a_i}\sin\theta\cos\phi, \frac{\delta r}{\delta a_i}\cos(\theta)\sin(\phi) + \frac{\delta r_\theta}{\delta a_i}\sin(\theta)\sin(\phi),\\ &\frac{\delta r_\theta}{\delta a_i}\cos\theta - \frac{\delta r}{\delta a_i}\sin\theta\Bigg].\end{aligned} \tag{135}$$

Finally, we compute the variations of L, M, and N. From (115),

$$\begin{aligned}\frac{\delta L}{\delta a_i} &= \frac{-1}{R^2}\frac{\delta R}{\delta a_i}\left(-2rr_\theta^2\sin(\theta) + r^2 r_{\theta\theta}\sin(\theta) - r^3\sin(\theta)\right)\\ &\quad + \frac{1}{R}\Big(- 2\frac{\delta r}{\delta a_i}r_\theta^2\sin(\theta) - 4rr_\theta\frac{\delta r_\theta}{\delta a_i}\sin(\theta)\\ &\quad + 2r\frac{\delta r}{\delta a_i}r_{\theta\theta}\sin(\theta) + r^2\frac{\delta r_{\theta\theta}}{\delta a_i}\sin(\theta) - 3r^2\frac{\delta r}{\delta a_i}\sin(\theta)\Big).\end{aligned}$$

Notice that the first line contains a term of L and we obtain a simplified expression

$$\frac{\delta L}{\delta a_i} = \frac{-1}{R}\frac{\delta R}{\delta a_i}L + \frac{1}{R}\sin(\theta)\Big(- 2\frac{\delta r}{\delta a_i}r_\theta^2 - 4rr_\theta\frac{\delta r_\theta}{\delta a_i} + 2r\frac{\delta r}{\delta a_i}r_{\theta\theta} + r^2\frac{\delta r_{\theta\theta}}{\delta a_i} - 3r^2\frac{\delta r}{\delta a_i}\Big). \tag{136}$$

Similar simplifications can be done to obtain δM and δN. From (116) and (117),

$$\begin{aligned}\frac{\delta M}{\delta a_i} = \frac{-1}{R}\frac{\delta R}{\delta a_i}M + \frac{1}{R}\Bigg(&\sin(\theta)\Big(2\frac{\delta r}{\delta a_i}r_\phi r_\theta + 2r\frac{\delta r_\phi}{\delta a_i}r_\theta + 2rr_\phi\frac{\delta r_\theta}{\delta a_i}\\ &- 2r\frac{\delta r}{\delta a_i}r_{\theta\phi} - r^2\frac{\delta r_{\theta\phi}}{\delta a_i}\Big) + \cos(\theta)\Big(2r\frac{\delta r}{\delta a_i}r_\phi + r^2\frac{\delta r_\phi}{\delta a_i}\Big)\Bigg),\end{aligned} \tag{137}$$

$$\begin{aligned}\frac{\delta N}{\delta a_i} = \frac{-1}{R}\frac{\delta R}{\delta a_i}N + \frac{1}{R}\sin(\theta)\Bigg(& - 3r^2\frac{\delta r}{\delta a_i}\sin^2(\theta) + 2r\frac{\delta r}{\delta a_i}r_{\phi\phi} + r^2\frac{\delta r_{\phi\phi}}{\delta a_i}\\ &+ 2r\frac{\delta r}{\delta a_i}r_\theta\cos(\theta)\sin(\theta) + r^2\frac{\delta r_\theta}{\delta a_i}\cos(\theta)\sin(\theta) - 2\frac{\delta r}{\delta a_i}r_\phi^2 - 4rr_\phi\frac{\delta r_\phi}{\delta a_i}\Bigg).\end{aligned} \tag{138}$$

3.6.6. Variation of surface area, volume, and curvature. The variation of the surface area with respect to a surface harmonic mode a_i can be computed directly from (120) as

$$\delta S_A = \int_0^{2\pi} \int_0^{\pi} \frac{\delta \omega}{\delta a_i} \, d\theta \, d\phi, \tag{139}$$

where the variation of ω is computed from (119),

$$\begin{aligned} \frac{\delta \omega}{\delta a_i} &= \frac{\delta r}{\delta a_i} [r_\phi^2 + r_\theta^2 \sin^2(\theta) + r^2 \sin^2(\theta)]^{1/2} \\ &\quad + \frac{r}{2} \left(\frac{2 r_\phi \dfrac{\delta r_\phi}{\delta a_i} + 2 r_\theta \dfrac{\delta r_\theta}{\delta a_i} \sin^2(\theta) + 2r \dfrac{\delta r}{\delta a_i} \sin^2(\theta)}{\sqrt{r_\phi^2 + r_\theta^2 \sin^2(\theta) + r^2 \sin^2(\theta)}} \right). \end{aligned} \tag{140}$$

Similarly, the variation of the volume can be computed directly from (121),

$$\delta V = \int_0^{2\pi} \int_0^{\pi} r^2 \frac{\delta r}{\delta a_i} \sin(\theta) \, d\theta \, d\phi. \tag{141}$$

The expression for the mean curvature H is given by (122). There are many products and quotients of r in (122), so the variation δH will involve using the product and quotient rules multiple times. This direct computation is straightforward but exceedingly messy, and hence is not given here. Instead, and in practice, we compute the variation of the mean curvature H via (67) using the variations of the fundamental form coefficients. The variation is given by

$$\begin{aligned} \frac{\delta H}{\delta a_i} &= \frac{\dfrac{\delta E}{\delta a_i} N + E \dfrac{\delta N}{\delta a_i} + \dfrac{\delta G}{\delta a_i} L + G \dfrac{\delta L}{\delta a_i} - 2 \left(\dfrac{\delta F}{\delta a_i} M + F \dfrac{\delta M}{\delta a_i} \right)}{2(EG - F^2)} \\ &\quad - \frac{(EN + GL - 2FM) \left(2 \dfrac{\delta E}{\delta a_i} G + 2E \dfrac{\delta G}{\delta a_i} - 4F \dfrac{\delta F}{\delta a_i} \right)}{4(EG - F^2)^2}. \end{aligned} \tag{142}$$

3.6.7. Variation of mechanical energy. Finally, we are ready to numerically solve the shape equation. To do this, we assume that the Gaussian modulus $\mathscr{K}_G$ is uniform over the membrane surface, and so the Gaussian curvature integrates to a constant $\int_\Gamma K dS =$

$4\pi(1-g)$, where g is the genus of the membrane topology, according to the Gauss-Bonet Theorem [95]. Thus, the variation of the total mechanical energy with respect to a surface harmonic mode a_i is

$$\delta_\Gamma E[\Gamma(\vec{a});\theta,\phi] = \int_\Gamma \left[\mathscr{K}_C 2(2H - C_0)(\delta H)\,\omega + \mathscr{K}_C \frac{1}{2}(2H - C_0)^2(\delta\omega) \right] d\theta d\phi \\ + k_S(S_A - \bar{S})\delta S_A + k_V(V - \bar{V})\delta V. \tag{143}$$

With the surface Γ expressed in terms of the surface harmonic coefficients $\vec{a}$, the new shape equation is completed by setting (143) to zero.

CHAPTER 4

BIOMOLECULAR MECHANICS: NUMERICAL RESULTS

In this chapter, we numerically solve the variational problem (76) parameterized by surface harmonics and present results. We emphasize that this algorithm for solving the equilibrium shapes of vesicle membranes is fast, due to the reduced number of degrees of freedom compared to other methods, and the choice of nonlinear conjugate gradient method, which requires only the first derivative (no computation of the Hessian matrix is required).

4.1. NONLINEAR CONJUGATE GRADIENT (NCG)

We employ a Fletcher-Reeves type nonlinear conjugate gradient (NCG) method to minimize the total energy functional (76). For the parameter β, we chose the Hestenes-Stiefel formula. For a description of the method, please refer to [78]. Psuedocode is provided below. We found that $K = 14$ in line 18 of Algorithm 4.1 and $\alpha_m = 0$ and $\alpha_M = 0.15$ on line 1 of Algorithm 4.2 provide optimal results.

Algorithm 4.1 Nonlinear conjugate gradient (NCG)

```
Define initial SHF modes $\vec{a}_0$
Define tolerances $\epsilon_g, \epsilon_a$, $\epsilon_E$, $M$
Compute $E_0 \leftarrow I(\vec{a}_0)$, $\vec{g}_0 \leftarrow \delta_\Gamma I(\vec{a}_0)$
Define direction $\vec{d}_0 \leftarrow -\vec{g}_0$
$k \leftarrow 0$
for $k$ from 1 to $M$ do:
    Compute step size $\alpha_k \leftarrow \mathit{LineSearch}(\vec{a}_k, \vec{d}_k)$
    Step in direction $\vec{a}_{k+1} \leftarrow \vec{a}_k + \alpha_k \vec{d}_k$
    Update energy and gradient $E_{k+1} \leftarrow I(\vec{a}_{k+1})$, $\vec{g}_{k+1} \leftarrow \delta_\Gamma I(\vec{a}_{k+1})$
    if $||\vec{g}_{k+1} - \vec{g}_k|| < \epsilon_g$ then:
        break for
    end if
    Compute $\beta_k \leftarrow (\vec{g}_{k+1}^T(\vec{g}_{k+1} - \vec{g}_k))/((\vec{g}_{k+1} - \vec{g}_k)^T \vec{d}_k)$
    Update direction $\vec{d}_{k+1} \leftarrow -\vec{g}_{k+1} + \beta_k \vec{d}_k$
    if $||\vec{a}_{k+1} - \vec{a}_k|| < \epsilon_a$ then:
        break for
    end if
    if $|E_{k+1} - E_k|/E_{k+1} < \epsilon_E$ and $k > K$ then
        break for
    end if
    $k \leftarrow k + 1$
end for
return $\vec{a}_k$
```

Algorithm 4.2 Line Search $(\vec{a}, \vec{d})$

```
Define $\alpha_m, \alpha_M, M, \epsilon$
Compute $E_m \leftarrow I(\vec{a} + \alpha_m \cdot \vec{d})$, $E_M \leftarrow I(\vec{a} + \alpha_M \cdot \vec{d})$
if $E_m < E_M$ then:
    $\alpha_l \leftarrow \alpha_m$; $\alpha_u \leftarrow \alpha_M$
    $E_l \leftarrow E_m$; $E_u \leftarrow E_M$
else
    $\alpha_l \leftarrow \alpha_M$; $\alpha_u \leftarrow \alpha_m$
    $E_l \leftarrow E_M$; $E_u \leftarrow E_m$
end if
for $i$ from 1 to $M$ do:
    $\alpha_t \leftarrow (\alpha_l + \alpha_u)/2$
    $E_t \leftarrow I(\vec{a} + \alpha_t \cdot \vec{d})$
    if $E_t > E_l$ then:
        $\alpha_u \leftarrow \alpha_t$
    else
        $\vec{g} \leftarrow \delta_\Gamma I(\vec{a} + \alpha_t \cdot \vec{d})$
        $(D\phi) \leftarrow \vec{g}^T \vec{d}$
        if $(D\phi) \cdot (\alpha_l - \alpha_t) > 0$ then:
            $\alpha_l \leftarrow \alpha_t$
        else
            $\alpha_u \leftarrow \alpha_l$; $\alpha_l \leftarrow \alpha_t$
        end if
        $E_l \leftarrow E_t$
    end if
    if $|\alpha_u - \alpha_l| < \epsilon$ then
        break for
    end if
end for
return $\alpha_t$
```

4.2. EXPANSION MODES AND QUADRATURE

Numerically, the surface is approximated by truncating the surface harmonic expansion at some appropriate value N, as in equation (93). The uniform convergence properties of spherical harmonics are shared by surface harmonics, and so we expect the result to become more accurate as N gets large. Too large of a value will result in a slow numerical procedure, so we want to choose N small enough for computation time, but large enough for accuracy.

To determine an appropriate truncation value N, we reconstructed three surfaces and examined the root mean square error in the surface reconstruction pointwise, and the relative error in the volume, surface area, and energy. For many vesicle structures, increasing N achieves higher accuracy in the energy as well as in the pointwise error. However, for some vesicle structures, increasing N transiently actually gives a worse approximation *for the energy*, which is the problem of interest. Choosing N is not quite as simple as it looks.

The first surface we reconstructed was an energy minimizing axisymmetric prolate from Seifert et. al., [91]. Instructions for reconstructing this surface can be found in Appendix B of [91], with choice of parameters $\bar{P} = 0.1$, $\bar{\Sigma} = -1.1\bar{P}^{2/3}$, $C_0 = 0$, and $U(0) = 0.56$. Next, we reconstructed statistically fitted parameterizations of a red blood cell (RBC) from [32]. The height of the profile of the surface is given by

$$h(x) = \frac{\pm 0.5}{R_0}(1 - x^2)(C_0 + C_2x^2 + C_4x^4) \qquad x \in [-1, 1]. \tag{144}$$

Table 4 in [32] includes values for R_0, C_0, C_2, and C_4 for producing RBC shapes with tonicities 300 and 217 mO. The values are reproduced here in Table 4.1. We chose two linear combinations of the parameters given for averaged shapes from the ones in [32]. The profiles

Table 4.1: Shape coefficients for average RBC

Tonicity (mO)	R_0 (μm)	C_0 (μm)	C_2 (μm)	C_4 (μm)
300	3.91	0.81	7.83	-4.39
217	3.80	2.10	7.58	-5.59

for the three sample surfaces and their reconstructed surfaces with $N = 4$ are included in Figure 4.1.

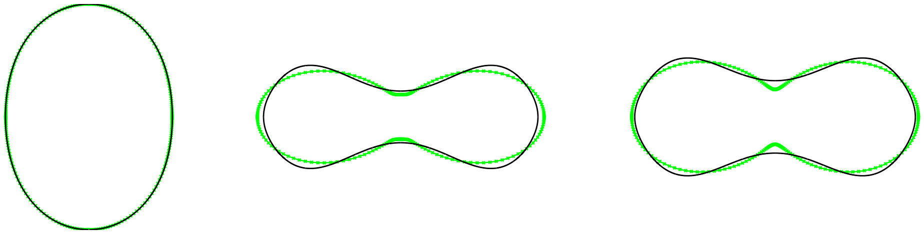

Figure 4.1: Profile of various test surfaces (black) and their reconstructions using surface harmonics with $N = 4$ (green). The full surfaces are generated by rotation about the y-axis. Left: prolate from [91], middle and right: RBC from [32] with 50% and 90% weight on tonicity 217 mO coefficients, respectively.

The coefficients of the surface harmonic parameterizations of these three surfaces are computed using the formula

$$a_n^m = \int_0^{2\pi} \int_0^{\pi} r(\theta, \phi) S_n^m(\theta, \phi)\, d\theta\, d\phi. \tag{145}$$

For the reconstruction, the integration was computed numerically over 230 cubature points. Using the coefficients from (145), the reconstructed radius $\tilde{r}$ was determined by (93). The root mean square distance error in the reconstruction is defined over the cubature points by

$$E_{rmsd} = \sum_{i=1}^{230} \frac{1}{230} [r(\theta_i, \phi_i) - \tilde{r}(\theta_i, \phi_i)]^2.$$

The pointwise error and the relative error in the volume, surface area, and energy are provided in Tables 4.2-4.4 for various N.

For the prolate surface, the reconstruction accuracy increases in all categories as N increases. The most relevant observation to this work is that the error in the energy is less than 1% using $N = 2$ and greater. For a simple prolate structure, only $(N + 1)^2 = 9$ modes are necessary to achieve 99% accuracy.

For the RBC structures, initially the errors decrease as N increases, but increasing the number of modes beyond a certain threshold actually increases the error in the energy computation. For RBC 1, the best possible error in the energy is 5.34%, with $N = 4$ or $N = 5$

Table 4.2: Error from truncation in surface harmonic expansion for prolate sample surface.

N	E_{rms}	E_{Vol}	E_{SA}	E_{Eng}
1	2.06×10^{-1}	2.57×10^{-2}	2.22×10^{-2}	3.73×10^{-2}
2	8.59×10^{-4}	2.22×10^{-4}	1.08×10^{-2}	8.37×10^{-3}
3	8.59×10^{-4}	2.22×10^{-4}	1.08×10^{-2}	8.37×10^{-3}
4	5.02×10^{-7}	2.56×10^{-6}	1.11×10^{-2}	7.19×10^{-3}
5	5.06×10^{-7}	2.56×10^{-6}	1.11×10^{-2}	7.19×10^{-3}
6	1.46×10^{-7}	2.76×10^{-6}	1.11×10^{-2}	7.18×10^{-3}
7	1.53×10^{-7}	2.76×10^{-6}	1.11×10^{-2}	7.18×10^{-3}
8	3.35×10^{-8}	2.76×10^{-6}	1.11×10^{-2}	7.18×10^{-3}

Table 4.3: Error from truncation in surface harmonic expansion for RBC 1 (50% weight) sample surface.

N	E_{rms}	E_{Vol}	E_{SA}	E_{Eng}
1	9.80×10^{-2}	4.00×10^{-1}	4.20×10^{-1}	4.21×10^{-1}
2	6.65×10^{-3}	4.80×10^{-2}	4.99×10^{-2}	8.36×10^{-1}
3	6.65×10^{-3}	4.80×10^{-2}	4.99×10^{-2}	8.36×10^{-1}
4	2.29×10^{-3}	1.93×10^{-3}	1.72×10^{-2}	5.34×10^{-2}
5	2.29×10^{-3}	1.93×10^{-3}	1.72×10^{-2}	5.34×10^{-2}
6	1.39×10^{-3}	4.94×10^{-3}	8.35×10^{-3}	1.62
7	1.39×10^{-3}	4.94×10^{-3}	8.35×10^{-3}	1.62
8	4.13×10^{-4}	3.29×10^{-5}	1.44×10^{-2}	7.97×10^{-1}

Table 4.4: Error from truncation in surface harmonic expansion for RBC 2 (90% weight) sample surface.

N	E_{rms}	E_{Vol}	E_{SA}	E_{Eng}
1	7.13×10^{-2}	2.82×10^{-1}	3.12×10^{-1}	3.82×10^{-1}
2	2.06×10^{-3}	1.35×10^{-2}	9.60×10^{-3}	3.96×10^{-1}
3	2.06×10^{-3}	1.35×10^{-2}	9.60×10^{-3}	3.96×10^{-1}
4	1.26×10^{-3}	3.36×10^{-3}	5.71×10^{-3}	7.75×10^{-2}
5	1.26×10^{-3}	3.36×10^{-3}	5.71×10^{-3}	7.75×10^{-2}
6	3.07×10^{-4}	1.92×10^{-3}	5.79×10^{-3}	4.24×10^{-1}
7	3.07×10^{-4}	1.92×10^{-3}	5.79×10^{-3}	4.24×10^{-1}
8	2.15×10^{-4}	1.21×10^{-3}	7.14×10^{-3}	9.97×10^{-2}

modes. For RBC 2, the best error is 7.75% with the same N. We suggest the reason for this is because higher modes contain more bulges than the lower modes, akin to Runge's phenomenon in high order polynomials. In the reconstruction, the coefficients are chosen to minimize E_{rms}. While transiently increasing N does improve the accuracy of E_{rms}, it may introduce local oscillations, near $\theta = 0$ (which presents a singularity in (140) when $r_\phi = 0$, for example). Since the energy is a function of the square mean curvature, these oscillations contribute significantly to the curvature energy. In Figure 4.2, RBC 1 is reconstructed with $N = 4$ and $N = 12$, for comparison.

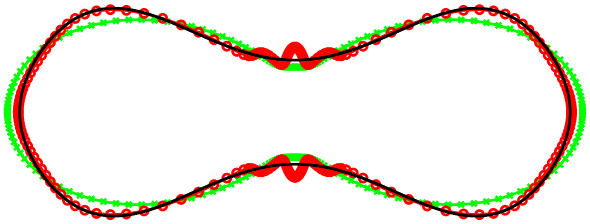

Figure 4.2: Effect of large N for RBC 1. The analytical surface is in black, the reconstructed surfaces for $N = 4$ and $N = 12$ are in green and red, respectively. Increasing N from 4 improves the pointwise accuracy especially near the edges, but also introduces small oscillations near the center with high energy cost. For $N = 12$, the pointwise error in the surface is improved at 1.18×10^{-4}, but the error in the energy is 258%.

4.3. EXAMPLES: REDUCED VOLUME

In this section, we provide numerical examples to test our method. First, observe that the integration of the square local mean curvature $(2H - C_0)^2$ is a dimensionless quantity. The mechanical bending energy (76) is completely governed by this dimensionless quantity and is therefore scale-invariant. Thus, for vesicle shapes with $C_0 = 0$, the minimum energy is completely determined by a single dimensionless quantity called the reduced volume v. If we denote the current vesicle volume and surface area V and S_A, respectively, then the reduced volume scales the current volume V by the volume of a sphere with surface area S_A. Since spheres maximize volume for a given surface area, the reduced volume satisfies $v \leq 1$. The reduced volume is given by the formula

$$v = \frac{V}{4\pi/3R_0^3}, \tag{146}$$

where $R_0 = \sqrt{S_A/4\pi}$. In terms of the surface area, the reduced volume is

$$v = \frac{6\sqrt{\pi}V}{(S_A)^{3/2}}. \tag{147}$$

Seifert et. al. have compiled a library of reduced volumes and their corresponding minimum energies for axisymmetric shapes in [91] by solving the Euler-Lagrange equations using a parameterization of the vesicle shape with an axis of symmetry. For verification purposes, we compare our axisymmetric results for various reduced volumes to theirs. We set the constraint volume $\bar{V}$ to be proportional to V by the (projected) reduced volume v. The volume constraint is in violation and NCG begins to change the shape to relax this configuration. If we begin with a perfectly spherical vesicle, NCG will simply scale the sphere to a sphere with a smaller volume, and the final reduced volume will be 1. Therefore, we take a slightly perturbed sphere to be our initial configuration. After NCG has converged, we calculate the final reduced volume v and the final energy E scaled by the energy of a spherical vesicle $E_0 = 8\pi\mathscr{K}_C$.

From the reconstruction examples, $N = 4$ is a reasonable truncation for the surface harmonic expansion. During the iterations of NCG, 20 quadrature points are used in each dimension, for a total of 400 points. We have three criteria for convergence. We say that NCG converges if (i) the L_2 norm of the change in gradient is less than $\epsilon_g = 10^{-10}$, (ii) the change in the modes is less than $\epsilon_a = 10^{-6}$, or (iii) the relative change in the energy is less than $\epsilon_E = 10^{-4}$ provided a minimum number of iterations is reached ($K = 15$). When the final configuration is achieved, the total energy is evaluated with 64 quadrature points in each dimension to provide a more accurate computation and to ensure that enough quadrature points are used.

4.3.1. OBLATES. We present examples for the case when $C_0 = 0$. In the line search (Algorithm 4.2), we chose $\alpha_m = 0$ to ensure that the step size is positive. If the step is negative, then the algorithm may step in a direction toward the gradient, rather than away from the gradient (recall the gradient direction is the direction of greatest *increase*). With this choice, our algorithm gives strictly oblate shapes. An oblate is a spheroid where the polar axis is shorter than the equatorial diameter. A familiar oblate spheroid is a football. A prolate is a spheroid where the polar axis is greater than the equatorial diameter. The two shapes are contrasted in Figure 4.3.

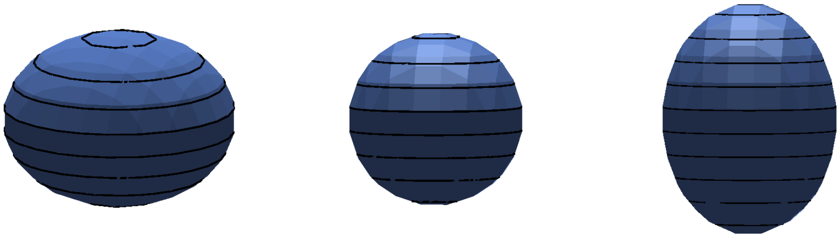

Figure 4.3: Oblate (left), sphere (middle), and prolate (right) shapes.

RBCs are biological examples of oblates which exhibit zero spontaneous curvature, and thus serve as great model verification. For reduced volumes above approximately $v = 0.75$, the numerical energy is within 10% of the analytical values calculated by Seifert et. al. (see Table 4.5). However, for reduced volumes less than this, the error exceeds 10%. If the number of modes is increased to $N = 6$ (since $N = 5$ gives the same numerical results as $N = 4$ as demonstrated in Tables 4.2-4.4), the relative error is reduced. However, there is a significant difference between the energy evaluated at 20 quadrature points than at 64 quadrature points at the final iteration. This is because the added oscillation from the higher order modes is not absorbed by NCG with only 20 quadrature points. Using 30 quadrature points when $N = 6$, the relative error is less than 1% when compared to 64 points. For surfaces with reduced volume $0.65 \leq v \leq 0.75$, using $N = 6$ and 30 quadrature points per dimension, the relative error in the final energy is less than 10%. For surfaces with reduced volume $0.5 \leq v < 0.65$, we determined that 40 quadrature points are needed with $N = 8$; however, the error is still above 10%, and the use of $N = 8$ fared no better than $N = 6$. Our method could not reconstruct surfaces with these reduced volumes well. These data are plotted in Figure 4.4, overlayed by the analytic solution from Seifert [91].

In summary, for surfaces with $0.75 \leq v \leq 1$, we used $N = 4$ and 20 quadrature points in each dimension, for surfaces with $0.65 \leq v < 0.75$, we used $N = 6$ and 30 quadrature points

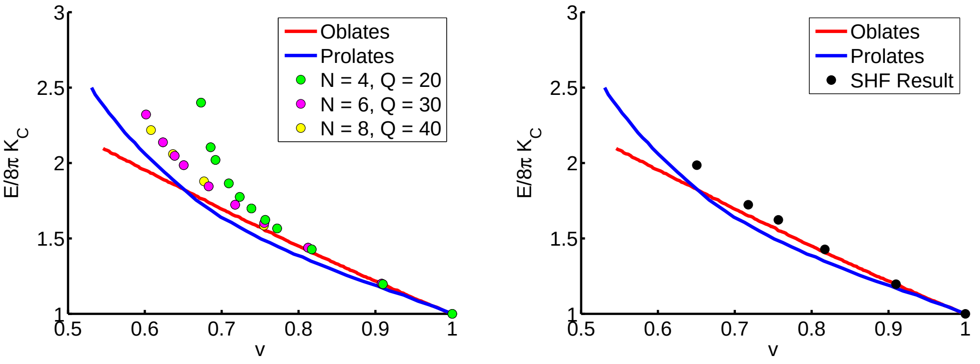

Figure 4.4: Vesicle energy vs. reduced volume for oblate vesicles in comparison with [91]. Left: All data points used to determine cutoff values for N given a reduced volume v. Right: Kept data according to the cutoff values. All data points are within 10% error of the appropriate analytical curve.

in each dimension. The results using this cutoff are overlayed by Seifert's data in Figure 4.4. Finally, the surfaces corresponding to the data in Table 4.5 are shown in Figure 4.5.

Table 4.5: Oblate vesicle energy vs. reduced volume.

v	1.0	0.91	0.82	0.75	0.72	0.65
E/E_0, [91]	1.0	1.19	1.43	1.62	1.72	1.98
E/E_0, SHF	1.0	1.19	1.41	1.56	1.65	1.83
Rel. error	0.00%	0.14%	1.60%	4.24%	4.41%	8.79%
Iterations	1	48	30	40	46	64

Figure 4.6 shows an actual RBC photographed with a scanning electron microscope in comparison to the model energy minimizing shape.

We note that the results of the numerical procedure may be only local minima and therefore only locally stable. With enough perturbation through some external force, another configuration with a lower energy may be achieved. In the range of $0.64 \leq v \leq 1$, oblate shapes are local energy minimizers, but prolates are global minimizers for axisymmetric shapes. However, it may be possible to obtain a non-axisymmetric shape with lower energy than a prolate.

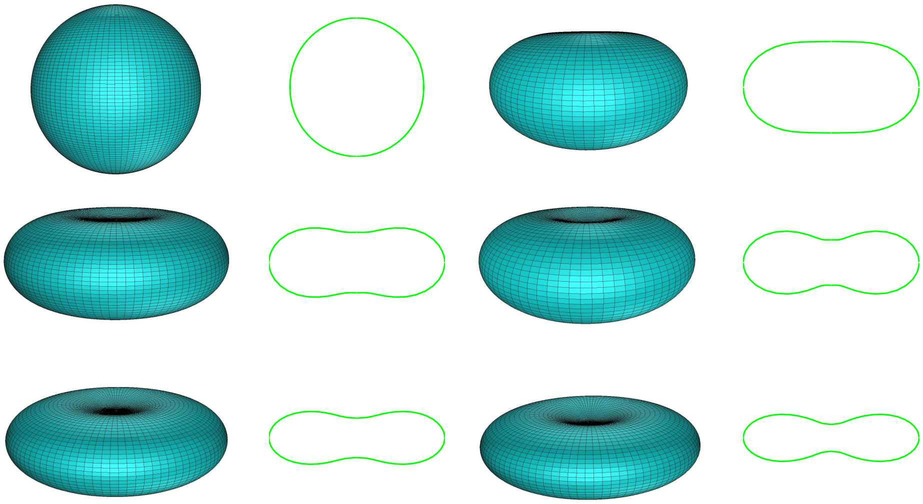

Figure 4.5: Oblate vesicles with various reduced volumes. Organized by row, $v = 1.00, 0.90; 0.81, 0.76; 0.70, 0.65$. The shapes here correspond to the data in Table 4.5. The full volumes are angled slightly down, while the profiles are not angled.

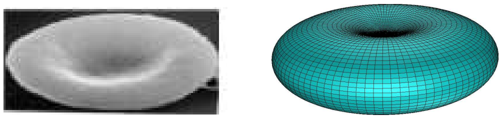

Figure 4.6: Real RBC (left) compared to model RBC (right).

4.3.2. Prolates. Our model is capable of producing prolate shapes as well (see Figure 4.3 (c)). Interestingly, this is accomplished by allowing the step size α_m to be negative. This means that the algorithm can step in a direction that increases the energy. We offer the following explanation: since the algorithm produces local extrema, it may be possible to obtain a different local extrema, but a transient increase of energy is required to overcome the energy barriers. Furthermore, in the regime $0.58 \leq v \leq 1$, prolate shapes are better minimizers of the energy than oblate shapes. Table 4.6 shows the results for prolate shapes with similar reduced volumes as obtained in the algorithm for oblate shapes. Sometimes, more iterations are required to produce these shapes. If the algorithm is moving in the direction of an increase in energy to overcome an energy barrier, this makes sense. The shapes corresponding to the data in Table 4.6 are shown in Figure 4.7. The reduced volume vs. energy plot is shown in Figure 4.8.

Table 4.6: Prolate vesicle energy vs. reduced volume.

v	1.0	0.90	0.79	0.76	0.71	0.65
E/E_0, [91]	1.0	1.20	1.40	1.49	1.61	1.81
E/E_0, SHF	1.0	1.20	1.42	1.52	1.63	1.91
Rel. error	0.00%	0.20%	1.40%	2.46%	1.49%	5.42%
Iterations	1	56	44	60	124	168

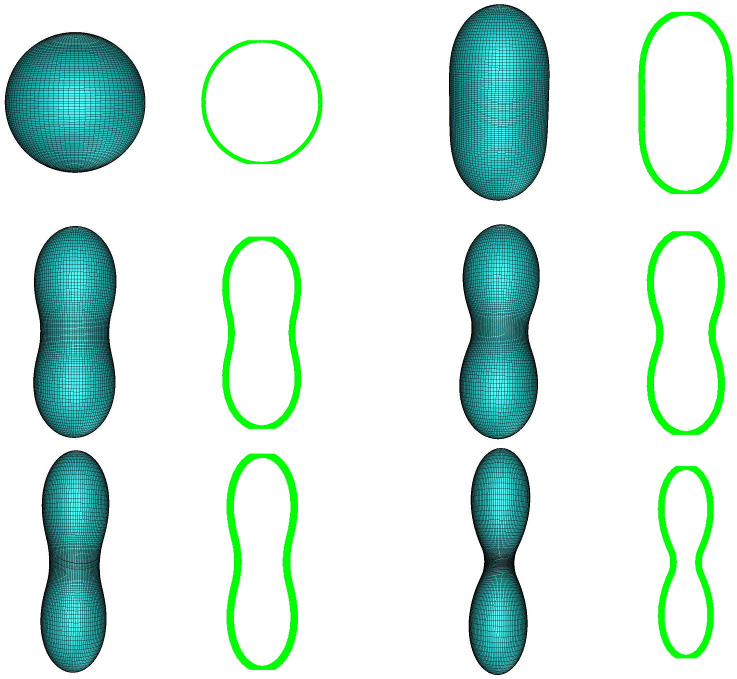

Figure 4.7: Prolate vesicles with various reduced volumes. Organized by row, $v = 1.00, 0.90; 0.79, 0.76; 0.71, 0.65$. The shapes here correspond to the data in Table 4.6.

In summary, our model is able to reproduce both prolate and oblate shapes. The data from Tables 4.5 and 4.6 (also Figures 4.5 and 4.7) are combined in Figure 4.9.

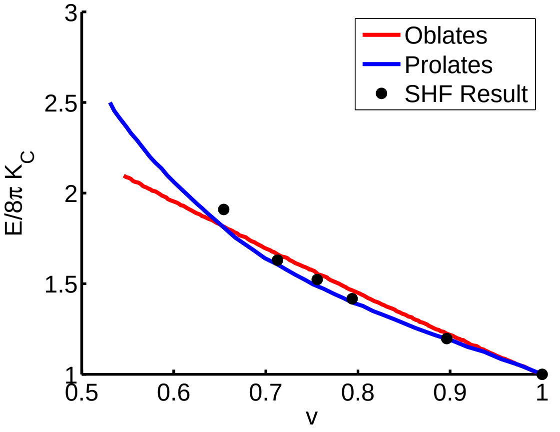

Figure 4.8: Vesicle energy vs. reduced volume for prolate vesicles in comparison with [91]. The SHF results correspond to the data in Table 4.6.

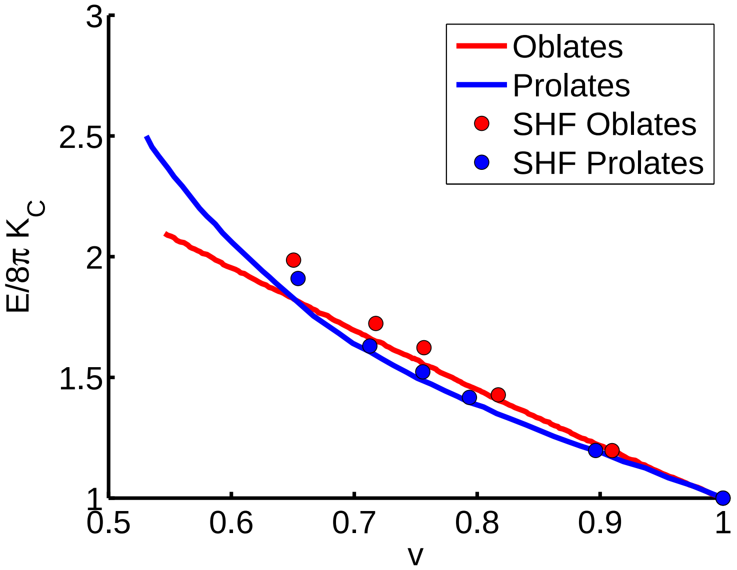

Figure 4.9: Vesicle energy vs. reduced volume for both oblate and prolate shaped in comparison with [91]. The SHF results correspond to the data in Tables 4.5 and 4.6 (also Figures 4.5 and 4.7).

CHAPTER 5

Biomolecular electrostatics

The classical theory of bilayer mechanics, introduced in Chapter 2 has been notably successful in modeling very large deformations of the membrane under external mechanical forces or constraints [37, 68]. We have further demonstrated the success of this model with the results in Chapter 4 [72]. In this chapter, we wish to introduce electrostatic interactions to the classical mechanical model. Consider a system with a vesicle and an external protein. The lipids on the vesicle membrane are charged, and the protein is also charged. Both the vesicle and the protein are placed in an ionic solvent. The mechanical energy given by equation (13) is on the same order of magnitude as the electrostatic potential energy, therefore the electrostatic interactions between the lipids, ions, and protein will play a significant role to the total energy of the system. Therefore, we wish to extend the mechanical model developed in Chapter 2 to an *electromechanical* model.

Suppose a protein and a lipid vesicle are placed in solvent. Denote the volume of the solvent by the open set $\Omega_s \subset \mathbb{R}^3$. This region appears outside of the protein and the vesicle as well as in the interior of the vesicle. The enclosed a volume of the vesicle is denoted $\Omega_m \subset \mathbb{R}^3$. The volume the protein occupies is denoted by the open set $\Omega_p \subset \mathbb{R}^3$. The entire containment region will be denoted by Ω. The interior boundary of the vesicle is called the *cytosolic face* and the exterior boundary is the *exoplasmic face*. Let the boundary of any domain be denoted $\Gamma \subset \mathbb{R}^2$ with appropriate subscripts, and let $\partial\Omega$ be the exterior boundary of Ω. Let n be the unit outward normal vector to any interface Γ. See Figure 5.1 for a picture of the domains.

In keeping with the theme of this thesis, we want to investigate the flow of the lipid membrane. As before, the flow is determined by the forces on the membrane, which includes the electrostatic force. To determine the electrostatic force, we need an expression for the electrostatic potential energy, which will be derived in this chapter. To compute the electrostatic potential energy in a continuum framework, dielectric permittivities are assigned

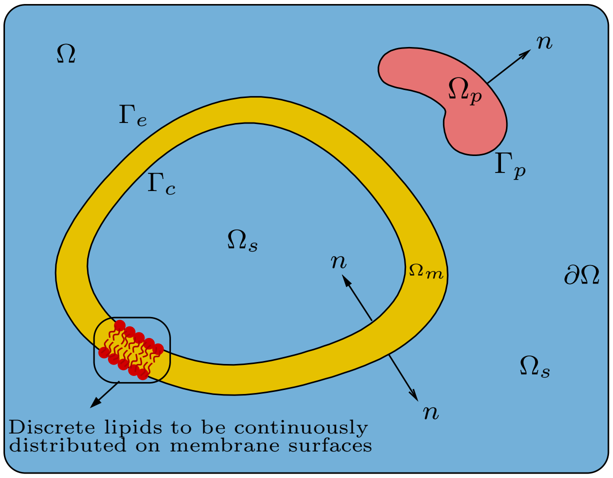

Figure 5.1: A mathematical description of the described solvation system. The volume of the membrane is Ω_m, contained by Γ_e and Γ_c representing the headgroups of each leaflet. The solvent both inside and outside of the vesicle is Ω_s. The protein is Ω_p with boundary Γ_p. The unit outward normal to any surface Γ is n.

to the interior of the membrane and the exterior, hence the membrane acts as a dielectric interface. The position of the membrane determines the electrostatic field, and this field determines the electrostatic potential energy. We first review some preliminary theory in electrostatics, covered in the following sections.

5.1. DIELECTRICS

To begin, we treat the protein, lipid membrane, and the solvent as dielectrics. A dielectric is an insulating material that can be polarized by an electric field $\vec{\mathbf{E}}$. The atoms within a dielectric material have a net neutral charge and their electrons are positioned randomly. But, when an electric field is applied, the electrons rearrange according to the direction of the applied field, as in Figure 5.2. This rearrangement, or polarization, creates an internal electric field which reduces the applied field. There are different degrees to which a material is polarizable. This is quantified by the relative permittivity, which will be denoted by ε_r. (This term may sometimes be referred to as the "dielectric constant," but this terminology is deprecated in the physics and engineering communities, since ε_r is often not a constant in the mathematical sense.) Every non-conducting medium has an associated relative permittivity.

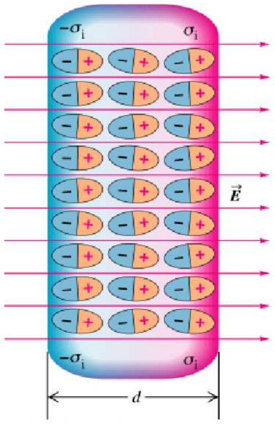

Figure 5.2: Polarization of a dielectric in an electric field $\vec{\mathbf{E}}$ [106].

For instance, a vacuum has $\varepsilon_r = 1$, air has $\varepsilon_r = 1.00059$, and water has $\varepsilon_r = 80.4$ (values taken at 20°C) [106]. The higher the relative permittivity, the greater the material's ability to be polarized, which reduces the effective strength of the electric field in the material.

Within the framework of the problem at hand, depicted in Figure 5.1, the lipids, protein, and solvent have different relative permittivities. This creates a discontinuity in the relative permittivity ε_r at each interface Γ_c, Γ_e, and Γ_p. The relative permittivities of the protein and membrane are denoted ε_p and ε_m, respectively, and usually range between $1 \le \varepsilon_p, \varepsilon_m \le 10$. On the other hand, the relative permittivity of the solvent, ε_s, is much greater, around 80, approximately the relative permittivity of water in normal conditions.

The dielectric is assumed to be isotropic and homogeneous in each distinct domain (e.g., the protein, membrane, and solvent). While the dielectric ε is often a three dimensional tensor, it is reduced to a (piecewise) scalar under these assumptions. We use the following definition for ε:

$$\varepsilon(x) = \begin{cases} \varepsilon_s & \text{if } x \in \Omega_s, \\ \varepsilon_p & \text{if } x \in \Omega_p, \\ \varepsilon_m & \text{if } x \in \Omega_m, \end{cases} \tag{148}$$

where $\varepsilon_s \approx 80$ and $\varepsilon_m \approx \varepsilon_p \approx 2$.

5.2. ELECTROSTATICS IN HOMOGENEOUS DIELECTRIC MEDIA

In this section, we derive Gauss' Law to describe electrostatics in dielectric media. We start with something simple. Coulomb's Law gives a physical description of the electrostatic interaction between two electrically charged particles. In a continuum model, it is more useful to consider the electric field generated by each point charge (from Coulomb's law) and then integrating over the whole space. The electric field $\vec{E}$ generated by a particle with charge q located at the origin is given by

$$\vec{E}(\vec{r}) = \frac{q\vec{e_r}}{4\pi\varepsilon r^2}, \tag{149}$$

where $\vec{r}$ is the displacement vector from the point charge, $\vec{e_r} = \vec{r}/|\vec{r}|$ is the unit vector in the direction of $\vec{r}$, $r = |\vec{r}|$ is the distance from the point charge, and ε is the absolute dielectric permittivity, $\varepsilon = \varepsilon_0\varepsilon_r$, where ε_0 is the permittivity of free space and ε_r is the relative permittivity of the material. For materials that do not have constant dielectric ε, like ours with the discontinuities on each interface Γ, it is more convenient to derive Gauss' Law using a linear constitutive relation for the displacement field,

$$\vec{D}(\vec{r}) = \varepsilon\vec{E}.$$

If the point charge is located at some other point $\vec{s} \in \Omega$, then Coulomb's Law is merely a shift of (149),

$$\vec{D}(\vec{r}) = \varepsilon\vec{E}(\vec{r}) = \frac{q}{4\pi|\vec{r}-\vec{s}|^2}\frac{\vec{r}-\vec{s}}{|\vec{r}-\vec{s}|} = \frac{q(\vec{r}-\vec{s})}{4\pi|\vec{r}-\vec{s}|^3}.$$

Notice that $\vec{D}(\vec{r})$ points in the direction of $\vec{r}-\vec{s}$ appropriately. The total displacement field at position $\vec{r}$ is obtained by integrating the individual electric fields from each point $\vec{s} \in \Omega$. Replacing the charge q by the charge density $\rho(\vec{s})$,

$$\vec{D}(\vec{r}) = \frac{1}{4\pi}\int_\Omega \frac{\rho(\vec{s})(\vec{r}-\vec{s})}{|\vec{r}-\vec{s}|^3}\, d^3\vec{s}.$$

Taking the divergence of both sides gives,

$$\begin{aligned}\nabla \cdot \vec{D}(\vec{r}) &= \frac{1}{4\pi}\int_\Omega \rho(\vec{s})\nabla \cdot \left(\frac{\vec{r}-\vec{s}}{|\vec{r}-\vec{s}|^3}\right)\, d^3\vec{s} \\ &= \int_\Omega \rho(\vec{s})\delta(\vec{r}-\vec{s})\, d^3\vec{s} \\ &= \rho(\vec{r}).\end{aligned}$$

This is the differential form of Gauss' Law,

$$\nabla \cdot \vec{D}(\vec{r}) = \rho(\vec{r}), \tag{150}$$

or alternatively,

$$\nabla \cdot \varepsilon \vec{E}(\vec{r}) = \rho(\vec{r}). \tag{151}$$

Thus, from Coulomb's Law, Gauss' Law is derived. To obtain the integral form, integrate the above result over any volume Ω and apply the divergence theorem,

$$\begin{aligned}\int_\Omega \rho(\vec{r})\, d^3\vec{r} &= \int_\Omega \nabla \cdot \vec{D}(\vec{r})\, d^3\vec{r} \\ &= \int_\Gamma \vec{D}(\vec{r}) \cdot \vec{n}\, d^2\vec{r},\end{aligned}$$

where Γ is any closed surface in Ω and $\vec{n}$ is the unit normal to the surface Γ. The integral form of Gauss' Law states that for a surface Γ that encloses a region $\Omega \subset \mathbb{R}^3$, the total flux of electric field is proportional to the total enclosed charge. That is,

$$\int_\Gamma \varepsilon \vec{E}(\vec{r}) \cdot \vec{n}\, dS = \int_\Omega \rho(\vec{r})\, dV. \tag{152}$$

Gauss' Law concerns the flux of an electric field, $(\vec{E} \cdot n)\, dS$ through some surface element dS. Suppose that a charge lies outside of the enclosed surface. The electric field from this charge will pass through one end of the surface dS_1 and then through the other dS_2. The net outward flux is zero due to the cancellation in the flux through dS_1 and dS_2. Now suppose that some distribution of charges lie inside the enclosed surface. No matter how the charges which create the electric field are distributed, they may be treated as a single change emanating from a point enclosed in a (Gaussian) sphere. The electric field due to this point charge is given by (152). The left side of the equation reduces to

$$\int_\Gamma \varepsilon \vec{E}_q(\vec{r}) \cdot \vec{n}\, dS = \frac{q}{4\pi r^2} \int_\Gamma \vec{e_r} \cdot \vec{n}\, dS = q,$$

since $\vec{e_r}$ and $\vec{n}$ are parallel unit vectors, and the surface area of a sphere is $4\pi r^2$. By superposition, the total flux is a sum of all of the charges inside the surface,

$$\int_\Gamma \varepsilon \vec{E}(\vec{r}) \cdot \vec{n}\, dS = \sum_{i=1}^{N} q_i, \qquad q_i \in S.$$

It is also convenient to write the electric field as the gradient of the electrostatic potential, $\vec{E} = -\nabla\phi$. If the field is emanating from a point charge, the potential is given by

$$\phi(r) = \frac{q}{4\pi\varepsilon r}. \tag{153}$$

This can be seen by taking the gradient of (153) with respect to $\vec{r}$ and obtaining (149). It is usually simpler to work in terms of ϕ rather than $\vec{E}$, since the potential is a scalar quantity. Using the differential form of Gauss' Law, Poisson's Equation is obtained. From (150),

$$\nabla \cdot (\nabla\phi) = \Delta\phi = -\frac{\rho(\vec{r})}{\varepsilon}. \tag{154}$$

If ε is discontinuous, then Poisson's equation must follow (151),

$$\nabla \cdot (\epsilon\nabla\phi) = -\rho(\vec{r}). \tag{155}$$

The derivation of Poisson's equation (155) can be found in any good book on electrostatics, e.g. [98, 51].

5.2.1. INTERFACE CONDITIONS. Suppose a surface Γ separates two regions with different dielectrics, as our model does. Let the relative permittivity of the interior be ε_1 and that of the exterior be ε_2. Now consider a cylindrical Gaussian surface Ω intersecting the boundary. The height of the cylinder is taken to be small so that the only contributions to the outward flux from the cylinder come from the top and bottom faces. The displacement field on the top face is denoted $\vec{D}_2$ and the displacement field on the bottom face is $\vec{D}_1$. Suppose for now that the boundary carries no charge, so that $\rho = 0$ inside the Gaussian cylinder. By (150),

$$\int_\Omega \nabla \cdot \vec{D}\, dV = 0.$$

By the divergence theorem (2),

$$\int_\Gamma \vec{D} \cdot \vec{n}\, dV = \vec{D}_1 \cdot \vec{n}_1 + \vec{D}_2 \cdot \vec{n}_2 = 0.$$

Since the normal vectors point in opposite directions, the above equation reduces to

$$\vec{D}_1 \cdot \vec{n} = \vec{D}_2 \cdot \vec{n}. \tag{156}$$

This is our first boundary condition, which may be applied to the protein-solvent boundary Γ_p, since this boundary is uncharged. In terms of the electrostatic potential, (156) becomes

$$\varepsilon_1 \nabla \phi_1 \cdot \vec{n} = \varepsilon_2 \nabla \phi_2 \cdot \vec{n}. \tag{157}$$

The condition (156) states that the displacement field is continuous across the interface Γ. However, the electric field is clearly discontinuous since the dielectric is discontinuous.

For the second boundary condition, consider a rectangular contour γ, denoted $ABCD$ that spans the interface, where the edge AB is in the exterior (with dielectric ε_2) parallel to Γ, and the edge DC is in the interior (with dielectric ε_1) perpendicular to Γ. Define dl to be the length of the rectangle so that $dl = |AB| = |DC|$, and define dw to be the width of the rectangle so that $dw = |AD| = |BC|$. The electric field is conservative, so no work is done along the contour γ traversing the rectangle. Let $E_{||}^{(1)}$ be the electric field parallel to the surface along DC and $E_{||}^{(2)}$ be the electric field parallel to the surface along AB. Then consider the contour integral

$$\oint_\gamma \vec{E} \cdot d\vec{l} = E_{||}^{(1)} dl - E_{||}^{(2)} dl + E dw + E dw = 0.$$

If we take $dw \to 0$, the electric field contributions from sides BC and DA are negligible, and hence

$$E_{||}^{(1)} = E_{||}^{(2)}, \tag{158}$$

which implies that the tangential component of the electric field is continuous across the boundary. This condition (158) applies to all boundaries Γ in our setup, for it remains unchanged with charged interfaces. In terms of the electrostatic potential, (158) becomes

$$\phi_1 = \phi_2. \tag{159}$$

If the boundary Γ is itself charged (such as the boundaries where the charged lipid heads lie, Γ_c and Γ_e), the first boundary condition must be modified. The continuity of $E_{||}$ and ϕ remains the same. However, the displacement field condition must be modified to include the surface charge density σ,

$$\vec{D}_1 \cdot \vec{n} - \vec{D}_2 \cdot \vec{n} = \sigma. \tag{160}$$

In terms of the electrostatic potential, the boundary condition modified from (157) is

$$-\varepsilon_1 \nabla \phi_1 \cdot \vec{n} = -\varepsilon_2 \nabla \phi_2 \cdot \vec{n} + \sigma. \tag{161}$$

We use the notation ρ for a distribution of lipids on the surface Γ_e and Γ_c, and hence ρ has dimensions 1/Length^2. The charge per lipid q_l has units of charge, C. Then, σ, the charge density per unit area is defined as $\sigma = \rho q_l$, hence the boundary condition

$$\varepsilon_1 \nabla \phi_1 \cdot \vec{n} = \varepsilon_2 \nabla \phi_2 \cdot \vec{n} - \rho q_l. \tag{162}$$

This condition applies to the membrane boundaries Γ_c and Γ_e. Our final interface conditions in terms of the electrostatic potential are (157), (159), and (162).

5.2.2. Molecular interfaces. There are several different ways to determine the position of the interface of a molecule upon which the boundary conditions discussed in Section 5.2.1 are imposed. Three common methods are discussed here.

The simplest way to model the interface of a molecule is by its van der Waals surface. This idea is to consider each atom of the molecule and its van der Waals radius, which are often determined by the atomic spacing between unbounded atoms in crystals. This radius is of course a hypothetical value. Each atom in the molecule is given a van der Waals radius and pieced together to create a van der Waals surface. The green line in Figure 5.3 shows the van der Waals surface, and Figure 5.4(a) illustrates an example of the van der Waals surface for a particular molecule.

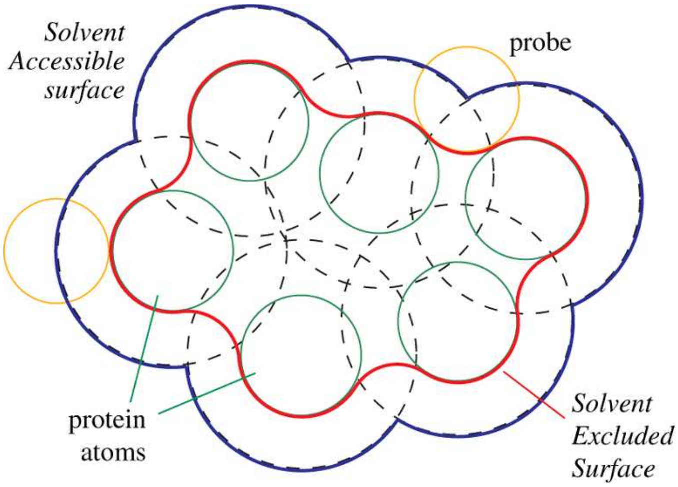

Figure 5.3: The van der Waals, solvent excluded, and solvent accessible surfaces [58].

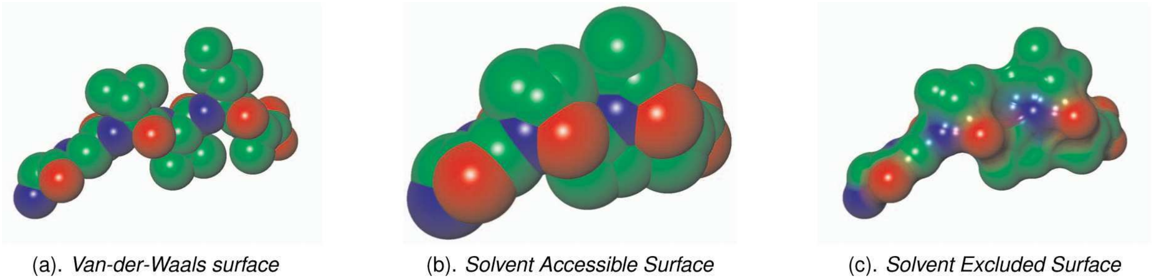
(a). *Van-der-Waals surface*
(b). *Solvent Accessible Surface*
(c). *Solvent Excluded Surface*

Figure 5.4: Illustration of van der Waals, solvent excluded, and solvent accessible surfaces for a sample molecule [58].

The solvent excluded surface is obtained by smoothing out the van der Waals surface. This smoothing is calculated in a specific way. A sphere of solvent with a particular radius, called the probe sphere, is rolled across the van der Waals surface of the molecule. If the probe sphere touches the van der Waals surface, then the solvent excluded surface is the same as the van der Waals surface at that point. When the probe sphere gets caught in between two or more atoms from the molecule, it traces a smooth connecting line in between the atoms. Therefore, the solvent excluded surface always encompasses more volume than the van der Waals surface. The solvent excluded surface is sometimes simply called the molecular surface. The red line in Figure 5.3 shows the solvent excluded surface, and Figure 5.4(c) illustrates an example of the solvent excluded surface for a particular molecule.

A third way to describe the molecular interface is by the solvent accessible surface. Like the solvent excluded surface, the solvent accessible surfaces traces a smooth connection between the van der Waals spheres by using a probe sphere of solvent. The point of connection is not the point of contact, but rather the center of the probe sphere. That is, the solvent accessible surface is just the solvent excluded surface increased by the radius of the probe sphere, and again, the solvent accessible surface always encompasses more volume than the solvent excluded surface. The blue line in Figure 5.3 shows the solvent accessible surface, and Figure 5.4(b) illustrates an example of the solvent accessible surface for a particular molecule.

We prefer the solvent excluded or solvent accessible surface for our model so that the surfaces are smooth.

5.3. POISSON EQUATION

Now we piece together the electrostatic theory for our particular problem. We developed the partial differential equation for the electrostatic potential ϕ in (155), namely, the Poisson equation. We also developed the boundary conditions (159) for every boundary Γ, (157) for the protein boundary Γ_p, and (162) for the lipid boundaries Γ_c and Γ_e. We define a function $g \in W^{2,\infty}(\Omega)$ for the electrostatic potential on the containment boundary $\partial\Omega$, where $W^{2,\infty}$

is the Sobolev space of twice differentiable functions whose derivatives up to second order are essentially bounded (i.e. bounded up to a set of measure zero). Assembling all of these equations together, we obtain the Poisson equation with boundary conditions for our system,

$$\begin{cases} \nabla \cdot (\varepsilon \nabla \phi) = -\rho_\Omega, & \text{in } \Omega, \\ [\phi] = 0, & \text{on } \Gamma_c, \Gamma_e, \Gamma_p, \\ \varepsilon_s \dfrac{\partial \phi^s}{\partial n} = \varepsilon_m \dfrac{\partial \phi^m}{\partial n} - \rho[\Gamma] q_l, & \text{on } \Gamma_c, \Gamma_e, \\ \varepsilon_s \dfrac{\partial \phi^s}{\partial n} = \varepsilon_p \dfrac{\partial \phi^p}{\partial n}, & \text{on } \Gamma_p, \\ \phi = g, & \text{on } \partial\Omega. \end{cases} \tag{163}$$

The notation $[\phi]$ denotes the jump in ϕ, i.e. $[\phi] = \phi_1 - \phi_2$, where ϕ_i, $i = 1, 2$ is the value of ϕ on each side of the boundary. This boundary condition in (163) is equivalent to saying that ϕ is continuous across the boundary as in (159).

We still need to describe the distribution of charges ρ_Ω in the first equation of (163). This term accounts for the distribution of charges in the volumes $\Omega_s, \Omega_p, \Omega_m \subset \Omega \subset \mathbb{R}^3$. This includes the charges from the ions in the solvent Ω_s as well as the charges from the atoms in the protein Ω_p. Since the charges from the lipids are modeled on the headgroups Γ_c and Γ_e, there is no charge distribution arising from Ω_m. Therefore, we have

$$\rho_\Omega = \rho_p + \rho_i, \tag{164}$$

where ρ_p describes the distribution of charge in the protein, and ρ_i describes the distribution of charge in the solvent. In the next section, we discuss the distribution of charge in the protein ρ_p. In the following section, we define a Boltzmann distribution for ρ_i. With these two results, we finish the first equation of (163) to describe the term ρ_Ω.

5.4. Protein structure and charge distribution

In this section, we model the distribution of charge in a protein, ρ_p. Proteins are rigid structures, meaning that the position of the atoms and hence the charges associated are fixed. For review, we briefly discuss protein structure next.

When atoms bond with other atoms, they form a *primary structure* of amino acids. While there are hundreds of different amino acids, there are only 20 that play a role in the formation of proteins. Amino acids can bend and fold into regular patterns known as *secondary structures* such as α-helices and β-sheets (these two structures are the most common in protein formation). When several of these secondary structures are assembled together, a *tertiary structure*, or polypeptide chain is made. These can look quite complex, but are essentially just the folds of secondary structures that place them into an energy minimizing position. These tertiary structures are subunits of a *quaternary structure*, which is the full protein complex. An illustration of the protein structure is found in Figure 5.5. Of course, all of the linking, bending, and merging will move the charges to different positions in space. Most proteins are overall weakly charged, however, even if the net charge of a protein is balanced to zero, a protein may still be polar, and charges from one side of a protein may be relevant.

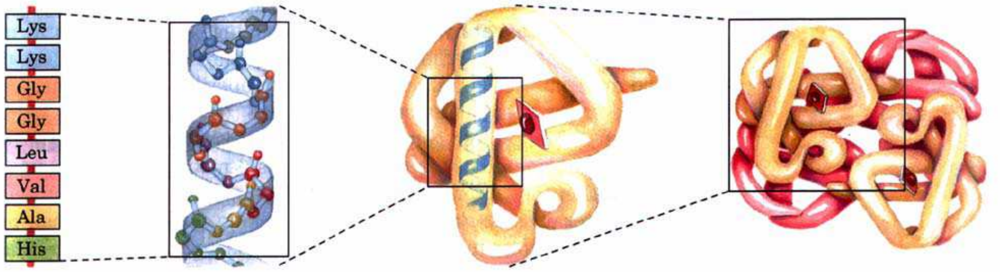

Figure 5.5: The structure of proteins. From left to right: Primary structure of amino acid residues, secondary structure of an α-helix, tertiary structure of a polypeptide chain, quaternary structure of assembled subunits [75].

We model a protein composed of N atoms located at the points $x_1, x_2, \ldots x_N$ with charges $Q_1, Q_2, \ldots, Q_N$, respectively. The charge of each atom is located in the atom's center. We assume the protein will not make any conformational changes, and therefore the charge distribution will remain fixed at the atoms' centers. Such a description is found in [4, 5],

$$\rho_p(x) = \frac{4\pi e_c^2}{k_B T} \sum_{i=1}^{N} q_i \delta(x - x_i), \tag{165}$$

where e_c is the charge of an electron, k_B is the Boltzmann constant, and T the temperature so that the product $k_B T$ is the thermal energy of the system. The delta function ensures that the charge is located at the atom's center x_i for each i.

The form of equation (165) assumes that the charges arise from the centers of each atom in the protein. This function $\rho_p \in L^1(\Omega)$, since the distribution $\delta(x) \in L^1(\Omega)$, but $\rho_p \notin H^1(\Omega)$, a condition that will be needed in the computation of the dielectric boundary force. Therefore, the model given by (165) is not used in our definition of the electrostatic potential energy, but instead, a smooth approximation of the delta function is used, such as those in [60, 94, 85]. In this way, the analysis of the energy functional is easier to treat [62]. We assume the charge follows some nonzero distribution across the entire van der Waals surface. This way, $\rho_p \in H^1(\Omega)$, as desired. To further satisfy some distance requirements to be made later in equation (210), the boundary Γ should be defined by the solvent accessible surface, rather than the van der Waals surface. (See Figures 5.3 and 5.4 for a depiction of the van der Waals and solvent accessible surfaces.)

5.5. Boltzmann distribution

In this section, we describe the charge distribution of ions in the solvent, ρ_i in (164) to complete the Poisson equation (163). Recall that the membrane-protein system is placed in an ion-concentrated solution (solvent). Ions are atoms with an unbalanced number of protons and electrons, and therefore possess electric charge. We model the distribution of ions as a Boltzmann distribution, assuming that (i) all particles are equivalent, (ii) the particles are indistinguishable, (iii) there are no particle-particle interactions except to transfer energy in brief collisions, and (iv) the particles are in thermal equilibrium.

Consider a system with N equivalent, indistinguishable particles (ions) with no interactions between them except for very brief collisions in which they exchange energy and momentum. We seek the distribution of particles in thermal equilibrium. We will compute the entropy of this system and assume that the distribution of particles maximizes entropy, in accordance with the second law of thermodynamics. (Entropy is a measure of the number of ways a system can be arranged, or equivalently, a measure of disorder.)

The particles can assume K distinct energy levels, and assume N is large. Denote the energy of each energy level by e_i. We take the fundamental assumption of statistical thermodynamics (also called the fundamental postulate of statistical mechanics), which states that the probability of a particle occupying any microstate is equally likely. To expand on this assumption, suppose that the distribution of the particles in the K energy levels is random. The particles are moving around, each with some speed. When two particles collide, they transfer energy to each other, resulting in a change of energy level. The probability of increasing the energy of a given particle is equally likely as the probability of decreasing in energy, and since there are so many particles (N is large), the particles are continuously changing energy levels. Next, suppose there are n_i particles in each energy level i so that $\sum_{i=1}^{K} n_i = N$. The n_i is called the occupation number of the energy level i. The total energy of the system is

$$E = \sum_{i=1}^{K} e_i n_i. \tag{166}$$

The number of ways of selecting n objects from a set of N is $\binom{N}{n} = N!/(n!(N-n)!)$. Here, we have K distinct "energy sets" from which to pick. Select n_1 objects from N and place them in set 1 (energy level e_1), then from the remaining $N-n_1$ objects, select n_2 objects and place them into set 2 (energy level e_2), and so on. The remaining $N - n_1 - n_2 - \cdots - n_{K-1}$ objects are placed into set K (energy level e_K). The total number of ways this can be done is

$$W = \frac{N!}{n_1!(N-n_1)!} \times \frac{(N-n_1)!}{n_2!(N-n_1-n_2)!} \times \cdots \times \frac{(N-n_1-n_2-\cdots-n_{K-1})!}{n_K!(N-n_1-n_2-\cdots-n_K)!} \tag{167}$$
$$= \frac{N!}{n_1!n_2!n_3!\cdots n_K!}.$$

The equation simplifies by telescoping terms on the denominator with the corresponding term on the subsequent numerator, and knowing that the term in the final denominator $(N-n_1-n_2-\cdots-n_K)! = 1$ since $\sum_{i=1}^{K} n_i = N$.

Before we continue, we need to make a correction to (167) concerning the degeneracy of energy levels. In quantum mechanics, an energy level is said to be degenerate if it corresponds to two or more different measurable states or distributions. Denote the degeneracy of the ith energy level by g_i. This means there are really g_i ways to express the energy e_i, rather than just one. This will affect our probability calculation, since the number of ways of placing elements into the set i must be increased by the number of ways n_i can be distributed into the degenerate levels g_i. If the particles on each sublevel are indistinguishable, this number is $g_i^{n_i}$, where the superscript denotes exponentiation. If the energy of level i can be expressed in g_i different ways, and n_i particles belong in level i, then there are g_i choices for particle 1, g_i choices for particle 2, and so on, and g_i choices for particle n_i, for a total of $g_i^{n_i}$ choices. Therefore, the total number of ways N particles can be distributed into their energy levels, including degenerate states, is

$$W = N! \prod_{i=1}^{K} \frac{g_i^{n_i}}{n_i!}. \tag{168}$$

We can use (168) to compute the entropy of the system.

Entropy is a fundamental concept in thermodynamics, and is a measure of the number of ways a thermodynamic system can be arranged. Entropy is an additive measure, meaning that if we have two systems of with corresponding entropies S_1 and S_2, then the entropy of the two systems should be $S_1 + S_2$. But, the number of ways the full system is not the number of ways system 1 can be arranged plus the number of ways system 2 can be arranged.

Instead, the number of ways a system can be arranged grows combinatorially. In the 1870s, Ludwig Boltzmann showed that the entropy S of a system is logarithmically related to the number of ways the system could be arranged (168) in his fundamental equation,

$$S = k_B \ln W. \tag{169}$$

Logarithms exchange multiplicative problems (such as counting the number of ways two systems can be arranged) into additive problems, making entropy an additive quantity, as desired. Using this feature of natural logarithms, the entropy of the system is

$$S = k_B \ln \left(N! \prod_{i=1}^{K} \frac{g_i^{n_i}}{n_i!} \right) = k_B \left(\ln(N!) + \sum_{i=1}^{K} \left[n_i \ln(g_i) - \ln(n_i!) \right] \right). \tag{170}$$

Since N is large, we assume that each n_i is also large, so we can apply Stirling's approximation to both N and each n_i. Stirling's approximation says

$$\ln(n!) = n \ln(n) - n + O(\ln(n)). \tag{171}$$

This gives

$$S \approx k_B \left(N \ln(N) - N + \sum_{i=1}^{K} \left[n_i \ln(g_i) - n_i \ln(n_i) + n_i \right] \right). \tag{172}$$

Gibbs noticed that (172) does not give the correct entropy, known as Gibbs' paradox. The problem is that the particles considered are distinguishable, but in the calculation, we assumed they were indistinguishable. For instance, two particles may have different momenta, but the same energy. Hence, they are distinguishable. With this correction, we carry out the counting problem again. This is called Bose-Einstein statistics. Then, if $w(n_i, g_i)$ is the number of ways of distributing n_i distinguishable particles in g_i sublevels, it is given as a number of permutations,

$$w(n_i, g_i) = \left(\!\! \binom{g_i}{n_i} \!\! \right) = \binom{g_i + n_i - 1}{n_i} = \frac{(g_i + n_i - 1)!}{n_i!(g_i - 1)!}. \tag{173}$$

Then, the number of ways of arranging the entire system is the produce of the $w(n_i, g_i)$ for each i,

$$W = \prod_{i=1}^{K} \frac{(n_i + g_i - 1)!}{n_i!(g_i - 1)!}. \tag{174}$$

This distribution requires a temperature above 0K and low density, so we have the approximations $1 \ll n_i \ll g_i$, and hence we can still apply Stirling's approximation, but this time we will use the form,

$$n! \approx \sqrt{2\pi n}\, n^n e^{-n}. \tag{175}$$

Using this approximation on $(n_i + g_i)!$, $n_i!$, and $g_i!$, Equation (174) becomes

$$\begin{aligned} W &= \prod_{i=1}^{K} \frac{(n_i + g_i)! g_i}{n_i! g_i! n_i} \\ &= \prod_{i=1}^{K} \frac{\sqrt{2\pi(n_i + g_i)}\ (n_i + g_i)^{n_i + g_i} e^{-n_i - g_i} g_i}{\sqrt{2\pi n_i}\ n_i^{n_i} e^{-n_i} \sqrt{2\pi g_i}\ g_i^{g_i} e^{-g_i} (n_i + g_i)} \\ &= \prod_{i=1}^{K} \frac{(n_i + g_i)^{n_i + g_i}}{n_i^{n_i} g_i^{g_i}} \frac{g_i}{n_i + g_i}. \end{aligned}$$

The latter fraction $g_i/(n_i + g_i) \approx 1$ since $n_i \ll g_i$. Then, divide both the numerator and the denominator by $g_i^{(n_i + g_i)}$ to get

$$W \approx \prod_{i=1}^{K} \frac{(n_i + g_i)^{n_i + g_i}}{n_i^{n_i} g_i^{g_i}} = \prod_{i=1}^{K} \frac{g_i^{n_i} (n_i/g_i + 1)^{n_i + g_i}}{n_i^{n_i}}.$$

Recall the limit definition for the exponential function

$$e^x = \lim_{n \to \infty} \left(1 + \frac{x}{n}\right)^n. \tag{176}$$

This form appears in the numerator of W above, $e^{n_i} \approx (1 + n_i/g_i)^{g_i}$ since $g_i \gg n_i$. Using this, and using Stirling's approximation (175) in reverse, we have

$$W \approx \prod_{i=1}^{K} \frac{g_i^{n_i} e^{n_i}}{n_i^{n_i}} \approx \prod_{i=1}^{K} \frac{g_i^{n_i}}{n_i!}. \tag{177}$$

With this, so-called *correct Boltzmann counting*, the entropy is (using Stirling's approximation (171) yet again)

$$S = k_B \ln\left(\prod_{i=1}^{K} \frac{g_i^{n_i}}{n_i!}\right) = k_B\left(\sum_{i=1}^{K} n_i \ln(g_i) - \ln(n_i!)\right) \tag{178}$$

$$\approx k_B\left(\sum_{i=1}^{K} n_i \ln(g_i) - n_i\ln(n_i) + n_i\right).$$

The distribution of particles maximizes entropy, and so we look for values of n_i which maximize equation (178), while keeping the total number of particles and the total energy (166) fixed. For clarity, we use $\bar{N}$ and $\bar{E}$ to denote the respective fixed values. Using the method of Lagrange multipliers for the constraints, we maximize the following function,

$$f(n_1,\cdots,n_K) = \left(\sum_{i=1}^{K} n_i\ln(g_i) - n_i\ln(n_i) + n_i\right) + \alpha\left(\bar{N} - \sum_{i=1}^{K} n_i\right) + \beta\left(\bar{E} - \sum_{i=1}^{K} e_i n_i\right)$$

$$= \left(\sum_{i=1}^{K} n_i\ln(g_i) - n_i\ln(n_i) + n_i - \alpha n_i - \beta e_i n_i\right) + \alpha\bar{N} + \beta\bar{E}. \tag{179}$$

Taking partial derivatives with respect to n_i, we require

$$\frac{\partial f}{\partial n_i} = \ln(g_i) - \ln(n_i) - (\alpha + \beta e_i) \overset{\text{set}}{=} 0. \tag{180}$$

Solve (180) for each n_i to get

$$n_i = g_i e^{-(\alpha+\beta e_i)}. \tag{181}$$

Now, using (181), we have

$$\begin{aligned}\ln(W) &= \left(\sum_{i=1}^{K} n_i \ln(g_i) - n_i \ln(n_i) + n_i\right)\\ &= \left(\sum_{i=1}^{K} g_i e^{-(\alpha+\beta e_i)} \ln(g_i) - g_i e^{-(\alpha+\beta e_i)} \ln(g_i e^{-(\alpha+\beta e_i)}) + g_i e^{-(\alpha+\beta e_i)}\right)\\ &= \left(\sum_{i=1}^{K} g_i e^{-(\alpha+\beta e_i)}(\alpha+\beta e_i) + g_i e^{-(\alpha+\beta e_i)}\right)\\ &= \left(\sum_{i=1}^{K} n_i(\alpha+\beta e_i+1)\right)\\ &= (\alpha+1)N+\beta E.\end{aligned}$$

If we rearrange this and differentiate, we get

$$E = \frac{1}{\beta}\ln(W) - \frac{\alpha+1}{\beta}N, \tag{182}$$

$$dE = \frac{1}{\beta}\,d\ln(W) - \frac{\alpha+1}{\beta}\,dN. \tag{183}$$

But (183) is just the second law of thermodynamics,

$$dE = T\,dS + \mu\,dN = T\,d(k_B\ln(W)) + \mu\,dN, \tag{184}$$

so by matching terms in (183) and (184), we have $k_BT = 1/\beta$ and $\mu = -(\alpha+1)/\beta$. Solving for $\beta = 1/(k_BT)$ and $\alpha = -\mu/(k_BT) - 1$ allows us to rewrite (181) explicitly,

$$n_i = g_i \exp\left(\frac{\mu - e_i}{k_BT} + 1\right). \tag{185}$$

This equation (185) defines the form of a Boltzmann distribution. A *Boltzmann distribution* is defined to be a distribution that takes the form,

$$\rho(x) = c_\infty e^{-U/(k_BT)}, \tag{186}$$

where c_∞ is some constant of proportionality called the bulk number density, U is the free energy usually written as the product of the electrostatic potential ϕ with the charge q, and the constant $\beta = 1/(k_B T)$ is the inverse thermal energy.

For our purposes, we assume that the solvent contains M distinct ionic species. These counterions (so-called because they produce electric neutrality to the membrane-protein-solvent system in Figure 5.1) are modeled by a Boltzmann distribution as in [2, 20],

$$\rho_i(x) = \sum_{j=1}^{M} c_j^\infty q_j e^{-\beta q_j \phi(x)}, \tag{187}$$

where ϕ is the electrostatic potential, c_j^∞ is the bulk concentration, q_j the charge, and the subscript j represents the jth particular ionic species. We assume the condition of charge neutrality in the bulk, which is a reasonable assumption away from any charged surfaces,

$$\sum_{j=1}^{M} c_j^\infty q_j = 0. \tag{188}$$

One may generalize (187) as in [10, 5, 56] by enforcing ion-excluded volume effects, or steric effects. Steric effects occur when atoms come so close together that their electron clouds overlap. The steric potential, scaled by the inverse thermal energy, is added to the exponential of (187) is to ensure that the atoms from the protein, lipids, and the counterions do not overlap.

The results of this section can be found in any good textbook on statistical mechanics, e.g. [71].

5.6. POISSON-BOLTZMANN EQUATION

We use a Boltzmann distribution (187) for ρ_i to complete the Poisson equation (163). This leads the the Poisson-Boltzmann equation, which is equation governing the system. We restrict the distribution (187) to the solvent domain Ω_s by the characteristic function χ_s

which is 1 on Ω_s and 0 elsewhere and define (as in [62])

$$B(\phi) = \beta^{-1} \sum_{j=1}^{M} c_j^{\infty} (e^{-\beta q_j \phi} - 1). \tag{189}$$

Then, $\rho_i(x) = -B'(\phi)$. Using this notation, the Poisson equation (163) becomes the Poisson-Boltzmann equation,

$$\begin{cases} \nabla \cdot (\varepsilon \nabla \phi) - \chi_s B'(\phi) = -\rho_p, & \text{in } \Omega, \\ [\phi] = 0, & \text{on } \Gamma_c, \Gamma_e, \Gamma_p, \\ \varepsilon_s \dfrac{\partial \phi^s}{\partial n} = \varepsilon_m \dfrac{\partial \phi^m}{\partial n} - \rho[\Gamma] q_l, & \text{on } \Gamma_c, \Gamma_e, \\ \varepsilon_s \dfrac{\partial \phi^s}{\partial n} = \varepsilon_p \dfrac{\partial \phi^p}{\partial n}, & \text{on } \Gamma_p, \\ \phi = g, & \text{on } \partial\Omega, \end{cases} \tag{190}$$

where again, ε is the dielectric permittivity for each region defined by (148), ϕ is the electrostatic potential, ρ_p is the distribution of charges in the rigid protein which shall be assumed to be a sufficiently smooth and compactly supported approximation to (165), n is the outward unit normal vector to any interface Γ, $\rho[\Gamma]$ is the distribution of lipids on the vesicle membrane (to be defined later), q_l is the charge of a lipid, and $g \in W^{2,\infty}(\Omega)$ is the value of ϕ at the containment domain's boundary.

We remark that the Poisson-Boltzmann equation (190) is equivalent to the following elliptic interface problem.

$$
\begin{cases}
\varepsilon_p \Delta\phi = -\rho_p & \text{in } \Omega_p, \\
\varepsilon_m \Delta\phi = 0 & \text{in } \Omega_m, \\
\varepsilon_s \Delta\phi - B'(\psi) = 0 & \text{in } \Omega_s, \\
[\phi] = 0 & \text{on } \Gamma_c, \Gamma_e, \Gamma_p, \\
\varepsilon_s \nabla\phi^s \cdot n = \varepsilon_p \nabla\phi^p \cdot n & \text{on } \Gamma_p, \\
\varepsilon_s \nabla\phi^s \cdot n = \varepsilon_m \nabla\phi^m \cdot n - \rho[\Gamma]q_l & \text{on } \Gamma_c, \Gamma_e, \\
\phi = g & \text{on } \partial\Omega.
\end{cases}
\tag{191}
$$

A proof of the equivalence can be checked in [61] with appropriate inclusions for the lipids.

The Poisson-Boltzmann equation (190) is the standard equation for describing electrostatic forces on boundaries. The only term that does not have a formula is the distribution of lipids on the membrane surfaces Γ_c and Γ_e. In the following section, we define this distribution $\rho[\Gamma]$ and complete (190).

5.7. LIPID DISTRIBUTION

The drift-diffusion equation, also called the electrodiffusion equation, is used to model the movement of particles that are transferred due to the processes of diffusion and convection. Both processes are relevant in our system, since the lipids experience "drift" due to the electric field $\vec{E} = -\nabla\phi$ and may freely diffuse on the surface of the membrane. When an electric field is present, the lipids drift according to the direction of the field and the sign of their charge. Positively charged lipids drift in the opposite direction as negatively charged lipids. The drift-diffusion equation is

$$
\frac{\partial \rho}{\partial t} = \nabla \cdot (D\nabla\rho + D\beta q\rho\nabla\phi),
\tag{192}
$$

where ρ is the concentration of lipids, D is the diffusion coefficient, q is the charge of a lipid, and ϕ is the (electrostatic) potential.

The distribution of lipids should satisfy the drift-diffusion equation in its steady state. That is, the concentration of lipids is determined once the processes of drift and diffusion have settled into equilibrium. Therefore, ρ satisfies

$$0 = \nabla \cdot (D\nabla\rho + D\beta q\rho\nabla\phi). \tag{193}$$

To solve (193), it is convenient to represent ion concentration ρ using a "Slotboom variable" [93],

$$u = \rho e^{\beta q\phi}. \tag{194}$$

This variable transforms (193) to an equivalent, symmetric form,

$$0 = \nabla \cdot (De^{-\beta q\phi}\nabla u), \tag{195}$$

since the term inside the divergence operator matches,

$$\begin{aligned} De^{-\beta q\phi}\nabla u &= De^{-\beta q\phi}\nabla(\rho e^{\beta q\phi}) \\ &= De^{-\beta q\phi}\left((\nabla\rho)e^{\beta q\phi} + \beta q\rho e^{\beta q\phi}(\nabla\phi)\right) \\ &= D\nabla\rho + D\beta q\rho\nabla\phi. \end{aligned}$$

One solution to the drift diffusion equation given by (195) is $u = c$ for some constant c. It is quick to check this is a solution, since $\nabla u = 0$. Then, by (194), we have

$$c = \rho e^{\beta q\phi}. \tag{196}$$

Solving (196) for ρ gives us

$$\rho = c\mathrm{e}^{-\beta q\phi}. \tag{197}$$

If we let $c = c^{\infty}q$, then (197) matches the Boltzmann distribution (187) for a single species. Indeed, lipids are often arranged as a Boltzmann distribution on membranes [15]. We now wish to determine an appropriate c for the lipid distribution if the lipids do not satisfy the ideal Boltzmann distribution.

The practical distribution of lipids is subject to other constraints such as finite sizes and entropy conditions and may not follow the ideal Boltzmann distribution [53, 55, 108]. We generalize the distribution of lipids given by (200) in the following way.

The integration of the lipid concentration over the membrane Γ gives the total number of lipids on a leaflet. By the discussion in Section 2.1, this quantity is conserved. Using a Boltzmann distribution, we have

$$T = \int_\Gamma \rho \, dS = \int_\Gamma c e^{-q\beta\phi} \, dS. \tag{198}$$

We can factor the constant c and solve

$$c = \frac{T}{\displaystyle\int_\Gamma e^{-q\beta\phi} \, dS}. \tag{199}$$

Plugging (199) back into (197), we have the distribution of lipids with an ideal Boltzmann distribution,

$$\rho[\Gamma] = \frac{T e^{-q\beta\phi}}{\displaystyle\int_\Gamma e^{-q\beta\phi} \, dS}. \tag{200}$$

For the generalization, define

$$\rho[\Gamma] = \frac{-C\gamma'(\phi)}{\beta q_l \displaystyle\int_\Gamma \gamma(\phi) \, dS}, \tag{201}$$

where C is a dimensionless quantity related to T (the total number of lipids), and $\gamma : \Omega \to \mathbb{R}$ captures the generalization. Notice that if

$$\gamma(\phi) = e^{-q_l\beta\phi}, \tag{202}$$

and if $C = T$, then the general lipid distribution (201) follows the Boltzmann distribution (200).

With (201), we have a formula for every term in the Poisson-Boltzmann equation (190). In the next section, we use (190) to define the electrostatic potential energy for the protein-membrane system.

5.8. Electrostatic potential energy

In the calculus of variations, the stationary functions of a functional are the solutions to the Euler-Lagrange equation corresponding to that functional. In our context, we seek an energy functional whose Euler-Lagrange equation is the Poisson-Boltzmann equation. In this way, the electrostatic potential energy ϕ that satisfies the Poisson-Boltzmann equation (190) will be a stationary solution to the energy functional. In this section, we define an energy functional for the electrostatic potential energy and prove that the stationary solution to the functional is also a weak solution to the Poisson-Boltzmann equation.

Consider the following electrostatic potential energy,

$$G[\Gamma;\phi] = \int_\Omega \left[-\frac{\varepsilon}{2}|\nabla\phi|^2 + \rho_p\phi - \chi_s B(\phi)\right] d\Omega - \frac{C}{\beta}\ln\left(\int_{\Gamma_{c,e}} \gamma(\phi)\, dS \Big/ \int_{\Gamma_{c,e}} dS\right), \tag{203}$$

where the notation $\Gamma_{c,e} = \Gamma_c \cup \Gamma_e$ emphasizes that the integration of the lipid distribution only occurs in the lipid membranes (and not on Γ_p).

We remark that this energy functional is concave down, and so a stationary function of this electrostatic potential energy will be the *maximizer* of the energy functional. This may seem confusing, since we try to perform energy *minimizing* computations. However it is conventional to define the electrostatic potential energy in this way. It is easy to find the energy minimizing solution by simply negating (203) above. E.g.,

$$G[\Gamma;\phi]^* = \int_\Omega \left[\frac{\varepsilon}{2}|\nabla\phi|^2 - \rho_p\phi + \chi_s B(\phi)\right] d\Omega + \frac{C}{\beta}\ln\left(\int_{\Gamma_{c,e}} \gamma(\phi)\, dS \Big/ \int_{\Gamma_{c,e}} dS\right). \tag{204}$$

This energy formulation is concave up, so a stationary function will be the energy *minimizer* of G^*. This form is in accordance with Dirichlet's principle for energy minimization (e.g., see Section 2.5.5 of [34]). We proceed with the conventional electrostatic energy in (203).

The reader should keep in mind that energy *maximization* can be easily replaced with energy *minimization* with the use of (204).

We also remark that if $\gamma(\phi) = 1$, then $\gamma'(\phi) = 0$, and so by (201), there are no lipids on the membrane surface. In terms of the energy, the second term will be zero, since $\ln(1) = 0$. Note that if $\gamma = c$ for $c \neq 1$, there will be no lipids, yet there will be an energy cost of $C/\beta \ln(c)$. Therefore, we require that $\gamma(\phi)$ be a non-constant function of ϕ.

In addition, consider the notation for the Hilbert space with boundary,

$$H^1_g(\Omega) = \{\phi \in H^1(\Omega) \mid \phi = g \text{ on } \partial\Omega\}, \tag{205}$$

where $H^1 = W^{1,2}$ is the usual Hilbert space whose functions are square integrable and have square integrable partial derivatives up to first order.

We justify our choice of the energy function (203) by the following theorem.

Theorem 5.8.1. *Let the electrostatic potential energy G be given by* (203)*, where Γ is any smooth boundary in Ω. Then there exists a critical point $\psi_0 \in H^1_g(\Omega)$ of $G[\Gamma;\cdot]$ which is also the weak solution of the nonlinear Poisson-Boltzmann equation* (190)*.*

Proof. Let $\psi \in H^1_0(\Omega)$. Consider the variation of the electrostatic potential energy:

$$\begin{aligned}\left.\frac{dG[\Gamma;\phi+t\psi]}{dt}\right|_{t=0} &= \frac{d}{dt}\left(\int_\Omega \left[-\frac{\varepsilon}{2}|\nabla(\phi+t\psi)|^2 - \chi_s B(\phi+t\psi) + \rho_p(\phi+t\psi)\right] d\Omega\right.\\ &\qquad \left.\left. -\frac{C}{\beta}\ln\left(\int_\Gamma \gamma(\phi+t\psi)\,dS \Big/ \int_\Gamma dS\right)\right)\right|_{t=0}\\ &= \int_\Omega -\varepsilon\nabla(\phi+t\psi)\cdot(\nabla\psi) - \chi_s B'(\phi+t\psi)\psi + \rho_p(\phi+t\psi)\,d\Omega - \frac{C}{\beta}\left.\left(\frac{\displaystyle\int_\Gamma \gamma'(\phi+t\psi)\psi\,dS}{\displaystyle\int_\Gamma \gamma(\phi+t\psi)\,dS}\right)\right|_{t=0}\\ &= \int_\Omega -\varepsilon(\nabla\phi)\cdot(\nabla\psi) - \chi_s B'(\phi)\psi + \rho_p\psi\,d\Omega - \int_\Gamma \frac{C\gamma'(\phi)\psi}{\beta\int_\Gamma \gamma(\phi)\,dS}\\ &= \int_\Omega -\varepsilon(\nabla\phi)\cdot(\nabla\psi) - \chi_s B'(\phi)\psi + \rho_p\psi\,d\Omega + \int_\Gamma \rho[\Gamma]q_l\psi\,dS.\end{aligned}$$

In the computation above, the notation Γ is used to indicate any boundary on which the integrand is defined (i.e., both Γ_e and Γ_c). Critical points of the electrostatic potential energy are obtained by setting the result above to 0,

$$\begin{aligned}(206)\qquad &\left(\int_{\Omega} -\varepsilon(\nabla\phi)\cdot(\nabla\psi)\;d\Omega - \int_{\Omega_s} B'(\phi)\psi\;d\Omega + \int_{\Omega} \rho_p\psi\;d\Omega\right)\\ &\qquad + \int_{\Gamma_c} \rho[\Gamma_c]q_l\psi\;dS + \int_{\Gamma_e} \rho[\Gamma_e]q_l\psi\;dS = 0.\end{aligned}$$

Standard calculations show (206) has a solution $\phi = \psi_0$ and that this critical point ψ_0 is the unique maximizer of $G[\Gamma;\cdot]$. The ideas follow the proof in [62], which proves the result for uncharged surfaces.

Next, we will show that (206) is equivalent to the weak form of the Poisson-Boltzmann equation (190). The weak form of the Poisson-Boltzmann equation for a smooth test function $\psi : \Omega \to \mathbb{R}$ is

$$(207)\qquad \int_{\Omega} \nabla\cdot(\varepsilon\nabla\phi)\psi\;d\Omega - \int_{\Omega} \chi_s B'(\phi)\psi\;d\Omega = \int_{\Omega} -\rho_p\psi\;d\Omega.$$

Splitting the first integral in the domains Ω_s, Ω_m, and Ω_p, and using the product rule gives

$$\begin{aligned}&\int_{\Omega_s} \nabla\cdot(\varepsilon_s\nabla\phi^s\psi)\;d\Omega - \int_{\Omega_s} \varepsilon_s(\nabla\phi^s)\cdot(\nabla\psi)\;d\Omega + \int_{\Omega_m} \nabla\cdot(\varepsilon_m\nabla\phi^m\psi)\;d\Omega\\ &\quad - \int_{\Omega_m} \varepsilon_m(\nabla\phi^m)\cdot(\nabla\psi)\;d\Omega + \int_{\Omega_p} \nabla\cdot(\varepsilon_p\nabla\phi^p\psi)\;d\Omega - \int_{\Omega_p} \varepsilon_p(\nabla\phi^p)\cdot(\nabla\psi)\;d\Omega\\ &\quad - \int_{\Omega_s} B'(\phi)\psi\;d\Omega = \int_{\Omega} -\rho_p\psi\;d\Omega.\end{aligned}$$

Now combine the second, fourth, and sixth integrals and use the divergence theorem on the first, third, and fifth integrals to get

$$\begin{aligned}&-\int_{\Omega} \varepsilon(\nabla\phi)\cdot(\nabla\psi)\;d\Omega + \int_{\partial\Omega} \varepsilon_s\psi(\nabla\phi^s)\cdot n\;dS - \int_{\Gamma_c} \varepsilon_s\psi(\nabla\phi^s)\cdot n\;dS\\ &\quad - \int_{\Gamma_e} \varepsilon_s\psi(\nabla\phi^s)\cdot n\;dS - \int_{\Gamma_p} \varepsilon_s\psi(\nabla\phi^s)\cdot n\;dS + \int_{\Gamma_e} \varepsilon_m\psi(\nabla\phi^m)\cdot n\;dS\\ &\quad + \int_{\Gamma_c} \varepsilon_m\psi(\nabla\phi^m)\cdot n\;dS + \int_{\Gamma_p} \varepsilon_p\psi(\nabla\phi^p)\cdot n\;dS - \int_{\Omega_s} B'(\phi)\psi\;d\Omega = -\int_{\Omega} \rho_p\psi\;d\Omega.\end{aligned}$$

Since the test function ψ is compactly supported on Ω, the boundary integrals over $\partial\Omega$ are zero. Combine the boundary integrals over Γ and obtain

$$\begin{aligned}
&\left(-\int_{\Omega} \varepsilon(\nabla\phi)\cdot(\nabla\psi)\, d\Omega - \int_{\Omega_s} B'(\phi)\psi\, d\Omega + \int_{\Omega} \rho_p \psi\, d\Omega \right) \\
&\quad + \left(\int_{\Gamma_c} \psi(\varepsilon_m \nabla\phi^m - \varepsilon_s \nabla\phi^s)\cdot n\, dS \right) + \left(\int_{\Gamma_e} \psi(\varepsilon_m \nabla\phi^m - \varepsilon_s \nabla\phi^s)\cdot n\, dS \right) \\
&\quad + \left(\int_{\Gamma_p} \psi(\varepsilon_p \nabla\phi^p - \varepsilon_s \nabla\phi^s)\cdot n\, dS \right) = 0.
\end{aligned}$$

Next, apply the boundary conditions to the last three integrals to obtain (206), the variational form of the electrostatic potential energy. Therefore, the maximizer ψ_0 of $G[\Gamma;\cdot]$ is also the weak solution to the nonlinear Poisson-Boltzmann equation. □

As a consequence of Theorem 5.8.1, the Euler Lagrange equation for the energy functional (203) is the Poisson-Boltzmann equation (190).

We define the maximization of the electrostatic potential energy to be

$$G[\Gamma] = \max_{\phi \in H^1_g(\Omega)} G[\Gamma;\phi] = G[\Gamma;\psi_0]. \tag{208}$$

Finally, we give a brief summary of the terms in the potential energy (203). The first term, $|\nabla\phi|^2$ describes the energy from the electric field potential, since $\vec{E} = -\nabla\phi$. The second term, $\rho_p\phi$ describes the energy from the charges in the protein. The third term, $B(\phi)$ describes the energy from the mobile ions in the solvent. The final term involving $\gamma(\phi)$ describes the energy from the charged lipids on each leaflet Γ_c and Γ_e.

We have now established the electrostatic energy functional for the protein-membrane system. In the next chapter, we compute the dielectric boundary force on the boundaries of the vesicle membrane Γ_e and Γ_c. This force governs the flow of the membrane.

CHAPTER 6

Dielectric Boundary Force

In this chapter, we compute the dielectric boundary force on the vesicle membrane. The results of this chapter are published in [73]. Recall the physical set up of the system depicted in Figure 5.1. The dielectric boundary force describes the movement of the membrane based on the electrostatic potential energy (203). In order to compute this force, we use techniques from shape calculus as in [62]. To compute the shape derivative, we define a diffeomorphism that perturbs the boundaries of the membrane. This perturbation is in the normal direction of the membrane. Then, important properties of this diffeomorphism are established in terms of its effect on volume elements of Ω and on surface area elements of Γ. Equipped with these properties, we establish the dielectric boundary force.

6.1. Transformation and velocity of the surface

The deformation of the vesicle membrane is governed by a smooth velocity field that vanishes at distances away from the membrane surfaces. We define the velocity function $V \in C^\infty(\mathbb{R}^3, \mathbb{R}^3)$ by the following dynamical system,

$$\begin{cases} \dfrac{dx}{dt} = V(x), \qquad \forall t > 0, \\ x(0) = X, \end{cases} \tag{209}$$

where X is the original position of the membrane and x is the transformed position. We require V to be compactly supported near the bilayer membrane surfaces. In other words, $V(x) = 0$ if $\operatorname{dist}(x, \Gamma) > d$ for some $d > 0$ where Γ is either Γ_c or Γ_e and

$$d < \frac{1}{2} \min \Big\{ \operatorname{dist}\,(\Gamma_e, \partial\Omega), \operatorname{dist}\,(\Gamma_c, \operatorname{supp}\,(\rho_p)), \operatorname{dist}\,(\Gamma_c, \operatorname{supp}\,(\rho_p)) \Big\}. \tag{210}$$

The condition (210) prevents the exterior membrane surface from stretching beyond the containment domain Ω and also prevents either membrane leaflet from overlapping the atoms within the protein.

The solution to (209) defines a diffeomorphism $T_t : \mathbb{R}^3 \to \mathbb{R}^3$ which sends the old coordinates X to the new coordinates x in the time t. We denote this transformation by $T_t(X) = x(t, X)$. We get an approximation for the transformation by computing a Taylor expansion of the velocity field centered at $t = 0$,

$$\begin{aligned} T_t(X) &= x(t, X) \\ &= x(0, X) + t\partial_t x(0, X) + \mathcal{O}(t^2) \\ &= X + tV(x(0, X)) + \mathcal{O}(t^2) \\ &= X + tV(X) + \mathcal{O}(t^2). \end{aligned} \tag{211}$$

In this way, the map $T_t(X)$ agrees with the perturbation of the identity up to the leading term.

The membrane configuration under the transformation $T_t(X)$ results in a new electrostatic potential energy,

$$G[\Gamma_t; \phi] = \int_{\Omega_t} \left[-\frac{\varepsilon}{2} |\nabla\phi|^2 + \rho_p \phi - \chi_s B(\phi) \right] dx + \frac{C}{\beta} \ln \left(\int_{\Gamma_t} \gamma(\phi)\, dS \Big/ \int_{\Gamma_t} dS \right), \tag{212}$$

where each of the functions are computed over the transformed regions $\Omega_t = T_t(\Omega)$, $\Gamma_t = T_t(\Gamma)$. As in (203), the integration on the membrane is not performed on the protein Γ_p, since no lipids are distributed here. Similar to the proof in Theorem 5.8.1, there is a unique maximizer $\psi_t \in H^1_g(\Omega) \cap L^\infty(\Omega)$ that maximizes (212) over $H^1_g(\Omega)$. The maximum is

$$G[\Gamma_t] = \max_{\phi \in H^1_g(\Omega)} G[\Gamma_t; \phi] = G[\Gamma_t; \psi_t]. \tag{213}$$

The same ψ_t is also the unique weak solution to the transformed boundary value problem of the Poisson-Boltzmann equation, given by

$$
\begin{cases}
\nabla \cdot (\varepsilon \nabla \phi) - \chi_s B'(\phi) = -\rho_p, & \text{in } \Omega_t, \\
[\phi] = 0, & \text{on } \Gamma_{c_t}, \Gamma_{e_t}, \Gamma_{p_t}, \\
\varepsilon_s \dfrac{\partial \phi^s}{\partial n}, = \varepsilon_m \dfrac{\partial \phi^m}{\partial n} - \rho[\Gamma_t] q_l, & \text{on } \Gamma_{c_t}, \Gamma_{e_t}, \\
\varepsilon_s \dfrac{\partial \phi^s}{\partial n} = \varepsilon_p \dfrac{\partial \phi^p}{\partial n}, & \text{on } \Gamma_{p_t}, \\
\phi = g, & \text{on } \partial\Omega.
\end{cases}
\tag{214}
$$

Notice that equation (214) is identical to the Poisson-Boltzmann equation (190), except that the domains are transformed by T_t. The transformation $T_t(X)$ defined by (211) acts on volumes and surfaces within Ω. Some useful properties of the transformation are outlined next.

6.1.1. PROPERTIES OF THE TRANSFORMATION ON VOLUMES. The following are properties of the transformation $T_t(X)$ given by (211) on a volume element $dX \in \mathbb{R}^3$. These properties will be used in the computation of the shape derivative and their justifications are found in [22], among other sources.

(T1) Let $X \in \mathbb{R}^3$ and $t \geq 0$. Let $\nabla T_t(X)$ be the Jacobian matrix of T_t at X defined by $(\nabla T_t(X))_{ij} = \partial_j T_t^i(X)$, where T_t^i is the ith component of T_t $(i = 1, 2, 3)$. Let

$$
J_t(X) = \det \nabla T_t(X). \tag{215}
$$

Then, for each X, the function $t \mapsto J_t(X)$ is in C^∞ and at X,

$$
\frac{dJ_t}{dt} = J_t (\nabla \cdot V) \circ T_t. \tag{216}
$$

At $t = 0$, since no time has passed, $\nabla T_0 = I$ for any x and so $J_0(X) = 1$. The continuity of J_t at $t = 0$ implies $J_t > 0$ for $t > 0$ small enough.

(T2) Define $A(t) : \Omega \to \mathbb{R}$ for $t \geq 0$ small enough by

$$A(t) = J_t(\nabla T_t)^{-1}(\nabla T_t)^{-T}, \tag{217}$$

where the notation $(\cdot)^{-T}$ denotes the inverse transpose. At each point in Ω,

$$\begin{aligned} A'(t) = \Big[&((\nabla \cdot V) \circ T_t) - (\nabla T_t)^{-1}\left((\nabla V) \circ T_t\right) \nabla T_t \\ &- (\nabla T_t)^{-1}\left((\nabla V) \circ T_t\right)^T (\nabla T_t)\Big] A(t). \end{aligned} \tag{218}$$

(T3) For any $u \in L^2(\Omega)$ and $t \geq 0$, $u \circ T_t^{-1} \in L^2(\Omega)$. Moreover,

$$\lim_{t\to 0} u \circ T_t = u \qquad \text{and} \qquad \lim_{t\to 0} u \circ T_t^{-1} = u \qquad \text{in } L^2(\Omega). \tag{219}$$

(T4) Let $t \geq 0$ and $u \in H^1(\Omega)$. Then both $u \mapsto u \circ T_t$ and $u \mapsto u \circ T_t^{-1}$ are one-to-one and onto maps from $H^1(\Omega)$ to $H^1(\Omega_t) = H^1(\Omega)$ and $H^1_g(\Omega)$ to $H^1_g(\Omega)$, respectively. Moreover, for any $u \in H^1(\Omega)$,

$$\nabla(u \circ T_t^{-1}) = (\nabla T_t^{-1})^T(\nabla u \circ T_t^{-1}) \qquad \text{and} \qquad \nabla(u \circ T_t) = (\nabla T_t)^T(\nabla u \circ T_t). \tag{220}$$

(T5) For any $u \in H^1(\Omega)$ and $t \geq 0$,

$$\frac{d}{dt}(u \circ T_t) = (\nabla u \cdot V) \circ T_t. \tag{221}$$

The properties are proved in Chapter 9.4 of [22].

6.1.2. PROPERTIES OF THE TRANSFORMATION ON AREAS.

In Section 6.1.1, the properties of the transformation of a volume element were derived. Because our energy functional (203) contains an integral over a 2D surface Γ, an analogous transformation of a surface element must be derived. In this section, we compute a useful property of the transformation T_t on a surface element $dS \in \mathbb{R}^2$. Define the Jacobian of the surface transformation by

$$J_s(X, t) = (\det \nabla T_t(X))\left|\nabla T_t^{-T} n(X)\right|, \tag{222}$$

as in [17], where $n(X)$ is the normal unit normal vector at X. Note that at time $t = 0$, $J_s(X, 0) = (\det I)|In_0| = |n_0(X)| = 1$, since $n(X)$ is a unit vector. Analogous to the transformation on a volume element, the differential surface element is transformed by $ds = J_s\, dS$. The surface transformation property we wish to establish is stated as the following theorem.

THEOREM 6.1.1. *The time derivative of the Jacobian of the surface transformation J_s at $t = 0$ is given by the surface divergence of the velocity,*

$$\left.\frac{dJ_s}{dt}\right|_{t=0} = \nabla_s \cdot V. \tag{223}$$

PROOF. Recall the formula for the Jacobian of the surface transformation given by (222). The derivative of (222) is given by

$$\frac{dJ_s}{dt} = (J_t(\nabla \cdot V) \circ T_t) \left|\nabla T_t^{-T} n\right| + \frac{\det \nabla T_t}{\left|\nabla T_t^{-T} n\right|} (\nabla T_t^{-T} n) \cdot \frac{d}{dt}(\nabla T_t^{-T} n). \tag{224}$$

The derivative in (224) was computed using the product rule, (216), and the fact that the derivative of $|\vec{x}|$ for any vector $\overrightarrow{x(t)} \in \mathbb{R}^3$ is given by

$$\begin{aligned} \frac{d|\vec{x}|}{dt} &= \frac{d}{dt}\sqrt{x_1^2 + x_2^2 + x_3^2} \\ &= \frac{1}{2}(x_1^2 + x_2^2 + x_3^2)^{-1/2}(2x_1\frac{dx_1}{dt} + 2x_2\frac{dx_2}{dt} + 2x_3\frac{dx_3}{dt}) \\ &= \frac{1}{|\vec{x}|}(\vec{x} \cdot \frac{d\vec{x}}{dt}), \end{aligned} \tag{225}$$

so that

$$\frac{d}{dt}\left|\nabla T_t^{-T} n\right| = \frac{1}{\left|\nabla T_t^{-T} n\right|}(\nabla T_t^{-T} n) \cdot \frac{d}{dt}(\nabla T_t^{-T} n).$$

We proceed by simplifying (224). The derivative with respect to t of $(\nabla T_t^{-T} n)$ is

$$\frac{d}{dt}(\nabla T_t^{-T} n) = \frac{d(\nabla T_t^{-T})}{dt} n + \nabla T_t^{-T} \frac{dn}{dt}. \tag{226}$$

There is another way to express (226) that will prove easier for further calculations. Let $\vec{a} = \nabla T_t^{-T} n$ so that $n = \nabla T_t^T \vec{a}$. Then, computing the derivative of n,

$$\frac{dn}{dt} = \frac{d(\nabla T_t^T \vec{a})}{dt} = \frac{d(\nabla T_t^T)}{dt}\vec{a} + \nabla T_t^T \frac{d\vec{a}}{dt}.$$

Therefore,

$$\frac{d\vec{a}}{dt} = (\nabla T_t^{-T}) \left(\frac{dn}{dt} - \frac{d(\nabla T_t^T)}{dt}\vec{a} \right).$$

Replacing $\vec{a}$ gives the alternative form of (226),

$$\frac{d}{dt}(\nabla T_t^{-T} n) = (\nabla T_t^{-T}) \left(\frac{dn}{dt} - \frac{d(\nabla T_t^T)}{dt}(\nabla T_t^{-T})n \right). \tag{227}$$

This equation is more advantageous than (226) because (226) involves computing the derivative of ∇T_t^{-T} whereas (227) only requires the derivative of ∇T_t^T. We compute the derivative of ∇T_t^T with respect to time t next.

First note that the velocity $V(x)$ (209) is $V(x) = dx/dt$. The transformation is defined through the velocity as $T_t(X) = x$. Then,

$$V \circ T_t = V(T_t(X)) = \frac{d(T_t(X))}{dt}.$$

We want to keep track of which variable, x or X, is the variable of differentiation when writing $\nabla(\cdot)$. Write $T_t(X) = T(t, X)$ to emphasize T is a function of X and t (but not x). This allows for the subscript notation of partial derivatives. We adopt the notation $\nabla_x(\cdot)$ or $\nabla_X(\cdot)$ to denote the variable of spatial differentiation x or X when computing $\nabla T(t, \cdot)$. Computing the derivative with respect to time of $\nabla_X T(t, X)$ yields

$$\begin{aligned}\frac{d}{dt}\nabla_X T(t,X) &= \frac{d}{dt}\left(\partial_{X_j} T_i\right)_{1\le i,j\le 3} = \left(\partial_{X_j}\frac{dT_i}{dt}\right)_{1\le i,j\le 3} = \left(\partial_{X_j} V_i(X)\right)_{1\le i,j\le 3} \\ &= \nabla_X V(X).\end{aligned}$$

Then,

$$\nabla_X V(X) = \begin{pmatrix} \frac{\partial V_1}{\partial X_1} & \frac{\partial V_1}{\partial X_2} & \frac{\partial V_1}{\partial X_3} \\ \vdots & \ddots & \vdots \\ \frac{\partial V_3}{\partial X_1} & \dots & \frac{\partial V_3}{\partial X_3} \end{pmatrix} = \begin{pmatrix} \frac{\partial V_1}{\partial x_1} & \frac{\partial V_1}{\partial x_2} & \frac{\partial V_1}{\partial x_3} \\ \vdots & \ddots & \vdots \\ \frac{\partial V_3}{\partial x_1} & \dots & \frac{\partial V_3}{\partial x_3} \end{pmatrix} \begin{pmatrix} \frac{\partial x_1}{\partial X_1} & \frac{\partial x_1}{\partial X_2} & \frac{\partial x_1}{\partial X_3} \\ \vdots & \ddots & \vdots \\ \frac{\partial x_3}{\partial X_1} & \dots & \frac{\partial x_3}{\partial X_3} \end{pmatrix}$$

$$= (\nabla_x V(x))(\nabla_X T(t, X)).$$

This establishes

$$\frac{d}{dt}\nabla_X T(t, X) = (\nabla_x V(x))(\nabla_X T(t, X)). \tag{228}$$

From (228) and the fact that the derivative of the transpose of a matrix is the transpose of the derivative,

$$\frac{d}{dt}\nabla T_t^T = \left((\nabla V)(\nabla T_t)\right)^T. \tag{229}$$

The equation (229) may be substituted in (227), which may in turn be substituted into (224), but we choose to substitute everything at the end of the section for neatness.

Next, we establish a formula for the normal derivative dn/dt at time $t = 0$. Let u and v parametrize a surface in $\mathbb{R}^3$ and define the surface by

$$\vec{r}(u, v) = (x(u, v), y(u, v), z(u, v)). \tag{230}$$

With this parameterization of the surface, the transformation T_t acting on the surface can be defined as

(231)

$$T_t(x(u, v), y(u, v), z(u, v)) = (x(u, v) + \alpha(u, v, t), y(u, v) + \beta(u, v, t), z(u, v) + \gamma(u, v, t))$$

$$= \vec{r}(u, v) + \vec{s}(u, v, t),$$

where $\vec{s}(u,v,t) = (\alpha(u,v,t), \beta(u,v,t), \gamma(u,v,t))$. Note that $\vec{s}$ depends in t but $\vec{r}$ is independent of t. Next, define the (initial) normal vector to the surface by the identity

$$n(X,0) = \frac{r_u \times r_v}{|r_u \times r_v|}, \tag{232}$$

where the subscripts denote partial derivatives. Then, at any time $t > 0$, the transformed normal vector is calculated by applying (231) to the initial normal vector (232),

$$n(X,t) = \frac{(r_u + s_u) \times (r_v + s_v)}{|(r_u + s_u) \times (r_v + s_v)|}. \tag{233}$$

For simplicity, let $\zeta = (r_u + s_u) \times (r_v + s_v)$. Next, the initial time rate of change of (233) is computed,

$$\begin{aligned} \frac{dn(X,0)}{dt} &= \frac{d}{dt}\left(\frac{\zeta}{|\zeta|}\right)\Bigg|_{t=0} \\ &= \left(\frac{1}{|\zeta|}\frac{d\zeta}{dt} + \zeta\frac{d}{dt}\left(\frac{1}{|\zeta|}\right)\right)\Bigg|_{t=0}. \end{aligned} \tag{234}$$

Define

$$P = \frac{1}{|\zeta|}\frac{d\zeta}{dt} \qquad \text{and} \qquad Q = \zeta\frac{d}{dt}\left(\frac{1}{|\zeta|}\right).$$

The time derivative $\frac{dP}{dt}$ can be computed using the product rule for cross products,

$$\frac{d}{dt}(A \times B) = \left(\frac{dA}{dt} \times B\right) + \left(A \times \frac{dB}{dt}\right). \tag{235}$$

Then the derivative of P at $t = 0$ is

$$\begin{aligned} \frac{dP}{dt}\bigg|_{t=0} &= \frac{1}{|\zeta|}\frac{d}{dt}((r_u + s_u) \times (r_v + s_v))\bigg|_{t=0} \\ &= \frac{1}{|\zeta|}\left[\left(\frac{d}{dt}(r_u + s_u)\right) \times (r_v + s_v) + (r_u + s_u) \times \left(\frac{d}{dt}(r_v + s_v)\right)\right]\Bigg|_{t=0} \\ &= \frac{1}{|(r_u + s_u) \times (r_v + s_v)|}\left(\frac{ds_u}{dt} \times (r_v + s_v) + (r_u + s_u) \times \frac{ds_v}{dt}\right)\Bigg|_{t=0} \\ &= \frac{1}{|r_u \times r_v|}\left(\frac{ds_u}{dt} \times r_v + r_u \times \frac{ds_v}{dt}\right). \end{aligned}$$

To compute the initial time derivative of Q, first notice that by using (225) and the chain rule, we have

$$\frac{d}{dt}\left(\frac{1}{|\vec{x}|}\right) = \frac{-1}{|\vec{x}|^3}\left(\vec{x}\cdot\frac{d\vec{x}}{dt}\right).$$

Using this result for $1/|\zeta|$, the initial derivative of Q is

$$\begin{aligned}\left.\frac{dQ}{dt}\right|_{t=0} &= \left((r_u+s_u)\times(r_v+s_v)\right)\left.\frac{d}{dt}\left(\frac{1}{|\zeta|}\right)\right|_{t=0}\\ &= \left((r_u+s_u)\times(r_v+s_v)\right)\left.\frac{-1}{|\zeta|^3}(\zeta\cdot\frac{d\zeta}{dt})\right|_{t=0}\\ &= (r_u\times r_v)\frac{-1}{|r_u\times r_v|^3}\left((r_u\times r_v)\cdot\left(\frac{ds_u}{dt}\times r_v + r_u\times\frac{ds_v}{dt}\right)\right).\end{aligned}$$

Now we have a formula for dn/dt,

$$\begin{aligned}\frac{dn(X,0)}{dt} &= \frac{1}{|r_u\times r_v|}\left(\frac{ds_u}{dt}\times r_v + r_u\times\frac{ds_v}{dt}\right)+\\ &\quad + (r_u\times r_v)\frac{-1}{|r_u\times r_v|^3}\left((r_u\times r_v)\cdot\left(\frac{ds_u}{dt}\times r_v + r_u\times\frac{ds_v}{dt}\right)\right).\end{aligned}\tag{236}$$

To simplify, we define

$$R = \frac{ds_u}{dt}\times r_v + r_u\times\frac{ds_v}{dt}.$$

Then

$$\begin{aligned}\frac{dn(X,0)}{dt} &= \frac{1}{|r_u\times r_v|}R + (r_u\times r_v)\frac{-1}{|r_u\times r_v|^3}\left((r_u\times r_v)\cdot R\right)\\ &= \frac{1}{|r_u\times r_v|}\left[R - \frac{r_u\times r_v}{|r_u\times r_v|}\left(\frac{r_u\times r_v}{|r_u\times r_v|}\cdot R\right)\right]\\ &= \frac{1}{|r_u\times r_v|}\left[R - n(X,0)\left(n(X,0)\cdot R\right)\right].\end{aligned}$$

That is,

$$\frac{dn(X,0)}{dt} = \frac{1}{|r_u\times r_v|}\left[R - n(X,0)\left(n(X,0)\cdot R\right)\right].\tag{237}$$

To finish simplifying the formula (224) requires substituting (229) and an expression lengthier than (236) into (227) and substituting the result into (224). The final expression for $\frac{dJ_s}{dt}$ for arbitrary $t > 0$ would be exceedingly long, and the expression is unnecessary for the calculations of the shape derivative of G_2. In fact, only the derivative of J_s evaluated at

$t = 0$ is useful. To compute this quantity, we notice that by (229) it follows

$$\left.\frac{d}{dt}\nabla T_t^T\right|_{t=0} = ((\nabla V)(\nabla T_0))^T = (\nabla V)^T, \tag{238}$$

where the ∇ operator acting on $T_t^T(X)$ is with respect to X and the one acting on $V(x)$ is with respect to x. Now, substituting (227), (238), and (237) into (224) when $t = 0$ gives the result,

$$\begin{aligned}
\left.\frac{dJ_s}{dt}\right|_{t=0} &= (J_0(\nabla \cdot V) \circ T_0) \left|\nabla T_0^{-T} n\right| \\
&\qquad + (\det \nabla T_0) \left(\frac{1}{\left|\nabla T_0^{-T} n\right|} (\nabla T_0^{-T} n) \cdot \left.\frac{d}{dt}(\nabla T_t^{-T} n)\right|_{t=0} \right) \\
&= \nabla \cdot V + \left.\left(n \cdot \frac{d}{dt}(\nabla T_t^{-T} n) \right)\right|_{t=0} \\
&= \nabla \cdot V + \left(n \cdot \left(\left.\frac{dn}{dt}\right|_{t=0} - \left.\left(\frac{d(\nabla T_t^T)}{dt} (\nabla T_t^{-T}) n \right)\right|_{t=0} \right) \right. \\
&= \nabla \cdot V + n \cdot \left(\frac{dn(X,0)}{dt} - (\nabla V)^T n \right) \\
&= \nabla \cdot V + n \cdot \frac{1}{|r_u \times r_v|} \left(R - n\,(n \cdot R)\right) - n \cdot (\nabla V)^T n,
\end{aligned}$$

where $n = n(X, 0)$ is the initial unit normal. Notice that $n(n \cdot R)$ is the component of R in the direction of n. Then, $R - n(n \cdot R)$ is the component of R perpendicular to n. Thus, $n \cdot (R - n(n \cdot R)) = 0$. This leads to

$$\left.\frac{dJ_s}{dt}\right|_{t=0} = \nabla \cdot V - n \cdot (\nabla V)^T n. \tag{239}$$

Next, notice that for any matrix A and vector $\vec{x}$, $x \cdot A^T x = x \cdot Ax$. This formula can be verified by expanding the matrix-vector product in component form and rearranging the terms. This reduces (239) to

$$\left.\frac{dJ_s}{dt}\right|_{t=0} = \nabla \cdot V - n \cdot (\nabla V) n. \tag{240}$$

Finally, notice that this is the formula for surface divergence, as in (5). This leads to the final form of the initial time derivative of J_s,

$$\left.\frac{dJ_s}{dt}\right|_{t=0} = \nabla_s \cdot V. \tag{241}$$

□

We conclude this section with a useful property for closed surfaces.

Lemma 6.1.1. *The surface divergence of any continuous function F on a closed surface is 0,*

$$\iint_\Gamma (\nabla_s \cdot F)\, dS = 0. \tag{242}$$

Proof. The proof follows directly from the 2D divergence theorem,

$$\iint_\Gamma (\nabla \cdot F)\, dS = \oint_{\partial\Gamma} F \cdot n \, d\sigma = \int_{\partial\Gamma} F \cdot n_1 \, d\sigma + \int_{\partial\Gamma} F \cdot n_2 \, d\sigma, \tag{243}$$

Since Γ is a closed surface, the outward normal directions to the boundary $\partial\Gamma$ are opposite in sign. Therefore, the two integrals in (243) cancel, giving the desired result. □

6.2. Shape derivative computation

In this section, we compute the shape derivative of the electrostatic potential energy with respect to the boundary. This computation provides a convenient way to extract F_n, the normal component of the dielectric boundary force, through the Hadamard-Zolésio structure theorem of Shape Calculus:

Theorem 6.2.1. *Consider the functional G with sufficiently smooth domain Γ. Then, for $F_n \in L^1(\Gamma)$, the shape derivative of G with respect to Γ in the direction of V is*

$$\delta_\Gamma G[\Gamma] = \int_\Gamma -F_n (V \cdot n)\, dS, \tag{244}$$

where n is the unit normal to the surface.

Proof. A proof of this theorem can be found in [23, 98]. $\square$

We point out that under these conditions, the shape derivative is in the direction normal to the velocity of the deformation; therefore, only the normal component of the dielectric boundary force determines the motion on the boundary. We will prove that the force is given by

$$\begin{aligned} F_n = &-\frac{\varepsilon_s}{2}|\nabla\psi_0^s|^2 + \frac{\varepsilon_m}{2}|\nabla\psi_0^m|^2 - \varepsilon_m|\nabla\psi_0^m\cdot n|^2 + \varepsilon_m(\nabla\psi_0^s\cdot n)(\nabla\psi_0^m\cdot n) \\ &- B(\psi_0) - q_l\rho[\Gamma](\nabla\psi_0^s\cdot n), \end{aligned} \tag{245}$$

which is the main result of this chapter.

To set up the theorem, let $V \in C^\infty(\mathbb{R}^3, \mathbb{R}^3)$ be a smooth map that vanishes outside a small neighborhood of the membrane surface Γ. That is, $V(X) = 0$ if $\operatorname{dist}(X, \Gamma) > d$ for some $d > 0$ satisfying (210). Let the transformations $T_t (t \geq 0)$ be defined by (209). For $t > 0$ the electrostatic free energy is given by (213), where the functional $G[\Gamma_t; \cdot]$ is given in (212) and ψ_t is the weak solution to (214). For $t = 0$, the electrostatic free energy is given by (208), where the functional $G[\Gamma; \cdot]$ is given in (203) and ψ_0 is the weak solution to (190).

Theorem 6.2.2. *Let $\rho_p \in H^1(\Omega)$. Then the shape derivative of the electrostatic free energy $G[\Gamma]$ given by* (203) *in the direction of V is given by*

$$\begin{aligned} \delta_\Gamma G[\Gamma] = \int_\Gamma \Bigg(&\frac{\varepsilon_s}{2}|\nabla\psi_0^s|^2 - \frac{\varepsilon_m}{2}|\nabla\psi_0^m|^2 + \varepsilon_m|\nabla\psi_0^m\cdot n|^2 - \varepsilon_m(\nabla\psi_0^s\cdot n)(\nabla\psi_0^m\cdot n) \\ &+ B(\psi_0) + q_l\rho[\Gamma](\nabla\psi_0^s\cdot n)\Bigg)(V\cdot n)\, dS. \end{aligned} \tag{246}$$

Proof. The proof is divided into four steps:

i First, the energy functional is computed in the transformed coordinates through a new function $z(t, \phi)$. A change of variables brings z back to the reference coordinates, and then z is differentiated with respect to time.

ii Second, the difference quotient corresponding to the shape derivative is squeezed between two realizations of $\partial_t z$.

iii Third, the inequality is passed to the limit as $t \to 0$ and it is shown that the two realizations of $\partial_t z$ are identical in the limit, and hence equal to the shape derivative.

iv Fourth and finally, the result is simplified to match the final form.

The computations to determine the shape derivative of (203) is completed in two calculations by splitting (203) into two components,

$$G_1[\Gamma;\phi] = \int_\Omega \left[-\frac{\varepsilon}{2}|\nabla\phi|^2 + \rho_p\phi - \chi_s B(\phi)\right] dX, \tag{247}$$

and

$$G_2[\Gamma;\phi] = -\frac{C}{\beta}\ln\left(\int_{\Gamma_{c,e}} \gamma(\phi)\, dS(X) \Big/ \int_{\Gamma_{c,e}} dS(X)\right), \tag{248}$$

where $G[\Gamma;\phi] = G_1[\Gamma;\phi] + G_2[\Gamma;\phi]$. We have the analagous splitting for (212),

$$G_1[\Gamma_t;\phi] = \int_{\Omega_t} \left[-\frac{\varepsilon}{2}|\nabla\phi|^2 + \rho_p\phi - \chi_s B(\phi)\right] dx, \tag{249}$$

and

$$G_2[\Gamma_t;\phi] = -\frac{C}{\beta}\ln\left(\int_{\Gamma_t} \gamma(\phi)\, dS(x) \Big/ \int_{\Gamma_t} dS(x)\right). \tag{250}$$

Step 1. *The energy functional is computed in the transformed coordinates through a new function $z(t,\phi)$. A change of variables brings z back to the reference coordinates, and then z is differentiated with respect to time.*

Let $t \geq 0$ be sufficiently small. Since each $\phi \in H_g^1(\Omega)$ corresponds uniquely to $\phi \circ T_t^{-1} \in H_g^1(\Omega)$, i.e., the map $\phi \in H_g^1(\Omega) \to \phi \circ T_t^{-1} \in H_g^1(\Omega)$ is an isomorphism, then by (213), we have

$$G[\Gamma_t] = \max_{\phi \in H_g^1(\Omega)} G[\Gamma_t, \phi \circ T_t^{-1}].$$

This takes the transformed coordinates $x = T_t(X)$ back into the original coordinates, for which information is known. Let $\phi \in H^1(\Omega) \cap L^\infty(\Omega)$ and $t \geq 0$ and denote

$$z(t, \phi) = G[\Gamma_t, \phi \circ T_t^{-1}]. \tag{251}$$

The function z is split into two components, z_1, corresponding the functional G_1 (247), and z_2 corresponding to the functional G_2 (248).

$$z_1(t, \phi) = G_1[\Gamma_t, \phi \circ T_t^{-1}], \tag{252}$$

$$z_2(t, \phi) = G_2[\Gamma_t, \phi \circ T_t^{-1}], \tag{253}$$

$$z(t, \phi) = z_1(t, \phi) + z_2(t, \phi). \tag{254}$$

The function $z_1(t, \phi)$ is considered first.

Remember that J_t =det$(\nabla T_t(X))$ by equation (215). Since $t \mapsto J_t(X)$ is continuous and $J_0(X) = 1$ at each $X \in \Omega$, $\exists\, \tau > 0$ such that $J_t(X) > 0$ $\forall t \in [0, \tau]$ and $\forall X \in \Omega$. Let $t \in [0, \tau]$ and $\phi \in H^1(\Omega) \cap L^\infty(\Omega)$. Consider

$$\begin{aligned}
z_1(t, \phi) &= G_1[\Gamma_t, \phi \circ T_t^{-1}], && \text{by (252)},\\
&= \int_\Omega \Big[-\frac{\varepsilon}{2} |\nabla(\phi \circ T_t^{-1})|^2 + \rho_p(\phi \circ T_t^{-1}) - \chi_s(B(\phi) \circ T_t^{-1}) \Big]\, dx, && \text{by (249)},\\
&= \int_\Omega \Big[-\frac{\varepsilon}{2} |\nabla(\phi \circ T_t^{-1})|^2 + \rho_p(\phi \circ T_t^{-1}) - \chi_s(B(\phi) \circ T_t^{-1}) \Big]\, dx, && \text{by (220)},\\
&= \int_\Omega \Big[-\frac{\varepsilon}{2} A(t) \nabla\phi \cdot \nabla\phi + (\rho_p \circ T_t)\phi J_t - \chi_s B(\phi) J_t \Big]\, dX, && \text{by } x = T_t(X),
\end{aligned}$$

where $A(t)$ is given by (217). The details of the transformation are not obvious. Note that the functions are transformed according to $\phi \circ T_t^{-1}(x) = \phi(X)$ and $\rho_p(x) = \rho_p(T_t(X)) = \rho_p \circ T_t(X)$. Remember that the gradient operators also need to be transformed. The details of the transformation of the first term is shown below.

$$\begin{aligned}
\int_\Omega |\nabla_x(\phi\circ T_t^{-1})(x)|^2\,dx &= \int_\Omega |\nabla_x\phi(X)|^2\ \det(\nabla T_t)\,dX \\
&= \int_\Omega \left| \begin{pmatrix} \frac{\partial X_1}{\partial x_1} & \frac{\partial X_2}{\partial x_1} & \frac{\partial X_3}{\partial x_1} \\ \vdots & \ddots & \vdots \\ \frac{\partial X_1}{\partial x_3} & \dots & \frac{\partial X_3}{\partial x_3} \end{pmatrix} \begin{pmatrix} \frac{\partial\phi}{\partial X_1} \\ \frac{\partial\phi}{\partial X_2} \\ \frac{\partial\phi}{\partial X_3} \end{pmatrix} \right|^2 \det(\nabla T_t)\,dX \\
&= \int_\Omega \left|(\nabla_X T_t)^{-T}(\nabla_X\phi)\right|^2 \det(\nabla T_t)\,dX \\
&= \int_\Omega \left((\nabla T_t)^{-T}\nabla\phi\right)^T\cdot\left((\nabla T_t)^{-T}\nabla\phi\right)\det(\nabla T_t)\,dX \\
&= \int_\Omega (\nabla\phi)^T(\nabla T_t)^{-1}(\nabla T_t)^{-T}(\nabla\phi)\det(\nabla T_t)\,dX.
\end{aligned}$$

Now, since $(\nabla T_t)^{-1}(\nabla T_t)^{-T}$ is symmetric, we can move it to the end and use $A(t)$ as in (217) to get the desired result,

$$\begin{aligned}
\int_\Omega (\nabla\phi)^T(\nabla T_t)^{-1}(\nabla T_t)^{-T}(\nabla\phi)\nabla T_t\,dX &= \int_\Omega (\nabla\phi)^T(\nabla\phi)\det(\nabla T_t)(\nabla T_t)^{-1}(\nabla T_t)^{-T}\,dX \\
&= \int_\Omega (\nabla\phi)^T(\nabla\phi)A(t)\,dX \\
&= \int_\Omega A(t)\nabla\phi\cdot\nabla\phi\,dX.
\end{aligned}$$

This shows the details of the first term in the change of coordinates. The other terms in $z_1(t,\phi)$ above are found in a similar fashion.

By properties (T1), (T2), and (T5), each term in the integrand of $z_1(t,\phi)$ is differentiable with respect to t. Note that $\phi(X)$ does not depend on t. The following derivative is later proven to be the shape derivative at $t=0$,

$$\begin{aligned}
\partial_t z_1(t,\phi) &= \int_\Omega \Big[-\frac{\varepsilon}{2}A'(t)\nabla\phi\cdot\nabla\phi + (\partial_t(\rho_p\circ T_t))\phi J_t + (\rho_p\circ T_t)\phi\partial_t J_t - \chi_s B(\phi)\partial_t J_t\Big]\,dX \\
&= \int_\Omega \Big[-\frac{\varepsilon}{2}A'(t)\nabla\phi\cdot\nabla\phi + ((\nabla\rho_p\cdot V)\circ T_t))\phi J_t + (\rho_p\circ T_t)\phi((\nabla\cdot V)\circ T_t)J_t \\
&\qquad - \chi_s B(\phi)((\nabla\cdot V)\circ T_t)J_t\Big]\,dX,
\end{aligned}$$

where $A'(t)$ is given by (218). The second term follows from (221) and the third and fourth from (216). Continuing the calculation,

$$\begin{aligned}\partial_t z_1(t,\phi) = \int_\Omega \Big[& -\frac{\varepsilon}{2} A'(t)\nabla\phi\cdot\nabla\phi + ((\nabla\cdot(\rho_p V))\circ T_t)\phi J_t \\ & - \chi_s B(\phi)((\nabla\cdot V)\circ T_t)J_t\Big]\, dX.\end{aligned} \tag{255}$$

The middle terms reduced due to the product rule of the del operator (3), and for arbitrary functions f, g, h, $(fg)\circ h = (f\circ h)(g\circ h)$.

Next, the form of $z_2(t,\phi)$ is established. Using (253), (248), and a transformation of coordinates $x = T_t(X)$,

$$\begin{aligned} z_2(t,\phi) &= G_2[\Gamma_t; \phi\circ T_t^{-1}] \\ &= -\frac{C}{\beta}\ln\left(\int_{\Gamma_t}\gamma(\phi\circ T_t^{-1})(x)\, dS(x) \Big/ \int_{\Gamma_t} dS(x)\right) \\ &= -\frac{C}{\beta}\ln\left(\int_{\Gamma_0}\gamma(\phi(X))J_s(X,t)\, dS(X) \Big/ \int_{\Gamma_0} J_s(X,t)\, dS(X)\right), \end{aligned} \tag{256}$$

where the formula for J_s is given by (222). Differentiating with respect to t,

$$\partial_t z_2(t,\phi) = -\frac{C}{\beta}\left(\frac{\displaystyle\int_{\Gamma_0}\gamma(\phi)\frac{dJ_s(X,t)}{dt}\, dS(X)}{\displaystyle\int_{\Gamma_0}\gamma(\phi)J_s(X,t)\, dS(X)} - \frac{\displaystyle\int_{\Gamma_0}\frac{dJ_s(X,t)}{dt}\, dS(X)}{\displaystyle\int_{\Gamma_0}J_s(X,t)\, dS(X)}\right). \tag{257}$$

Then, the full form of $\partial_t z(t,\phi)$ is given by combining (255) and (257),

$$\begin{aligned} &\partial_t z(t,\phi) \\ &\quad = \int_\Omega \Big[-\frac{\varepsilon}{2}A'(t)\nabla\phi\cdot\nabla\phi + ((\nabla\cdot(\rho_p V))\circ T_t)\phi J_t - \chi_s B(\phi)((\nabla\cdot V)\circ T_t)J_t\Big]\, dX \\ &\qquad - \frac{C}{\beta}\left(\frac{\displaystyle\int_{\Gamma_0}\gamma(\phi)\frac{dJ_s(X,t)}{dt}\, dS(X)}{\displaystyle\int_{\Gamma_0}\gamma(\phi)J_s(X,t)\, dS(X)} - \frac{\displaystyle\int_{\Gamma_0}\frac{dJ_s(X,t)}{dt}\, dS(X)}{\displaystyle\int_{\Gamma_0}J_s(X,t)\, dS(X)}\right). \end{aligned} \tag{258}$$

Step 2. *The difference quotient corresponding to the shape derivative is squeezed between two realizations of* $\partial_t z$ (258)*.*

Let $t \in (0, \tau]$. Since $\psi_t \in H^1_g(\Omega) \cap L^\infty(\Omega)$ and $\psi_0 \in H^1_g(\Omega) \cap L^\infty(\Omega)$ maximize $G[\Gamma_t, \cdot]$ and $G[\Gamma, \cdot]$, respectively, over $H^1_g(\Omega)$ we have

$$G[\Gamma_t, \psi_0 \circ T_t^{-1}] \le G[\Gamma_t, \psi_t] = G[\Gamma_t], \tag{259}$$

$$G[\Gamma, \psi_t] \le G[\Gamma, \psi_0] = G[\Gamma], \tag{260}$$

$$G[\Gamma, \psi_t \circ T_t] \le G[\Gamma, \psi_0] = G[\Gamma]. \tag{261}$$

By (259),

$$\frac{G[\Gamma_t, \psi_0 \circ T_t^{-1}] - G[\Gamma, \psi_0]}{t} \le \frac{G[\Gamma_t] - G[\Gamma]}{t}.$$

By (261),

$$\frac{G[\Gamma_t] - G[\Gamma]}{t} \le \frac{G[\Gamma_t, \psi_t] - G[\Gamma, \psi_t \circ T_t]}{t}.$$

Putting the two inequalities together with the definition in (251) gives

$$\frac{z(t, \psi_0) - z(0, \psi_0)}{t} \le \frac{G[\Gamma_t] - G[\Gamma]}{t} \le \frac{z(t, \psi_t \circ T_t) - z(0, \psi_t \circ T_t)}{t}. \tag{262}$$

Notice that the far left expression of the inequality (262) is the secant line of $z(\cdot, \psi_0)$ from 0 to $t \le \tau$, and the far right expression is the secant line of $z(\cdot, \psi_t \circ T_t)$ from 0 to $t \le \tau$. Since z is differentiable on $t \ge 0$, we can apply the Mean Value Theorem to each expression. That is, there exists $\xi(t), \eta(t) \in [0, t]$ for each $t \in (0, \tau]$ such that

$$\partial_t z(\xi(t), \psi_0) \le \frac{G[\Gamma_t] - G[\Gamma]}{t} \le \partial_t z(\eta(t), \psi_t \circ T_t), \qquad \forall t \in (0, \tau]. \tag{263}$$

Step 3. *The inequality* (263) *is passed to the limit as* $t \to 0$*, and it is shown that the two realizations of* $\partial_t z$ *are identical in the limit and hence equal to the shape derivative.*

We claim

$$\lim_{t\to 0} \partial_t z(\xi(t), \psi_0) = \partial_t z(0, \psi_0), \tag{264}$$

$$\lim_{t\to 0} \partial_t z(\eta(t), \psi_t \circ T_t) = \partial_t z(0, \psi_0). \tag{265}$$

As in Step 1, the the proofs of (264) and (265) are split into the corresponding z_1 and z_2 components,

$$\lim_{t\to 0} \partial_t z_1(\xi(t), \psi_0) = \partial_t z_1(0, \psi_0), \tag{266}$$

$$\lim_{t\to 0} \partial_t z_1(\eta(t), \psi_t \circ T_t) = \partial_t z_1(0, \psi_0), \tag{267}$$

$$\lim_{t\to 0} \partial_t z_2(\xi(t), \psi_0) = \partial_t z_2(0, \psi_0), \tag{268}$$

$$\lim_{t\to 0} \partial_t z_2(\eta(t), \psi_t \circ T_t) = \partial_t z_2(0, \psi_0). \tag{269}$$

We will prove (269) here. The proofs for (266) and (267) are proved in [62] and the proof of (268) is similar and easier than (269). Let $\eta(t) \in [0, t]$ and consider passing $\partial_t z_2(\eta(t), \psi_t \circ T_t)$ to the limit as $t \to 0$,

$$\begin{aligned}
\partial_t z_2(\eta(t), \psi_t \circ T_t) &= -\frac{C}{\beta}\left(\frac{\displaystyle\int_{\Gamma_0} \gamma(\psi_t \circ T_t)\frac{dJ_s(X,\eta(t))}{dt}\, dS(X)}{\displaystyle\int_{\Gamma_0} \gamma(\psi_t \circ T_t) J_s(X,\eta(t))\, dS(X)} - \frac{\displaystyle\int_{\Gamma_0} \frac{dJ_s(X,\eta(t))}{dt}\, dS(X)}{\displaystyle\int_{\Gamma_0} J_s(X,\eta(t))\, dS(X)}\right) \\
&\to -\frac{C}{\beta}\left(\frac{\displaystyle\int_{\Gamma_0} \gamma(\psi_0)\frac{dJ_s(X,0)}{dt}\, dS(X)}{\displaystyle\int_{\Gamma_0} \gamma(\psi_0) J_s(X,0)\, dS(X)} - \frac{\displaystyle\int_{\Gamma_0} \frac{dJ_s(X,0)}{dt}\, dS(X)}{\displaystyle\int_{\Gamma_0} J_s(X,0)\, dS(X)}\right) \\
&= \partial_t z_2(0, \psi_0).
\end{aligned}$$

This establishes (269). Now take the limit of the inequality (263) as $t \to 0$ and use (264) and (265), with the computation (258) to get the shape derivative of G,

$$\begin{aligned} \delta_\Gamma G[\Gamma] &= \lim_{t\to 0} \frac{G[\Gamma_t] - G[\Gamma]}{t} = \partial_t z(0, \psi_0) \\ &= \int_\Omega \left[-\frac{\varepsilon}{2} A'(0) \nabla\psi_0 \cdot \nabla\psi_0 + (\nabla \cdot (\rho_p V))\psi_0 - \chi_s B(\psi_0)(\nabla \cdot V) \right] dX \\ &\quad - \frac{C}{\beta} \left(\frac{\displaystyle\int_{\Gamma_0} \gamma(\psi_0) \frac{dJ_s(X,0)}{dt} \, dS(X)}{\displaystyle\int_{\Gamma_0} \gamma(\psi_0) J_s(X,0) \, dS(X)} - \frac{\displaystyle\int_{\Gamma_0} \frac{dJ_s(X,0)}{dt} \, dS(X)}{\displaystyle\int_{\Gamma_0} J_s(X,0) \, dS(X)} \right). \end{aligned} \tag{270}$$

Step 4. *The final step is to simplify* (270) *to match the final form* (246).

As in the previous steps, we begin the simplifications with z_1 and then move to those for z_2. The combined results will give the shape derivative. The first part of (270) is

$$\partial_t z_1(0, \psi_0) = \int_\Omega \left[-\frac{\varepsilon}{2} A'(0) \nabla\psi_0 \cdot \nabla\psi_0 + (\nabla \cdot (\rho_p V))\psi_0 - \chi_s B(\psi_0)(\nabla \cdot V) \right] dX.$$

Since $A'(0) = (\nabla \cdot V - 2\nabla V)A(0)$, and $A(0) = I$, the above equation can be reduced to

$$\begin{aligned} \partial_t z_1(0, \psi_0) &= \int_\Omega -\frac{\varepsilon}{2} (\nabla \cdot V) \nabla\psi_0 \cdot \nabla\psi_0 \, dX + \int_\Omega \varepsilon (\nabla V) \nabla\psi_0 \cdot \nabla\psi_0 \, dX \\ &\quad + \int_\Omega (\nabla \cdot (\rho_p V))\psi_0 \, dX - \int_{\Omega_s} B(\psi_0)(\nabla \cdot V) \, dX. \end{aligned} \tag{271}$$

Consider the third term of (271). By applying the product rule for the divergence operator (3) successively,

$$\begin{aligned}
&\int_\Omega (\nabla \cdot (\rho_p V))\psi_0 \, dX \\
&\qquad = \int_\Omega \rho_p (\nabla \cdot V)\psi_0 \, dX + \int_\Omega V \cdot (\nabla \rho_p)\psi_0 \, dX \\
&\qquad = \int_\Omega \rho_p (\nabla \cdot (V\psi_0)) \, dX - \int_\Omega \rho_p (V \cdot \nabla \psi_0) \, dX + \int_\Omega V \cdot (\nabla \rho_p)\psi_0 \, dX \\
&\qquad = \int_\Omega \nabla \cdot (\rho_p V \psi_0) \, dX - \int_\Omega V\psi_0 \cdot \nabla \rho_p \, dX \\
&\qquad\quad - \int_\Omega \rho_p (V \cdot \nabla \psi_0) \, dX + \int_\Omega V \cdot (\nabla \rho_p)\psi_0 \, dX.
\end{aligned}$$

Notice that the second and fourth terms on the right-hand side cancel. Finally, use the divergence theorem (2) to see

$$\begin{aligned}
\int_\Omega (\nabla \cdot (\rho_p V))\psi_0 \, dX &= \int_\Omega \nabla \cdot (\rho_p V \psi_0) \, dX - \int_\Omega \rho_p (V \cdot \nabla \psi_0) \, dX \\
&= \int_{\partial\Omega} (\rho_p V \psi_0) \cdot n \, dS - \int_\Omega \rho_p (V \cdot \nabla \psi_0) \, dX.
\end{aligned}$$

But since $V = 0$ on $\partial\Omega$, and since ρ_p is only defined on Ω_p, the third term of (271) reduces to

$$\int_\Omega (\nabla \cdot (\rho_p V))\psi_0 \, dX = -\int_{\Omega_p} \rho_p (V \cdot \nabla \psi_0) \, dX. \tag{272}$$

Next, consider the final term of (271) disregarding the sign in front. Again by applying the product rule of the divergence operator (3),

$$\int_{\Omega_s} B(\psi_0)(\nabla \cdot V) \, dX = \int_{\Omega_s} \nabla \cdot (B(\psi_0)V) \, dX - \int_{\Omega_s} V \cdot (\nabla B(\psi_0)) \, dX$$

Now use the divergence theorem (2) again, noting that Ω_s has more than one boundary, namely $\partial\Omega$ and Γ (where Γ includes Γ_c, Γ_e, and Γ_p).

$$\begin{aligned}\int_{\Omega_s} B(\psi_0)(\nabla\cdot V)\,dX &= \int_{\Omega_s}\nabla\cdot(B(\psi_0)V)\,dX - \int_{\Omega_s} V\cdot(\nabla B(\psi_0))\,dX\\ &= \int_{\partial\Omega} B(\psi_0)V\cdot n\,dS - \int_{\Gamma} B(\psi_0)V\cdot n\,dS - \int_{\Omega_s} V\cdot(\nabla B(\psi_0))\,dX\end{aligned}$$

Notice that the second integral above is negative. This is because each n on Γ is defined to be the outward normal to Ω_m and Ω_p, but n is directed inwardly as observed from Ω_s (see Figure 5.1). Now, since $V = 0$ on $\partial\Omega$, the first integral above is 0. Furthermore, we can apply the chain rule to B and rearrange the order of the dot product in the third integral above to see

$$\int_{\Omega_s} B(\psi_0)(\nabla\cdot V)\,dX = -\int_{\Gamma} B(\psi_0)V\cdot n\,dS - \int_{\Omega_s} B'(\psi_0)(\nabla\psi_0\cdot V)\,dX. \tag{273}$$

Next, consider the first term of (271) restricted to Ω_s disregarding the sign in front. Using the same technique of applying (3) and (2), and keeping in mind the normal outward normal to Ω_s is actually $-n$,

$$\begin{aligned}\int_{\Omega_s}\frac{\varepsilon_s}{2}(\nabla\cdot V)\nabla\psi_0^s\cdot\nabla\psi_0^s\,dX &= \int_{\Omega_s}\frac{\varepsilon_s}{2}(\nabla\cdot V)|\nabla\psi_0^s|^2\,dX\\ &= \int_{\Omega_s}\frac{\varepsilon_s}{2}\nabla\cdot\left(V|\nabla\psi_0^s|^2\right)\,dX - \int_{\Omega_s}\frac{\varepsilon_s}{2}V\cdot\nabla\left(|\nabla\psi_0^s|^2\right)\,dX\\ &= \int_{\partial\Omega}\frac{\varepsilon_s}{2}\left(V|\nabla\psi_0^s|^2\right)\cdot n\,dS - \int_{\Gamma}\frac{\varepsilon_s}{2}\left(V|\nabla\psi_0^s|^2\right)\cdot n\,dS - \int_{\Omega_s}\frac{\varepsilon_s}{2}V\cdot\nabla\left(|\nabla\psi_0^s|^2\right)\,dX.\end{aligned}$$

Again, the first integral above is 0 since $V = 0$ on $\partial\Omega$. Write the final integral above in component form. Let V^i and n_i be the ith components of V and n, respectively. Using the Einstein summation convention, consider

$$\begin{aligned}\int_{\Omega_s}\frac{\varepsilon_s}{2}V\cdot\nabla\left(|\nabla\psi_0^s|^2\right)\,dX &= \int_{\Omega_s}\frac{\varepsilon_s}{2}V^i\left(2\,\partial_{X_j}\psi_0^s(\partial^2_{X_jX_i}\psi_0^s)\right)\,dX\\ &= \int_{\Omega_s}\varepsilon_s V^i\partial_{X_j}\psi_0^s\partial^2_{X_jX_i}\psi_0^s\,dX.\end{aligned}$$

Then, the first term of (271) restricted to Ω_s is

$$\int_{\Omega_s} -\frac{\varepsilon_s}{2}(\nabla \cdot V)\nabla\psi_0^s \cdot \nabla\psi_0^s \, dX = \int_{\Gamma} \frac{\varepsilon_s}{2}|\nabla\psi_0^s|^2(V \cdot n)\, dS + \int_{\Omega_s} \varepsilon_s V^i \partial_{X_j}\psi_0^s \partial^2_{X_j X_i}\psi_0^s \, dX.$$

By similar constructions, the first term of (271) in full is

$$\begin{aligned}
&\int_{\Omega} -\frac{\varepsilon}{2}(\nabla \cdot V)\nabla\psi_0 \cdot \nabla\psi_0 \, dX \\
&\quad = -\int_{\Gamma_p} \frac{\varepsilon_p}{2}|\nabla\psi_0^p|^2(V \cdot n)\, dS + \int_{\Omega_p} \varepsilon_p V^i \partial_{X_j}\psi_0^p \partial^2_{X_j X_i}\psi_0^p \, dX \\
&\qquad + \int_{\Gamma_{c,e,p}} \frac{\varepsilon_s}{2}|\nabla\psi_0^s|^2(V \cdot n)\, dS + \int_{\Omega_s} \varepsilon_s V^i \partial_{X_j}\psi_0^s \partial^2_{X_j X_i}\psi_0^s \, dX \\
&\qquad - \int_{\Gamma_{c,e}} \frac{\varepsilon_m}{2}|\nabla\psi_0^m|^2(V \cdot n)\, dS + \int_{\Omega_m} \varepsilon_m V^i \partial_{X_j}\psi_0^m \partial^2_{X_j X_i}\psi_0^m \, dX,
\end{aligned} \tag{274}$$

where the notation $\Gamma_{c,e,p} = \Gamma_c \cup \Gamma_e \cup \Gamma_p$ emphasizes all three boundaries contribute to the solvent potential, and $\Gamma_{c,e} = \Gamma_c \cup \Gamma_e$ emphasizes that only the boundaries of the membrane contribute to the membrane potential. The reason why the first and fifth integrals in (274) is negative is because from the domain Ω_p and Ω_m, the normal n is already the outward normal.

Finally, we reduce the second term of (271). As with the first term of (271), consider the second term restricted to Ω_s,

$$\begin{aligned}
&\int_{\Omega_s} \varepsilon_s(\nabla V)\nabla\psi_0^s \cdot \nabla\psi_0^s \, dX \\
&\quad = \int_{\Omega_s} \varepsilon_s(\partial_{X_j}V^i)(\partial_{X_j}\psi_0^s)(\partial_{X_i}\psi_0^s)\, dX \\
&\quad = \int_{\Omega_s} \varepsilon_s \partial_{X_j}(V^i \partial_{X_j}\psi_0^s \partial_{X_i}\psi_0^s)\, dX - \int_{\Omega_s} \varepsilon_s V^i \partial_{X_j}(\partial_{X_j}\psi_0^s \partial_{X_i}\psi_0^s)\, dX \\
&\quad = \int_{\Omega_s} \varepsilon_s \partial_{X_j}(\partial_{X_j}\psi_0^s V^i \partial_{X_i}\psi_0^s)\, dX - \int_{\Omega_s} \varepsilon_s V^i(\partial^2_{X_j X_j}\psi_0^s \partial_{X_i}\psi_0^s + \partial_{X_j}\psi_0^s \partial^2_{X_j X_j}\psi_0^s)\, dX \\
&\quad = \int_{\Omega_s} \varepsilon_s \nabla \cdot (\nabla\psi_0^s V^i \partial_{X_i}\psi_0^s)\, dX - \int_{\Omega_s} \varepsilon_s V^i(\partial^2_{X_j X_j}\psi_0^s \partial_{X_i}\psi_0^s + \partial_{X_j}\psi_0^s \partial^2_{X_j X_j}\psi_0^s)\, dX.
\end{aligned}$$

Leave the second integral in the above equation as it is and work on the first by applying the divergence theorem (2), remembering that there are multiple boundaries for Ω_s,

$$\int_{\Omega_s} \varepsilon_s \nabla \cdot (\nabla \psi_0^s V^i \partial_{X_i} \psi_0^s)\, dX = \int_{\partial\Omega} \varepsilon_s \nabla \psi_0^s (V^i \partial_{X_i} \psi_0^s) \cdot n\, dS + \int_{\Gamma} \varepsilon_s \nabla \psi_0^s (V^i \partial_{X_i} \psi_0^s) \cdot (-n)\, dS$$

Notice that the normal to Γ is the opposite direction of the normal to $\partial\Omega$, so it is negative. We have

$$\begin{aligned}
\int_{\Omega_s} \varepsilon_s \nabla \cdot (\nabla \psi_0^s V^i \partial_{X_i} \psi_0^s)\, dX &= -\int_{\Gamma_{c,e,p}} \varepsilon_s \nabla \psi_0^s (V^i \partial_{X_i} \psi_0^s) \cdot n\, dS \\
&= -\int_{\Gamma_{c,e,p}} \varepsilon_s (V^i \partial_{X_i} \psi_0^s)(\nabla \psi_0^s \cdot n)\, dS \\
&= -\int_{\Gamma_{c,e,p}} \varepsilon_s (V \cdot \nabla \psi_0^s)(\nabla \psi_0^s \cdot n)\, dS.
\end{aligned}$$

Therefore, the second term of (271) restricted to Ω_s reduces to

$$\begin{aligned}
&\int_{\Omega_s} \varepsilon_s (\nabla V) \nabla \psi_0^s \cdot \nabla \psi_0^s\, dX \\
&\quad = -\int_{\Gamma_{c,e,p}} \varepsilon_s (\nabla \psi_0^s \cdot n)(V \cdot \nabla \psi_0^s)\, dS - \int_{\Omega_s} \varepsilon_s V^i (\partial^2_{X_j X_j} \psi_0^s \partial_{X_i} \psi_0^s + \partial_{X_j} \psi_0^s \partial^2_{X_j X_j} \psi_0^s)\, dX.
\end{aligned}$$

Following the same logic, we reduce the second term of (271) in full form to

$$\begin{aligned}
(275)\quad &\int_{\Omega} \varepsilon (\nabla V) \nabla \psi_0 \cdot \nabla \psi_0\, dX \\
&= \int_{\Gamma_p} \varepsilon_p (\nabla \psi_0^p \cdot n)(V \cdot \nabla \psi_0^p)\, dS - \int_{\Omega_p} \varepsilon_p V^i (\partial^2_{X_j X_j} \psi_0^p \partial_{X_i} \psi_0^p + \partial_{X_j} \psi_0^p \partial^2_{X_i X_j} \psi_0^p\, dX \\
&\quad - \int_{\Gamma_{c,e,p}} \varepsilon_s (\nabla \psi_0^s \cdot n)(V \cdot \nabla \psi_0^s)\, dS - \int_{\Omega_s} \varepsilon_s V^i (\partial^2_{X_j X_j} \psi_0^s \partial_{X_i} \psi_0^s + \partial_{X_j} \psi_0^s \partial^2_{X_i X_j} \psi_0^s)\, dX \\
&+ \int_{\Gamma_{c,e}} \varepsilon_m (\nabla \psi_0^m \cdot n)(V \cdot \nabla \psi_0^m)\, dS - \int_{\Omega_m} \varepsilon_m V^i (\partial^2_{X_j X_j} \psi_0^m \partial_{X_i} \psi_0^m + \partial_{X_j} \psi_0^m \partial^2_{X_i X_j} \psi_0^m\, dX.
\end{aligned}$$

Now we have simplified each term of (271). Combining the reduced terms from (274), (275), (272) and (273), we have

$$
\begin{aligned}
&\partial_t z_1(0,\psi_0)\\
&\quad= -\int_{\Gamma_p} \frac{\varepsilon_p}{2}|\nabla\psi_0^p|^2(V\cdot n)\,dS + \int_{\Omega_p} \varepsilon_p V^i \partial_{X_j}\psi_0^p \partial^2_{X_jX_i}\psi_0^p\,dX\\
&\qquad+ \int_{\Gamma_{c,e,p}} \frac{\varepsilon_s}{2}|\nabla\psi_0^s|^2(V\cdot n)\,dS + \int_{\Omega_s} \varepsilon_s V^i \partial_{X_j}\psi_0^s \partial^2_{X_jX_i}\psi_0^s\,dX\\
&\qquad- \int_{\Gamma_{c,e}} \frac{\varepsilon_m}{2}|\nabla\psi_0^m|^2(V\cdot n)\,dS + \int_{\Omega_m} \varepsilon_m V^i \partial_{X_j}\psi_0^m \partial^2_{X_jX_i}\psi_0^m\,dX\\
&\qquad+ \int_{\Gamma_p} \varepsilon_p(\nabla\psi_0^p\cdot n)(V\cdot\nabla\psi_0^p)\,dS - \int_{\Omega_p} \varepsilon_p V^i(\partial^2_{X_jX_j}\psi_0^p\partial_{X_i}\psi_0^p + \partial_{X_j}\psi_0^p\partial^2_{X_iX_j}\psi_0^p)\,dX\\
&\qquad- \int_{\Gamma_{c,e,p}} \varepsilon_s(\nabla\psi_0^s\cdot n)(V\cdot\nabla\psi_0^s)\,dS - \int_{\Omega_s} \varepsilon_s V^i(\partial^2_{X_jX_j}\psi_0^s\partial_{X_i}\psi_0^s + \partial_{X_j}\psi_0^s\partial^2_{X_iX_j}\psi_0^s)\,dX\\
&\qquad+ \int_{\Gamma_{c,e}} \varepsilon_m(\nabla\psi_0^m\cdot n)(V\cdot\nabla\psi_0^m)\,dS - \int_{\Omega_m} \varepsilon_m V^i(\partial^2_{X_jX_j}\psi_0^m\partial_{X_i}\psi_0^m + \partial_{X_j}\psi_0^m\partial^2_{X_iX_j}\psi_0^m\,dX\\
&\qquad- \int_{\Omega_p} \rho_p(V\cdot\nabla\psi_0)\,dX + \int_{\Gamma_{c,e,p}} B(\psi_0)(V\cdot n)\,dS + \int_{\Omega_s} B'(\psi_0)(\nabla\psi_0\cdot V)\,dX.
\end{aligned}
$$

Thankfully, this simplifies as well. The second term cancels with the latter part of the eighth term, and the fourth term cancels with the latter part of the tenth term, and the sixth term with the latter part of the twelfth term. So we have

$$
\begin{aligned}
&\partial_t z_1(0,\psi_0)\\
&\quad= -\int_{\Gamma_p} \frac{\varepsilon_p}{2}|\nabla\psi_0^p|^2(V\cdot n)\,dS + \int_{\Gamma_{c,e,p}} \frac{\varepsilon_s}{2}|\nabla\psi_0^s|^2(V\cdot n)\,dS - \int_{\Gamma_{c,e}} \frac{\varepsilon_m}{2}|\nabla\psi_0^m|^2(V\cdot n)\,dS\\
&\qquad+ \int_{\Gamma_p} \varepsilon_p(\nabla\psi_0^p\cdot n)(V\cdot\nabla\psi_0^p)\,dS - \int_{\Omega_p} \varepsilon_p V^i \partial^2_{X_jX_j}\psi_0^p\partial_{X_i}\psi_0^p\,dX\\
&\qquad- \int_{\Gamma_{c,e,p}} \varepsilon_s(\nabla\psi_0^s\cdot n)(V\cdot\nabla\psi_0^s)\,dS - \int_{\Omega_s} \varepsilon_s V^i \partial^2_{X_jX_j}\psi_0^s\partial_{X_i}\psi_0^s\,dX\\
&\qquad+ \int_{\Gamma_{c,e}} \varepsilon_m(\nabla\psi_0^m\cdot n)(V\cdot\nabla\psi_0^m)\,dS - \int_{\Omega_m} \varepsilon_m V^i \partial^2_{X_jX_j}\psi_0^m\partial_{X_i}\psi_0^m\,dX\\
&\qquad- \int_{\Omega_p} \rho_p(V\cdot\nabla\psi_0)\,dX + \int_{\Gamma_{c,e,p}} B(\psi_0)(V\cdot n)\,dS + \int_{\Omega_s} B'(\psi_0)(\nabla\psi_0\cdot V)\,dX.
\end{aligned}
$$

Putting everything back into vector form and combining terms gives

$$\begin{aligned}
&\partial_t z_1(0,\psi_0)\\
&\quad= -\int_{\Gamma_p} \frac{\varepsilon_p}{2}|\nabla \psi_0^p|^2 (V\cdot n)\, dS + \int_{\Gamma_{c,e,p}} \frac{\varepsilon_s}{2}|\nabla \psi_0^s|^2 (V\cdot n)\, dS - \int_{\Gamma_{c,e}} \frac{\varepsilon_m}{2}|\nabla \psi_0^m|^2 (V\cdot n)\, dS\\
&\qquad+ \int_{\Gamma_p} \varepsilon_p (\nabla \psi_0^p \cdot n)(V\cdot \nabla \psi_0^p) dS - \int_{\Omega_p} \varepsilon_p \Delta \psi_0 (\nabla \psi_0 \cdot V)\, dX\\
&\qquad- \int_{\Gamma_{c,e,p}} \varepsilon_s (\nabla \psi_0^s \cdot n)(V\cdot \nabla \psi_0^s)\, dS - \int_{\Omega_s} \varepsilon_s \Delta \psi_0 (\nabla \psi_0 \cdot V)\, dX\\
&\qquad+ \int_{\Gamma_{c,e}} \varepsilon_m (\nabla \psi_0^m \cdot n)(V\cdot \nabla \psi_0^m) dS - \int_{\Omega_m} \varepsilon_m \Delta \psi_0 (\nabla \psi_0 \cdot V)\, dX\\
&\qquad- \int_{\Omega_p} \rho_p (V\cdot \nabla \psi_0)\, dX + \int_{\Gamma_{c,e,p}} B(\psi_0)(V\cdot n)\, dS + \int_{\Omega_s} B'(\psi_0)(\nabla \psi_0 \cdot V)\, dX
\end{aligned}$$

$$\begin{aligned}
&\quad= -\int_{\Gamma_p} \frac{\varepsilon_p}{2}|\nabla \psi_0^p|^2 (V\cdot n)\, dS + \int_{\Gamma_{c,e,p}} \frac{\varepsilon_s}{2}|\nabla \psi_0^s|^2 (V\cdot n)\, dS - \int_{\Gamma_{c,e}} \frac{\varepsilon_m}{2}|\nabla \psi_0^m|^2 (V\cdot n)\, dS\\
&\qquad+ \int_{\Gamma_p} \varepsilon_p (\nabla \psi_0^p \cdot n)(V\cdot \nabla \psi_0^p)\, dS - \int_{\Gamma_{c,e,p}} \varepsilon_s (\nabla \psi_0^s \cdot n)(V\cdot \nabla \psi_0^s)\, dS\\
&\qquad+ \int_{\Gamma_{c,e}} \varepsilon_m (\nabla \psi_0^m \cdot n)(V\cdot \nabla \psi_0^m) dS - \int_{\Omega_p} (\varepsilon_p \Delta \psi_0 + \rho_p)(\nabla \psi_0 \cdot V)\, dX\\
&\qquad- \int_{\Omega_s} (\varepsilon_s \Delta \psi_0 - B'(\psi_0))(\nabla \psi_0 \cdot V)\, dX - \int_{\Omega_m} (\varepsilon_m \Delta \psi_0)(\nabla \psi_0 \cdot V)\, dX\\
&\qquad+ \int_{\Gamma_{c,e,p}} B(\psi_0)(V\cdot n)\, dS.
\end{aligned}$$

By the elliptic interface conditions in (191), we have $\varepsilon_s \Delta\psi_0 = B'(\psi_0)$ in Ω_s, $\varepsilon_p \Delta\psi_0 = -\rho_p$ in Ω_p, and $\varepsilon_m \Delta\psi_0 = 0$ in Ω_m which leaves us with

$$
\begin{aligned}
(276)\quad & \partial_t z_1(0,\psi_0) \\
&= -\int_{\Gamma_p} \frac{\varepsilon_p}{2} |\nabla\psi_0^p|^2 (V\cdot n)\, dS + \int_{\Gamma_{c,e,p}} \frac{\varepsilon_s}{2} |\nabla\psi_0^s|^2 (V\cdot n)\, dS - \int_{\Gamma_{c,e}} \frac{\varepsilon_m}{2} |\nabla\psi_0^m|^2 (V\cdot n)\, dS \\
&\quad + \int_{\Gamma_p} \varepsilon_p (\nabla\psi_0^p \cdot n)(V\cdot\nabla\psi_0^p)\, dS - \int_{\Gamma_p} \varepsilon_s (\nabla\psi_0^s \cdot n)(V\cdot\nabla\psi_0^s)\, dS \\
&\quad + \int_{\Gamma_{c,e}} \varepsilon_m (\nabla\psi_0^m \cdot n)(V\cdot\nabla\psi_0^m)\, dS - \int_{\Gamma_{c,e}} \varepsilon_s (\nabla\psi_0^s \cdot n)(V\cdot\nabla\psi_0^s)\, dS \\
&\quad + \int_{\Gamma_{c,e,p}} B(\psi_0)(V\cdot n)\, dS.
\end{aligned}
$$

By the boundary conditions in the Poisson-Boltzmann equation (190), there is continuity of ψ_0 across $\Gamma_{c,e,p}$. That is, the tangential components are equal, but the normal components are not equal. Any difference occurs only in the direction of n. In terms of the jump across the membrane interfaces,

$$
(277)\qquad \nabla(\psi_0^m - \psi_0^s) = (\nabla\psi_0^m \cdot n - \nabla\psi_0^s \cdot n)n \qquad \text{on } \Gamma_{c,e}.
$$

Similarly, across the protein interface,

$$
(278)\qquad \nabla(\psi_0^p - \psi_0^s) = (\nabla\psi_0^p \cdot n - \nabla\psi_0^s \cdot n)n \qquad \text{on } \Gamma_p.
$$

There are two equally correct approaches from here. Consider the second line of (276) (where the integrals are on Γ_p). Substituting the boundary condition in (191) on Γ_p and using (277) gives

$$
\begin{aligned}
&\int_{\Gamma_p} \varepsilon_p(\nabla\psi_0^p \cdot n)(V \cdot \nabla\psi_0^p)\, dS - \int_{\Gamma_p} \varepsilon_s(\nabla\psi_0^s \cdot n)(V \cdot \nabla\psi_0^s)\, dS \\
&\quad = \int_{\Gamma_p} \varepsilon_p(\nabla\psi_0^p \cdot n)(V \cdot \nabla\psi_0^p)\, dS - \int_{\Gamma_p} \varepsilon_p(\nabla\psi_0^p \cdot n)(V \cdot \nabla\psi_0^s)\, dS \\
&\quad = \int_{\Gamma_p} \varepsilon_p(\nabla\psi_0^p \cdot n)(V \cdot \nabla(\psi_0^p - \psi_0^s))\, dS \\
&\quad = \int_{\Gamma_p} \varepsilon_p(\nabla\psi_0^p \cdot n)(V \cdot (\nabla\psi_0^p \cdot n - \nabla\psi_0^s \cdot n)n)\, dS \\
&\quad = \int_{\Gamma_p} \varepsilon_p \left|\nabla\psi_0^p \cdot n\right|^2 (V \cdot n) - \varepsilon_p(\nabla\psi_0^p \cdot n)(\nabla\psi_0^s \cdot n)(V \cdot n)\, dS.
\end{aligned}
$$

Similarly, consider the the third line in (276) (where the integrals are on $\Gamma_{c,e}$). Substituting the boundary condition in (191) on $\Gamma_{c,e}$ and using (278) gives,

$$
\begin{aligned}
&\int_{\Gamma_{c,e}} \varepsilon_m(\nabla\psi_0^m \cdot n)(V \cdot \nabla\psi_0^m)\, dS - \int_{\Gamma_{c,e}} \varepsilon_s(\nabla\psi_0^s \cdot n)(V \cdot \nabla\psi_0^s)\, dS \\
&\quad = \int_{\Gamma_{c,e}} \varepsilon_m(\nabla\psi_0^m \cdot n)(V \cdot \nabla\psi_0^m)\, dS - \int_{\Gamma_{c,e}} (\varepsilon_m\nabla\psi_0^m \cdot n - \rho[\Gamma]q_l)(V \cdot \nabla\psi_0^s)\, dS \\
&\quad = \int_{\Gamma_{c,e}} \varepsilon_m(\nabla\psi_0^m \cdot n)(V \cdot \nabla(\psi_0^m - \psi_0^s)) + \rho[\Gamma]q_l(V \cdot \nabla\psi_0^s)\, dS \\
&\quad = \int_{\Gamma_{c,e}} \varepsilon_m(\nabla\psi_0^m \cdot n)(V \cdot (\nabla\psi_0^m \cdot n - \nabla\psi_0^s \cdot n)n) + \rho[\Gamma]q_l(V \cdot \nabla\psi_0^s)\, dS \\
&\quad = \int_{\Gamma_{c,e}} \varepsilon_m \left|\nabla\psi_0^m \cdot n\right|^2 (V \cdot n) - \varepsilon_m(\nabla\psi_0^m \cdot n)(\nabla\psi_0^s \cdot n)(V \cdot n) + \rho[\Gamma]q_l(V \cdot \nabla\psi_0^s)\, dS.
\end{aligned}
$$

Substituting these term back into (276) and combining terms will lead to the final result for $\partial_t z_1$,

$$\begin{aligned}
&\partial_t z_1(0,\psi_0)\\
&\quad= -\int_{\Gamma_p} \frac{\varepsilon_p}{2}|\nabla\psi_0^p|^2(V\cdot n)\,dS + \int_{\Gamma_{c,e,p}} \frac{\varepsilon_s}{2}|\nabla\psi_0^s|^2(V\cdot n)\,dS - \int_{\Gamma_{c,e}} \frac{\varepsilon_m}{2}|\nabla\psi_0^m|^2(V\cdot n)\,dS\\
&\qquad + \int_{\Gamma_p} \varepsilon_p\left|\nabla\psi_0^p\cdot n\right|^2(V\cdot n) - \varepsilon_p(\nabla\psi_0^p\cdot n)(\nabla\psi_0^s\cdot n)(V\cdot n)\,dS\\
&\qquad + \int_{\Gamma_{c,e}} \varepsilon_m\left|\nabla\psi_0^m\cdot n\right|^2(V\cdot n) - \varepsilon_m(\nabla\psi_0^m\cdot n)(\nabla\psi_0^s\cdot n)(V\cdot n) + \rho[\Gamma]q_l(V\cdot\nabla\psi_0^s)\,dS\\
&\qquad + \int_{\Gamma_{c,e,p}} B(\psi_0)(V\cdot n)\,dS.
\end{aligned}$$

Since we are interested in the dielectric boundary force of the *membrane* and not the protein boundary, we restrict our attention to $\Gamma_{c,e}$. Then the final result for $\partial_t z_1$ is

$$\begin{aligned}
(279)\qquad &\partial_t z_1(0,\psi_0)\Big|_{\Gamma_{c,e}}\\
&\quad= \int_{\Gamma_{c,e}} \Big[\Big(\frac{\varepsilon_s}{2}|\nabla\psi_0^s|^2 - \frac{\varepsilon_m}{2}|\nabla\psi_0^m|^2 + \varepsilon_m|\nabla\psi_0^m\cdot n|^2\\
&\qquad - \varepsilon_m(\nabla\psi_0^m\cdot n)(\nabla\psi_0^s\cdot n) + B(\psi_0)\Big)(V\cdot n) + \rho[\Gamma]q_l(V\cdot\nabla\psi_0^s)\Big]\,dS.
\end{aligned}$$

An alternative form of (279) can be obtained by substituting the boundary conditions of (191) and keeping the solvent term ($\varepsilon_s\nabla\psi_0^s\cdot n$) rather than the term corresponding to the membrane.

Next, the shape derivative from $\partial_t z_2$ will be simplified. Evaluating (257) at $t=0$ and $\phi=\psi_0$ gives

$$\partial_t z_2(0,\psi_0) = -\frac{C}{\beta}\left(\frac{\displaystyle\int_{\Gamma_0}\gamma(\psi_0)\frac{dJ_s(X,0)}{dt}\,dS(X)}{\displaystyle\int_{\Gamma_0}\gamma(\psi_0)J_s(X,0)\,dS(X)} - \frac{\displaystyle\int_{\Gamma_0}\frac{dJ_s(X,0)}{dt}\,dS(X)}{\displaystyle\int_{\Gamma_0}J_s(X,0)\,dS(X)}\right).$$

We emphasize again that Γ_0 corresponds to the non-transformed boundaries of $\Gamma_{c,e}$. The time derivative of J_s at $t=0$ is the surface divergence of the velocity, as calculated in (241). Recall from Section 6.1.2 that $J_s(X,0)=1$. Using these two facts, the above equation is equivalent to

$$\partial_t z_2(0,\psi_0) = -\frac{C}{\beta}\left(\frac{\displaystyle\int_{\Gamma_0}\gamma(\psi_0)(\nabla_s\cdot V)\,dS(X)}{\displaystyle\int_{\Gamma_0}\gamma(\psi_0)\,dS(X)} - \frac{\displaystyle\int_{\Gamma_0}(\nabla_s\cdot V)\,dS(X)}{\displaystyle\int_{\Gamma_0}dS(X)}\right). \tag{280}$$

By Lemma 6.1.1, since the velocity V is a continuous function, the second term of (280) is zero. Applying the product rule (3) to the remaining term,

$$\partial_t z_2(0,\psi_0) = -\frac{C}{\beta}\left(\frac{\displaystyle\int_{\Gamma_0}\nabla_s\cdot(V\gamma(\psi_0)) - V\cdot(\nabla_s\gamma(\psi_0))\,dS(X)}{\displaystyle\int_{\Gamma_0}\gamma(\psi_0)\,dS(X)}\right). \tag{281}$$

By applying Lemma 6.1.1 again to (281) to remove the surface divergence of the continuous function $V\gamma(\psi_0)$, and by expanding the surface gradient in the remaining term, we have

$$\begin{aligned}\partial_t z_2(0,\psi_0) &= -\frac{C}{\beta}\left(\frac{\displaystyle\int_{\Gamma_0}-V\cdot(\gamma'(\psi_0)\nabla_s\psi_0)\,dS(X)}{\displaystyle\int_{\Gamma_0}\gamma(\psi_0)\,dS(X)}\right)\\ &= -\int_{\Gamma_0}\rho[\Gamma]q_l(V\cdot\nabla_s\psi_0)\,dS(X),\end{aligned} \tag{282}$$

where the last step uses the definition of $\rho[\Gamma]$ in (201) at $\phi=\psi_0$.

Finally, combine (279) and (282) for the full form of the shape derivative,

$$\begin{aligned}\delta_\Gamma G[\Gamma] &= \partial_t z_1(0,\psi_0) + \partial_t z_2(0,\psi_0)\\ &= \int_{\Gamma_0}\Big[\Big(\frac{\varepsilon_s}{2}|\nabla\psi_0^s|^2 - \frac{\varepsilon_m}{2}|\nabla\psi_0^m|^2 + \varepsilon_m|\nabla\psi_0^m\cdot n|^2 - \varepsilon_m(\nabla\psi_0^m\cdot n)(\nabla\psi_0^s\cdot n)\\ &\qquad + B(\psi_0)\Big)(V\cdot n) + \rho[\Gamma]q_l(V\cdot\nabla\psi_0^s)\Big]\,dS - \int_{\Gamma_0}\rho[\Gamma]q_l(V\cdot\nabla_s\psi_0)\,dS.\end{aligned}$$

By continuity of ψ_0, we have $\psi_0^s = \psi_0^m = \psi_0$ on Γ_0, and hence the last two terms reduce, using the definition of surface divergence in (5),

$$\begin{aligned}
&\int_{\Gamma_0} \rho[\Gamma] q_l (V \cdot \nabla \psi_0^s)\, dS - \int_{\Gamma_0} \rho[\Gamma] q_l (V \cdot \nabla_s \psi_0)\, dS \\
&\quad = \int_{\Gamma_0} \rho[\Gamma] q_l V \cdot (\nabla \psi_0^s - \nabla_s \psi_0^s)\, dS \\
&\quad = \int_{\Gamma_0} \rho[\Gamma] q_l V \cdot (\nabla \psi_0^s - [\nabla \psi_0^s - (\nabla \psi_0^s \cdot n) n])\, dS \\
&\quad = \int_{\Gamma_0} \rho[\Gamma] q_l (\nabla \psi_0^s \cdot n)(V \cdot n)\, dS.
\end{aligned}$$

Using this result, the shape derivative is simplified to the final result,

$$\begin{aligned}
\delta_\Gamma G[\Gamma] = \int_{\Gamma_0} \Bigg(&\frac{\varepsilon_s}{2} |\nabla \psi_0^s|^2 - \frac{\varepsilon_m}{2} |\nabla \psi_0^m|^2 + \varepsilon_m |\nabla \psi_0^m \cdot n|^2 - \varepsilon_m (\nabla \psi_0^s \cdot n)(\nabla \psi_0^m \cdot n) \\
&+ B(\psi_0) + q_l \rho[\Gamma](\nabla \psi_0^s \cdot n) \Bigg)(V \cdot n)\, dS.
\end{aligned} \tag{283}$$

The alternative form of $\delta_\Gamma G[\Gamma]$ based on the alternative form of (279) is given by

$$\begin{aligned}
\delta_\Gamma^{(\mathrm{alt})} G[\Gamma] = \int_{\Gamma_0} \Bigg(&\frac{\varepsilon_s}{2} |\nabla \psi_0^s|^2 - \frac{\varepsilon_m}{2} |\nabla \psi_0^m|^2 - \varepsilon_s |\nabla \psi_0^s \cdot n|^2 + \varepsilon_s (\nabla \psi_0^s \cdot n)(\nabla \psi_0^m \cdot n) \\
&+ B(\psi_0) + q_l \rho[\Gamma](\nabla \psi_0^m \cdot n) \Bigg)(V \cdot n)\, dS.
\end{aligned} \tag{284}$$

Notice that the two forms are equivalent, since subtracting (283) from (284) using the interface condition over $\Gamma_{c,e}$ in (190) results in zero.

$$
\begin{aligned}
&\delta_\Gamma^{(\mathrm{alt})} G[\Gamma] - \delta_\Gamma G[\Gamma] = \\
&\quad = \Bigg(\Big(-\varepsilon_s |\nabla\psi_0^s \cdot n|^2 + \varepsilon_s (\nabla\psi_0^s \cdot n)(\nabla\psi_0^m \cdot n) + q_l \rho[\Gamma](\nabla\psi_0^m \cdot n) \Big) \\
&\qquad - \Big(\varepsilon_m |\nabla\psi_0^m \cdot n|^2 - \varepsilon_m (\nabla\psi_0^s \cdot n)(\nabla\psi_0^m \cdot n) + q_l \rho[\Gamma](\nabla\psi_0^s \cdot n) \Big) \Bigg) \Big(V \cdot n \Big) \\
&\quad = \Bigg(-\varepsilon_s |\nabla\psi_0^s \cdot n|^2 + \varepsilon_s (\nabla\psi_0^s \cdot n)(\nabla\psi_0^m \cdot n) + \Big(\varepsilon_m (\nabla\psi_0^m \cdot n) - \varepsilon_s (\nabla\psi_0^s \cdot n) \Big) \Big(\nabla\psi_0^m \cdot n \Big) \\
&\qquad - \varepsilon_m |\nabla\psi_0^m \cdot n|^2 + \varepsilon_m (\nabla\psi_0^s \cdot n)(\nabla\psi_0^m \cdot n) - \Big(\varepsilon_m (\nabla\psi_0^m \cdot n) - \varepsilon_s (\nabla\psi_0^s \cdot n) \Big) \Big(\nabla\psi_0^s \cdot n \Big) \Bigg) \Big(V \cdot n \Big) \\
&\quad = 0.
\end{aligned}
$$

□

Using the result of Theorem 6.2.2, we can extract the dielectric boundary force as (245) by Theorem 6.2.1.

6.3. EQUIVALENCE TO THE MAXWELL STRESS TENSOR

In classical electromechanics, the force on charged interfaces is given by the jump in the divergence of the Maxwell stress tensor [41, 59, 92, 98]. The Maxwell stress tensor is defined by

$$
M = \varepsilon E \otimes E - \frac{\varepsilon}{2} |E|^2 I - \chi_s B(\psi) I, \tag{285}
$$

where $E = -\nabla\psi$ is the electric field, not to be confused with the bending energy. Since ε and $\nabla\psi$ are discontinuous across the membrane interfaces $\Gamma_{c,e}$, the Maxwell stress tensor M is also discontinuous. In the domains Ω_m and Ω_s, we refer to the Maxwell stress tensor as M^m and M^s, respectively. We verify that the force F_n computed by the shape derivative (246) as in Theorem 6.2.2 can also be expressed as the jump in the divergence of the Maxwell stress tensor [11],

$$
\begin{aligned}
(286) \qquad F_n &= n \cdot M^s n - n \cdot M^m n \\
&= \Big(\varepsilon_s |\nabla\psi^s \cdot n|^2 - \frac{\varepsilon_s}{2}|\nabla\psi^s|^2 - \chi_s B(\psi^s)\Big) - \Big(\varepsilon_m |\nabla\psi^m \cdot n|^2 - \frac{\varepsilon_m}{2}|\nabla\psi^m|^2\Big) \\
&= -\frac{\varepsilon_s}{2}|\nabla\psi^s|^2 + \frac{\varepsilon_m}{2}|\nabla\psi^m|^2 + \varepsilon_s|\nabla\psi^s \cdot n|^2 - \varepsilon_m|\nabla\psi^m \cdot n|^2 - B(\psi) \\
&= -\frac{\varepsilon_s}{2}|\nabla\psi^s|^2 + \frac{\varepsilon_m}{2}|\nabla\psi^m|^2 + \varepsilon_s(\nabla\psi^s \cdot n)(\nabla\psi^s \cdot n) - \varepsilon_m(\nabla\psi^m \cdot n)(\nabla\psi^s \cdot n) \\
&\qquad + \varepsilon_m(\nabla\psi^s \cdot n)(\nabla\psi^m \cdot n) - \varepsilon_m(\nabla\psi^m \cdot n)(\nabla\psi^m \cdot n) - B(\psi) \\
&= -\frac{\varepsilon_s}{2}|\nabla\psi^s|^2 + \frac{\varepsilon_m}{2}|\nabla\psi^m|^2 - \varepsilon_m|\nabla\psi^m \cdot n|^2 + \varepsilon_m(\nabla\psi^s \cdot n)(\nabla\psi^m \cdot n) \\
&\qquad - B(\psi) + \Big(\varepsilon_s(\nabla\psi^s \cdot n) - \varepsilon_m(\nabla\psi^m \cdot n)\Big)(\nabla\psi^s \cdot n) \\
&= -\frac{\varepsilon_s}{2}|\nabla\psi^s|^2 + \frac{\varepsilon_m}{2}|\nabla\psi^m|^2 - \varepsilon_m|\nabla\psi^m \cdot n|^2 + \varepsilon_m(\nabla\psi^s \cdot n)(\nabla\psi^m \cdot n) \\
&\qquad - B(\psi) - q_l\rho[\Gamma](\nabla\psi^s \cdot n).
\end{aligned}
$$

This matches (245) exactly, suggesting that our definition of the electrostatic forces on charged dielectric interfaces is physical.

CHAPTER 7

Topological vesicle deformation

7.1. Introduction

When a protein induces a force that produces a topological change to the membrane surface, such as the merging or separating of membranes, the sharp-interface model fails. Recall that the integration of the Gaussian curvature over a closed surface is a topological constant. Changing the topology creates a discontinuity in the energy functional (12). Moreover, a change in topology requires the surface to be discontinuous for a moment, which is impossible to model using an explicit parameterization. An effective way to treat topological changes is to increase the dimensionality of the problem and track the surface as a level set of a 3D function. This method is called the phase field method or diffuse-interface method [27, 28, 100]. The membrane is defined by a level set of a phase field function, ϕ, and the motion of the membrane is governed by the motion of the phase field function. In this way, the membrane is never explicitly tracked, and topological changes can occur. This approach has the obvious advantage over sharp interface models since it provides a way to describe topological changes to the membrane. However, a disadvantage of this method is that it is difficult for this method to describe local forces on the membrane. If local forces need to be modeled, one should use the sharp-interface method. Furthermore, this method requires solving a higher dimensional system, since the energy functional is computed over the entire space $\Omega \subset \mathbb{R}^3$ rather than just a manifold $\Gamma \subset \mathbb{R}^2$. This is the price we must pay to describe membrane merging and separating.

7.2. Lagrangian and Eulerian formulation

A simple version of the mechanical bending energy (13) is given by the Lagrangian formulation,

$$E_L = \int_\Gamma k(H - C_0)^2 \, dS, \tag{287}$$

where H is the mean curvature of the membrane Γ, C_0 is the spontaneous curvature of the membrane, and k is the bending modulus. The above equation neglects surface tension and stretching rigidity. The surface tension is constant in vesicles with fixed surface area giving justification of our simplification [28]. We refer the reader to [27] for adding stretching rigidity to (287). The Lagrangian formulation above is derived from basic physical principles in Chapter 2. For the phase field model, we recast the energy functional in an Eulerian formulation through a function ϕ which separates the interior of the membrane from the exterior in the following way. Let Ω be a domain containing a membrane Γ. Let Ω_i represent the region interior to Γ and Ω_e be the region exterior to Γ. We require a phase function with following properties: the set $\{x : \phi(x) = 0\}$ represents the membrane Γ, the set $\{x : \phi(x) > 0\}$ represents points inside the membrane, $x \in \Omega_i$, and the set $\{x : \phi(x) \leq 0\}$ represents points outside the membrane, $x \in \Omega_e$. These properties are illustrated in Figure 7.1.

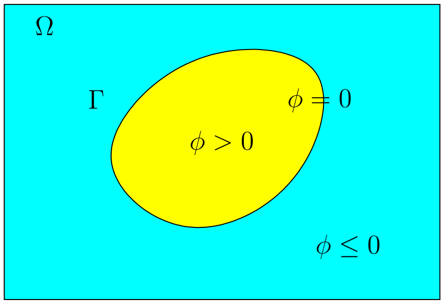

Figure 7.1: Properties of phase function ϕ within the domain Ω.

Define the phase field function by

$$\phi(x) = q\left(\frac{d(x)}{\epsilon}\right), \tag{288}$$

where q is some nonlinear function. The function $d(x)$ is a signed distance for any point $x \in \Omega$ to the surface Γ. It satisfies the properties that $d(x) = 0$ for $x \in \Gamma$, $d(x) > 0$ for $x \in \Omega_e$ and $d(x) < 0$ for $x \in \Omega_i$. The parameter $0 < \epsilon \ll 1$ is a parameter adjusting the transition of ϕ across the membrane. The dilation $1/\epsilon$ gives ϕ a steep sigmoid shape.

Define the Eulerian formulation of the bending energy by

$$E_E = \int_\Omega \frac{k\epsilon}{2} \left| \Delta\phi - \frac{1}{\epsilon^2}(\phi^2 - 1)(\phi + C\epsilon) \right|^2 \, dx \tag{289}$$

where $C = \sqrt{2}C_0$. If we substitute (288) into (289) and take the limit $\epsilon \to 0$, the Lagrangian formulation (287) is recovered [26]. Thus, the minimization of the Lagrangian formulation is equivalent to the minimization of the Eulerian formulation. The details of the substitution are shown below. Notice that $\nabla q(d(x)/\epsilon) = q'(d(x)/\epsilon)\frac{1}{\epsilon}\nabla d$ and $\Delta q = q''(d(x)/\epsilon)\frac{1}{\epsilon^2} + q'(d(x)/\epsilon)\frac{1}{\epsilon}\Delta d$ since $|\nabla d(x)| = 1$ for signed distance functions[1]. Note that in the next equation, when we write q, we mean $q(\frac{d(x)}{\epsilon})$.

$$\begin{aligned}
E_E &= \int_\Omega \frac{k\epsilon}{2} \left| \Delta q - \frac{1}{\epsilon^2}\left(q^2 - 1\right)\left(q + C\epsilon\right) \right|^2 \, dx \\
&= \int_\Omega \frac{k\epsilon}{2} \left| q''\frac{1}{\epsilon^2} + q'\frac{1}{\epsilon}\Delta d - \frac{1}{\epsilon^2}(q^2 - 1)(q + C\epsilon) \right|^2 \, dx \\
&= \int_\Omega \frac{k\epsilon}{2} \left| \frac{1}{\epsilon}\left(q''\frac{1}{\epsilon} + q'\Delta d - \frac{1}{\epsilon}\left((q^2 - 1)q + (q^2 - 1)C\epsilon\right) \right) \right|^2 \, dx \\
&= \int_\Omega \frac{k}{2\epsilon} \left| q'\Delta d + \frac{1}{\epsilon}\Big(q'' - (q^2 - 1)q\Big) - C(q^2 - 1) \right|^2 \, dx.
\end{aligned}$$

The leading order term of the Eulerian formulation for small ϵ is $|(q'' - (q^2 - 1)q)|^2$. If E_E is to be minimized, this term must vanish as $\epsilon \to 0$. Solving the second order differential equation

$$q'' - (q^2 - 1)q = 0 \tag{290}$$

yields $q(x) = \tanh(x/\sqrt{2})$. Therefore in the minimization of E_E as $\epsilon \to 0$, $q(\cdot) \to \tanh(\cdot/\sqrt{2})$. Plots of $\tanh(x/(\sqrt{2}\epsilon))$ are shown in Figure 7.2 for different ϵ. Numerically, we use the phase

---

[1] To justify $|\nabla d(x)| = 1$, consider the path from a point $x \in \Omega$ to its nearest point $x_\Gamma \in \Gamma$. The shortest path connecting these two points is a vector that points from x to x_Γ. This is the path of steepest descent, so $-\nabla d$ is the direction of the vector from x to x_Γ. The length of the vector is the shortest distance, $|d(x)|$. Using this, the decomposed vector from x to x_Γ is given by $\vec{r} = d|\nabla d|$. The length of $\vec{r}$ can also be expressed as $|\vec{r}| = |d||\nabla d|$, but we already know the length of $\vec{r}$ is $|d|$. Solving this equality, we see that $|\nabla d| = 1$. We must be careful in that this only holds when x has a unique point closest to the interface, x_Γ. However, $|\nabla d(x)| \approx 1$ for these points, [81].

field function

$$\phi = \tanh\left(\frac{d(x)}{\sqrt{2}\epsilon}\right), \tag{291}$$

which approaches the Heaviside step function for a sharp interface as $\epsilon \to 0$.

$$H_{-1}(x) = \begin{cases} 1, & \text{if } x > 0, \\ -1, & \text{it } x < 0. \end{cases} \tag{292}$$

That is, as $\epsilon \to 0$, $\phi(x) = 1$ if $x \in \Omega_i$ and $\phi(x) = -1$ if $x \in \Omega_e$. This is a sharp interface from Ω_i to Ω_e. Next we show the convergence of the Eulerian form of the bending energy (289) to the Lagrangian form of the bending energy (287). Consider,

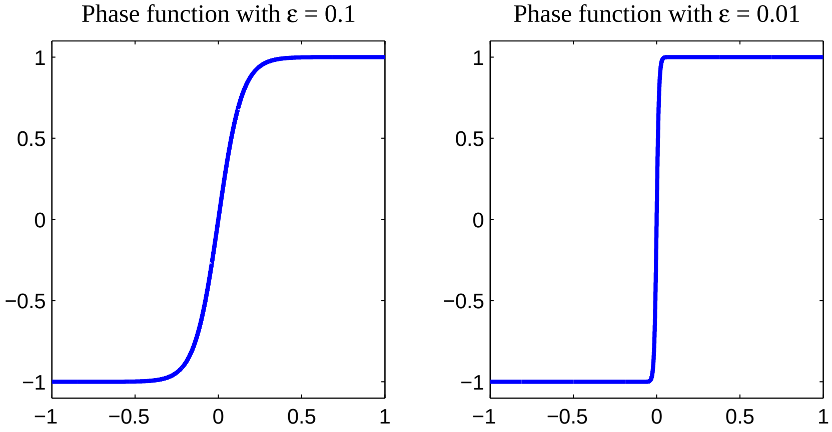

Figure 7.2: Plots of a phase function ϕ as $\epsilon \to 0$. Notice that $\phi \to H_{-1}(x)$ as $\epsilon \to 0$, giving a sharp interface.

$$\nabla\phi = \frac{1}{\epsilon}q'\nabla d, \qquad \Delta\phi = \frac{1}{2\epsilon^2}q''\nabla_i d\nabla_j d + \frac{1}{\epsilon}q'\Delta d,$$
$$q'(x) = \frac{d}{dx}\tanh(x/\sqrt{2}) = \operatorname{sech}^2(x/\sqrt{2})/\sqrt{2} = (1-\tanh^2(x/\sqrt{2}))/\sqrt{2} = (1-q^2(x))/\sqrt{2},$$
$$q''(x) = -2\tanh(x/\sqrt{2})\operatorname{sech}^2(x/\sqrt{2}) = -2q(x)(1-q^2(x)).$$

By the above relations, we find that

$$\Delta d = \left(\Delta\phi - \frac{1}{2\epsilon^2}q''\nabla_i d\nabla_j d\right)\frac{\epsilon}{q'}.$$

Replace ∇d with $(\nabla\phi)\epsilon/q'$ and q'' with $-2q(1-q^2)$ to get

$$\begin{aligned}\Delta d &= \left(\Delta\phi - \frac{1}{2\epsilon^2}2q(1-q^2)\nabla_i\phi\frac{\epsilon}{q'}\nabla_j\phi\frac{\epsilon}{q'}\right)\frac{\epsilon}{q'} \\ &= \frac{\epsilon}{q'}\left(\Delta\phi - \frac{q(1-q^2)}{(q')^2}\nabla_i\phi\nabla_j\phi\right).\end{aligned}$$

Now replace q' with $(1-q^2)/\sqrt{2}$ and factor to get

$$\begin{aligned}\Delta d &= \frac{\sqrt{2}\epsilon}{1-q^2}\left(\Delta\phi + \frac{q(1-q^2)}{(1-q^2)^2/2}\nabla_i\phi\nabla_j\phi\right) \\ &= \frac{\sqrt{2}\epsilon}{1-q^2}\left(\Delta\phi - \frac{2q}{q^2-1}\nabla_i\phi\nabla_j\phi\right).\end{aligned}$$

Finally, replace q with ϕ to get

$$\Delta d = \frac{\sqrt{2}\epsilon}{1-\phi^2}\left(\Delta\phi + \frac{2\phi}{\phi^2-1}\left|\nabla\phi\right|^2\right). \tag{293}$$

The unit normal vector to the interface is given by $n = \nabla d$ and the mean curvature is defined as $H = -1/2\ \nabla\cdot n$; therefore, the above quantity (293) is proportional to the mean curvature. Using this, and the fact that $\left|\nabla\phi\right|^2 = \frac{1}{2\epsilon^2}(1-q^2)^2 = \frac{1}{2\epsilon^2}(1-\phi^2)^2$, we have

$$\begin{aligned}H &= -\frac{1}{2}\Delta d \\ &= -\frac{\sqrt{2}\epsilon}{2(1-\phi^2)}\left(\Delta\phi - \frac{2\phi}{\phi^2-1}\left|\nabla\phi\right|^2\right) \\ &= \frac{\sqrt{2}\epsilon}{2(\phi^2-1)}\left(\Delta\phi - \frac{1}{\epsilon^2}\phi(\phi^2-1)\right). \qquad (294)\end{aligned}$$

Consider the integral

$$\begin{aligned}
\int_{-\infty}^{\infty}\left(1-q^2\left(\frac{x}{\sqrt{2}\epsilon}\right)\right)^2\,dx &= 2\int_0^{\infty}\operatorname{sech}^4\left(\frac{x}{\sqrt{2}\epsilon}\right)\,dx\\
&= \frac{\sqrt{2}\epsilon}{3}\left(3\sinh\left(\frac{x}{\sqrt{2}\epsilon}\right)+\sinh\left(\frac{3x}{\sqrt{2}\epsilon}\right)\right)\operatorname{sech}^3\left(\frac{x}{\sqrt{2}\epsilon}\right)\Bigg|_{x=0}^{\infty}\\
&= \frac{\sqrt{2}\epsilon}{3}\lim_{x\to\infty}\left(3\sinh\left(\frac{x}{\sqrt{2}\epsilon}\right)+\sinh\left(\frac{3x}{\sqrt{2}\epsilon}\right)\right)\operatorname{sech}^3\left(\frac{x}{\sqrt{2}\epsilon}\right)\\
&= \frac{\sqrt{2}\epsilon}{3}\lim_{x\to\infty}\left(\frac{3}{2}\left(e^{\frac{x}{\sqrt{2}\epsilon}}-e^{\frac{x}{\sqrt{2}\epsilon}}\right)+\frac{1}{2}e^{\frac{3x}{\sqrt{2}\epsilon}}-e^{\frac{-3x}{\sqrt{2}\epsilon}}\right)\left(\frac{2}{e^{\frac{x}{\sqrt{2}\epsilon}}+e^{\frac{-x}{\sqrt{2}\epsilon}}}\right)^3\\
&= \frac{\sqrt{2}\epsilon}{3}\lim_{x\to\infty}\left(\frac{4e^{\frac{3x}{\sqrt{2}\epsilon}}+\text{Lower order terms}}{e^{\frac{3x}{\sqrt{2}\epsilon}}+\text{Lower order terms}}\right)=\frac{4\sqrt{2}\epsilon}{3}.
\end{aligned}$$

By the above computation, the two forms for the bending energy are equivalent up to constant multiple:

$$\begin{aligned}
E_L &= \int_{\Gamma}k(H-C_0)^2\,dx = \frac{3}{4\sqrt{2}\epsilon}\int_{-\infty}^{\infty}\left(1-q^2\left(\frac{x}{\sqrt{2}\epsilon}\right)\right)^2\,dx\;\int_{\Gamma}k(H-C_0)^2\,dx\\
&= \frac{3}{4\sqrt{2}\epsilon}\int_{-\infty}^{\infty}(1-\phi^2(x))^2\,dx\;\int_{\Gamma}k\left(\frac{\sqrt{2}\epsilon}{2(\phi^2-1)}\left(\Delta\phi-\frac{1}{\epsilon^2}\phi(\phi^2-1)\right)-C_0\right)^2\,dx\\
&\sim \frac{3k}{4\sqrt{2}\epsilon}\int_{\Omega}(\phi^2(x)-1)^2\,\left(\frac{\epsilon}{\sqrt{2}(\phi^2-1)}\left(\Delta\phi-\frac{1}{\epsilon^2}\phi(\phi^2-1)\right)-C_0\right)^2\,dx\\
&= \frac{3k}{8\sqrt{2}\epsilon}\int_{\Omega}\left(\epsilon\Delta\phi-\frac{1}{\epsilon}\phi(\phi^2-1)-\sqrt{2}(\phi^2-1)C_0\right)^2\,dx\\
&= \frac{3k}{8\sqrt{2}\epsilon}\int_{\Omega}\left(\epsilon\Delta\phi-\left(\frac{1}{\epsilon}\phi+C_0\sqrt{2}\right)(\phi^2-1)\right)^2\,dx\\
&= \frac{3}{4\sqrt{2}}\int_{\Omega}\frac{k\epsilon}{2}\left(\Delta\phi-\frac{1}{\epsilon^2}(\phi+C\epsilon)(\phi^2-1)\right)^2\,dx=\frac{3}{4\sqrt{2}}E_E.
\end{aligned}$$

To justify the combination of integrals in line 3 above, note that the surface Γ can be continuously dilated and contracted in Ω. Therefore the combination of integrals can be thought of as integrating over the surface infinitely many times until it fills the domain. The approximation to the integral over Ω is justified since the integrand $(1-\phi^2)^2$ essentially has compact support, i.e., the integral from $-\infty$ to ∞ is essentially the same as the integral from one end of the boundary of Ω to another, provided Ω is sufficiently large.

In addition to the Eulerian formulation for the bending energy, we define the following area and volume constraints. The volume constraint is given by

$$A(\phi) = \int_\Omega \phi(x)\, dx. \tag{295}$$

Notice that the integral defined by (295) gives

$$\int_\Omega \phi\, dx = \int_{\Omega_i} \phi\, dx + \int_{\Omega_e} \phi\, dx \xrightarrow{\epsilon \to 0} \int_{\Omega_i} 1\, dx + \int_{\Omega_e} -1\, dx,$$

That is, $A(\phi)$ approaches the difference between the interior and exterior volumes. The surface area constraint is defined by

$$B(\phi) = \int_\Omega \left(\frac{\epsilon}{2} \left|\nabla \phi\right|^2 + \frac{1}{4\epsilon}(\phi^2 - 1)^2 \right)\, dx. \tag{296}$$

For small ϵ, the integrand of (296) is significant only near the interface Γ, and as $\epsilon \to 0$, $\phi(x) = q(d(x)/\epsilon) \to \tanh(d(x)/(\sqrt{2}\epsilon))$, so that $B(\phi) \to 2\sqrt{2}/3 \cdot \text{area}(\Gamma)$. This computation can be done by decomposing the integral over Ω into an integral over Γ and a 1D integral, the latter of which will have two terms that each integrate to $\sqrt{2}/3$,

$$\begin{aligned}
B(\phi) &= \int_\Omega \left(\frac{\epsilon}{2} \left|\nabla \phi\right|^2 + \frac{1}{4\epsilon}(1 - \phi^2)^2 \right)\, dx. \\
&\to \int_{-\infty}^{\infty} \frac{\epsilon}{2} \left(q'(\frac{x}{\sqrt{2}\epsilon}) \right)^2 + \frac{1}{4\epsilon} \left(1 - q^2(\frac{x}{\sqrt{2}\epsilon}) \right)^2 dx \int_\Gamma dS \\
&= \int_{-\infty}^{\infty} \frac{\epsilon}{2} \left(\left(1 - q^2(\frac{x}{\sqrt{2}\epsilon}) \right) \frac{1}{\sqrt{2}\epsilon} \right)^2 + \frac{1}{4\epsilon} \left(1 - q^2(\frac{x}{\sqrt{2}\epsilon}) \right)^2 dx \cdot \text{area}(\Gamma) \\
&= \left(\frac{\epsilon}{2} \frac{4\sqrt{2}\epsilon}{3} \frac{1}{2\epsilon^2} + \frac{1}{4\epsilon} \frac{4\sqrt{2}\epsilon}{3} \right) \cdot \text{area}(\Gamma) = \frac{2\sqrt{2}}{3} \cdot \text{area}(\Gamma).
\end{aligned} \tag{297}$$

7.3. GRADIENT FLOW

To ensure a decrease in the energy while keeping the surface area and volume enclosed fixed, we require that the motion of ϕ in time is governed by gradient flow,

$$\phi_t = -\gamma \frac{\delta E}{\delta \phi} = -\gamma \frac{\delta E_E}{\delta \phi} + \lambda_1 \frac{\delta A}{\delta \phi} - \lambda_2 \frac{\delta B}{\delta \phi}, \tag{298}$$

where λ_1 and λ_2 are Lagrange multipliers for the volume and area constraints. Next, we compute the functional derivatives. For simplicity, define

$$h = \Delta(\phi + \tau\psi) + \frac{1}{\epsilon^2}(\phi + \tau\psi + C\epsilon)(1 - (\phi + \tau\psi)^2),$$

$$f_c(\phi) = \epsilon\Delta\phi - \frac{1}{\epsilon}(\phi^2 - 1)(\phi + C\epsilon), \tag{299}$$

$$f(\phi) = \epsilon\Delta\phi - \frac{1}{\epsilon}(\phi^2 - 1)\phi, \tag{300}$$

$$g(\phi) = k\left(\Delta f_c - \frac{1}{\epsilon^2}(3\phi^2 + 2C\epsilon\phi - 1)f_c\right). \tag{301}$$

Then, using (6), we compute the functional derivative of E_E with respect to ϕ,

$$\begin{aligned}
\frac{d}{d\tau}E_E(\phi + \tau\psi) &= \frac{d}{d\tau}\int_\Omega \frac{k\epsilon}{2}\,|h|^2\,dx\,\bigg|_{\tau=0} = \int_\Omega \frac{k\epsilon}{2}2|h|\frac{h}{|h|}\left(\frac{dh}{d\tau}\right)dx\,\bigg|_{\tau=0} \\
&= \int_\Omega k\epsilon h\cdot\left(\Delta\psi + \frac{1}{\epsilon^2}\Big[\psi(1 - (\phi + \tau\psi)^2) + (\phi + \tau\psi + C\epsilon)(-2(\phi + \tau\psi)\psi)\Big]\right)dx\,\bigg|_{\tau=0} \\
&= \int_\Omega k\left(\epsilon\Delta\phi - \frac{1}{\epsilon}(\phi + C\epsilon)(\phi^2 - 1)\right)\left(\Delta\psi + \frac{1}{\epsilon^2}\psi\Big[1 - \phi^2 + (\phi + C\epsilon)(-2\phi)\Big]\right)\,dx \\
&= \int_\Omega kf_c\left(\Delta\psi - \frac{1}{\epsilon^2}\psi\Big[3\phi^2 + 2C\epsilon\phi - 1\Big]\right)\,dx \\
&= \int_\Omega -k\nabla f_c\cdot\nabla\psi\,dx - \int_\Omega k\frac{1}{\epsilon^2}\psi\Big[3\phi^2 + 2C\epsilon\phi - 1\Big]f_c\,dx \\
&= \int_\Omega k\Delta f_c\psi\,dx - \int_\Omega k\frac{1}{\epsilon^2}\psi\Big[3\phi^2 + 2C\epsilon\phi - 1\Big]f_c\,dx,
\end{aligned}$$

where the last two lines are obtained using integration by parts (1), assuming the test function ψ is compactly supported in Ω. (Note that the test function need not be zero on Γ, since the interface is not a boundary for the phase function ϕ, $\partial\Omega$ is the boundary.) Therefore, the functional derivative is

$$\frac{\delta E_E}{\delta\phi} = k\left(\Delta f_c - \frac{1}{\epsilon^2}(3\phi^2 + 2C\epsilon\phi - 1)f_c\right) = g. \tag{302}$$

Similarly, the functional derivatives for the boundary conditions are

$$\begin{aligned}\frac{\delta A}{\delta\phi} &= 1,\\ \frac{\delta B}{\delta\phi} &= -\epsilon\Delta\phi + \frac{1}{\epsilon}(\phi^2-1)\phi = -f.\end{aligned}$$

Therefore, the equation for gradient flow is simplified to

$$\phi_t = -\gamma g + \lambda_1 + \lambda_2 f. \tag{303}$$

To derive expressions for the Lagrange multipliers, we integrate (303) over the containment domain Ω. Since the integral of ϕ over Ω is the volume constraint $A(\phi)$, which is constant, $\int_\Omega \phi_t\, dx = 0$. Therefore, integrating (303) over Ω gives

$$\lambda_1|\Omega| + \lambda_2\int_\Omega f\, dx = \gamma\int_\Omega g\, dx. \tag{304}$$

Similarly, since $B(\phi)$ is proportional to the surface area, which is also constant, the time derivative is also zero,

$$\begin{aligned} 0 = \frac{d}{dt}B(\phi) &= \int_\Omega \epsilon\nabla\phi\cdot\nabla\phi_t + \frac{1}{\epsilon}(\phi^2-1)\phi\phi_t\, dx\\ &= \int_{\partial\Omega}\epsilon\phi_t(\nabla\phi\cdot n)\, dx - \int_\Omega \epsilon\phi_t\Delta\phi\, dx + \int_\Omega \frac{1}{\epsilon}(\phi^2-1)\phi\phi_t\, dx\\ &= \int_\Omega -\left(\epsilon\Delta\phi - \frac{1}{\epsilon}(\phi^2-1)\phi\right)\phi_t\, dx\\ &= \int_\Omega -f\phi_t\, dx\\ &= \int_\Omega f\phi_t\, dx, \end{aligned}$$

since $\nabla\phi\cdot n = 0$ on the boundary of Ω. Now, substituting in (303) above gives

$$\gamma\int_\Omega fg\, dx = \lambda_1\int_\Omega f\, dx + \lambda_2\int_\Omega f^2\, dx. \tag{305}$$

Equations (303), (304), and (305) give the system

$$\begin{cases} \phi_t + \gamma g - \lambda_1 - \lambda_2 f = 0, \\ \lambda_1 |\Omega| + \lambda_2 \int_\Omega f \, dx - \gamma \int_\Omega g \, dx = 0, \\ \lambda_1 \int_\Omega f \, dx + \lambda_2 \int_\Omega f^2 \, dx - \gamma \int_\Omega fg \, dx = 0. \end{cases} \tag{306}$$

Recall that f and g are given by (300), and (301), respectively.

Given some initial value $\phi(x, 0) = \phi_0(x)$ and boundary conditions for $\partial\Omega$, the system (306) defines the deformation of vesicles under curvature-driven membrane flow. As in [28], we apply periodic boundary conditions so that the Fourier transform is easier to apply. Figures 7.1 and 7.2 show why this is an acceptable boundary condition. The computation domain Ω is large enough so that the phase function ϕ is always close to -1 on the boundary $\partial\Omega$. Therefore, although a Dirichlet boundary condition of $\phi|_{\partial\Omega} = -1$ is perhaps a more natural condition, periodic boundary conditions are justifiable when Ω is large enough, allowing us to use Fourier transforms.

As a verification of the numerical procedure, we derive the energy dissipation law as follows. By taking the time derivative of (289),

$$\frac{dE_E}{dt} = \int_\Omega \frac{\delta E_E}{\delta \phi} \frac{d\phi}{dt} \, dx = \int_\Omega g \phi_t \, dx.$$

The last equality was obtained using the fact that the functional derivative of E_E is g. Then, by using the first two equations of (306), the energy dissipation law is

$$\begin{aligned} \frac{dE_E}{dt} &= \int_\Omega \frac{1}{\gamma} \left(-\phi_t + \lambda_1 + \lambda_2 f\right) \phi_t \, dx \\ &= -\frac{1}{\gamma} \int_\Omega \phi_t^2 \, dx + \frac{1}{\gamma} \int_\Omega (\lambda_1 + \lambda_2 f) \phi_t \, dx \\ &= -\frac{1}{\gamma} \int_\Omega \Big(\gamma g - \lambda_1 - \lambda_2 f\Big)^2 \, dx. \end{aligned} \tag{307}$$

The first line is obtained by substituting g using the first equation of (306), and the third line is obtained by substituting ϕ_t using the first equation then and employing the second equation on the second integral. This result will serve as a numerical check in the implementation.

7.4. NUMERICAL IMPLEMENTATION

For the numerical solution to the system (306), we follow the procedure of [28] and use the Crank-Nicholson method for the time discretization coupled with the Fourier spectral method for the spatial discretization. Since nonlinear systems are introduced with the time discretization, interior iterations are introduced to use an implicit method on the linear terms and an explicit method on the nonlinear terms.

7.4.1. THE FOURIER TRANSFORM. The Fourier Transform of a multivariable scalar-valued function $f(\vec{x}) \in L^1(\Omega)$, $\vec{x} \in \Omega \subset \mathbb{R}^3$ is defined in this context as

$$\mathcal{F}\Big(f(\vec{x})\Big)(\xi) = \int_\Omega f(\vec{x}) e^{-2\pi i \vec{x}\cdot\xi}\, d\vec{x}. \tag{308}$$

Using the definition (308), integration by parts and the fact that $f \in L^1$, the familiar property on derivatives holds

$$\mathcal{F}\left(\frac{\partial f(\vec{x})}{\partial x}\right) = (2\pi i u)\mathcal{F}\big(f(\vec{x})\big), \tag{309}$$

where u is the frequency in the x-component, i.e., if $\vec{x} \in \mathbb{R}^3$, $\xi = [u, v, w]$.

For the second derivatives,

$$\mathcal{F}\left(\frac{\partial^2 f(\vec{x})}{\partial x^2}\right) = -4\pi^2 u^2 \mathcal{F}\big(f(\vec{x})\big). \tag{310}$$

We can use these properties to derive properties for vector calculus. Let $f : \Omega \subset \mathbb{R}^3 \to \mathbb{R}$ be a multivariate real-valued absolutely integrable function. Then,

$$\begin{aligned} \mathcal{F}(\Delta\phi) &= \mathcal{F}\left(\frac{\partial^2\phi}{\partial x^2} + \frac{\partial^2\phi}{\partial y^2} + \frac{\partial^2\phi}{\partial z^2}\right) \\ &= (2\pi i u)^2\mathcal{F}(\phi) + (2\pi i v)^2\mathcal{F}(\phi) + (2\pi i w)^2\mathcal{F}(\phi) \\ &= -4\pi^2(u^2+v^2+w^2)\mathcal{F}(\phi). \end{aligned} \tag{311}$$

Similarly, $\Delta^2\phi$ can be computed from

$$\begin{aligned} \mathcal{F}(\Delta^2\phi) &= \mathcal{F}\left(\frac{\partial^4\phi}{\partial x^4} + \frac{\partial^4\phi}{\partial y^4} + \frac{\partial^4\phi}{\partial z^4} + 2\frac{\partial^4\phi}{\partial x^2 y^2} + 2\frac{\partial^4\phi}{\partial x^2 z^2} + 2\frac{\partial^4\phi}{\partial y^2 z^2}\right) \\ &= (2\pi i u)^4\mathcal{F}(\phi) + (2\pi i v)^4\mathcal{F}(\phi) + (2\pi i w)^4\mathcal{F}(\phi) \\ &\quad + 2\left((2\pi i)^4u^2v^2 + (2\pi i)^4u^2w^2 + (2\pi i)^4v^2w^2\right)\mathcal{F}(\phi) \\ &= 16\pi^4\left(u^4+v^4+w^4+2u^2v^2+2u^2w^2+2v^2w^2\right)\mathcal{F}(\phi) \\ &= 16\pi^4(u^2+v^2+w^2)^2\mathcal{F}(\phi). \end{aligned} \tag{312}$$

We chose these properties out of convenience for our application, but other properties that may be derived are similar.

7.4.2. Time discretization. To begin, we average the functions in the first equation in (306) over the current and next step ϕ_n and ϕ_{n+1}, and use a linear approximation on the derivative to obtain,

$$\frac{\phi_{n+1}-\phi_n}{\Delta t} + \gamma g(\phi_{n+1},\phi_n) - \lambda_1 - \lambda_2 f(\phi_{n+1},\phi_n) = 0, \tag{313}$$

where the averaged functions are defined using the Crank-Nicholson method

$$f(\phi_{n+1},\phi_n) = \frac{\epsilon}{2}\Delta(\phi_{n+1}+\phi_n) - \frac{1}{4\epsilon}(\phi_{n+1}^2+\phi_n^2-2)(\phi_{n+1}+\phi_n), \tag{314}$$

$$\begin{aligned} g(\phi_{n+1},\phi_n) &= \frac{k}{2}\Delta\left(f_c(\phi_{n+1}) + f_c(\phi_n)\right) \\ &\quad - \frac{k}{2\epsilon^2}\left(\phi_{n+1}^2 + \phi_{n+1}\phi_n + \phi_n^2 + C\epsilon(\phi_{n+1}+\phi_n) - 1\right)\left(f_c(\phi_{n+1}) + f_c(\phi_n)\right), \end{aligned} \tag{315}$$

and the function $f_c(\cdot)$ is defined in (299), unchanged. We want to solve this system for ϕ_{n+1}, but note that the functions (314) and (315) are nonlinear in ϕ_{n+1}. To treat the nonlinearities, we define an interior iteration ψ_m, where $\psi_m \to \phi_{n+1}$ as $m \to \infty$. Then, replacing ϕ_{n+1} with ψ_m in the nonlinear parts and ψ_{m+1} in the linear parts, we have the predictor-corrector scheme:

$$\frac{\psi_{m+1} - \phi_n}{\Delta t} + \gamma g(\psi_{m+1}, \psi_m, \phi_n) - \lambda_1 - \lambda_2 f(\psi_{m+1}, \psi_m, \phi_n) = 0, \tag{316}$$

where the new averaged functions are defined by

$$f(\psi_{m+1}, \psi_m, \phi_n) = \frac{\epsilon}{2}\Delta(\psi_{m+1} + \phi_n) - \frac{1}{4\epsilon}(\psi_m^2 + \phi_n^2 - 2)(\psi_m + \phi_n), \tag{317}$$

$$f_c'(\psi_{m+1}, \psi_m, \phi_n) = \frac{\epsilon}{2}\Delta(\psi_{m+1} + \phi_n) - \frac{1}{4\epsilon}(\psi_m^2 + \phi_n^2 - 2)(\psi_m + \phi_n + 2C\epsilon), \tag{318}$$

$$\begin{aligned} g(\psi_{m+1}, \psi_m, \phi_n) = {} & \Delta\left(f_c'(\psi_{m+1}, \psi_m, \phi_n)\right) \\ & - \frac{1}{2\epsilon^2}\left(\psi_m^2 + \psi_m\psi_n + \phi_n^2 - 1 + C\epsilon(\psi_m + \phi_n)\right)\left(f_c(\psi_m) + f_c(\phi_n)\right). \end{aligned} \tag{319}$$

The single variable function $f_c(\cdot)$ appearing at the end of (319) is still defined in (299). We first iterate over the interior index m. Numerically, once $\|\psi_{m+1} - \psi_m\|$ is less than some tolerance, we say that ψ_m has converged and update $\phi_{n+1} = \psi_m$. Then, we advance over the index n and repeat the process until convergence.

7.4.3. SPECTRAL METHODS. To solve the system (316) for ψ_{m+1}, we define intermediate functions to separate out the terms involving ψ_{m+1},

$$f_{lin}(\psi_{m+1}) = \frac{\epsilon}{2}\Delta\psi_{m+1}, \tag{320}$$

$$f_{nlin}(\psi_m, \phi_n) = \frac{\epsilon}{2}\Delta\phi_n - \frac{1}{4\epsilon}(\psi_m^2 + \phi_n^2 - 2)(\psi_m + \phi_n), \tag{321}$$

$$f_{c_{lin}}'(\psi_{m+1}) = \frac{\epsilon}{2}\Delta\psi_{m+1}, \tag{322}$$

$$f_{c_{nlin}}'(\psi_m, \phi_n) = \frac{\epsilon}{2}\Delta\phi_n - \frac{1}{4\epsilon}(\psi_m^2 + \phi_n^2 - 2)(\psi_m + \phi_n + 2C\epsilon), \tag{323}$$

$$g_{lin} = \Delta f'_{c_{lin}}(\psi_{m+1}), \tag{324}$$

$$\begin{aligned} g_{nlin} &= \Delta f'_{c_{nlin}}(\psi_m, \phi_n) \\ &\quad - \frac{1}{2\epsilon^2}\left(\psi_m^2 + \psi_m\psi_n + \phi_n^2 - 1 + C\epsilon(\psi_m + \phi_n)\right)(f_c(\psi_m) + f_c(\phi_n)). \end{aligned} \tag{325}$$

The implicit scheme for (316) is now given by

$$\frac{\psi_{m+1} - \phi_n}{\Delta t} = \lambda_1 + \lambda_2\left(f_{lin} + f_{nlin}\right) - \gamma\left(g_{lin} + g_{nlin}\right). \tag{326}$$

Now, gathering all the terms with ψ_{m+1}, using the formulas for f_{lin} and g_{lin}, we have

$$\psi_{m+1} - \lambda_2\Delta t f_{lin} + \gamma\Delta t g_{lin} = \left(\lambda_1 + \lambda_2 f_{nlin} - \gamma g_{nlin}\right)\Delta t + \phi_n,$$

$$\left(1 - \lambda_2\Delta t\frac{\epsilon}{2}\Delta + \gamma\Delta t\frac{\epsilon}{2}\Delta^2\right)\psi_{m+1} = \left(\lambda_1 + \lambda_2 f_{nlin} - \gamma g_{nlin}\right)\Delta t + \phi_n. \tag{327}$$

Since the left-hand side of (327) is linear in ψ_{m+1}, we can use Fourier transforms to solve the equation. Take the Fourier transform of both sides of (327) and use (311) and (312) to get

$$\begin{aligned} &\left(1 - \lambda_2\Delta t\frac{\epsilon}{2}\left(-4\pi^2(u^2+v^2+w^2)\right) + \gamma\Delta t\frac{\epsilon}{2}\left(16\pi^4(u^2+v^2+w^2)^2\right)\right)\mathcal{F}(\psi_{m+1}) \\ &\quad = \mathcal{F}(\left(\lambda_1 + \lambda_2 f_{nlin} - \gamma g_{nlin}\right)\Delta t + \phi_n). \end{aligned}$$

Finally, divide and take an inverse Fourier transform to obtain the iterative method,

$$\psi_{m+1} = \mathcal{F}^{-1}\left(\frac{\mathcal{F}\left(\left(\lambda_1 + \lambda_2 f_{nlin} - \gamma g_{nlin}\right)\Delta t + \phi_n\right)}{1 + 2\pi^2\epsilon\lambda_2\Delta t\left(u^2+v^2+w^2\right) + 8\pi^4\epsilon\gamma\Delta t\left(u^2+v^2+w^2\right)^2}\right). \tag{328}$$

7.4.4. LAGRANGE MULTIPLIERS. For the computation of the Lagrange multipliers in (306), we use the implicit scheme analogous to (313). The conditions for the Lagrange multipliers are modified from the second and third equations in (306) to

$$\begin{cases} \lambda_1|\Omega| + \lambda_2\displaystyle\int_\Omega f(\psi_m, \phi_n)\,dx - \gamma\int_\Omega g(\psi_m, \phi_n)\,dx = 0, \\ \lambda_1\displaystyle\int_\Omega f(\psi_m, \phi_n)\,dx + \lambda_2\int_\Omega f^2(\psi_m, \phi_n)\,dx - \gamma\int_\Omega f(\psi_m, \phi_n)g(\psi_m, \phi_n)\,dx = 0, \end{cases} \tag{329}$$

where the functions f and g follow

$$f(\psi_m,\phi_n) = \frac{\epsilon}{2}\Delta(\psi_m+\phi_n) + \frac{1}{4\epsilon}(\psi_m^2+\phi_n^2-2)(\psi_m+\phi_n), \tag{330}$$

$$\begin{aligned} g(\psi_m,\phi_n) = {} & \frac{k}{2}\Delta\left(f_c(\psi_m)+f_c(\phi_n)\right) \\ & - \frac{k}{2\epsilon^2}\left(\psi_m^2+\psi_m\phi_n+\phi_n^2+C\epsilon(\psi_m+\phi_n)-1\right)\left(f_c(\psi_m)+f_c(\phi_n)\right), \end{aligned} \tag{331}$$

We can solve (329) for λ_1 and λ_2 easily as a system of two equations. Define intermediate variables

$$a = |\Omega|, \tag{332}$$

$$b = \int_\Omega f(\psi_m,\phi_n)\,dx, \tag{333}$$

$$d = \int_\Omega f^2(\phi_{n+1},\phi_n)\,dx, \tag{334}$$

$$v_1 = \gamma\int_\Omega g(\psi_m,\phi_n)\,dx, \tag{335}$$

$$v_2 = \gamma\int_\Omega f(\psi_m,\phi_n)g(\psi_m,\phi_n)\,dx. \tag{336}$$

The variables that are integrals can all be computed quickly by using the zero-frequency component of the Fourier transform of the respective integrands. Then, (329) is equivalent to the linear system,

$$\begin{bmatrix} a & b \\ b & d \end{bmatrix}\begin{pmatrix}\lambda_1\\ \lambda_2\end{pmatrix} = \begin{pmatrix} v_1 \\ v_2\end{pmatrix}, \tag{337}$$

whose solution is given by

$$\begin{aligned} \lambda_1 &= \frac{v_2 - dv_1/b}{b - ad/b}, \\ \lambda_2 &= \frac{v_2 - bv_1/a}{d - b^2/a}. \end{aligned} \tag{338}$$

7.4.5. CONSERVATION AND DISSIPATION LAWS. We can write the expression $\delta A/\delta\phi = 1$ in discrete form

$$\begin{aligned} A(\phi_{n+1}) - A(\phi_n) &= \int_\Omega (\phi_{n+1} - \phi_n)\, dx \\ &= -\Delta t \int_\Omega \Big(\gamma g(\phi_{n+1}, \phi_n) - \lambda_1 - \lambda_2 f(\phi_{n+1}, \phi_n)\Big)\, dx \\ &= 0. \end{aligned}$$

The second equality is from (313), and the result is zero by the first equation of (329), since $\psi_m \to \phi_{n+1}$. The equality guarantees that the total volume is conserved. In a similar way, the surface area is conserved, since $\delta B/\delta\phi = -f$,

$$\begin{aligned} B(\phi_{n+1}) - B(\phi_n) &= -\int_\Omega (\phi_{n+1} - \phi_n) f(\phi_{n+1}, \phi_n)\, dx \\ &= -\Delta t \int_\Omega \Big(\gamma g(\phi_{n+1}, \phi_n) - \lambda_1 - \lambda_2 f(\phi_{n+1}, \phi_n)\Big) f(\phi_{n+1}, \phi_n)\, dx \\ &= 0, \end{aligned}$$

where the minus sign is added to match the form of the conservation law for the volume constraint. Here, the second equality is from (313) as before, and the result is zero by the second equation of (329), since $\psi_m \to \phi_{n+1}$. Finally, we can apply the same procedure to derive the discrete form of the energy dissipation law (307):

$$\begin{aligned} E_E(\phi_{n+1}) - E_E(\phi_n) &= \int_\Omega (\phi_{n+1} - \phi_n) g(\phi_{n+1}, \phi_n)\, dx \\ &= -\Delta t \int_\Omega \Big(\gamma g(\phi_{n+1}, \phi_n) - \lambda_1 - \lambda_2 f(\phi_{n+1}, \phi_n)\Big) g(\phi_{n+1}, \phi_n)\, dx \\ &= -\frac{\Delta t}{\gamma} \int_\Omega \Big(\gamma g(\phi_{n+1}, \phi_n) - \lambda_1 - \lambda_2 f(\phi_{n+1}, \phi_n)\Big)^2\, dx. \end{aligned}$$

7.4.6. FULL ALGORITHM FOR PHASE FIELD METHOD AND RESULTS. The complete algorithm is given by

$$
\begin{cases}
\dfrac{\psi_{m+1}-\phi_n}{\Delta t} + \gamma g(\psi_{m+1},\psi_m,\phi_n) - \lambda_1 - \lambda_2 f(\psi_{m+1},\psi_m,\phi_n) = 0, \\
\lambda_1|\Omega| + \lambda_2 \displaystyle\int_\Omega f(\psi_m,\phi_n)\,dx - \gamma \int_\Omega g(\psi_m,\phi_n)\,dx = 0, \\
\lambda_1 \displaystyle\int_\Omega f(\psi_m,\phi_n)\,dx + \lambda_2 \int_\Omega f^2(\psi_m,\phi_n)\,dx - \gamma \int_\Omega f(\psi_m,\phi_n)g(\psi_m,\phi_n)\,dx = 0, \\
\phi_{n+1} = \psi_m.
\end{cases}
\tag{339}
$$

The algorithm is summarized as follows:

Algorithm 7.1 Computing phase field function ϕ_{n+1}

```
Define initial phase field function $\phi_0$ via (291)
Compute constraints (295) and (296) using zero frequency component of FFT
Compute initial energy $E(\phi_0)$ by (289)
for $n$ from 0 to $N$ do:
    $m \leftarrow 0$
    Initialize $\psi_m \leftarrow \phi_n$
    while $||\psi_{m+1} - \psi_m||^2 \geq 10^{-7}$ do:
        Compute $f(\psi_m, \phi_n)$ and $g(\psi_m, \phi_n)$ using (330) and (331)
        Compute $\lambda_1$ and $\lambda_2$ by (338)
        Compute $f_{nlin}$ and $g_{nlin}$ using (321) and (325)
        Update $\psi_{m+1}$ using (328)
        Update $m \leftarrow m + 1$
    end while
    Update $\phi_{n+1} \leftarrow \psi_m$
end for
```

We run a few numerical tests to illustrate the method. In each of the tests, we use a $64 \times 64 \times 64$ grid over the domain $\Omega = [-\pi, \pi]^3$. We chose $\epsilon = 0.1$ and used a timestep of $\Delta t = 2.5 \times 10^{-5}$. We matched the choice in [103] with the Lagrange multiplier $\gamma = 3$.

First, we begin with two spheres of equal radius, separated by a small distance. Note that there is no force that brings the vesicles closer together in this model (yet). Electrostatic forces may drive the vesicles closer together until they touch, and then our model can simulate the curvature energy minimization from this point. After running Algorithm 7.1, the spheres merged together to minimize the curvature cost. The results are show in Figure 7.3. The interior iterations converged in 7 steps initially, but then quickly converged in 3 steps as time elapsed.

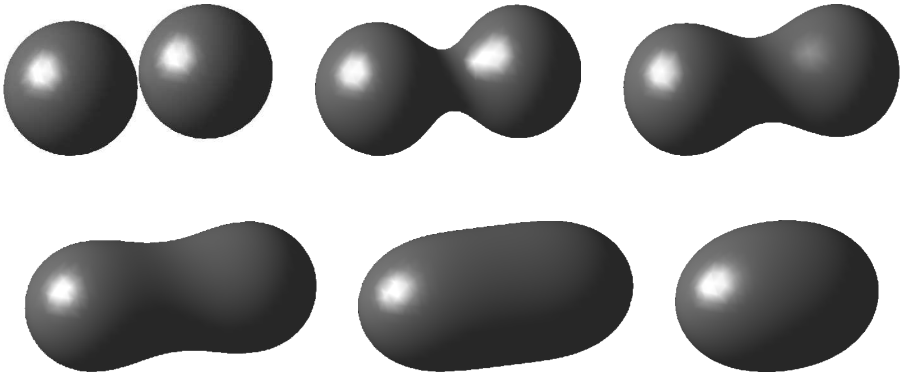

Figure 7.3: Two spheres merging according to Algorithm 7.1.

Next, of course, what's more interesting than two spheres... three! Figure 7.4 illustrates the merging of three spheres under Algorithm 7.1. The interior iterations converged in 7 steps initially, but then quickly converged in 3 steps as time elapsed.

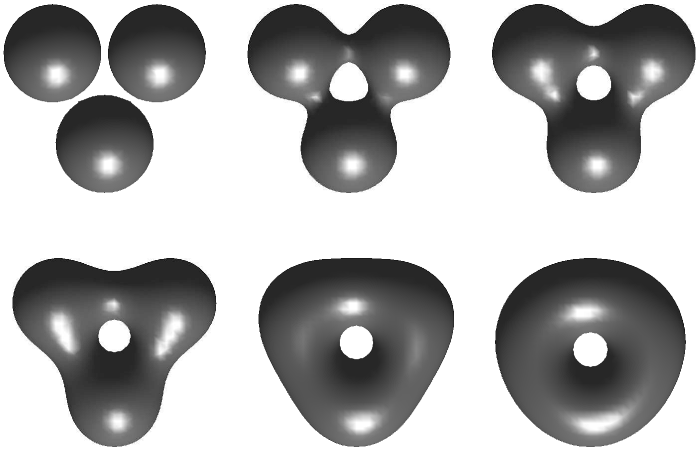

Figure 7.4: Three spheres merging according to Algorithm 7.1.

Finally, perhaps more biologically interesting is the merging of a smaller vesicle into a larger one, similar to the process of endocytosis. This is demonstrated in Figure 7.5. The interior iterations converged in 6 steps initially, but then quickly converged in 3 steps as time elapsed. Of course, this description is an oversimplification of endocytosis, since it neglects

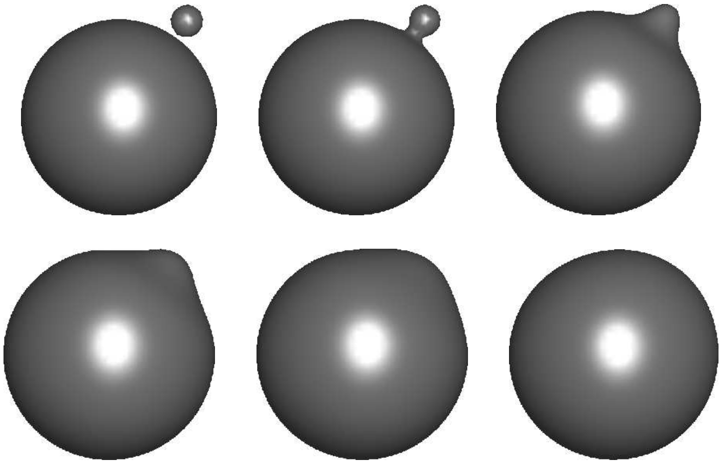

Figure 7.5: “Endocytosis” according to Algorithm 7.1.

the inversion of the membranes. The merging process, however, is well-captured.

We note that there are many other interesting configurations that can be described under this method, as well as a variety of other applications for phase field models. We extend the model in the following section.

CHAPTER 8

Curvature-driven protein localization

In practice, vesicles are not strictly composed of a single species of lipids. Experiments suggest that multiple species of lipids arrange themselves into distinct domains called rafts, which play an important role in protein activity [48, 101, 102]. Modeling multiple species on the vesicle membrane requires an extension of the single phase-field function model of Chapter 7. Du, et. al., have modeled two lipid species by using two phase functions [103]. The phase functions are orthogonal and their intersections define the separation of the two lipid species. They have been able to reproduce numerous vesicle shapes, such as the ones shown in Figure 8.1. While this approach has produced results matching experiments [7], the model is limiting in the following way. Lipid species may arrange themselves into distinct phases; however, proteins do not necessarily form phases [54]. Therefore, a dual phase field model may account for multiple lipid species, but it cannot account for the effect of diffusive proteins in lipid membranes.

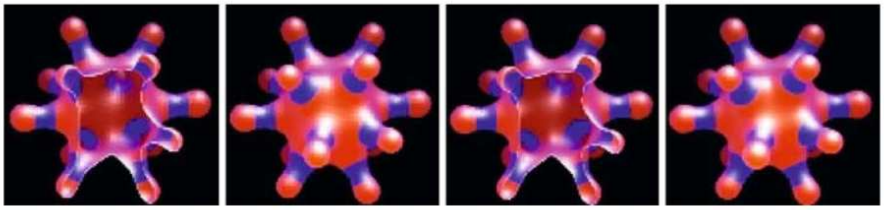

Figure 8.1: Various shapes of two-component membranes [103]. The different colors correspond to the two components.

8.1. Proteins and membrane curvature

Experiments suggest that diffusive proteins within lipid membranes play a significant role in membrane curvature [6, 109, 3, 19, 82, 96, 50]. A fraction between 30% and 90% of all membrane proteins can freely diffuse along the membrane [35, 54]. A few mechanisms of protein induced curvature are presented in Figure 8.2. In Figure 8.2 (a), rigid proteins

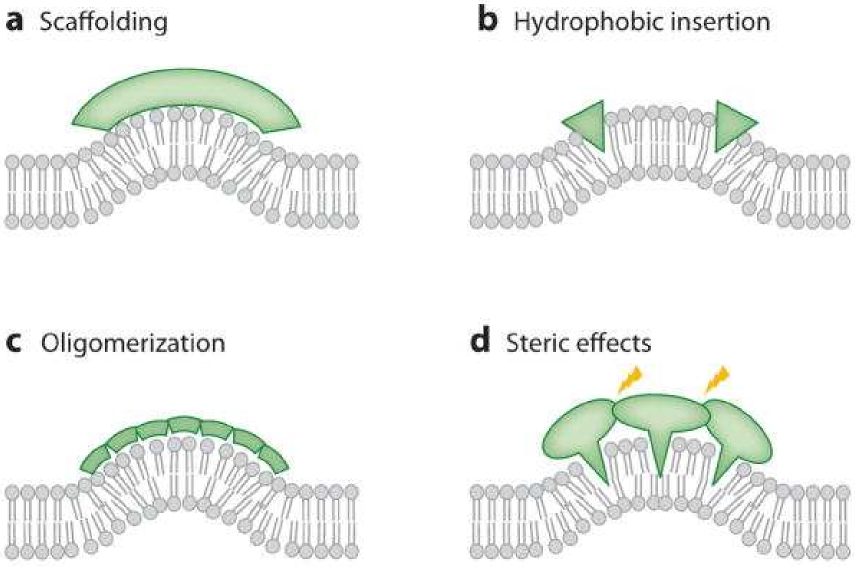

Figure 8.2: Mechanisms of protein-induced membrane curvature [6].

such as those in the BAR (Bin/Amphiphysin/Rvs) domain family can act as a scaffold to the membrane. These proteins have an intrinsic curvature and, upon attachment, the membrane bends to match the protein curvature. Similarly, in Figure 8.2 (c), several proteins can oligomerize to create a rigid shape and bend the membrane. Protein coats such as clathrin, COPI (COat Protein I) and COPII (COat Protein II) are examples of this type. Other proteins may insert themselves into the membrane as shown in Figure 8.2 (b). There may be a difference between the length of the hydrophobic region of a membrane protein and the thickness of the hydrophobic core of the lipid bilayer in which it is embedded, thereby inducing curvature in the membrane [82]. Epsin proteins do this by forming an α-helix known as H0 upon binding to the membrane, and this helix inserts itself into the membrane [6]. Finally, local protein crowding of peripheral proteins can cause membrane bending by creating an asymmetry of the monolayer areas and thereby curling the membrane away from the side which the crowding occurred, as shown in Figure 8.2 (d). This effect is experimentally demonstrated in [96].

Further illustrating the importance of proteins in membranes, Schmidt et. al. showed that the M2 protein plays an essential role in generating regions of high curvature in the influenza A virus membrane [88]. This specific protein accumulates in regions of negative Gaussian curvature and can generate curvature in the membrane itself, allowing the virus to replicate. The process is depicted in Figure 8.3.

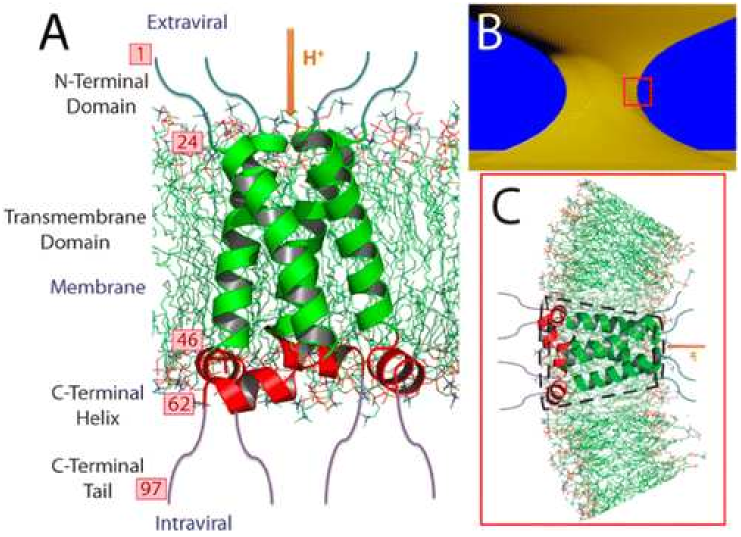

Figure 8.3: (A) Structure of M2 protein, (B) The neck of a bud, (C) M2 protein in membrane. Figure from [88].

While these examples should provide sufficient motivation to include proteins to the model, we note that all endocytosis and exocytosis processes are promoted in one way or another by proteins. Therefore, any viral replication process requires proteins. Antagonizing the curvature effects of proteins is a viable antiviral strategy [88]. Mathematically modeling these processes is beneficial toward this end.

8.2. Surface diffusion model

As stated previously, a phase field method simulates topological changes successfully, but a more physically relevant model for vesicle budding and scission must include proteins which diffuse along the surface of the membrane but do not form separate phases. Dual phase field models always produces phase separation, so we must use a different approach to model the diffusive proteins on the membrane.

To describe effect of the proteins in a continuum framework, we treat the proteins as diffusive particles on the membrane surface. Both the proteins and lipids follow some mass conservation law incorporating the effects of diffusion and advection on the membrane. A continuum model is physically justifiable by the relative length scales of the proteins embedded in the membrane, which are typically 4-5nm. thick, to the cell, which can be up to 100 μm in diameter. (In the aforementioned virus replication example, the spherical virions produced from the budding are typically 100nm in diameter [87].) At such length scales, we may consider the proteins as diffusive particles that are attracted toward necking regions.

Notice that in Figure 8.3 (C), the protein is embedded in the membrane and induces some curvature to the membrane. We call this induced curvature the spontaneous curvature of the diffusive protein species, just as we have defined separate spontaneous curvatures for the lipids. This can be calculated by measuring the curvature difference in the membrane when the protein is embedded to that of the membrane without the protein, as depicted in Figure 8.4.

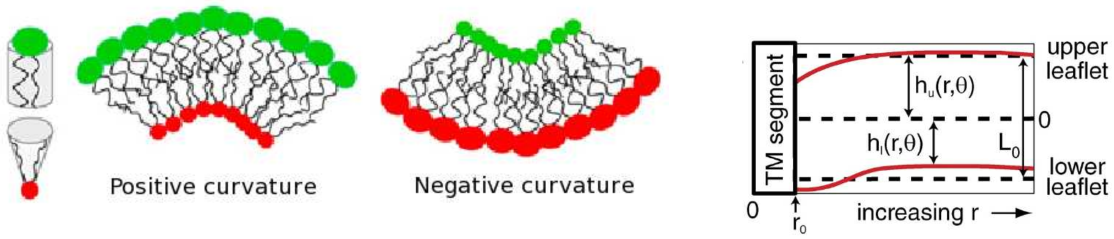

Figure 8.4: Left: Depiction of lipid spontaneous curvature [105]. Right: Depiction of protein spontaneous curvature in the sense that the membrane bends after protein insertion [12].

We wish to solve the advection-diffusion equation on a surface. Various techniques have been established for this purpose. Dziuk used finite element methods to solve elliptic partial differential equations on stationary surfaces [29]. This work was expanded with Elliott for parabolic equations on moving surfaces [30]. This work was extended even further with Deckelnick and Heine by solving the equation using a narrow band around the surface [21]. Other approaches for PDEs on surfaces include [100, 43, 1, 104, 79] and references therein. In all of the aforementioned approaches, mesh refinement is required to accurately resolve the numerical solution. These methods work well for stationary surfaces, but mesh refinement for dynamic surfaces can be a significant computational challenge, since the mesh must be changed with each movement of the membrane.

For this reason, we use the Fourier spectral method as we did for the solution of the shape equation of the membrane in Chapter 7. Fourier methods have so-called exponential convergence, meaning that the error decreases faster than any power of the grid size [97]. Therefore, mesh refinement near the interface is not necessary in Fourier (global) approaches as it is in finite element and finite difference (local) approaches. Since the surface is given as a level set of the phase function ϕ, no explicit tracking of the surface is necessary, and no parameterization of the surface is required. Finally, since the framework is consistent, we may solve the diffusion equation on surfaces given by Algorithm 7.1. That is, we may simultaneously solve for the shape of the membrane and the concentration of diffusive species on the membrane. The results of this coupled procedure should produce effects that are not easily observable in experiments.

Our model is summarized as follows. The total energy for the system is defined and minimized using the phase field approach formulated in Chapter 7. Multiple lipid and protein species are allowed to diffuse and advect on the surface of the membrane, governed by a curvature-driven diffusion equation similar to (192). The difference between this diffusion equation and (192) is that the flux should be proportional to a diffusion potential which is governed by the curvature energy (287). The movement of the diffusive species will induce a curvature on the membrane through the spatially variable and concentration dependent spontaneous curvature.

8.3. Energy formulation

The total energy of the system is now composed of the membrane bending energy in Eulerian form (289), modified to include the effects of the multiple lipid and protein species on the spontaneous curvature and the entropic energy from the sizes of the lipids and proteins. Eventually, we should include the electrostatic potential energy arising from the charges on the proteins, lipids, and ions. This will be a future project. We remove the electrostatic contribution of the energy for now so that the Poisson equation does not need to be solved. Consider the following energy,

$$E_{\text{tot}} = E_{\text{mem}} + E_{\text{ent}}. \tag{340}$$

The membrane energy (289) is modified through a density dependent spontaneous curvature C as follows,

$$E_{\text{mem}} = \int_\Omega \frac{\epsilon}{2} \left| \Delta\phi - \frac{1}{\epsilon^2}(\phi^2 - 1)(\phi + C(\rho_l^{\text{lip}}, \rho^{\text{pro}})\epsilon) \right|^2 dx, \tag{341}$$

where ρ_l^{lip} is the concentration of lipid species l, $l = 1, \ldots, m$, and ρ^{pro} is the concentration of the single protein species. Throughout our notation, we use subscripts to denote the species number and superscripts to denote the species type, i.e., the concentration of lipid species l is ρ_l^{lip}, the concentration of the proteins is ρ^{pro}, and the concentration of ion species i is ρ_i^{ion}. We consider only one species of protein; however, the model can easily be extended with the use of subscripts. The explicit function for $C(\rho_l^{\text{lip}}, \rho^{\text{pro}})$ is defined by the weighted average of the spontaneous curvatures of the contributing species,

$$C_0 = \left(\frac{\sum_{l=0}^{m} C_0^l (a_l^{\text{lip}})^2 \rho_l^{\text{lip}} + C_0^{\text{pro}} (a^{\text{pro}})^2 \rho^{\text{pro}}}{\sum_{l=0}^{m} (a_l^{\text{lip}})^2 \rho_l^{\text{lip}} + (a^{\text{pro}})^2 \rho^{\text{pro}}} \right), \qquad \forall \vec{x} \in \Omega, \tag{342}$$

where C_0^l is the spontaneous curvature of lipid species l and C_0^{pro} is the spontaneous curvature of the protein at each point $\vec{x}$ in the domain Ω [6]. The scaling $C = \sqrt{2}C_0$ is maintained to include the spontaneous curvature (342) into the curvature energy (341) with the equivalence to the 2D energy (287) in the sharp interface limit. The a_l^{lip} are the effective sizes for the charged lipids $l = 1, \ldots, m$; m is the total number of charged lipids in the bilayer; and a_0^{lip} is the effective size of the neutral lipids. Each lipid is modeled as a hard disk occupying some surface area in the membrane, hence we take $(a_l^{\text{lip}})^2$ for an effective surface area. Similarly, the a^{pro} is the effective size of the protein embedded in the membrane, occupying some surface area $(a^{\text{pro}})^2$. The concentration of particles on the membrane cannot exceed the available space, so the concentrations must satisfy the equation

$$\sum_{l=0}^{m}(a_l^{\text{lip}})^2\rho_l^{\text{lip}} + (a^{\text{pro}})^2\rho^{\text{pro}} = 1. \tag{343}$$

This equation (343) simplifies the spontaneous curvature (342) to

$$C_0 = \sum_{l=0}^{m} C_0^l (a_l^{\text{lip}})^2\rho_l^{\text{lip}} + C_0^{\text{pro}}(a^{\text{pro}})^2\rho^{\text{pro}}, \qquad \forall \vec{x} \in \Omega, \tag{344}$$

$$C = \sqrt{2}C_0. \tag{345}$$

In the spirit of (169), the entropic energy for the membrane with embedded proteins is defined by

$$\begin{aligned} E_{\text{ent}} = {} & \frac{1}{\beta}\int_\Omega \left(\sum_{i=0}^{r} \rho_i^{\text{ion}}\left[\ln\left(\rho_i^{\text{ion}}(a_i^{\text{ion}})^3\right) - 1\right]\right) dx \\ & + \frac{1}{\beta}\int_\Omega \left(\sum_{l=0}^{m} \rho_l^{\text{lip}}\left[\ln\left(\rho_l^{\text{lip}}(a_l^{\text{lip}})^2\right) - 1\right]\right) dx \\ & + \frac{1}{\beta}\int_\Omega \left(\rho^{\text{pro}}\left[\ln\left(\rho^{\text{pro}}(a^{\text{pro}})^2\right) - 1\right]\right) dx, \end{aligned} \tag{346}$$

where β is still the inverse thermal energy $\beta = 1/(k_B T)$ [108]. The a_i^{ion} are the effective ion sizes for $i = 1, \ldots, r$, r is the total number of ionic species in the solvent, and a_0^{ion} is the effective size of the solvent molecules. Each ion is modeled as a sphere occupying some volume in the solvent, hence we take $(a_i^{\text{ion}})^3$ for an effective volume. The concnetration of the ions in the solvent cannot exceed the available space, therefore the effective ion sizes must satisfy

$$\rho_0^{\text{ion}}(a_0^{\text{ion}})^3 + \sum_{i=1}^{r}\rho_i^{\text{ion}}(a_i^{\text{ion}})^3 = 1. \tag{347}$$

Note that there are no functions which depend explicitly upon the phase field function ϕ in the entropic energy (346). Therefore the gradient flow equations given by (328) remain the same, since $\frac{\delta E_{\text{ent}}}{\delta \phi} = 0$. The entropic energy is defined without the use of any surface delta functions, as the domain restrictions are imposed by the initial conditions and the differential equation. We require the initial distribution of ions to be localized in the bulk, away from the membrane, and the flux shall only occur in the bulk. This restricts the ions to the bulk, away from the membrane. Similarly, we require the initial distribution of lipids and proteins to be localized to the membrane, away from the bulk, and the flux shall only occur on the membrane. In this way, no delta functions are required in the entropic energy equation. This is consistent with the framework of the curvature energy (341).

8.4. MASS CONSERVATION LAW

We begin with a mathematical treatment for the diffusive lipids and proteins. Different species are allowed to advect and diffuse across the membrane. The concentrations of lipids and proteins satisfy a general mass conservation law for a general concentration ρ,

$$\frac{\partial \rho}{\partial t} + v \cdot \nabla \rho = -\nabla \cdot J, \qquad x \in \Omega, \tag{348}$$

where v is the velocity of the surface Γ, and J is the surface flux. A constitutive relation for the flux is given by the Nernst-Planck formula as an extension of Fick's first law,

$$J = -D\delta_\Gamma \beta \rho \nabla \mu, \tag{349}$$

where μ is the diffusion potential and D is the diffusion coefficient [108]. Note that this diffusion potential is based on the curvature energy; therefore the flux is curvature-driven. The flux is restricted by the surface delta function δ_Γ so that diffusion is nonzero only on the the membrane Γ, rather than the entire domain Ω. The surface delta function δ_Γ is defined by the property

$$\int_\Gamma f(x)\, d\Gamma = \int_\Omega f(x) \delta_\Gamma \, dx. \tag{350}$$

There are many choices to use for the surface delta function. A good catalog can be found in [60]. A good choice must maintain the property that $\int_\Omega \delta_\Gamma \, dx \propto \text{area}(\Gamma)$, as in (297). It may be convenient to choose a function without a $|\nabla \phi|$ term for the sake of the simplicity of the variation computations with respect to ϕ, (e.g., in equation (302)). We present our choice later in equation (441).

Finally, note that there is a corresponding mass conservation equation (348) and a corresponding Nernst-Planck flux (349) for each lipid species, ion species, and the proteins, using the appropriate subscripts and superscripts. For the ion species, however, the flux is given by

$$J^{\text{ion}} = -D(1 - \delta_\Gamma)\beta\rho\nabla\mu, \tag{351}$$

since the flux of ions should only occur outside of the membrane.

8.4.1. VELOCITY COMPUTATION. The fact that the surface deformation is driven by energy minimization requires the smallest possible velocity for any deformation. That is, any component of the velocity that is tangential to the surface will cost unnecessary energy for the deformation. Therefore, v must be normal to the surface. The velocity of the deformation is nonzero only in a small neighborhood of the surface Γ.

The velocity in the diffusion equation (348) can be computed by considering two realizations of the surface $\phi = 0$, one at time t and position x, and another at a later time $t + dt$ and at the deformed position $x + dx$. Consider a first order Taylor expansion for ϕ about (t, x),

$$\phi(x + dx, t + dt) = \phi(x, t) + \phi_t(x, t)\ dt + \nabla\phi(x, t)\ dx + \mathcal{O}(dt^2, dx^2). \tag{352}$$

We are only interested in the surface, where $\phi = 0$, so (352) up to first order becomes

$$0 = \phi_t\ dt + \nabla\phi\ dx. \tag{353}$$

From (353), we can see that

$$\nabla\phi \frac{dx}{dt} = -\phi_t. \tag{354}$$

Then we can define the normal component of the velocity using the fact that the surface normal is given by $n = \nabla\phi/|\nabla\phi|$,

$$v_n = n \cdot \frac{dx}{dt} = \frac{\nabla\phi}{|\nabla\phi|}\frac{dx}{dt} = \frac{-\phi_t}{|\nabla\phi|}. \tag{355}$$

The formula for the normal velocity (355) is the formula for the velocity under our assumption that the tangential velocity is zero. In fact, there are no computational techniques to our knowledge for the computation of the tangential velocity using phase field methods, but we do not require one for our model.

8.4.2. Surface flux and diffusion potential. The diffusion potentials are defined as the functional derivatives of the total energy (340) with respect to the appropriate concentrations,

$$\mu_i^{\text{ion}} = \frac{\delta E_{\text{tot}}}{\delta\rho_i^{\text{ion}}} = \frac{\delta E_{\text{mem}}}{\delta\rho_i^{\text{ion}}} + \frac{\delta E_{\text{ent}}}{\delta\rho_i^{\text{ion}}}, \qquad i = 1, \dots, r; \tag{356}$$

$$\mu_l^{\text{lip}} = \frac{\delta E_{\text{tot}}}{\delta\rho_l^{\text{lip}}} = \frac{\delta E_{\text{mem}}}{\delta\rho_l^{\text{lip}}} + \frac{\delta E_{\text{ent}}}{\delta\rho_l^{\text{lip}}}, \qquad l = 1, \dots, m; \tag{357}$$

$$\mu^{\text{pro}} = \frac{\delta E_{\text{tot}}}{\delta\rho^{\text{pro}}} = \frac{\delta E_{\text{mem}}}{\delta\rho^{\text{pro}}} + \frac{\delta E_{\text{ent}}}{\delta\rho^{\text{pro}}}. \tag{358}$$

For the computation of the diffusion potentials, we can solve (347) and (343) for $\rho_0^{\text{ion}}(a_0^{\text{ion}})^3$ and $\rho_0^{\text{lip}}(a_0^{\text{lip}})^2$ respectively and substitute these quantities in the entropic energy (346) to obtain an easier form for differentiating. For convenience, we also split the entropic energy into two components: one for the ion contribution to the volume, and the other for the lipid and protein contribution to the surface area. Define

$$\begin{aligned} E_{\text{ent}}^{\text{ion}} = \frac{1}{\beta}\int_\Omega \Bigg(\frac{1}{(a_0^{\text{ion}})^3}\left(1 - \sum_{i=1}^r \rho_i^{\text{ion}}(a_i^{\text{ion}})^3\right)\left[\ln\left(1 - \sum_{i=1}^r \rho_i^{\text{ion}}(a_i^{\text{ion}})^3\right) - 1\right] \\ + \sum_{i=1}^r \rho_i^{\text{ion}}\left[\ln\left(\rho_i^{\text{ion}}(a_i^{\text{ion}})^3\right) - 1\right]\Bigg)\, dx, \end{aligned} \tag{359}$$

$$E_{\text{ent}}^{\text{lip}} = \frac{1}{\beta}\int_{\Omega}\left(\frac{1}{\left(a_0^{\text{lip}}\right)^2}\left(1-\rho^{\text{pro}}(a_0^{\text{pro}})^2-\sum_{l=1}^{m}\rho_l^{\text{lip}}(a_l^{\text{lip}})^2\right)\right.$$
$$\times\left[\ln\left(1-\rho^{\text{pro}}(a_0^{\text{pro}})^2-\sum_{l=1}^{m}\rho_l^{\text{lip}}(a_l^{\text{lip}})^2\right)-1\right]$$
$$\left.+\sum_{l=1}^{m}\rho_l^{\text{lip}}\left[\ln\left(\rho_l^{\text{lip}}(a_l^{\text{lip}})^2\right)-1\right]+\rho^{\text{pro}}\left[\ln\left(\rho^{\text{pro}}(a^{\text{pro}})^2\right)-1\right]\right)dx, \tag{360}$$

where $E_{\text{ent}} = E_{\text{ent}}^{\text{ion}} + E_{\text{ent}}^{\text{lip}}$. We emphasize that the notation $E_{\text{ent}}^{\text{lip}}$ includes both the entropic energy from the lipids and the proteins, since both reside on the membrane. First, it should be clear that $\delta E_{\text{mem}}/\delta\rho_i^{\text{ion}} = 0$ and $\delta E_{\text{ent}}^{\text{lip}}/\delta\rho_i^{\text{ion}} = 0$, and so μ_i^{ion} depends only upon the ionic entropic energy. The diffusion potential for the ions is the same as in [108]. The computations are

$$\frac{\delta E_{\text{ent}}^{\text{ion}}}{\delta\rho_i^{\text{ion}}} = \frac{1}{\beta}\left(\frac{1}{(a_0^{\text{ion}})^3}\left(-(a_i^{\text{ion}})^3\right)\left[\ln\left(1-\sum_{j=1}^{r}\rho_j^{\text{ion}}(a_j^{\text{ion}})^3\right)-1\right]\right.$$
$$+\frac{1}{(a_0^{\text{ion}})^3}\left(1-\sum_{j=1}^{r}\rho_j^{\text{ion}}(a_j^{\text{ion}})^3\right)\left[\frac{-(a_i^{\text{ion}})^3}{1-\sum_{j=1}^{r}\rho_j^{\text{ion}}(a_j^{\text{ion}})^3}\right]$$
$$\left.+\left[\ln(\rho_i^{\text{ion}}(a_i^{\text{ion}})^3)-1\right]+\rho_i^{\text{ion}}\frac{(a_i^{\text{ion}})^3}{\rho_i^{\text{ion}}(a_i^{\text{ion}})^3}\right)$$
$$=\frac{1}{\beta}\left(\frac{-(a_i^{\text{ion}})^3}{(a_0^{\text{ion}})^3}\ln\left(1-\sum_{j=1}^{r}\rho_j^{\text{ion}}(a_j^{\text{ion}})^3\right)+\ln(\rho_i^{\text{ion}}(a_i^{\text{ion}})^3)\right), \qquad \forall i = 1,\ldots,r.$$

Therefore,

$$\mu_i^{\text{ion}} = \left(k_BT\left[\ln\left(\rho_i^{\text{ion}}(a_i^{\text{ion}})^3\right)-\frac{(a_i^{\text{ion}})^3}{(a_0^{\text{ion}})^3}\ln\left(1-\sum_{j=1}^{n}\rho_j^{\text{ion}}(a_j^{\text{ion}})^3\right)\right]\right), \quad i = 1,\ldots,r. \tag{361}$$

The diffusion potential for the ions should be nonzero only where the ions are present, i.e. only on Ω/Γ. We do not add any restriction to the function to accomplish this (e.g. multiplying the equation by $(1-\delta_\Gamma)$). This restriction is enforced by the initial condition and the diffusion equation. The initial concentration of ions is to be distributed only along the domain without the membrane, and the ion flux (351) is restricted to the bulk by a $(1-\delta_\Gamma)$ term.

For the lipid diffusion potential, $\delta E_{\text{ent}}^{\text{ion}}/\delta \rho_l^{\text{lip}} = 0$. The nonzero contribution includes the entropic energy and the membrane energy. The first is

$$
\begin{aligned}
\frac{\delta E_{\text{ent}}^{\text{lip}}}{\delta \rho_l^{\text{lip}}} = \frac{1}{\beta}\Bigg(& \frac{1}{(a_0^{\text{lip}})^2}\left(-(a_l^{\text{lip}})^2\right)\left[\ln\left(1-\rho^{\text{pro}}(a_0^{\text{pro}})^2-\sum_{j=1}^{m}\rho_j^{\text{lip}}(a_j^{\text{lip}})^2\right)-1\right] \\
& + \frac{1}{(a_0^{\text{lip}})^2}\left(1-\rho^{\text{pro}}(a_0^{\text{pro}})^2-\sum_{j=1}^{m}\rho_j^{\text{lip}}(a_j^{\text{lip}})^2)\right)\left[\frac{-(a_l^{\text{lip}})^2}{1-\rho^{\text{pro}}(a_0^{\text{pro}})^2-\sum_{j=1}^{m}\rho_j^{\text{lip}}(a_j^{\text{lip}})^2}\right] \\
& + \left[\ln(\rho_l^{\text{lip}}(a_l^{\text{lip}})^2)-1\right]+\rho_l^{\text{lip}}\frac{(a_l^{\text{lip}})^2}{\rho_l^{\text{lip}}(a_l^{\text{lip}})^2}\Bigg) \\
= \frac{1}{\beta}\Bigg(& \frac{-(a_l^{\text{lip}})^2}{(a_0^{\text{lip}})^2}\ln\left(1-\rho^{\text{pro}}(a_0^{\text{pro}})^2-\sum_{j=1}^{m}\rho_j^{\text{lip}}(a_j^{\text{lip}})^2\right)+\ln(\rho_l^{\text{lip}}(a_l^{\text{lip}})^2)\Bigg), \qquad \forall i = 1,\ldots,r.
\end{aligned}
$$

The variation of the membrane energy with respect to the concentration requires a bit more thought. Recall that the membrane energy E_{mem}, given in 3D by Equation (341) is an approximation to the two-dimensional curvature energy penalty in Lagrangian formulation E_L, given by Equation (287), i.e. $E_{\text{mem}} \to E_L$ as $\epsilon \to 0$. We really only want to track the curvature of the zero level set of the phase field function, yet the 3D energy (341) is defined everywhere. Rather than computing the diffusion potential from the 3D energy functional which is only an approximation, we will compute the variation from the 2D energy functional and then approximate. The variation of E_L is given by

$$
\frac{\delta E_L}{\delta \rho_l^{\text{lip}}} = 2(C_0 - H)\frac{\delta C_0}{\delta \rho_l^{\text{lip}}}. \tag{362}
$$

As for the 3D analog, we have an expression for the mean curvature H given by (294); however, this expression is only valid near the $\phi = 0$ level set. Therefore, we really want to restrict the mean curvature with a surface delta function so that it is only computed on (a narrow band around) the surface. The mean curvature at other level sets of ϕ could be extremely temperamental and give numerical troubles (and they do!). Using this idea with the phase field approximation to the mean curvature in (294) and the variation of the spontaneous curvature (344), we have

$$\frac{\delta E_{mem}}{\delta \rho_l^{\text{lip}}} \sim 2C_0^l (a_l^{\text{lip}})^2 \left(C_0 - \frac{\varepsilon}{\sqrt{2}(\phi^2 - 1)} \left(\Delta\phi - \frac{1}{\varepsilon^2}\phi(\phi^2 - 1) \right) \delta_\Gamma \right). \tag{363}$$

Therefore,

$$\begin{aligned} \mu_l^{\text{lip}} = k_B T &\left[\frac{-(a_l^{\text{lip}})^2}{(a_0^{\text{lip}})^2} \ln \left(1 - \rho^{\text{pro}} (a_0^{\text{pro}})^2 - \sum_{j=1}^m \rho_j^{\text{lip}} (a_j^{\text{lip}})^2 \right) + \ln(\rho_l^{\text{lip}} (a_l^{\text{lip}})^2) \right] \\ &+ 2C_0^l (a_l^{\text{lip}})^2 \left(C_0 - \frac{\varepsilon}{\sqrt{2}(\phi^2 - 1)} \left(\Delta\phi - \frac{1}{\varepsilon^2}\phi(\phi^2 - 1) \right) \delta_\Gamma \right). \end{aligned} \tag{364}$$

Similar to the diffusion potential for the ions, the diffusion potential for the lipids is defined over all of Ω, but should be nonzero only near the membrane Γ. We do not introduce any δ_Γ term multiplying all of (364) to enforce this condition; however, there is a δ_Γ term acting on the mean curvature as motivated above. The concentrations are initially distributed on the membrane only, and it is clear in (349) that the flux is restricted to the membrane only so these terms will remain zero away from Γ. This is also the case for the spontaneous curvature C_0, since it depends upon the concentrations. However, the mean curvature may be nonzero away from Γ, since this computation depends only upon ϕ, but we are interested only in the $\phi = 0$ level set. Therefore, we introduce a surface delta function to this term only to avoid large and nonphysical mean curvatures away from the $\phi = 0$ level set.

Finally, for the protein diffusion potential, $\delta E_{\text{ent}}^{\text{ion}} / \delta \rho^{\text{pro}} = 0$, and the nonzero contributions are

$$\begin{aligned} \frac{\delta E_{\text{ent}}^{\text{lip}}}{\delta \rho^{\text{pro}}} &= \frac{1}{\beta} \Bigg(\frac{1}{(a_0^{\text{lip}})^2} \left(-(a^{\text{pro}})^2 \right) \left[\ln \left(1 - \rho^{\text{pro}} (a_0^{\text{pro}})^2 - \sum_{j=1}^m \rho_j^{\text{lip}} (a_j^{\text{lip}})^2 \right) - 1 \right] \\ &\qquad + \frac{1}{(a_0^{\text{lip}})^2} \left(1 - \rho^{\text{pro}} (a_0^{\text{pro}})^2 - \sum_{j=1}^m \rho_j^{\text{lip}} (a_j^{\text{lip}})^2 \right) \left[\frac{-(a^{\text{pro}})^2}{1 - \rho^{\text{pro}} (a_0^{\text{pro}})^2 - \sum_{j=1}^m \rho_j^{\text{lip}} (a_j^{\text{lip}})^2} \right] \\ &\qquad + \left[\ln(\rho^{\text{pro}} (a^{\text{pro}})^2) - 1 \right] + \rho^{\text{pro}} \frac{(a^{\text{pro}})^2}{\rho^{\text{pro}} (a^{\text{pro}})^2} \Bigg) \\ &= \frac{1}{\beta} \Bigg(\frac{-(a^{\text{pro}})^2}{(a_0^{\text{lip}})^2} \ln \left(1 - \rho^{\text{pro}} (a_0^{\text{pro}})^2 - \sum_{j=1}^m \rho_j^{\text{lip}} (a_j^{\text{lip}})^2 \right) + \ln(\rho^{\text{pro}} (a^{\text{pro}})^2) \Bigg), \end{aligned}$$

$$\frac{\delta E_{\text{mem}}}{\delta \rho_l^{\text{pro}}} \sim 2C_0^{\text{pro}}(a^{\text{pro}})^2 \left(C_0 - \frac{\varepsilon}{\sqrt{2}(\phi^2-1)} \left(\Delta\phi - \frac{1}{\varepsilon^2}\phi(\phi^2-1) \right) \delta_\Gamma \right)$$

Therefore,

$$\begin{aligned} \mu^{\text{pro}} = k_B T \left[\frac{-(a^{\text{pro}})^2}{(a_0^{\text{lip}})^2} \ln \left(1 - \rho^{\text{pro}}(a_0^{\text{pro}})^2 - \sum_{j=1}^{m} \rho_j^{\text{lip}}(a_j^{\text{lip}})^2 \right) + \ln(\rho^{\text{pro}}(a^{\text{pro}})^2) \right] \\ + 2C_0^{\text{pro}}(a^{\text{pro}})^2 \left(C_0 - \frac{\varepsilon}{\sqrt{2}(\phi^2-1)} \left(\Delta\phi - \frac{1}{\varepsilon^2}\phi(\phi^2-1) \right) \delta_\Gamma \right). \end{aligned} \tag{365}$$

The appearance of δ_Γ in (365) is for the same reason as cited for that on (364). We have now described the terms in the conservation equations (348).

8.5. Curvature-driven protein localization

In this section, we give a simple formulation for protein localization. Rather than coupling the phase field function with the protein localization and allowing the membrane to deform with the mass conservation equations simultaneously, we simplify our model by fixing the boundary and solving the curvature-driven diffusion equation on a fixed membrane. The membrane is still defined as a level set of the phase function. Solving the curvature-driven diffusion equation using Fourier spectral methods is novel work even with this simplification of a fixed boundary. Eventually, we should solve the concentration equations on a moving boundary (with electrostatics!). For now, we wish to solve the curvature-driven surface diffusion equation (348) for ρ_l^{lip} and ρ^{pro} with fixed ϕ (neglecting the bulk). First, we introduce a few temporary variables to stay organized. Define

$$L^{\text{lip}}(\rho_l^{\text{lip}}) = \ln(\rho_l^{\text{lip}}(a_l^{\text{lip}})^2), \tag{366}$$

$$R^{\text{lip}}(\rho_l^{\text{lip}}, \rho^{\text{pro}}) = \frac{-(a_l^{\text{lip}})^2}{(a_0^{\text{lip}})^2} \ln \left(1 - \rho^{\text{pro}}(a_0^{\text{pro}})^2 - \sum_{j=1}^{m} \rho_j^{\text{lip}}(a_j^{\text{lip}})^2 \right), \tag{367}$$

$$L^{\text{pro}}(\rho^{\text{pro}}) = \ln(\rho^{\text{pro}}(a^{\text{pro}})^2), \tag{368}$$

$$R^{\text{pro}}(\rho_l^{\text{lip}}, \rho^{\text{pro}}) = \frac{-(a^{\text{pro}})^2}{(a_0^{\text{lip}})^2} \ln \left(1 - \rho^{\text{pro}}(a_0^{\text{pro}})^2 - \sum_{j=1}^{m} \rho_j^{\text{lip}}(a_j^{\text{lip}})^2 \right), \tag{369}$$

$$P(\phi, \rho_l^{\text{lip}}, \rho^{\text{pro}}) = \left(C_0(\rho_l^{\text{lip}}, \rho^{\text{pro}}) - \frac{\varepsilon}{\sqrt{2}(\phi^2 - 1)} \left(\Delta\phi - \frac{1}{\varepsilon^2}\phi(\phi^2 - 1) \right) \delta_\Gamma \right). \tag{370}$$

The notation is indicative of leading order terms for the lipids and proteins (L), remaining terms corresponding to the size restrictions (R), and a term corresponding to the curvature determined by the phase field function (P). Using (366)-(370) and suppressing the notation describing each function's independent variables, the diffusion potential (364) becomes

$$\mu_l^{\text{lip}} = \frac{1}{\beta}(L^{\text{lip}} + R^{\text{lip}}) + 2C_0^l(a_l^{\text{lip}})^2 P, \tag{371}$$

and (365) becomes

$$\mu^{\text{pro}} = \frac{1}{\beta}(L^{\text{pro}} + R^{\text{pro}}) + 2C_0^{\text{pro}}(a^{\text{pro}})^2 P. \tag{372}$$

Then we have

$$\nabla\mu_l^{\text{lip}} = \frac{1}{\beta}(\nabla L^{\text{lip}} + \nabla R^{\text{lip}}) + 2C_0^l(a_l^{\text{lip}})^2 \nabla P, \tag{373}$$

$$\nabla\mu^{\text{pro}} = \frac{1}{\beta}(\nabla L^{\text{pro}} + \nabla R^{\text{pro}}) + 2C_0^{\text{pro}}(a^{\text{pro}})^2 \nabla P, \tag{374}$$

where

$$\nabla L^{\text{lip}} = \frac{\nabla\rho_l^{\text{lip}}}{\rho_l^{\text{lip}}}, \tag{375}$$

$$\nabla R^{\text{lip}} = \frac{-(a_l^{\text{lip}})^2}{(a_0^{\text{lip}})^2} \left(\frac{-(a_0^{\text{pro}})^2 \nabla\rho^{\text{pro}} - \sum_{j=1}^{m} (a_j^{\text{lip}})^2 \nabla\rho_j^{\text{lip}}}{1 - \rho^{\text{pro}}(a_0^{\text{pro}})^2 - \sum_{j=1}^{m} \rho_j^{\text{lip}} (a_j^{\text{lip}})^2} \right), \tag{376}$$

$$\nabla L^{\text{pro}} = \frac{\nabla\rho^{\text{pro}}}{\rho^{\text{pro}}}, \tag{377}$$

$$\nabla R^{\text{pro}} = \frac{-(a^{\text{pro}})^2}{(a_0^{\text{lip}})^2} \left(\frac{-(a_0^{\text{pro}})^2 \nabla\rho^{\text{pro}} - \sum_{j=1}^{m} (a_j^{\text{lip}})^2 \nabla\rho_j^{\text{lip}}}{1 - \rho^{\text{pro}}(a_0^{\text{pro}})^2 - \sum_{j=1}^{m} \rho_j^{\text{lip}} (a_j^{\text{lip}})^2} \right), \tag{378}$$

$$\nabla P = \nabla C_0 - \nabla(H\delta_\Gamma), \tag{379}$$

$$\nabla C_0 = \sum_{l=0}^{m} C_0^l (a_l^{\text{lip}})^2 \nabla \rho_l^{\text{lip}} + C_0^{\text{pro}} (a^{\text{pro}})^2 \nabla \rho^{\text{pro}}. \tag{380}$$

To make our final equation simpler, define the constants

$$M_l^{\text{lip}} = 2\beta C_0^l (a_l^{\text{lip}})^2, \tag{381}$$

$$M^{\text{pro}} = 2\beta C_0^{\text{pro}} (a^{\text{pro}})^2. \tag{382}$$

Substituting (373) into the diffusion equation (348) for the lipids with the assumption of a fixed phase field ϕ gives

$$\frac{\partial \rho_l^{\text{lip}}}{\partial t} = D_l^{\text{lip}} \nabla \cdot \left\{ \delta_\Gamma \rho_l^{\text{lip}} (\nabla L^{\text{lip}} + \nabla R^{\text{lip}}) + M_l^{\text{lip}} \delta_\Gamma \rho_l^{\text{lip}} \nabla P \right\}. \tag{383}$$

Now substitute the derivative of the leading order term (375) directly into (383) to get

$$\frac{\partial \rho_l^{\text{lip}}}{\partial t} = D_l^{\text{lip}} \nabla \cdot \left\{ \delta_\Gamma \nabla \rho_l^{\text{lip}} + \delta_\Gamma \rho_l^{\text{lip}} \nabla R^{\text{lip}} + M_l^{\text{lip}} \delta_\Gamma \rho_l^{\text{lip}} \nabla P \right\}. \tag{384}$$

The derivation for the protein conservation equation is similar and results in

$$\frac{\partial \rho^{\text{pro}}}{\partial t} = D^{\text{pro}} \nabla \cdot \left\{ \delta_\Gamma \nabla \rho^{\text{pro}} + \delta_\Gamma \rho^{\text{pro}} \nabla R^{\text{pro}} + M^{\text{pro}} \delta_\Gamma \rho^{\text{pro}} \nabla P \right\}. \tag{385}$$

8.5.1. VARIABLE DIFFUSION COEFFICIENT. The equation (384) is organized such that the leading order term appears first. For simplicity, define

$$H_l^{\text{lip}}(\rho_l^{\text{lip}}, \rho^{\text{pro}}, \phi) = \delta_\Gamma \rho_l^{\text{lip}} \nabla R^{\text{lip}} + M_l^{\text{lip}} \delta_\Gamma \rho_l^{\text{lip}} \nabla P \tag{386}$$

so that (384) may be written as

$$\frac{\partial \rho_l^{\text{lip}}}{\partial t} = D_l^{\text{lip}} \nabla \cdot \left\{ \delta_\Gamma \nabla \rho_l^{\text{lip}} + H_l^{\text{lip}} \right\}. \tag{387}$$

Expanding the divergence operator in (387) gives

$$\frac{\partial \rho_l^{\text{lip}}}{\partial t} = D_l^{\text{lip}} \nabla \cdot \left\{ \delta_\Gamma \nabla \rho_l^{\text{lip}} + H_l^{\text{lip}} \right\} = D_l^{\text{lip}} \left\{ \delta_\Gamma \Delta \rho_l^{\text{lip}} + \nabla \delta_\Gamma \cdot \nabla \rho_l^{\text{lip}} + \nabla \cdot H_l^{\text{lip}} \right\}. \tag{388}$$

The first term in (388) is the leading order term in the variable for we wish to solve (ρ_l^{lip}), and it involves a product with the surface delta function δ_Γ. We cannot directly employ the same procedures as in Section 7.4 on this equation, since the Fourier transform of a product of two spatially variable functions is the convolution of the Fourier transforms. Therefore we cannot perform a simple division to obtain a formula akin to (328).

To perform numerical computations on (387), we use the technique developed in [18], where a treatment of elliptic equations with variable coefficients is provided. There are two modifications we make to this scheme as we have two characteristically different features in our equation (387) to that in [18]. In [18], the equation solved is

$$f = \nabla \cdot (a \nabla u), \tag{389}$$

where f, a, and u are multidimensional functions. In their treatment of (389), division by the coefficient a is necessary. But applying this step to our problem (387) is troublesome, since our variable coefficient, δ_Γ, is zero almost everywhere in Ω. Therefore, we first modify our equation to

$$\begin{aligned} \frac{\partial \rho_l^{\text{lip}}}{\partial t} &= D_l^{\text{lip}} \nabla \cdot \left\{ (\delta_\Gamma^* - 1) \nabla \rho_l^{\text{lip}} + H_l^{\text{lip}} \right\} \\ &= D_l^{\text{lip}} \nabla \cdot \left\{ \delta_\Gamma^* \nabla \rho_l^{\text{lip}} \right\} - D_l^{\text{lip}} \Delta \rho_l^{\text{lip}} + D_l^{\text{lip}} \nabla \cdot H_l^{\text{lip}}, \end{aligned} \tag{390}$$

where

$$\delta_\Gamma^* = \delta_\Gamma + 1. \tag{391}$$

In this way, the delta function in shifted up by one, so that it is never close to zero, making division by δ_Γ^* possible.

The second difference is that equation (389) is an elliptic equation, and our equation (390) is parabolic. Therefore, we treat the time derivative using Crank-Nicholson methods to transform (390) into an elliptic equation before applying the technique. If this is not done, the problem of convolutions remains. For simplicity, use the notation $\rho_n^l = \rho_l^{\text{lip}}(t)$ and $\rho_{n+1}^l = \rho_l^{\text{lip}}(t+\Delta t)$. Similarly, let $H_{n+\frac{1}{2}}^l$ be the average of (386) at times t and $t + \Delta t$. Using Crank-Nicholson in time gives

$$\begin{aligned}\frac{\rho_{n+1}^l - \rho_n^l}{\Delta t} &= D_l^{\text{lip}} \nabla \cdot \left(\delta_\Gamma^* \nabla \rho_{n+\frac{1}{2}}^l\right) - D_l^{\text{lip}} \Delta \rho_{n+\frac{1}{2}}^l + D_l^{\text{lip}} \nabla \cdot H_{n+\frac{1}{2}}^l \\ &= \frac{D_l^{\text{lip}}}{2} \left(\delta_\Gamma^* \Delta \rho_{n+1}^l + \delta_\Gamma^* \Delta \rho_n^l + \nabla \delta_\Gamma^* \cdot \nabla \rho_{n+1}^l + \nabla \delta_\Gamma^* \cdot \nabla \rho_n^l\right) \\ &\quad - \frac{D_l^{\text{lip}}}{2} \left(\Delta \rho_n^l + \Delta \rho_{n+1}^l\right) + D_l^{\text{lip}} \nabla \cdot H_{n+\frac{1}{2}}^l.\end{aligned}$$

Next, we isolate the terms for ρ_{n+1} on the left-hand side, except for the terms within $H_{n+\frac{1}{2}}^l$ (we will treat these with extra care later). This gives us

$$\begin{aligned}&\rho_{n+1}^l - \frac{D_l^{\text{lip}} \Delta t}{2} \left(\delta_\Gamma^* \Delta \rho_{n+1}^l + \nabla \delta_\Gamma^* \cdot \nabla \rho_{n+1}^l - \Delta \rho_{n+1}^l\right) \\ &\quad = \rho_n^l + \frac{D_l^{\text{lip}} \Delta t}{2} \left(\delta_\Gamma^* \Delta \rho_n^l + \nabla \delta_\Gamma^* \cdot \nabla \rho_n^l - \Delta \rho_n^l\right) + D_l^{\text{lip}} \Delta t \, \nabla \cdot H_{n+\frac{1}{2}}^l.\end{aligned}$$

Divide the entire equation by $\sqrt{\delta_\Gamma^*}$ and obtain

$$\begin{aligned}(392)\quad &\frac{\rho_{n+1}^l}{\sqrt{\delta_\Gamma^*}} - \frac{D_l^{\text{lip}} \Delta t}{2} \sqrt{\delta_\Gamma^*} \Delta \rho_{n+1}^l - \frac{D_l^{\text{lip}} \Delta t}{2} \frac{\nabla \delta_\Gamma^*}{\sqrt{\delta_\Gamma^*}} \cdot \nabla \rho_{n+1}^l + \frac{D_l^{\text{lip}} \Delta t}{2\sqrt{\delta_\Gamma^*}} \Delta \rho_{n+1}^l \\ &= \frac{\rho_n^l}{\sqrt{\delta_\Gamma^*}} + \frac{D_l^{\text{lip}} \Delta t}{2} \sqrt{\delta_\Gamma^*} \Delta \rho_n^l + \frac{D_l^{\text{lip}} \Delta t}{2} \frac{\nabla \delta_\Gamma^*}{\sqrt{\delta_\Gamma^*}} \cdot \nabla \rho_n^l - \frac{D_l^{\text{lip}} \Delta t}{2\sqrt{\delta_\Gamma^*}} \Delta \rho_n^l + \frac{D_l^{\text{lip}} \Delta t}{\sqrt{\delta_\Gamma^*}} \nabla \cdot H_{n+\frac{1}{2}}^l.\end{aligned}$$

Now use the fact that

$$\sqrt{\delta_\Gamma^*} \Delta \rho = \Delta(\sqrt{\delta_\Gamma^*} \rho) - 2 \nabla \sqrt{\delta_\Gamma^*} \cdot \nabla \rho - \Delta \sqrt{\delta_\Gamma^*} \rho$$

for the second term of (392) on both the left-hand and right-hand sides to obtain

$$\begin{aligned}(393)\qquad &\frac{\rho^l_{n+1}}{\sqrt{\delta^*_\Gamma}} - \frac{D^{\text{lip}}_l \Delta t}{2}\left(\Delta(\sqrt{\delta^*_\Gamma}\rho^l_{n+1}) - 2\nabla\sqrt{\delta^*_\Gamma}\cdot\nabla\rho^l_{n+1} - \Delta\sqrt{\delta^*_\Gamma}\rho^l_{n+1}\right)\\ &\quad - \frac{D^{\text{lip}}_l \Delta t}{2}\frac{\nabla\delta^*_\Gamma}{\sqrt{\delta^*_\Gamma}}\cdot\nabla\rho^l_{n+1} + \frac{D^{\text{lip}}_l \Delta t}{2\sqrt{\delta^*_\Gamma}}\Delta\rho^l_{n+1}\\ &= \frac{\rho^l_n}{\sqrt{\delta^*_\Gamma}} + \frac{D^{\text{lip}}_l \Delta t}{2}\left(\Delta(\sqrt{\delta^*_\Gamma}\rho^l_n) - 2\nabla\sqrt{\delta^*_\Gamma}\cdot\nabla\rho^l_n - \Delta\sqrt{\delta^*_\Gamma}\rho^l_n\right)\\ &\quad + \frac{D^{\text{lip}}_l \Delta t}{2}\frac{\nabla\delta^*_\Gamma}{\sqrt{\delta^*_\Gamma}}\cdot\nabla\rho^l_n - \frac{D^{\text{lip}}_l \Delta t}{2\sqrt{\delta^*_\Gamma}}\Delta\rho^l_n + \frac{D^{\text{lip}}_l \Delta t}{\sqrt{\delta^*_\Gamma}}\nabla\cdot H^l_{n+\frac{1}{2}}.\end{aligned}$$

Finally, notice that two terms cancel on each side of (393) since

$$\nabla\sqrt{\delta^*_\Gamma} = \frac{1}{2\sqrt{\delta^*_\Gamma}}\nabla\delta^*_\Gamma.$$

This gives us

$$\begin{aligned}(394)\qquad &\frac{\rho^l_{n+1}}{\sqrt{\delta^*_\Gamma}} - \frac{D^{\text{lip}}_l \Delta t}{2}\left(\Delta(\sqrt{\delta^*_\Gamma}\rho^l_{n+1}) - \Delta\sqrt{\delta^*_\Gamma}\rho^l_{n+1}\right) + \frac{D^{\text{lip}}_l \Delta t}{2\sqrt{\delta^*_\Gamma}}\Delta\rho^l_{n+1}\\ &= \frac{\rho^l_n}{\sqrt{\delta^*_\Gamma}} + \frac{D^{\text{lip}}_l \Delta t}{2}\left(\Delta(\sqrt{\delta^*_\Gamma}\rho^l_n) - \Delta\sqrt{\delta^*_\Gamma}\rho^l_n\right) - \frac{D^{\text{lip}}_l \Delta t}{2\sqrt{\delta^*_\Gamma}}\Delta\rho^l_n + \frac{D^{\text{lip}}_l \Delta t}{\sqrt{\delta^*_\Gamma}}\nabla\cdot H^l_{n+\frac{1}{2}}.\end{aligned}$$

Now define $\omega^l = \sqrt{\delta^*_\Gamma}\rho^l$ with appropriate subscripts for the time step to obtain the following iterative procedure, based on (394),

$$\begin{aligned}(395)\qquad &\frac{\omega^l_{n+1}}{\delta^*_\Gamma} - \frac{D^{\text{lip}}_l \Delta t}{2}\left(\Delta\omega^l_{n+1} - \frac{\Delta\sqrt{\delta^*_\Gamma}}{\sqrt{\delta^*_\Gamma}}\omega^l_{n+1} - \frac{1}{\sqrt{\delta^*_\Gamma}}\Delta\left(\frac{\omega^l_{n+1}}{\sqrt{\delta^*_\Gamma}}\right)\right)\\ &= \frac{\omega^l_n}{\delta^*_\Gamma} + \frac{D^{\text{lip}}_l \Delta t}{2}\left(\Delta\omega^l_n - \frac{\Delta\sqrt{\delta^*_\Gamma}}{\sqrt{\delta^*_\Gamma}}\omega^l_n - \frac{1}{\sqrt{\delta^*_\Gamma}}\Delta\left(\frac{\omega^l_n}{\sqrt{\delta^*_\Gamma}}\right)\right) + \frac{D^{\text{lip}}_l \Delta t}{\sqrt{\delta^*_\Gamma}}\nabla\cdot H^l_{n+\frac{1}{2}}.\end{aligned}$$

Rearranging the left-hand side according to the order of derivative, we have

$$\begin{aligned}(396)\qquad &-\frac{D^{\text{lip}}_l \Delta t}{2}\Delta\omega^l_{n+1} + \frac{D^{\text{lip}}_l \Delta t}{2\sqrt{\delta^*_\Gamma}}\Delta\left(\frac{\omega^l_{n+1}}{\sqrt{\delta^*_\Gamma}}\right) + \left(\frac{1}{\delta^*_\Gamma} + \frac{D^{\text{lip}}_l \Delta t}{2}\frac{\Delta\sqrt{\delta^*_\Gamma}}{\sqrt{\delta^*_\Gamma}}\right)\omega^l_{n+1}\\ &= \frac{\omega^l_n}{\delta^*_\Gamma} + \frac{D^{\text{lip}}_l \Delta t}{2}\left(\Delta\omega^l_n - \frac{\Delta\sqrt{\delta^*_\Gamma}}{\sqrt{\delta^*_\Gamma}}\omega^l_n - \frac{1}{\sqrt{\delta^*_\Gamma}}\Delta\left(\frac{\omega^l_n}{\sqrt{\delta^*_\Gamma}}\right)\right) + \frac{D^{\text{lip}}_l \Delta t}{\sqrt{\delta^*_\Gamma}}\nabla\cdot H^l_{n+\frac{1}{2}}.\end{aligned}$$

In (396), notice that the product on the leading order term with a spatially varying function is now removed, so that we can treat $\Delta\omega_{n+1}^l$ with Fourier transforms. However, there is a nonlinear product with δ_Γ^* on the second and third terms that we must handle. To take care of this, we use the interior iteration in m for ω^l with the notation ν_m^l where $\nu_m^l \to \omega_{n+1}^l$ as $m \to \infty$. In our scheme (396), we treat the nonlinear terms using only previous interior step ν_m^l and the linear terms using the current interior step ν_{m+1}^l. (Of course, we are not replacing any appearances of ω_n^l.) Note that since the higher order term $H_{n+\frac{1}{2}}^l$ given by (386) is entirely nonlinear, it will only depend upon ω_n^l and ν_m^l, and not on ν_{m+1}^l; therefore, it remains entirely on the right-hand side. The iteration scheme for finding ω_{n+1}^l is

$$\begin{aligned}(397)\quad & -\frac{D_l^{\text{lip}}\Delta t}{2}\Delta\nu_{m+1}^l + \frac{D_l^{\text{lip}}\Delta t}{2\sqrt{\delta_\Gamma^*}}\Delta\left(\frac{\nu_m^l}{\sqrt{\delta_\Gamma^*}}\right) + \left(\frac{1}{\delta_\Gamma^*} + \frac{D_l^{\text{lip}}\Delta t}{2}\frac{\Delta\sqrt{\delta_\Gamma^*}}{\sqrt{\delta_\Gamma^*}}\right)\nu_m^l \\ &= \frac{\omega_n^l}{\delta_\Gamma^*} + \frac{D_l^{\text{lip}}\Delta t}{2}\left(\Delta\omega_n^l - \frac{\Delta\sqrt{\delta_\Gamma^*}}{\sqrt{\delta_\Gamma^*}}\omega_n^l - \frac{1}{\sqrt{\delta_\Gamma^*}}\Delta\left(\frac{\omega_n^l}{\sqrt{\delta_\Gamma^*}}\right)\right) + \frac{D_l^{\text{lip}}\Delta t}{\sqrt{\delta_\Gamma^*}}\nabla\cdot H_{n+\frac{1}{2}}^l(\omega_n,\nu_m).\end{aligned}$$

Now isolating (397) for ν_{m+1}^l on the left-hand side, with all other terms on the right-hand side, and applying the scheme developed in [18], we have

$$\begin{aligned}(398)\quad & -\frac{D_l^{\text{lip}}\Delta t}{2}\Delta\nu_{m+1}^l + K\nu_{m+1}^l = -\left(\frac{1}{\delta_\Gamma^*} + \frac{D_l^{\text{lip}}\Delta t}{2}\frac{\Delta\sqrt{\delta_\Gamma^*}}{\sqrt{\delta_\Gamma^*}} - K\right)\nu_m^l - \frac{D_l^{\text{lip}}\Delta t}{2\sqrt{\delta_\Gamma^*}}\Delta\left(\frac{\nu_m^l}{\sqrt{\delta_\Gamma^*}}\right) \\ &+ \frac{\omega_n^l}{\delta_\Gamma^*} + \frac{D_l^{\text{lip}}\Delta t}{2}\left(\Delta\omega_n^l - \frac{\Delta\sqrt{\delta_\Gamma^*}}{\sqrt{\delta_\Gamma^*}}\omega_n^l - \frac{1}{\sqrt{\delta_\Gamma^*}}\Delta\left(\frac{\omega_n^l}{\sqrt{\delta_\Gamma^*}}\right)\right) + \frac{D_l^{\text{lip}}\Delta t}{\sqrt{\delta_\Gamma^*}}\nabla\cdot H_{n+\frac{1}{2}}^l(\omega_n,\nu_m),\end{aligned}$$

where K is added so that the form of the iterative scheme matches the form of (396). That is, in both equations there is a second order term and a zero-order term on ν_{m+1}. This parameter K is optimally defined as in [18] as

$$(399)\qquad K = \frac{1}{2}\left(\min\left\{\frac{1}{\delta_\Gamma^*} + \frac{D_l^{\text{lip}}\Delta t}{2}\frac{\Delta\sqrt{\delta_\Gamma^*}}{\sqrt{\delta_\Gamma^*}}\right\} + \max\left\{\frac{1}{\delta_\Gamma^*} + \frac{D_l^{\text{lip}}\Delta t}{2}\frac{\Delta\sqrt{\delta_\Gamma^*}}{\sqrt{\delta_\Gamma^*}}\right\}\right).$$

For an efficient numerical implementation of the scheme in (398), we wish to solve for the terms that do not include the interior iteration ν_m^l outside of the iteration in m. Therefore, the practical scheme is given by

$$
\begin{aligned}
(400)\qquad -\frac{D_l^{\mathrm{lip}}\Delta t}{2}\Delta\nu_{m+1}^l + K\nu_{m+1}^l = &-\left(\frac{1}{\delta_\Gamma^*} + \frac{D_l^{\mathrm{lip}}\Delta t}{2}\frac{\Delta\sqrt{\delta_\Gamma^*}}{\sqrt{\delta_\Gamma^*}} - K\right)\nu_m^l \\
&- \frac{D_l^{\mathrm{lip}}\Delta t}{2\sqrt{\delta_\Gamma^*}}\Delta\left(\frac{\nu_m^l}{\sqrt{\delta_\Gamma^*}}\right) + \frac{D_l^{\mathrm{lip}}\Delta t}{\sqrt{\delta_\Gamma^*}}\nabla\cdot H_m^l(\omega_n,\nu_m) + G^l(\omega_n),
\end{aligned}
$$

where $G^l(\omega_n)$ is defined by

$$
\begin{aligned}
(401)\qquad G^l(\omega_n) = &\frac{\omega_n^l}{\delta_\Gamma^*} + \frac{D_l^{\mathrm{lip}}\Delta t}{2}\left(\Delta\omega_n^l - \frac{\Delta\sqrt{\delta_\Gamma^*}}{\sqrt{\delta_\Gamma^*}}\omega_n^l - \frac{1}{\sqrt{\delta_\Gamma^*}}\Delta\left(\frac{\omega_n^l}{\sqrt{\delta_\Gamma^*}}\right)\right) \\
&+ \frac{D_l^{\mathrm{lip}}\Delta t}{\sqrt{\delta_\Gamma^*}}\nabla\cdot H_n^l(\omega_n).
\end{aligned}
$$

As promised, we now handle $H_{n+\frac{1}{2}}^{\mathrm{lip}}$ appearing in the scheme (398) with special care. This term was split in (400) and (401). The term $H_n^l(\omega_n)$ is the portion of $H_{n+\frac{1}{2}}^l$ that only includes terms with ω_n, and the term $H_m^l(\omega_n,\nu_m)$ is the portion of $H_{n+\frac{1}{2}}^l$ that includes terms with ν_m (and may also include terms with ω_n). A complete separation of terms cannot be performed due to the nonlinearity of (366) and (367) appearing in $H_{n+\frac{1}{2}}^{\mathrm{lip}}$. Instead, we isolate as many terms involving ν_m as we can, and define the splitting

$$
(402)\qquad H_{n+\frac{1}{2}}^{\mathrm{lip}}(\omega_n,\nu_m) = H_n^l(\omega_n) + H_m^l(\nu_m,\omega_n).
$$

Now we derive the splitting (402) above. To match the iteration scheme, we must apply the scaling $\omega^l = \sqrt{\delta_\Gamma^*}\rho^l$ to the definition of H^l in (386). This scaling involves the new delta function given in (391), whereas the definition involves the original delta function without the additional factor to allow division. Therefore, we first rewrite (386) in terms of the new delta, δ_Γ^*, and then perform the scaling.

$$
\begin{aligned}
(403)\quad H_{n+\frac{1}{2}}^l &= \delta_\Gamma^*\rho_{n+\frac{1}{2}}^l\nabla R_{n+\frac{1}{2}}^l - \rho_{n+\frac{1}{2}}^l\nabla R_{n+\frac{1}{2}}^l + M_l^{\mathrm{lip}}\delta_\Gamma^*\rho_{n+\frac{1}{2}}^l\nabla P_{n+\frac{1}{2}} - M_l^{\mathrm{lip}}\rho_{n+\frac{1}{2}}^l\nabla P_{n+\frac{1}{2}} \\
&= \sqrt{\delta_\Gamma^*}\omega_{n+\frac{1}{2}}^l\nabla R_{n+\frac{1}{2}}^l - \frac{\omega_{n+\frac{1}{2}}^l}{\sqrt{\delta_\Gamma^*}}\nabla R_{n+\frac{1}{2}}^l + M_l^{\mathrm{lip}}\sqrt{\delta_\Gamma^*}\omega_{n+\frac{1}{2}}^l\nabla P_{n+\frac{1}{2}} - M_l^{\mathrm{lip}}\frac{\omega_{n+\frac{1}{2}}^l}{\sqrt{\delta_\Gamma^*}}\nabla P_{n+\frac{1}{2}}.
\end{aligned}
$$

The terms of (403) are given below:

$$\omega_{n+\frac{1}{2}} = \frac{1}{2}\left(\omega_n + \nu_m\right), \tag{404}$$

$$\nabla\omega^l_{n+\frac{1}{2}} = \frac{1}{2}\left(\nabla\omega^l_n + \nabla\nu^l_m\right), \tag{405}$$

$$\nabla R^l_{n+\frac{1}{2}} = \frac{-(a^{\text{lip}}_l)^2}{(a^{\text{lip}}_0)^2}\left(\frac{-(a^{\text{pro}}_0)^2\nabla\left(\frac{\omega^{\text{pro}}_{n+\frac{1}{2}}}{\sqrt{\delta^*_\Gamma}}\right) - \sum_{j=1}^{m}(a^{\text{lip}}_j)^2\nabla\left(\frac{\omega^j_{n+\frac{1}{2}}}{\sqrt{\delta^*_\Gamma}}\right)}{1 - \frac{(a^{\text{pro}}_0)^2}{\sqrt{\delta^*_\Gamma}}\omega^{\text{pro}}_{n+\frac{1}{2}} - \sum_{j=1}^{m}\frac{(a^{\text{lip}}_j)^2}{\sqrt{\delta^*_\Gamma}}\omega^j_{n+\frac{1}{2}}}\right), \tag{406}$$

$$\nabla P_{n+\frac{1}{2}} = \nabla C_{n+\frac{1}{2}} - \nabla(H\delta_\Gamma), \tag{407}$$

$$C_{n+\frac{1}{2}} = \sum_{l=0}^{m} C^l_0(a^{\text{lip}}_l)^2\rho^l_{n+\frac{1}{2}} + C^{\text{pro}}_0(a^{\text{pro}})^2\rho^{\text{pro}}_{n+\frac{1}{2}}, \tag{408}$$

$$\nabla C_{n+\frac{1}{2}} = \sum_{l=0}^{m} C^l_0(a^{\text{lip}}_l)^2\nabla\rho^l_{n+\frac{1}{2}} + C^{\text{pro}}_0(a^{\text{pro}})^2\nabla\rho^{\text{pro}}_{n+\frac{1}{2}}. \tag{409}$$

Note that $\nabla R^l_{n+\frac{1}{2}}$ is a nonlinear function of ω_n and ν_m, and therefore cannot be separated. However, $\nabla P_{n+\frac{1}{2}}$ is a linear functions of ω_n and ν_m, and can be separated. The separation is allowable through the spontaneous curvature, so we begin here,

$$C_{n+\frac{1}{2}} = \frac{1}{2}\Big(C_n(\omega_n) + C_m(\nu_m)\Big), \tag{410}$$

$$C_n(\omega_n) = \sum_{l=0}^{m} C^l_0(a^{\text{lip}}_l)^2\rho^l_n + C^{\text{pro}}_0(a^{\text{pro}})^2\rho^{\text{pro}}_n, \tag{411}$$

$$C_m(\nu_m) = \sum_{l=0}^{m} C^l_0(a^{\text{lip}}_l)^2\rho^l_{n+1} + C^{\text{pro}}_0(a^{\text{pro}})^2\rho^{\text{pro}}_{n+1}. \tag{412}$$

It is simpler in the implementation to retain the original coordinates ρ rather than ω and ν. In (412) above, $\rho_{n+1} = \nu_m/\sqrt{\delta^*_\Gamma}$ for each species. Next, we split the gradient of the spontaneous curvature.

$$\nabla C_{n+\frac{1}{2}} = \frac{1}{2}\Big(\nabla C_n(\omega_n) + \nabla C_m(\nu_m)\Big), \tag{413}$$

$$\nabla C_n(\omega_n) = \sum_{l=0}^{m} C_0^l (a_l^{\text{lip}})^2 \nabla \rho_n^l + C_0^{\text{pro}} (a^{\text{pro}})^2 \nabla \rho_n^{\text{pro}}, \tag{414}$$

$$\nabla C_m(\nu_m) = \sum_{l=0}^{m} C_0^l (a_l^{\text{lip}})^2 \nabla \rho_{n+1}^l + C_0^{\text{pro}} (a^{\text{pro}})^2 \nabla \rho_{n+1}^{\text{pro}}. \tag{415}$$

As before, in (415) above, $\rho_{n+1} = \nu_m/\sqrt{\delta_\Gamma^*}$ for each species, and similar transformations are made for (414). Define the separation by

$$\nabla P_{n+\frac{1}{2}} = \nabla P_n(\omega_n) + \nabla P_m(\nu_m), \tag{416}$$

where

$$\nabla P_n(\omega_n) = \frac{1}{2}\nabla C_n - \nabla(H\delta_\Gamma), \tag{417}$$

$$\nabla P_m(\nu_m) = \frac{1}{2}\nabla C_m. \tag{418}$$

Now we can finally split $H_{n+\frac{1}{2}}^l$. The part that does not include any interior iterations is defined by

$$H_n^l(\omega_n) = \frac{M_l^{\text{lip}}}{2}\Bigg(\delta_\Gamma^* \rho_n^l \nabla P_n - \rho_n^l \nabla P_n\Bigg), \tag{419}$$

where ∇P_n is defined in (417). Similarly, the part involving the interior iteration in m is

$$\begin{aligned} H_m^l(\nu_m, \omega_n) = {} & \sqrt{\delta_\Gamma^*}\omega_{n+\frac{1}{2}}^l \nabla R_{n+\frac{1}{2}}^l - \frac{\omega_{n+\frac{1}{2}}^l}{\sqrt{\delta_\Gamma^*}} \nabla R_{n+\frac{1}{2}}^l \\ & + \frac{M_l^{\text{lip}}}{2}\Bigg(\delta_\Gamma^* \rho_n^l \nabla P_m + \delta_\Gamma^* \rho_{n+1}^l \nabla P_{n+\frac{1}{2}} - \rho_n^l \nabla P_m - \rho_{n+1}^l \nabla P_{n+\frac{1}{2}}\Bigg). \end{aligned} \tag{420}$$

These equations define the split in (402).

This completes the terms required to solve the iterative scheme in (400). The iterative scheme corresponding to the concentrations of the proteins are defined in a similar fashion. We can solve (400) using Fourier transforms as before using the property (311).

The derivation of the protein concentration equations is similar, with appropriate changes in subscripts and superscripts. The governing equation is given by

$$\begin{aligned} -\frac{D^{\text{pro}}\Delta t}{2}\Delta\nu^{\text{pro}}_{m+1} + K\nu^{\text{pro}}_{m+1} &= -\left(\frac{1}{\delta^*_\Gamma} + \frac{D^{\text{pro}}\Delta t}{2}\frac{\Delta\sqrt{\delta^*_\Gamma}}{\sqrt{\delta^*_\Gamma}} - K\right)\nu^{\text{pro}}_m \\ &\quad - \frac{D^{\text{pro}}\Delta t}{2\sqrt{\delta^*_\Gamma}}\Delta\left(\frac{\nu^{\text{pro}}_m}{\sqrt{\delta^*_\Gamma}}\right) + \frac{D^{\text{pro}}\Delta t}{\sqrt{\delta^*_\Gamma}}\nabla\cdot H^{\text{pro}}_m(\omega_n,\nu_m) + G^{\text{pro}}(\omega_n), \end{aligned} \tag{421}$$

where $G(\omega_n)$ is defined by

$$\begin{aligned} G^{\text{pro}}(\omega_n) = \frac{\omega^{\text{pro}}_n}{\delta^*_\Gamma} &+ \frac{D^{\text{pro}}\Delta t}{2}\left(\Delta\omega^{\text{pro}}_n - \frac{\Delta\sqrt{\delta^*_\Gamma}}{\sqrt{\delta^*_\Gamma}}\omega^{\text{pro}}_n - \frac{1}{\sqrt{\delta^*_\Gamma}}\Delta\left(\frac{\omega^{\text{pro}}_n}{\sqrt{\delta^*_\Gamma}}\right)\right) \\ &+ \frac{D^{\text{pro}}\Delta t}{\sqrt{\delta^*_\Gamma}}\nabla\cdot H^{\text{pro}}_n(\omega_n). \end{aligned} \tag{422}$$

The parameter K in (421) is given by

$$K = \frac{1}{2}\left(\min\left\{\frac{1}{\delta^*_\Gamma} + \frac{D^{\text{pro}}\Delta t}{2}\frac{\Delta\sqrt{\delta^*_\Gamma}}{\sqrt{\delta^*_\Gamma}}\right\} + \max\left\{\frac{1}{\delta^*_\Gamma} + \frac{D^{\text{pro}}\Delta t}{2}\frac{\Delta\sqrt{\delta^*_\Gamma}}{\sqrt{\delta^*_\Gamma}}\right\}\right). \tag{423}$$

The higher order term for the proteins is defined similarly as well and results in

$$H^{\text{pro}}_n(\omega_n) = \frac{M^{\text{pro}}}{2}\left(\delta^*_\Gamma\rho^{\text{pro}}_n\nabla P_n - \rho^{\text{pro}}_{n+1}\nabla P_n\right), \tag{424}$$

where ∇P_n is the same as defined in (417). Therefore, the only differences between (424) for the proteins and (419) for the lipids are the concentrations and spontaneous curvatures. The interior iteration remainder term is given by

$$\begin{aligned} H^{\text{pro}}_m(\nu_m,\omega_n) &= \sqrt{\delta^*_\Gamma}\omega^{\text{pro}}_{n+\frac{1}{2}}\nabla R^{\text{pro}}_{n+\frac{1}{2}} - \frac{\omega^{\text{pro}}_{n+\frac{1}{2}}}{\sqrt{\delta^*_\Gamma}}\nabla R^{\text{pro}}_{n+\frac{1}{2}} \\ &+ \frac{M^{\text{pro}}}{2}\left(\delta^*_\Gamma\rho^{\text{pro}}_n\nabla P_m + \delta^*_\Gamma\rho^{\text{pro}}_{n+1}\nabla P_{n+\frac{1}{2}} - \rho^{\text{pro}}_n\nabla P_m - \rho^{\text{pro}}_{n+1}\nabla P_{n+\frac{1}{2}}\right). \end{aligned} \tag{425}$$

The equation for $\nabla R^{\text{pro}}_{n+\frac{1}{2}}$ previously given by (406) needs to be updated with appropriate changes to match the protein equation to finish the formula in (425). Finally, in the formulas (421)-(425), the concentrations are given by

$$\omega^{\text{pro}}_n = \sqrt{\delta^*_\Gamma}\rho^{\text{pro}}_n, \tag{426}$$

$$\nu^{\text{pro}}_m \to \omega^{\text{pro}}_{n+1} = \sqrt{\delta^*_\Gamma}\rho^{\text{pro}}_{n+1}. \tag{427}$$

8.6. Two species model

In the numerical simulations, we solve the concentration equations for two competing species, one diffusive, the other background. To simplify the notation, let the diffusive species have concentration ρ^{dif} with spontaneous curvature C_0^{dif}, and the background species have concentration ρ^{bak} with spontaneous curvature C_0^{bak}. Other terms are notated similarly. By using a two species model, we only need to solve one governing equation, since the concentration of the second (background) species can be computed directly from the concentration of the diffusive species, $\rho^{\text{bak}} = (1-(a^{\text{dif}})^2\rho^{\text{dif}})/(a^{\text{bak}})^2$ according to equation (343).

To further simplify things, we also consider only the leading order diffusive term (L, (366)) without the correction term accounting for the size effect (R (367)); however, we do consider the correction term accounting for the curvature effect (P (370)). With these assumptions, the overall spontaneous curvature is now given by

$$C_0 = C_0^{\text{dif}}(a^{\text{dif}})^2\rho^{\text{dif}} + C_0^{\text{bak}}(1-(a^{\text{dif}})^2\rho^{\text{dif}}) \tag{428}$$

$$= \left(C_0^{\text{dif}} - C_0^{\text{bak}}\right)(a^{\text{dif}})^2\rho^{\text{dif}} + C_0^{\text{bak}} \tag{429}$$

$$= C_0^{\text{frac}}\rho^{\text{dif}} + C_0^{\text{bak}}, \qquad \forall \vec{x} \in \Omega, \tag{430}$$

where

$$C_0^{\text{frac}} = \left(C_0^{\text{dif}} - C_0^{\text{bak}}\right)(a^{\text{dif}})^2. \tag{431}$$

Note that if $C_0^{\text{dif}} = C_0^{\text{bak}}$, then (430) reduces to the constant $C_0 = C_0^{\text{dif}} = C_0^{\text{bak}}$, otherwise the spontaneous curvature is spatially dependent. The splitting of C is given by (410), where

$$C_n(\omega_n) = C_0^{\text{frac}} \rho_n^{\text{dif}} + C_0^{\text{bak}}, \tag{432}$$

$$C_m(\nu_m) = C_0^{\text{frac}} \rho_{n+1}^{\text{dif}} + C_0^{\text{bak}}. \tag{433}$$

The splitting of ∇C is given by (413), where

$$\nabla C_n(\omega_n) = C_0^{\text{frac}} \nabla \rho_n^{\text{dif}}, \tag{434}$$

$$\nabla C_m(\nu_m) = C_0^{\text{frac}} \nabla \rho_{n+1}^{\text{dif}}. \tag{435}$$

The splitting of ∇P is still given by (416) with terms matching the forms of (417) and (418). This leads to the splitting of the correction term, which takes the same form as (419). One important note is that the constants defined in (381) and (382) will be different, due to the change in (430). There is only one, and it is defined by

$$M^{\text{dif}} = 2\beta (a^{\text{dif}})^2 (C_0^{\text{dif}} - C_0^{\text{bak}}). \tag{436}$$

This will affect the conservation equation in (419). The splitting of the correction term involving the interior iteration in m is different, since the R terms are removed:

$$H_m^{\text{dif}}(\nu_m, \omega_n) = \frac{M^{\text{dif}}}{2} \left(\delta_\Gamma^* \rho_n^{\text{dif}} \nabla P_m + \delta_\Gamma^* \rho_{n+1}^{\text{dif}} \nabla P_{n+\frac{1}{2}} - \rho_n^{\text{dif}} \nabla P_m - \rho_{n+1}^{\text{dif}} \nabla P_{n+\frac{1}{2}} \right). \tag{437}$$

8.7. MASS CONSERVATION

In the scheme as stated so far, there is no guarantee that the solution ρ_{n+1} will converge to ρ^* for each time step t. This is because $\tilde{\rho} = \rho^* + C$ for any constant C is also a solution to (390). Therefore, the method may converge to $\rho_{n+1} = \rho^* + C$, where C is some unknown constant. To get the desired result, we impose the conservation of the total mass on Ω. For each time t,

$$\int_\Omega \rho^*(\vec{x}, t)\, d\Omega = \int_\Omega \rho_0(\vec{x}, 0) + D_l^{\text{lip}} \nabla \cdot H^l(\vec{x}, t)\, d\Omega = M, \tag{438}$$

where M is the total mass of the initial concentration plus the added mass due to the source term. In other words, the mass at is conserved. This condition (438) can be enforced using Fourier transforms, since the zero-frequency component of the Fourier transform is the integral of a function. This fact can be seen from the definition (308) when $\xi = 0$.

To enforce (438), we can perform the following procedure:

$$\rho_{n+1}(\vec{x},t) = \rho_{n+1}(\vec{x},t) - \frac{\displaystyle\int_\Omega \rho_{n+1}(\vec{x},t)\ d\Omega}{\displaystyle\int_\Omega d\Omega} + \frac{M}{\displaystyle\int_\Omega d\Omega}, \quad \forall t \tag{439}$$

The final procedure is stated in Algorithm 8.1.

Algorithm 8.1 Solve equation (390) with mass conservation

```
Define initial phase field function $\phi_0$ via (291)
Define initial concentrations $\rho^{\text{dif}}, \rho^{\text{bak}}$
Initialize $n \leftarrow 0$
for $n = 0$ to $T$ do:
    Update current time $t \leftarrow (n+1) \cdot dt$
    Define stationary curvature term $H_n^l$ by (419)
    Define parameter $K$ using (399)
    Define $G(\omega_n)$ using (401)
    Initialize $m \leftarrow 0$
    Initialize $\nu_m \leftarrow \omega_n$
    while $||\nu_{m+1} - \nu_m||^2 \geq 10^{-7}$ do:
        Define variable curvature term $H_m^l$ by (437)
        Update $\nu_{m+1}$ using (400)
        Update $m \leftarrow m + 1$
    end while
    Update $\omega_{n+1} \leftarrow \nu_m$
    Scale back $\rho_{n+1}^{\text{dif}} \leftarrow \omega_{n+1}/\sqrt{a}$
    Enforce mass conservation by (439)
    Update $n \leftarrow n + 1$
end for
```

CHAPTER 9

Curvature-driven protein localization: numerical results

9.1. Choosing initial conditions and delta function

In order to use the Fourier spectral method, we must use an initial condition which is smoothly distributed along the surface. Fourier methods exhibit Gibbs phenomenon when applied to discontinuous functions [49]. There should be no discontinuities in the distribution of the concentration, otherwise the spectral method fails. Furthermore, in order to capture the derivatives numerically, we need to define the surface in a narrow 3D band around the surface, rather than a 2D sheet. If the concentration is only defined on the 2D surface, there would be a sharp transition from outside the surface, where the concentration is zero, to on the surface, where the concentration is nonzero. We also want this transition to be smooth. That is, the concentration should be near zero on the outer edges of the surface band, and positive in the center of the band, where the surface is located. We define the narrow band as the set of points at which

$$\delta_\Gamma^* \geq 1 + b, \tag{440}$$

where $b > 0$ and δ_Γ^* is given in (391). Recall that δ_Γ^* is 1 outside the surface and 2 on the surface, with a smooth but sharp transition. We propose a new delta function in addition to those sampled in [60], defined by

$$\delta_\Gamma = \begin{cases} \tanh(D(\phi+1)), & -1 \leq \phi \leq 0, \\ -\tanh(D(\phi-1)), & 0 \leq \phi \leq 1. \end{cases} \tag{441}$$

The parameter D is chosen to be sufficiently large. Note that this function is continuous at $\phi = 0$; however, it does not have a continuous derivative. But, if D is large enough, the effect is negligible, since $\operatorname{sech}^2(D) \to -\operatorname{sech}^2(-D)$ as $D \to \infty$. A plot of (441) is given in Figure 9.1 for various D.

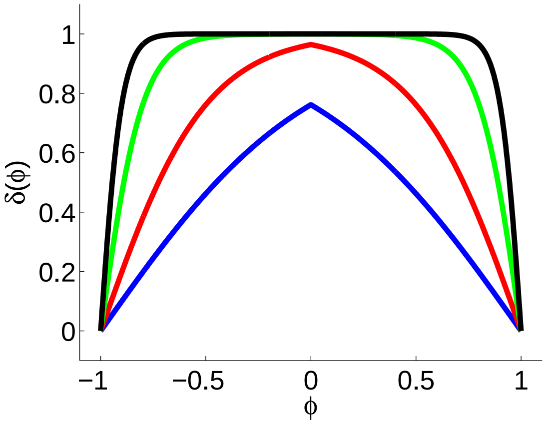

Figure 9.1: Plot of delta function defined by (441). Black: $D = 10$, Green: $D = 5$, Red: $D = 2$, Blue: $D = 1$.

Throughout the results, we consistently choose $D = 10$ for the definition of the delta function (441) and used a bandwidth of $b = 0.5$ for the surface band (440). Additionally, we choose $\epsilon = 0.1$ throughout the results as we did before, and we use a timestep of $\Delta t = 10^{-3}$ in each example.

9.2. PURE DIFFUSION

We being testing our algorithm using the simplest possible case: pure diffusion without any curvature effects. In this case, we neglect any curvature effects and follow Algorithm 8.1 with $H_n^{\text{dif}} = H_m^{\text{dif}} = 0$ for equations (419) and (437). Recall that there are no corresponding $H_{n,m}^{\text{bak}}$ terms since the concentration of the background species follows immediately from the concentration of the diffusive species.

9.2.1. DIFFUSION ON A SPHERE. For the simplest case of diffusion, we use the surface of a sphere of radius 1 centered at the origin. We conduct our first computation over a uniform grid of $64 \times 64 \times 64$ points on a domain of $[-\pi, \pi]^3$. Various cross sections of the delta function for this surface are plotted in Figure 9.2. Notice that there are approximately 4-5 grid points in one dimension in the narrow band of the surface with $b = 0.5$.

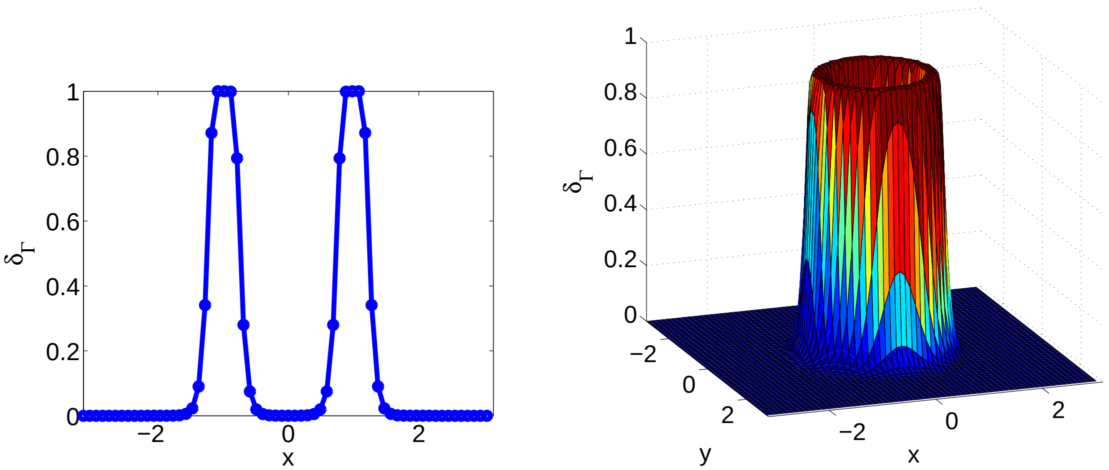

Figure 9.2: Profile of delta function for a sphere with 64 × 64 × 64 mesh. Left: 1D profile across the x grid points. Right: 2D profile across x and y grid points.

To create a smooth initial concentration which may be transformed accurately using Fourier spectral methods, we define the initial concentration as follows,

$$\rho(x, y, z, 0) = S \cdot \exp\left(-\sqrt{\mathrm{x}^2 + \mathrm{y}^2 + (\mathrm{z} - 1)^2}\right)(\delta_\Gamma - \mathrm{b}), \tag{442}$$

where δ_Γ is given by (441) and $b = 0.5$, and S is chosen so that the maximum concentration is exactly 1. In this way, the maximum concentration is given at the north pole of the sphere, but is smoothly distributed along the surface according to the distance away from the north pole. Also, at the edge of the band defining the surface, $\delta_\Gamma = b$; therefore, the concentration smoothly transitions to 0 from the inside of the band to the outside.

We ran Algorithm 8.1 (neglecting curvature effects) using the initial condition (447). The algorithm showed good convergence, using approximately $m = 12$ interior iterations at each time step (n). Furthermore, the concentration behaves as expected, diffusing along the narrow band around the sphere's surface. Figure 9.3 shows these results. It is important to note that due to the mass conservation in the narrow band, the concentration is always zero outside of the surface band, and mass is conserved within the surface band. The bottom

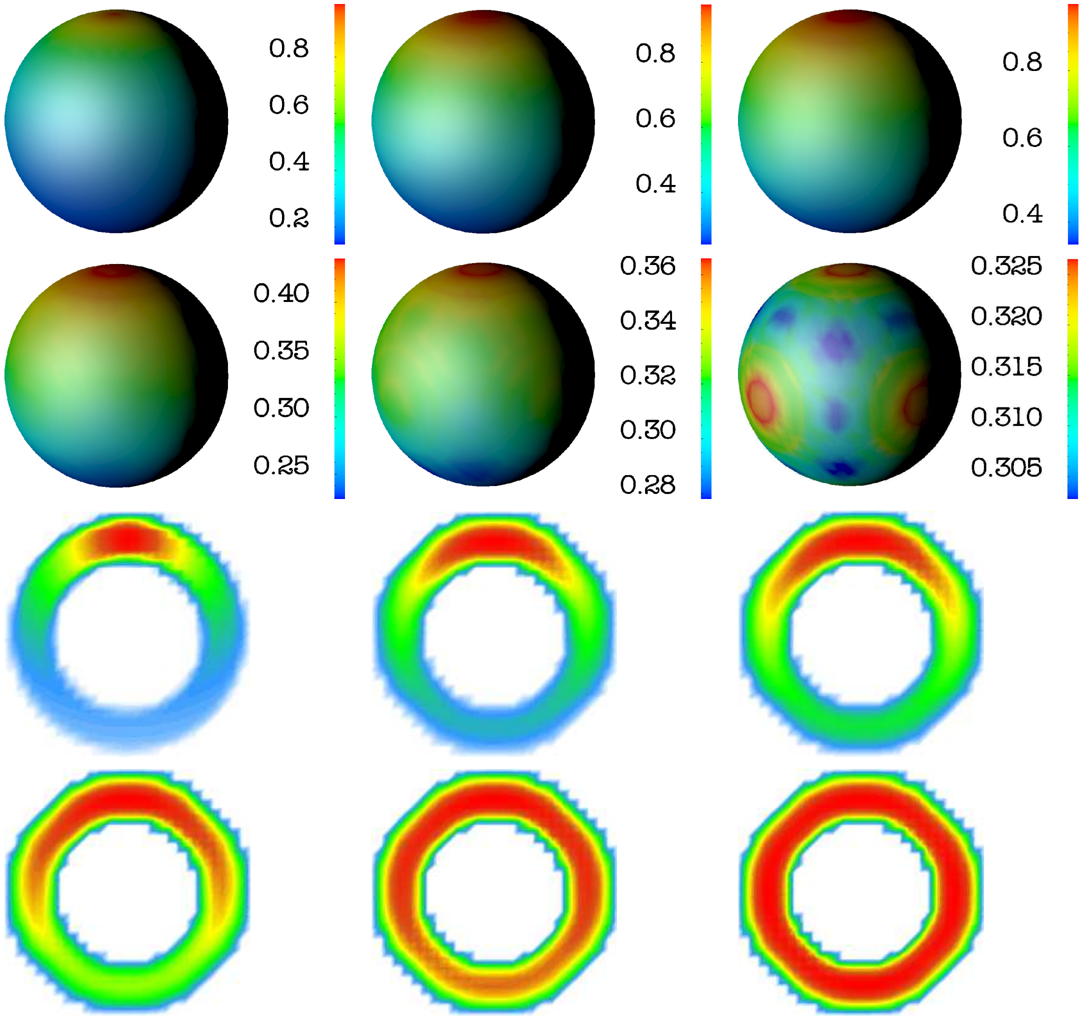

Figure 9.3: Concentration of diffusive species on surface and on a 2D cross section of sphere governed by pure diffusion with $64 \times 64 \times 64$ mesh. Times shown are $t = 0, 0.1, 0.25, 0.5, 1.0$, and 5.0. Bottom two rows: the color scale changes with each picture and does not correspond to the colorbar for the top two rows.

two rows of Figure 9.3 shows the same results along a cross section, so that the transition through the surface can be seen.

9.2.2. Diffusion on Torus. Next, we choose a more interesting (but still analytically defined) surface: a torus. We choose a torus because it has regions of positive Gaussian curvature and regions of negative Gaussian curvature so that we can eventually test the curvature effects. The surface is defined by

$$\left(R - \sqrt{x^2 + y^2}\right)^2 + z^2 = r^2, \tag{443}$$

where R and r are the major and minor radii, respectively. The major radius R is the distance from the center of the tube to the center of the torus, and the minor radius r is the radius of the tube. The torus may be parameterized by θ and ϕ,

$$\vec{x} = \begin{pmatrix} (R + r\cos\theta)\cos\phi \\ (R + r\cos\theta)\sin\phi \\ r\sin\phi \end{pmatrix}, \tag{444}$$

where the parameters $0 \leq \theta, \phi \leq 2\pi$. The angle ϕ is the angle made from the surface to the positive x-axis (projected on the xy-plane), and the angle θ is the angle made from the surface the the center of the tube. We consider a ring torus, where $R > r$.

We need to choose the radii carefully so that enough resolution is provided for the derivatives to be computed. We selected the torus with major radius $R = 2.0$ and minor radius $r = 1.1$, solved over a grid of $[-4, 4]^3$, beginning with a $64 \times 64 \times 64$ mesh.

The initial condition is chosen to be localized at the highest point of the positive y-axis, smoothly distributed along the surface, and smoothly distributed from the surface to the domain. We chose for the initial condition

$$\begin{aligned} \rho(x, y, z, 0) = S \cdot \exp &\left(-\sqrt{\mathrm{x}^2 + (\mathrm{y} - \mathrm{R})^2 + \mathrm{z}^2}\right) \\ &\cdot \exp\left(-2\left(\mathrm{r} - \sqrt{(\mathrm{x} - \mathrm{c_x})^2 + (\mathrm{y} - \mathrm{c_y})^2 + \mathrm{z}^2}\right)\right). \end{aligned} \tag{445}$$

The first exponential in (445) controls the smoothness of the concentration along the surface of the torus, and the second controls the smoothness of the concentration from the torus to the domain, akin to the term $(\delta_\Gamma - b)$ for a sphere. The point $(c_x, c_y, 0)$ is the center of the torus tube at a given angle ϕ. Finally, S is chosen so that the maximum of the concentration is 1 on the torus surface.

The profile of the delta function for the torus is shown in Figure 9.4. The 1D cross section

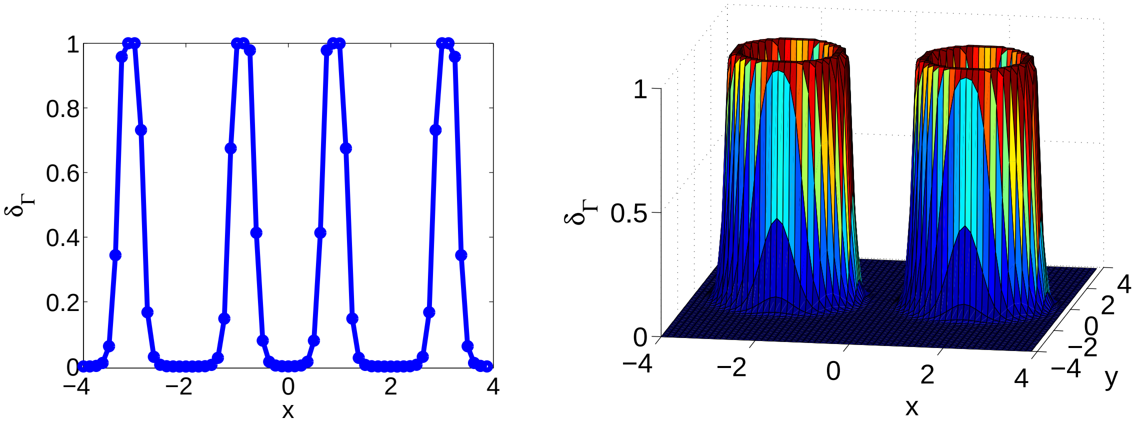

Figure 9.4: Profile of delta function for the torus with radii $R = 2.0$ and $r = 1.1$ with $64 \times 64 \times 64$ mesh. Left: 1D profile across the x grid points. Right: 2D profile across x and y grid points.

of the delta function as seen in Figure 9.4 shows that the surface is well resolved over the $y = z = 0$ cross section. That is, there is a clear transition from the outside to the inside of each ring, and the delta function settles to zero in the empty space.

The results of pure diffusion according to Algorithm 8.1 neglecting curvature effects are presented in Figure 9.5. It is clear from Figure 9.5 that the concentration is not distributed uniformly across the surface as expected, but seems to be stuck toward the inner ring of the torus. This is more evident in the 2D plots along the $x = 0$ cross-section in the bottom two rows of Figure 9.5. We attribute the unexpected result to numerical error due to a very coarse mesh. The grid spacing in each dimension is $\Delta x = 8/64 = 0.125$, which is not very small indeed. The radius of the torus tube is $r = 1.1$, giving only 8-9 points from one end of the tube to the other.

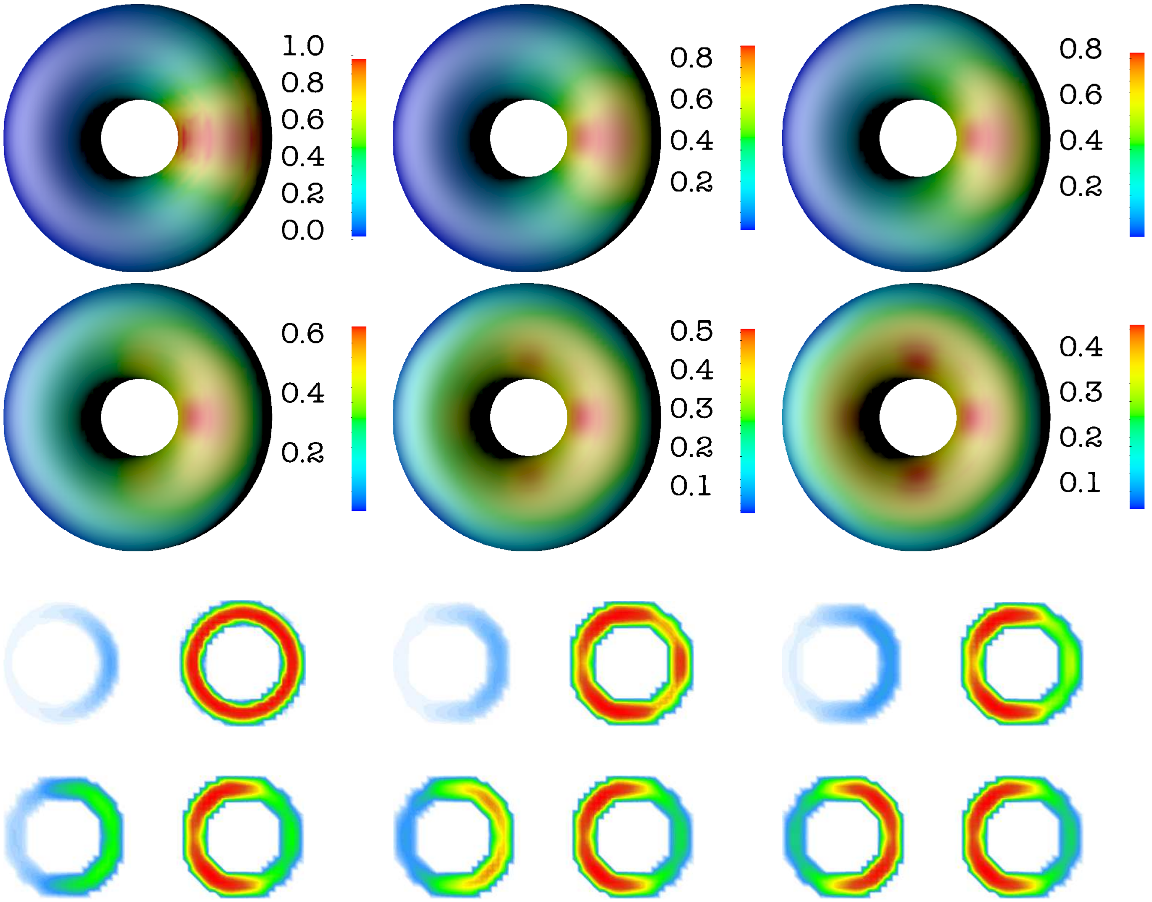

Figure 9.5: Concentration of diffusive species on surface and on a 2D cross section of the torus, governed by pure diffusion with $64\times 64\times 64$ mesh. Times shown are $t = 0, 0.25, 1.0, 2.5,$ 5.0, and 10.0. Bottom two rows: the color scale changes with each picture and does not correspond to the colorbar for the top two rows.

9.2.2.1. *Diffusion on torus with refined mesh.* Moving to a finer mesh of $128 \times 128 \times 128$, we can double the number of points in the torus tube. The grid spacing is now $\Delta x = 8/128 = 0.0625$. This is still not very small, but since the 3D computation can be very expensive for a finer mesh, we did not increase the mesh past 128 grid points in each dimension. The profile of the delta function for the torus with the "fine" mesh is shown in Figure 9.6.

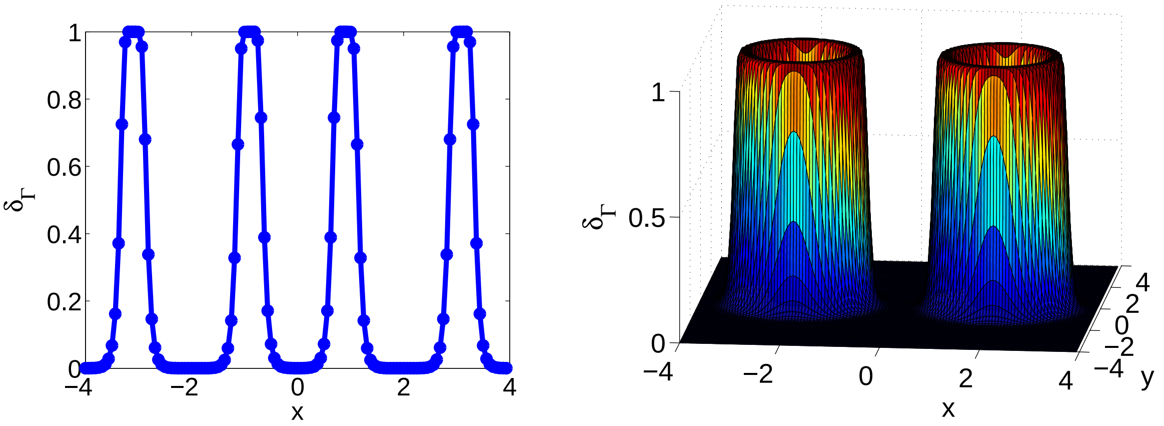

Figure 9.6: Profile of delta function for the torus with radii $R = 2.0$ and $r = 1.1$ under a $128 \times 128 \times 128$ mesh. Left: 1D profile across the x grid points. Right: 2D profile across x and y grid points.

The results of pure diffusion according to Algorithm 8.1 neglecting curvature effects with the new mesh are presented in Figure 9.7. Figure 9.8 shows that the undesirable effect of getting “stuck” in the middle of the torus is better resolved with this finer mesh.

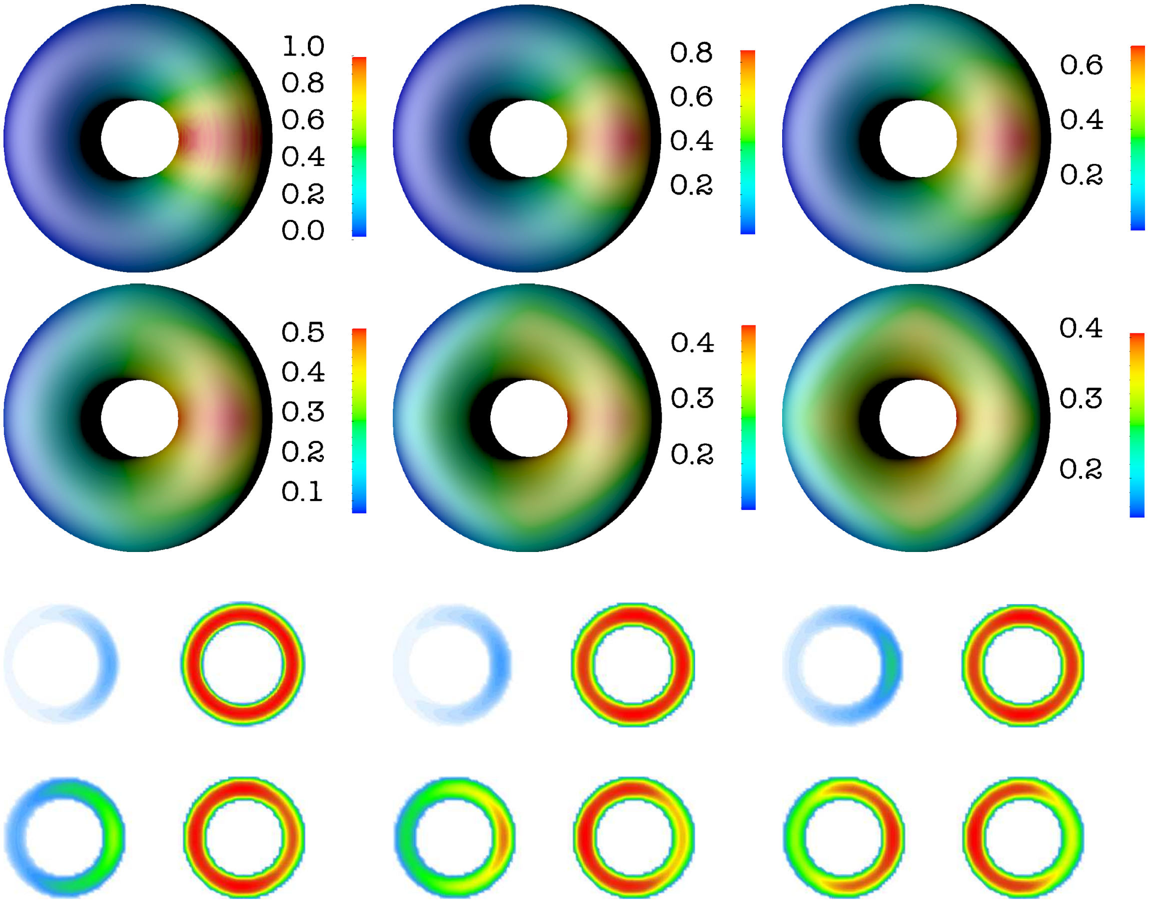

Figure 9.7: Concentration of diffusive species on surface and on a 2D cross section of the torus, governed by pure diffusion with 128 × 128 × 128 mesh. Times shown are $t = 0, 0.25, 1.0, 2.5,$ 5.0, and 10.0. Bottom two rows: the color scale changes with each picture and does not correspond to the colorbar for the top two rows.

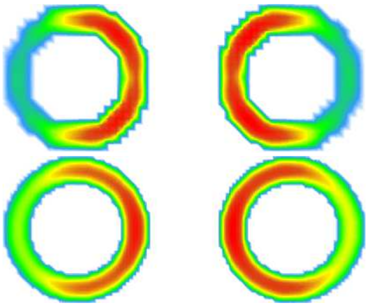

Figure 9.8: Comparison of diffusion on a torus with $64\times64\times64$ mesh (top) and $128\times128\times128$ mesh (bottom). Time shown is $t = 10.0$. Notice that the effect of getting "stuck" in the middle is reduced with the finer mesh (even though it is still not completely resolved).

9.2.3. Diffusion on two spheres merged. Finally, we test pure diffusion on a more interesting and more practical surface. This example illustrates the feasibility of eventually solving the phase equation that defines the surface simultaneously with the concentration equation. We take as a test surface the result from Algorithm 7.1 with a phase field initialized by two spheres of radius $\pi/4$. The merging of the spheres was illustrated in Figure 7.3. We stopped the Algorithm after $t = 0.02$ and used the result as the surface to test Algorithm 8.1 with pure diffusion. Using the coarse mesh of $64 \times 64 \times 64$, the merged surface requires a reinitialization of the phase function, since after advancing Algorithm 7.1, the inside of the surface does not satisfy $\phi = 1$ very well (see Figure 9.9). This can have detrimental effects when evaluating the delta function with this ϕ. Any input to the delta function that is not sufficiently close to 1 or -1 is regarded as the surface band. Therefore, it is critically important that the inside of the surface satisfy $\phi \approx 1$ sufficiently close, and the outside of the surface satisfy $\phi \approx -1$ sufficiently close, so that none of these positions are treated as surface points. A reinitialization of the $\tanh(\cdot)$ profile of the phase field ϕ is performed before running Algorithm 8.1. There are many methods of reinitialization, most employ a

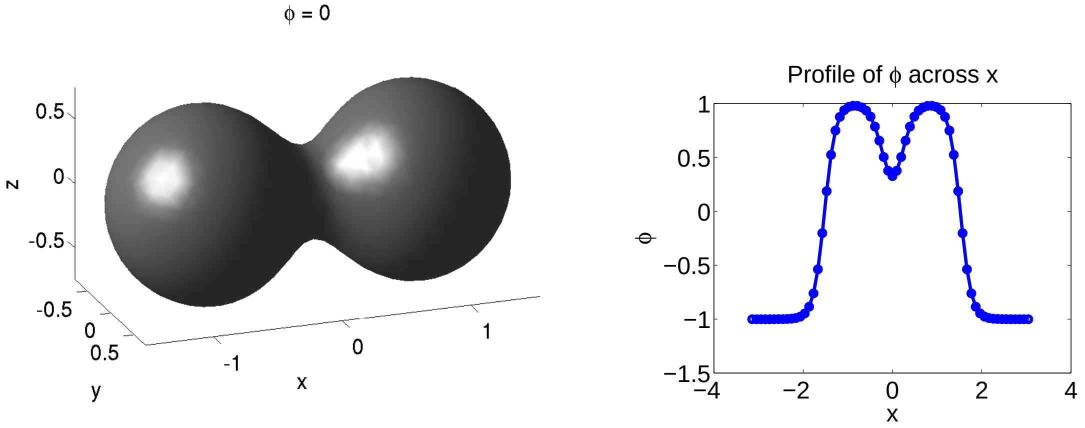

Figure 9.9: Left: Surface given by Algorithm 7.1 from two spheres merging, stopped at $t = 0.02$ with $64 \times 64 \times 64$ mesh. Right: 1D profile of surface. Notice the dip in ϕ near $x = 0$. While this point is clearly inside of the surface (it is the center point), $0 < \phi \ll 1$, rendering reinitialization necessary for the mesh of $64 \times 64 \times 64$.

reinitialization to a signed distance function by solving the equation

$$\frac{\partial d}{\partial t} = sign(d_0)(1 - |\nabla d|). \tag{446}$$

This equation penalizes any deviation of the signed distance function d from satisfying the Eikonal equation $|\nabla d| = 1$, while preserving the original sign convention of d_0. The function $sign(d)$ is the sign function that is positive 1 when $d > 0$, negative 1 when $d < 0$ and zero when $d = 0$. There are other methods that preserve the profile by coupling the phase equations with an energy penalty for the deviation of $|\nabla d|$ from 1 [63, 103]. These methods do not require reinitialization.

In efforts for something simpler, the reinitialization we chose is briefly described as follows. We define a temporary function ψ to be 1 if $\phi \geq 0$ and 0 otherwise. This may be thought of as a heat source that is located on and inside of the surface. Then, we solve the heat equation $\partial\psi/\partial t = D_h \Delta \psi$ for a few time steps, where $D_h > 0$ is the diffusion coefficient. There will be some level set of ψ close to but less than 1 that will define the new surface. There may still be a slight dip in ψ in the center, since less "heat" is diffusing from the center. Therefore, we scale the result by $\psi_1 = \tanh(\psi + 3)$. This also makes the profile more like the original $\tanh(\cdot)$ profile. Then we perform a linear scaling so that $-1 \leq \psi_1 \leq 1$. This ψ_1 defines the new phase field function. Note that the longer time the heat equation is solved, the smoother the profile, however a profile that is too diffusive may be very different from the original phase field function. We want a profile smooth enough to include points in the transition from inside to outside, yet we want it to maintain the $\tanh(\cdot)$ shape. Figure 9.10 shows the profile after reinitialization, using spectral methods to solve the heat equation with $D_h = 1$ and $\Delta t = 10^{-3}$, for a total of 7 time steps.

With the reinitialized phase field function, we ran Algorithm 8.1. We used the initial concentration similar to (447), but modified so that the concentration would be localized toward the north pole of the leftmost sphere. The two phase field function was created from two spheres of radius $r = \pi/4$, each initially displaced by $\pi/4 + 0.025$ from the origin on either side. Therefore, the new initial condition is given by (neglecting the 0.025 separation

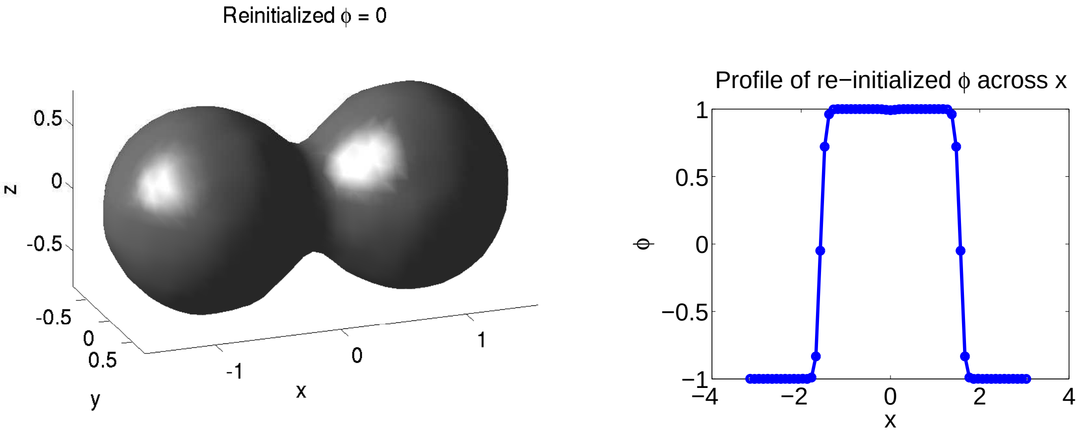

Figure 9.10: Left: Reinitialized surface with $64\times64\times64$ mesh. Right: 1D profile of reinitialized surface. In comparison with Figure 9.9, the profile is certainly better maintained, but the resolution along the transition region is sacrificed. This is intuitive since the transition region is sharper.

and any slight variations due to the merging process),

$$\rho(x,y,z,0)=S\cdot\exp\left(-\sqrt{\left(\mathrm{x}+\frac{\pi}{4}\right)^2+\mathrm{y}^2+\left(\mathrm{z}-\frac{\pi}{4}\right)^2}\right)(\delta_\Gamma-\mathrm{b}). \tag{447}$$

Again, S is chosen so that the maximum concentration is 1. The profile of the delta function for the reinitialized surface is shown in Figure 9.11.

The results of the pure diffusion algorithm on the reinitialized surface and the $z=0$ cross section are shown in Figure 9.12. One may notice some small patches of higher concentrations in the final figure, making the final distribution not perfectly uniform. This is a numerical artifact and can be resolved with a finer mesh, or better reinitialized surface ϕ. It is important to keep in mind that the mesh size using 64 grid points over 1 dimension on $[-\pi,\pi]$ results in a spacing of $\Delta x=2\pi/64\approx0.1$.

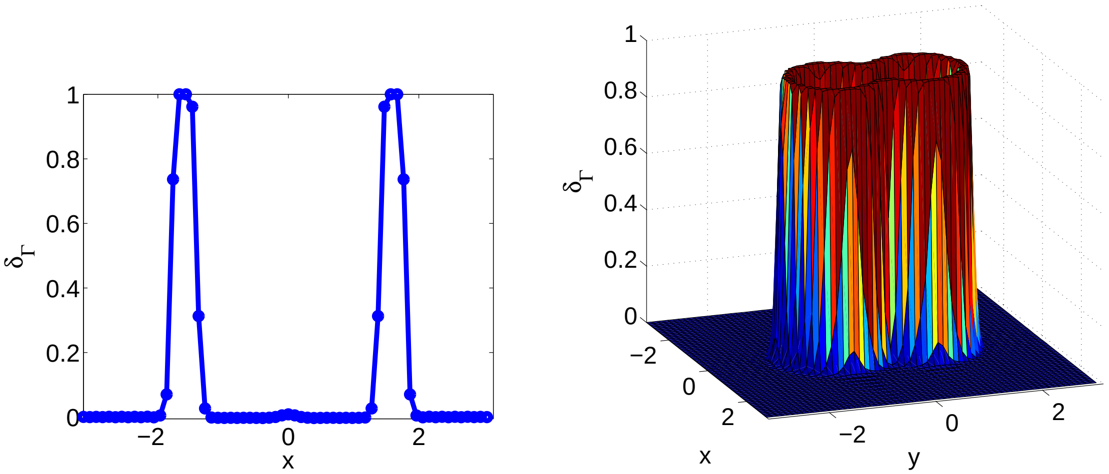

Figure 9.11: Profile of delta function across x with $y = z = 0$ for two spheres surface (reinitialized) with $64 \times 64 \times 64$ mesh. Left: 1D profile across the x grid points. Right: 2D profile across x and y grid points at $z = 0$.

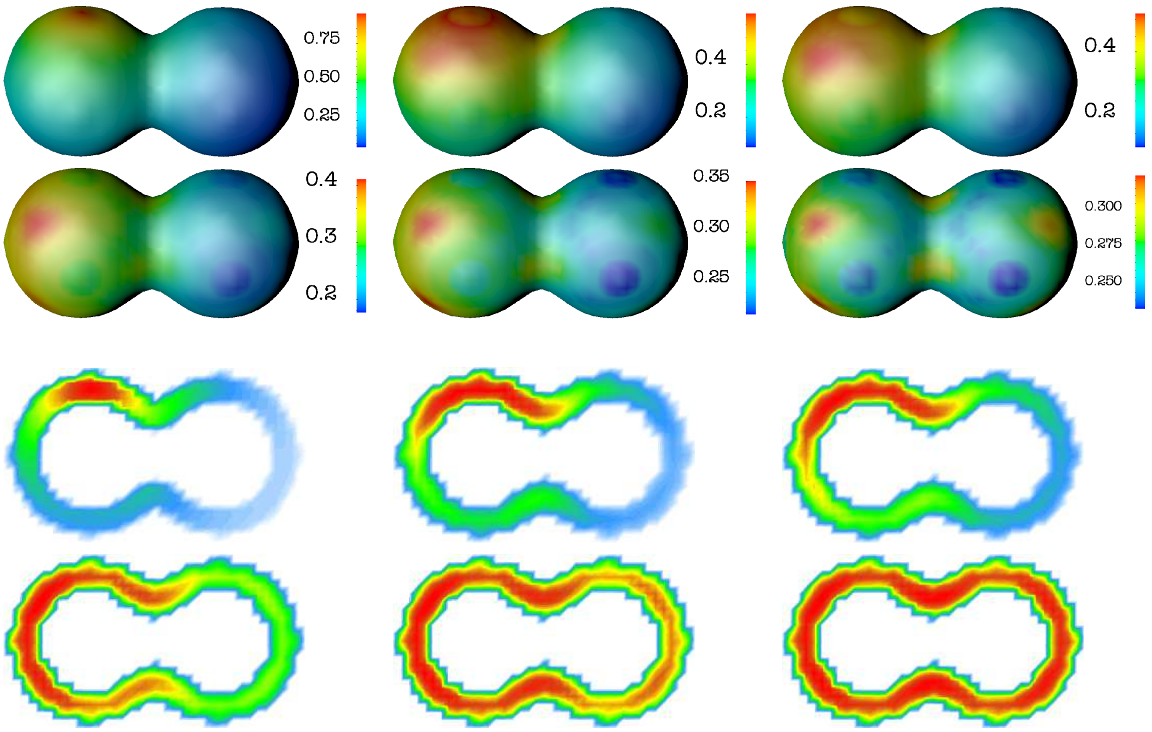

Figure 9.12: Concentration of diffusive species on reinitialized surface and on a 2D cross section of two spheres merged, governed by pure diffusion with $64 \times 64 \times 64$ mesh. Times shown are $t = 0, 0.1, 0.25, 1.0, 2.5$, and 5.0. Bottom two rows: the color scale changes with each picture and does not correspond to the colorbar for the top two rows.

9.2.3.1. *Diffusion on two spheres with refined mesh.* We now move to results on a finer mesh, using 128 × 128 × 128 grid points. We find that the merged spheres surface does not exceed the domain $[-2, 2]^3$, therefore we restrict $\Omega = [-2, 2]^3$ to reduce the grid spacing even further. The spacing between nodes is now $\Delta x = 4/128 = 0.03125$ in each dimension. We find that after advancing the phase field on this new domain with the new mesh, reinitialization of the profile was not as essential as before, and possibly unnecessary, as seen in Figure 9.13. With even further resolution of the mesh, reinitialization should be unnecessary.

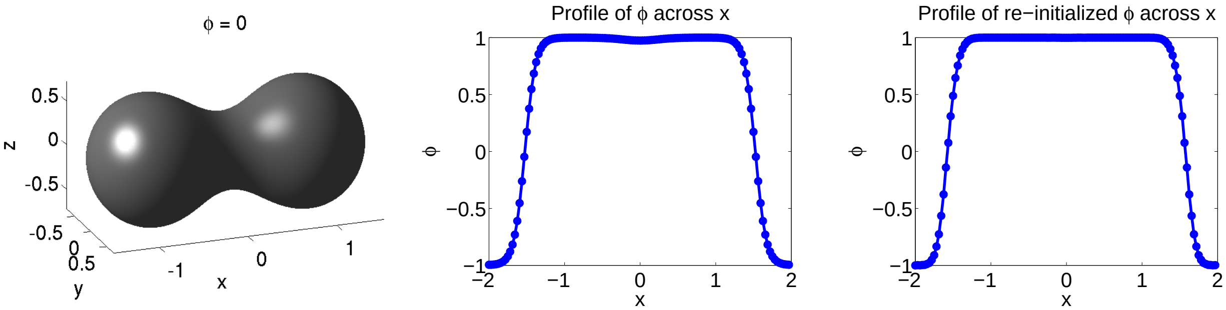

Figure 9.13: Left: Surface given by Algorithm 7.1 from two spheres merging on $\Omega = [-2, 2]^3$ with 128 × 128 × 128 mesh, stopped at $t = 0.02$. Middle: 1D profile of surface. Right: Reinitialized profile of surface. Note that reinitialization is not as dramatic as in the 64 × 64 × 64 mesh.

The profile of the delta function for the surface under the "fine" mesh is shown in Figure 9.14. Upon inspection of the delta function profile in Figure 9.14, it seems that a better choice for the domain is slightly greater than $[-2, 2]^3$, so that the tails of the delta profile are flat, giving no contribution to $\Delta\sqrt{\delta_\Gamma^*}$ in the algorithm, a term that appears in the diffusion equation (400). Unfortunately, time did not permit such a numerical test, but this should be done in the future.

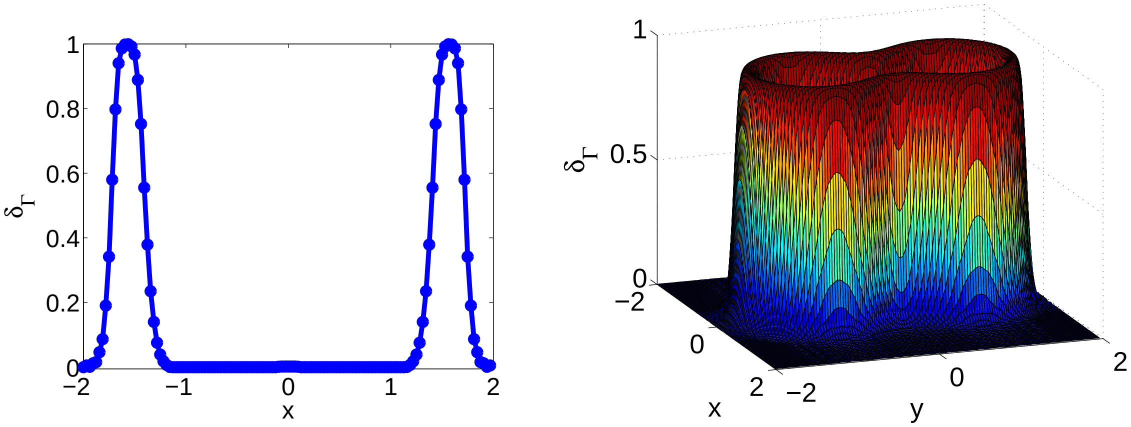

Figure 9.14: Profile of delta function (441) for the (reinitialized) two spheres surface with $128 \times 128 \times 128$ mesh. Left: 1D profile across the x grid points. Right: 2D profile across x and y grid points.

We use a consistent initial condition as (447), delta function (441), and bandwidth $b = 0.5$ for the $128 \times 128 \times 128$ mesh. The results of pure diffusion on the surface and along the $z = 0$ cross section are presented in Figure 9.15. In spite of the restrictive domain, the pure diffusion algorithm performed quite well. We note, however, that a careful choice of parameters was made to find such good results as those in Figure 9.15, and slight perturbations from these parameters results in unexpected behavior. In many cases, the concentration seems to be "stuck" in the center of the two spheres merged, much like what occurred in Figure 9.5. Again, this should be resolved with either (i) a larger domain than $[-2, 2]^3$ giving the delta function space to settle to zero, or (ii) a finer mesh.

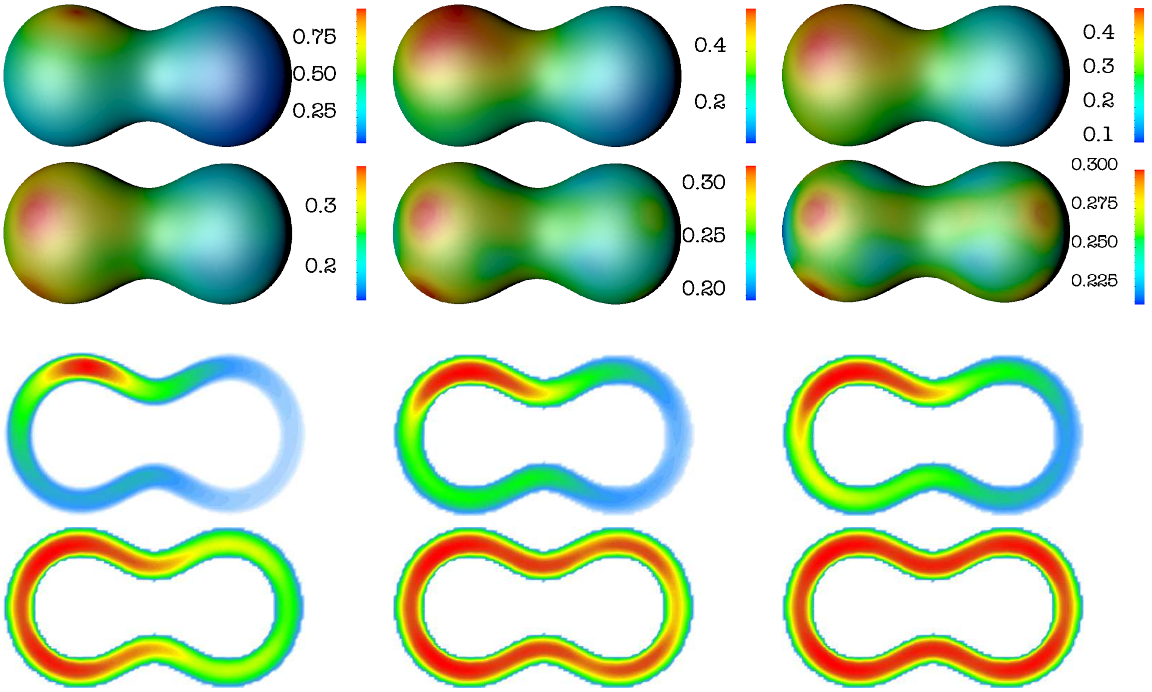

Figure 9.15: Concentration of diffusive species on surface and on a 2D cross section of two spheres merged, governed by pure diffusion with 128 × 128 × 128 mesh. Times shown are $t = 0, 0.1, 0.25, 1.0, 2.5,$ and 5.0. Bottom two rows: the color scale changes with each picture and does not correspond to the colorbar for the top two rows.

9.3. CURVATURE EFFECTS

Now we test our full algorithm by including the curvature effects. That is, we give the full version of Algorithm 8.1, and the correction terms H_n^{dif} and H_m^{dif} are given by (419) and (437). We choose the same delta as defined in (441) with $D = 10$ and $b = 0.5$ consistently.

9.3.1. CURVATURE EFFECTS ON A SPHERE.

We begin with the simple test case of curvature effects on a sphere of radius 1 centered at the origin. We solve this consistently on a grid of $[-\pi, \pi]^3$ and a mesh of $64 \times 64 \times 64$ for comparison. Analytically, a sphere has mean curvature $H = 1/r$ everywhere, where r is the radius of the sphere. This is exactly what we find when we plot the mean curvature given by the formula (294). A plot of the numerical mean curvature is given in Figure 9.25.

Since the mean curvature is constant everywhere along the sphere, we should expect a uniform distribution of the concentration for the equilibrium solution. Actually, the final

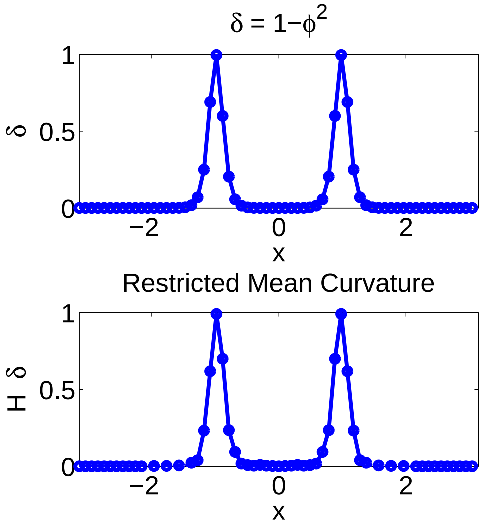

Figure 9.16: Mean curvature of a sphere with 64 × 64 × 64 mesh. Top: 1D cross section of delta function used to scale mean curvature. Bottom: 1D cross section of mean curvature of a sphere, scaled by the delta function.

result should be even better than regular diffusion: since the mean curvature is smoothed out by the delta function, the concentration will prefer positions where the curvature is closest to $1/r = 1$, which occurs in the center of the surface band. By setting the diffusive species to have spontaneous curvature $C_0^{\text{dif}} = 1$ and the background species to have curvature $C_0^{\text{bak}} = 0$, we see exactly this. The plots of a 2D cross section are more revealing than the surface visualization, since they show the preference of the diffusive species to the center of the band, where the curvature is 1. These plots are shown in Figure 9.17. Compared to the bottom two rows of Figure 9.3, the concentration of the diffusive species aggregates to the center of the band, which is desirable for the narrow band method. Pure diffusion should push the concentration away from the source, which causes leakage into the domain. This curvature preference actually resists this numerical artifact, keeping the concentration near the center of the narrow band.

On the other hand, if we set the diffusive species to prefer curvatures away from 1, the concentration will try to escape the center of the band, rather than be attracted to it. Let $C_0^{\text{dif}} = 0$ and $C_0^{\text{bak}} = 1$. On a sphere, the diffusive species has nowhere to travel to satisfy the

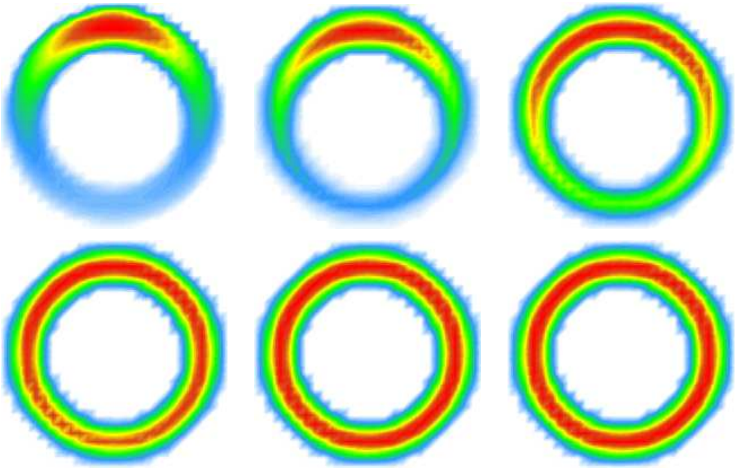

Figure 9.17: Concentration of diffusive species along the surface of sphere under diffusion with curvature effects using 64 × 64 × 64 mesh. The diffusive species prefers the curvature $C_0^{\mathrm{dif}} = 1.0$ and the background species prefers the curvature $C_0^{\mathrm{bak}} = 0$. The curvature is exactly 1 in the center of the band. Times shown are $t = 0$, 0.01, 0.1, 0.25, 0.5, and 1.0. The color is scaled by the maximum concentration in each plot.

curvature penalty except toward the domain, where $H = 0$. But, due to the conservation of mass, the diffusive species must stay inside the band. Figure 9.18 shows the results.

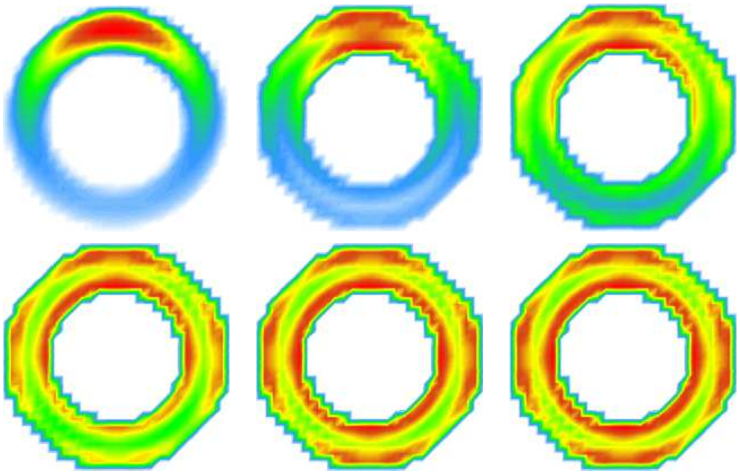

Figure 9.18: Concentration of diffusive species along surface of sphere under diffusion with curvature effects using $64 \times 64 \times 64$ mesh. The diffusive species prefers the curvature $C_0^{\mathrm{dif}} = 0$ and the background species prefers the curvature $C_0^{\mathrm{bak}} = 1$. The curvature is exactly 1 in the center of the band. Times shown are $t = 0$, 0.01, 0.1, 0.25, 0.5, and 1.0. The color is scaled by the maximum concentration in each plot.

9.3.2. CURVATURE EFFECTS ON A TORUS. Now we move to a more interesting example of the torus, where the surface has variable curvature. We choose the same parameters consistently for the torus as with the diffusive case. Analytically, the mean curvature of a torus is given by

$$H_{torus} = \frac{R + 2r\cos\theta}{2r(R + r\cos\theta)}, \tag{448}$$

where R, r, and θ are given in the parameterization (444). At the outer ring of the torus (with $\phi = 0$), $\theta = 0$. Therefore the mean curvature is $H_{torus} \approx 0.6158$. (On the other end when $\phi = \pi$, the outer ring has angle $\theta = -\pi$, and the signs cancel to give the same mean curvature, as expected by symmetry.) The outer ring is also a region of positive Gaussian curvature, since both principle curvatures are directed toward the center of the torus (in the same direction). At the inner ring of the torus, $\theta = \pi$ (with $\phi = 0$), and $H_{torus} \approx -0.1010$. The inner ring is also a region of negative Gaussian curvature, since one principle curvature is directed toward the center of the torus and the other is directed away from the center of the torus. Numerically, a 1D cross section of the mean curvature is shown in Figure 9.19.

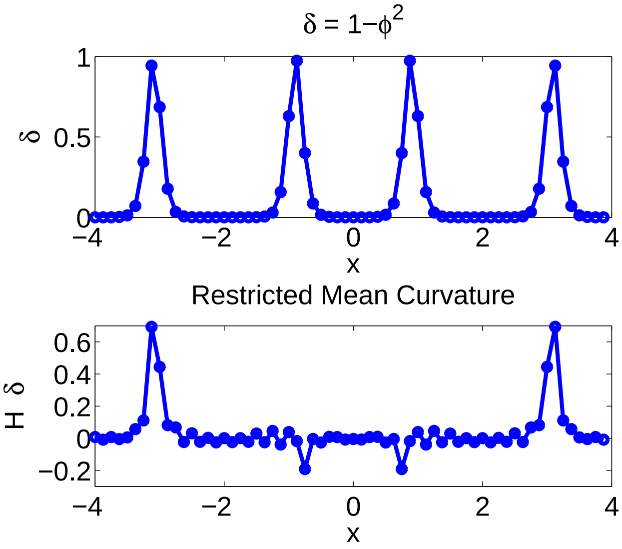

Figure 9.19: Mean curvature of a torus with 64 × 64 × 64 mesh. Top: 1D cross section of delta function used to scale mean curvature. Bottom: 1D cross section of mean curvature of a sphere, scaled by the delta function.

The plot matches the analytical values at the positions of the inner and outer rings well; however, some oscillation of the mean curvature is observed elsewhere in Figure 9.19. This is because the mean curvature H is approximated by equation (294), which depends on the phase field function ϕ at all level sets, and not just on the surface $\phi = 0$. The nonphysical values of H are supposed to be scaled away by the delta function, but with this coarse of a mesh, the delta function is not exactly zero in these regions. With a refined mesh, the mean curvature should be better resolved.

To drive the diffusive species to the outer ring and the background to the inner ring, we set the spontaneous curvatures $C_0^{\text{dif}} = 0.5$ and $C_0^{\text{bak}} = -0.1$, shown in Figure 9.20. Recall

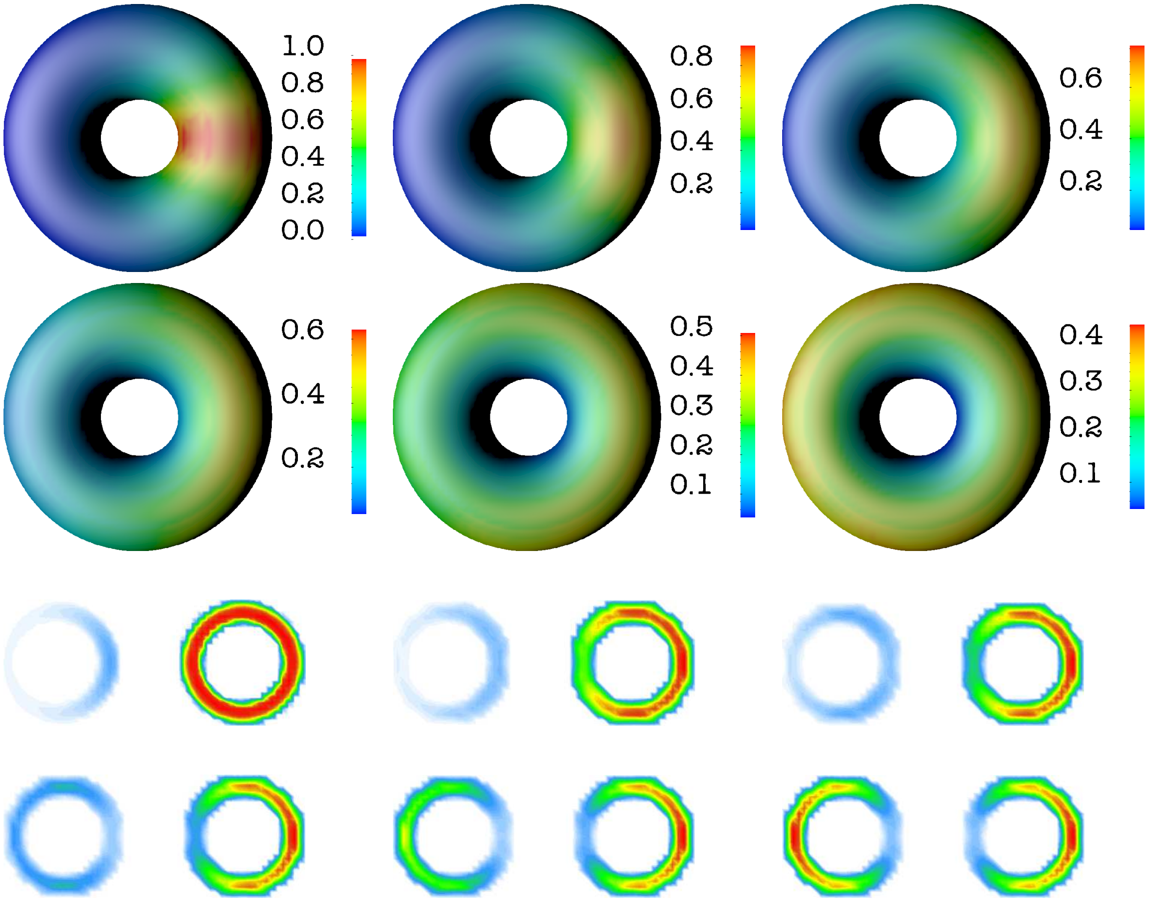

Figure 9.20: Concentration of diffusive species on the torus governed by diffusion with curvature effects using $64 \times 64 \times 64$ mesh. The diffusive species prefers the curvature $C_0^{\text{dif}} = 0.5$ (located on the outer ring) and the background species prefers the curvature $C_0^{\text{bak}} = -0.1$ (located on the inner ring). Times shown are $t = 0, 0.1, 0.25, 0.5$, 1.0, and 5.0. The color is scaled by the maximum concentration in each plot.

that under pure diffusion, the diffusive concentration tended toward the inner ring due to numerical error (see Figure 9.5). The curvature effect has this numerical error working against it. The curvature preference overcomes this. It is easy to see in Figure 9.20 the preference of the diffusive species toward the outer band.

Reversing the curvature preference, we now solve the equation with the diffusive species $C_0 = -0.1$ and the background species $C_0^{\text{bak}} = -0.1$. This is more like the motivating application of the M2 protein, preferring regions of negative Gaussian curvature (see Figure 8.3). The plots of the concentration with these curvature preferences together with the corresponding cross sections are shown in Figure 9.21.

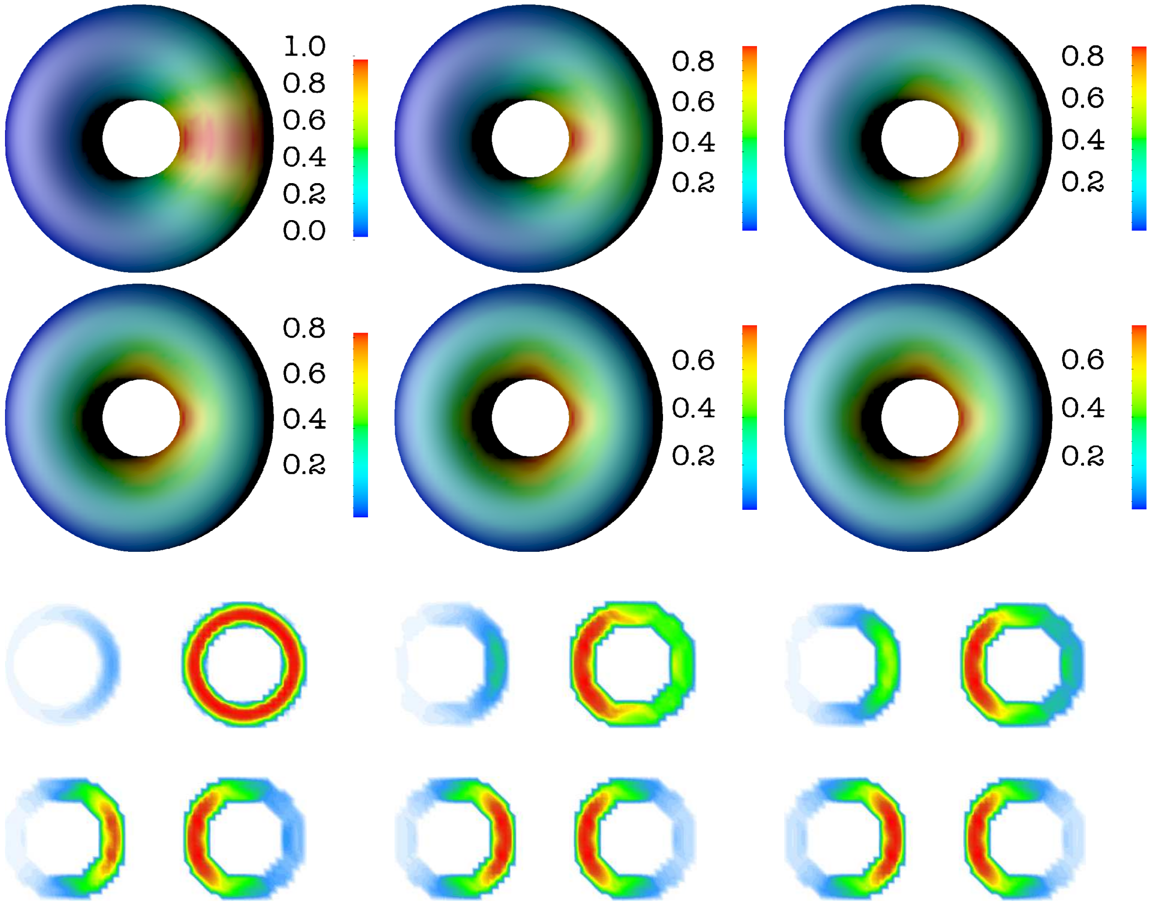

Figure 9.21: Concentration of diffusive species on the torus governed by diffusion with curvature effects using $64 \times 64 \times 64$ mesh. The diffusive species prefers the curvature $C_0^{\text{dif}} = -0.1$ (located on the inner ring) and the background species prefers the curvature $C_0^{\text{bak}} = 0.5$ (located on the outer ring). Times shown are $t = 0, 0.1, 0.25, 0.5$, 1.0, and 5.0.

9.3.2.1. *Curvature effects on torus with refined mesh.* Next, we move to the $128\times128\times128$ mesh. The plot of the mean curvature is resolved better when compared to that for the $64 \times 64 \times 64$ mesh (recall Figure 9.19). The mean curvature with the new mesh is given in Figure 9.22.

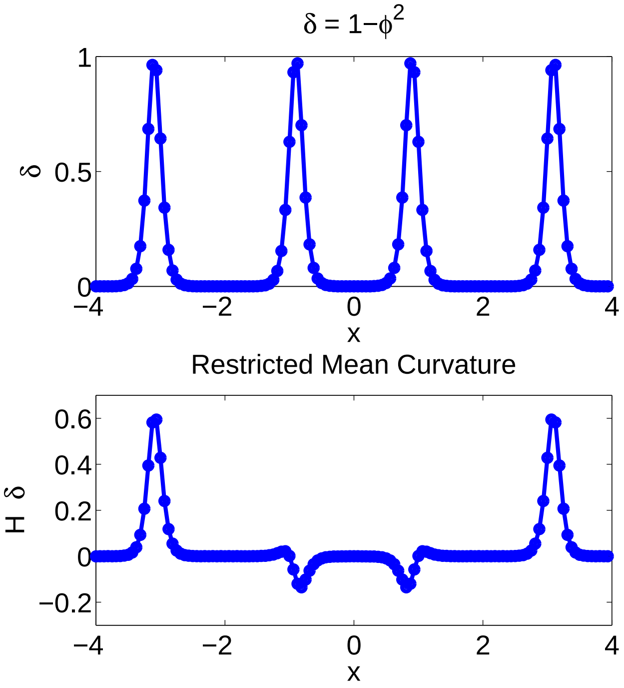

Figure 9.22: Mean curvature of a torus with $128 \times 128 \times 128$ mesh. Top: 1D cross section of delta function used to scale mean curvature. Bottom: 1D cross section of mean curvature of a sphere, scaled by the delta function above as in (370). Note the better resolution compare to Figure 9.19.

Figure 9.23 shows both the concentration on the surface and the corresponding $x = 0$ cross section. The diffusive species prefer the outer ring of the torus.

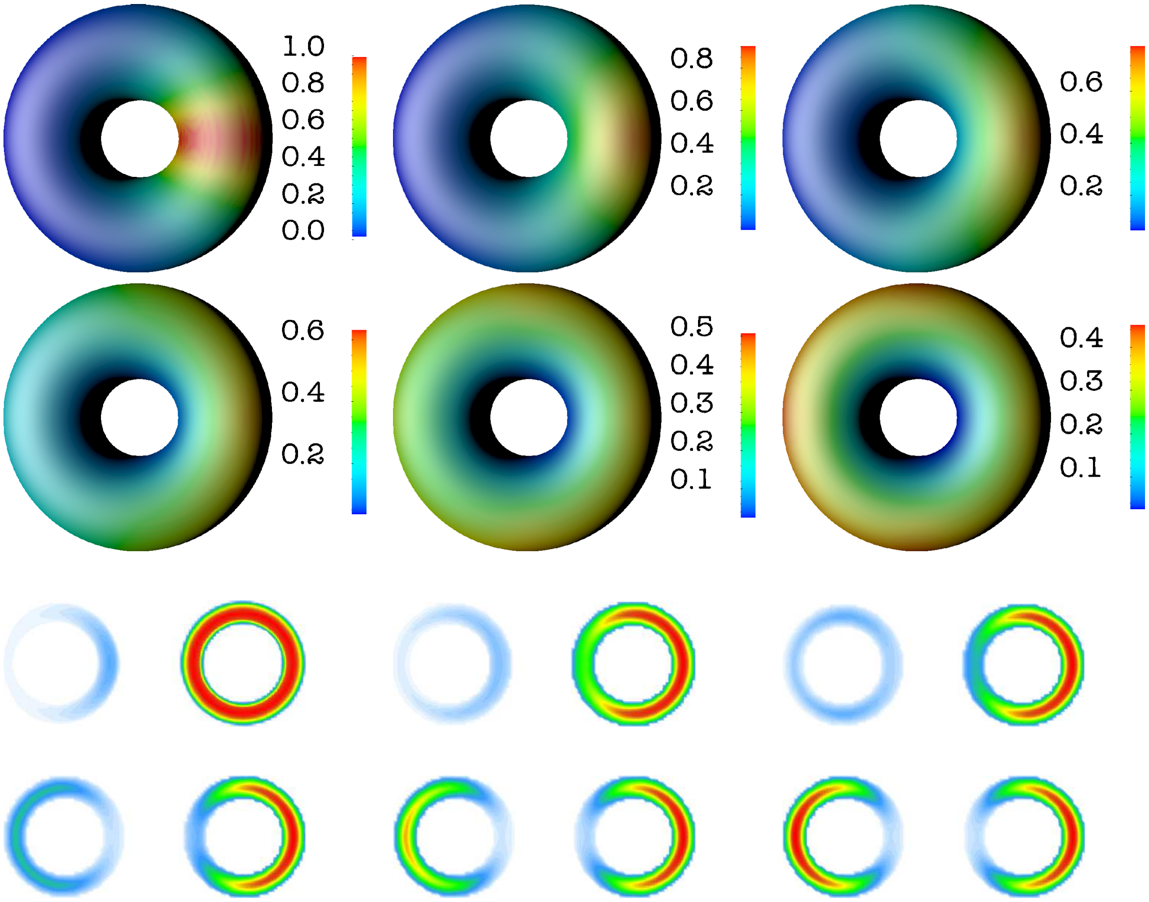

Figure 9.23: Concentration of diffusive species on the torus governed by diffusion with curvature effects using $128 \times 128 \times 128$ mesh. The diffusive species prefers the curvature $C_0^{\text{dif}} = 0.5$ (located on the outer ring) and the background species prefers the curvature $C_0^{\text{bak}} = -0.1$ (located on the inner ring). Times shown are $t = 0, 0.1, 0.25, 0.5$, 1.0, and 5.0. The color is scaled by the maximum concentration in each plot.

Reversing the curvature preferences, Figure 9.24 shows the concentration on the surface and the corresponding $x = 0$ cross section if the diffusive species prefers curvature toward the inner ring.

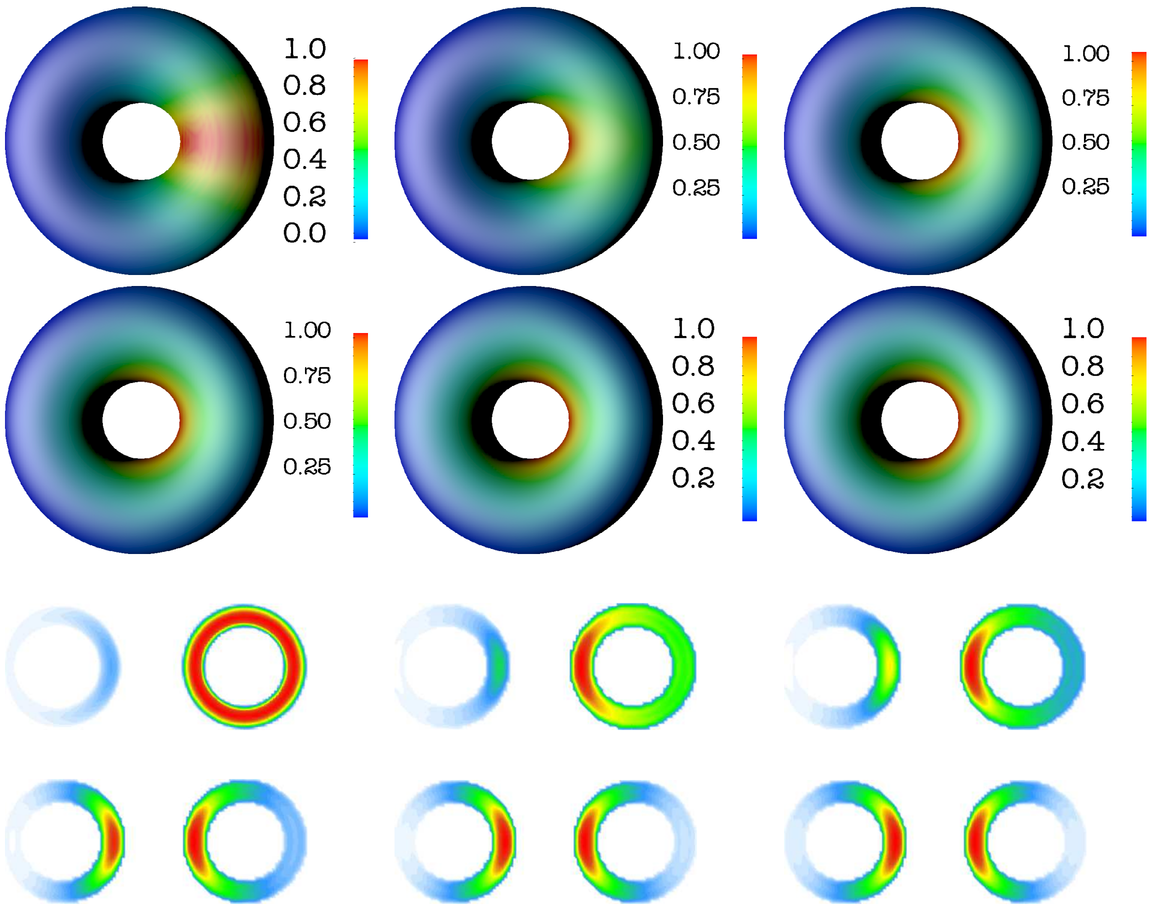

Figure 9.24: Concentration of diffusive species on the torus governed by diffusion with curvature effects with $128 \times 128 \times 128$ mesh. The diffusive species prefers the curvature $C_0^{\text{dif}} = -0.1$ (located on the inner ring) and the background species prefers the curvature $C_0^{\text{bak}} = 0.5$ (located on the outer ring). Times shown are $t = 0, 0.1, 0.25, 0.5,$ 1.0, and 5.0.

9.3.3. CURVATURE EFFECTS ON TWO SPHERES MERGED. Finally, we run diffusion with curvature effects on the surface given by two spheres merged as the finale of the thesis. Since the $64 \times 64 \times 64$ mesh required reinitialization, we skip this choice and move straight to the $128 \times 128 \times 128$ case (without reinitialization).

The plots of the mean curvature for the two spheres merged are given for two 1D cross sections in Figure 9.25. The first plot is the cross section across x, with $y = z = 0$, traversing the length of both spheres. The second plot is the cross section across z, with $x = y = 0$, traversing the location of the merge. The mean curvature across the x-direction appears to be very well controlled, with a maximum mean curvature of $H = 1.27$, and the mean

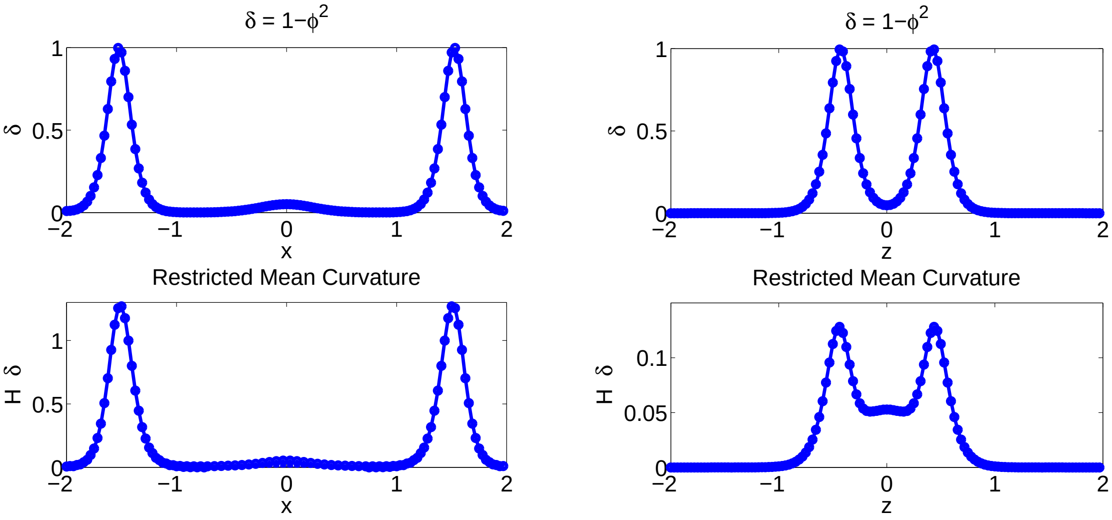
$\delta = 1-\phi^2$

$\delta = 1-\phi^2$

Restricted Mean Curvature

Restricted Mean Curvature

Figure 9.25: Mean curvature of two spheres surface with 128×128×128 mesh. Left: 1D profile across x-dimension. Right: 1D profile across $z-$ or $y-$ dimension (they are symmetric).

curvature is smoothly distributed across this dimension. However, the mean curvature does rise to $H = 0.05$ in the center of the sphere (where there is no surface). Because we did not reinitialize the surface, the delta function is greater than zero even in the very center of the surface. This can be seen in both plots, but it is more noticeable in the second mean curvature plot, since the maximum mean curvature across z is $H = 0.128$. The nonzero mean curvature along the interior of the surface is due to numerical error in the phase function, as seen in Figure 9.13. Even though there is only a slight "dip" in ϕ in the interior of the surface, this error is propagated when the delta function is computed in equation (441). Nevertheless, this is the surface we have to work with under the current resources.

We first set the diffusive species to prefer the curvature $C_0^{\text{dif}} = 1.25$ and the background species to prefer the curvature $C_0^{\text{bak}} = 0.1$. This should drive the concentration toward the outer edges of the surface. The results are seen in Figure 9.26.

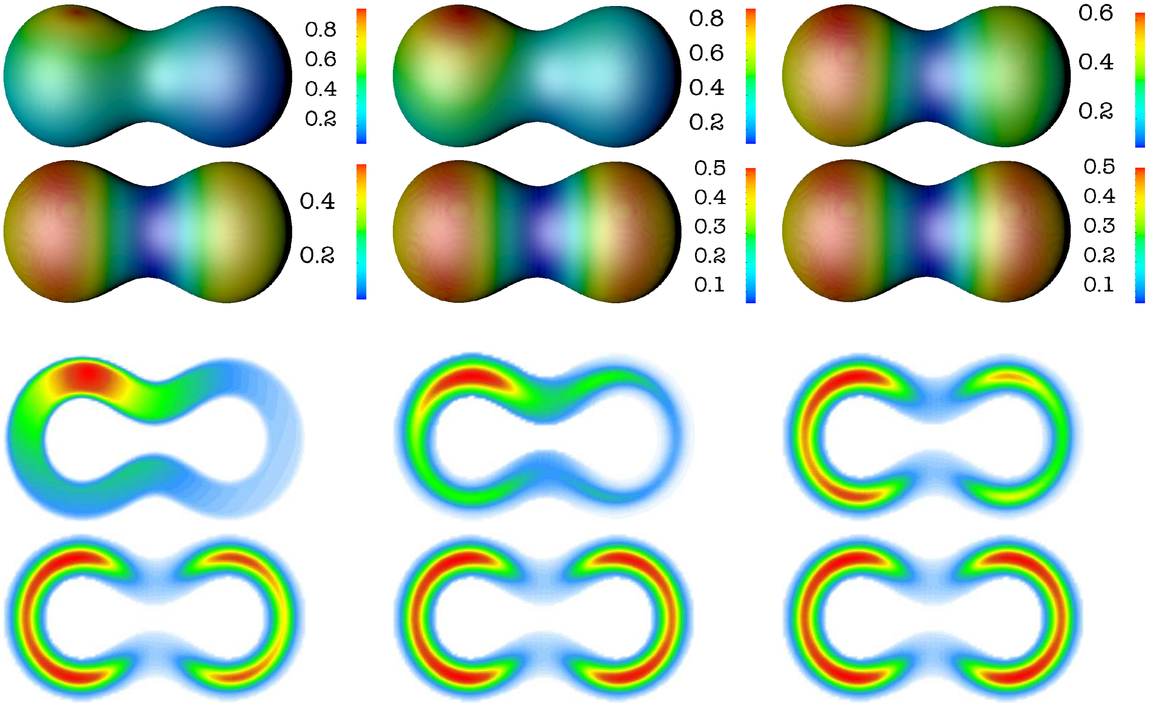

Figure 9.26: Concentration of diffusive species on two spheres merged governed by diffusion with curvature effects using $128 \times 128 \times 128$ mesh. The diffusive species prefers the curvature $C_0^{\text{dif}} = 1.25$ (located on the outer edges) and the background species prefers the curvature $C_0^{\text{bak}} = 0.1$ (located at the point of merging). Times shown are $t = 0$, 0.01, 0.1, 0.2, 0.4, and 0.5.

Finally, we reverse the curvature preferences and set $C_0^{\text{dif}} = 0.1$ and $C_0^{\text{bak}} = 1.2$. The diffusive species will prefer the region of the neck of the two spheres under these parameters. We note that in this region, the Gaussian curvature is negative, since the surface is a saddle here. This is exactly the feature we hope to capture with this model, matching the observation of the M2 protein [88]. The results are presented in Figure 9.27. Eventually, the model should be extended so that the shape may change along with the concentrations. Under the last set of parameters corresponding to Figure 9.27, the diffusive species aggregated in a necking region of the surface. This model successfully reproduced curvature-driven protein localization and is a promising start to many other applications.

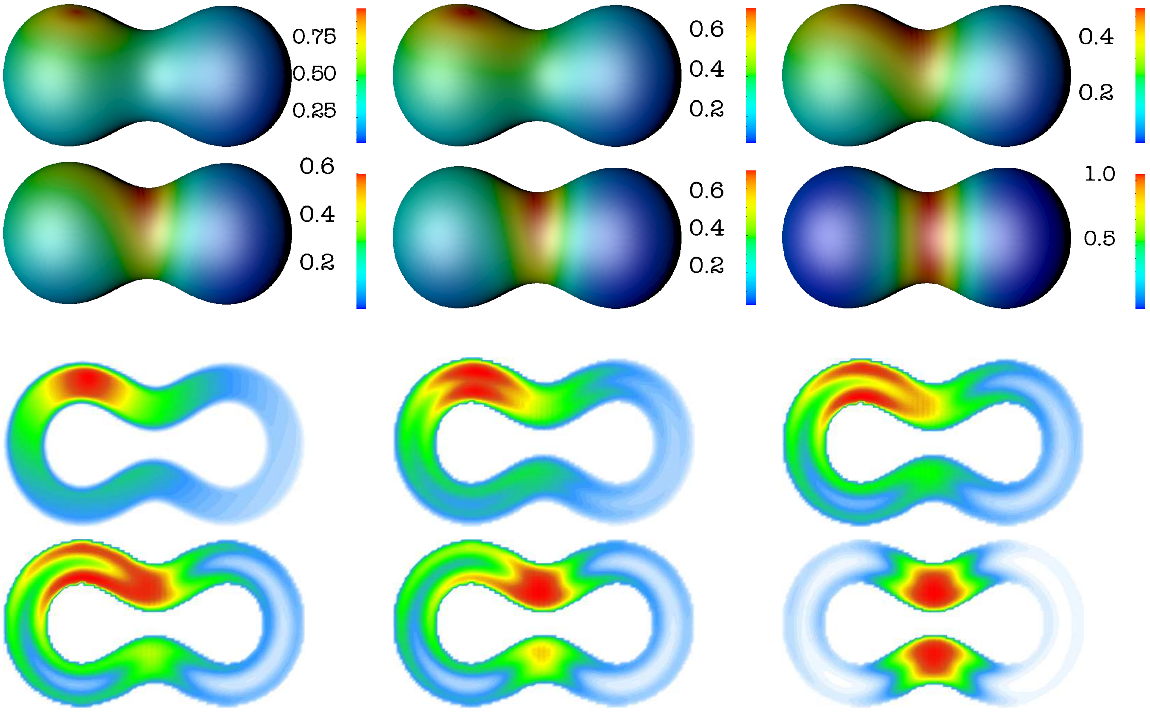

Figure 9.27: Concentration of diffusive species on two spheres merged governed by diffusion with curvature effects using $128 \times 128 \times 128$ mesh. The diffusive species prefers the curvature $C_0^{\mathrm{dif}} = 0.1$ (located at the point of merging) and the background species prefers the curvature $C_0^{\mathrm{bak}} = 1.25$ (located at the outer edges). Times shown are $t = 0$, 0.001, 0.005, 0.01, 0.02, and 0.1.

CHAPTER 10

Conclusions and future work

In this thesis, we have presented the mathematical theory and computational models for electromechanical and curvature-driven flows in lipid bilyaer membranes. In Chapter 1, we reviewed the biophysical background of lipid vesicles and motivated a need for continuum models. The rest of the thesis was organized into three sections: mechanical flows for lipid membranes, electrostatic flows for lipid membranes, and curvature-driven flows for lipid membranes.

In Chapters 2-4, we model mechanical flows for lipid membranes by numerically solving the shape equation using a surface harmonic parameterization [72]. Our method drastically reduced the degrees of freedom compared to alternative approaches and produces results which are physically relevant.

In Chapters 5 and 6, we model electrostatic flows for lipid membranes by computing the electrostatic force on the membrane with techniques from shape calculus [73]. We extended the computation for protein-solvent systems to include electrostatic contributions from charged lipids in a membrane-protein-solvent system. This work has a natural extension and coupling to the first project. It would be convenient to minimize the total electromechanical energy, expressed as a sum of equations (54) and (203), using the efficient surface harmonics parameterization and algorithm from Chapter 3. The variation of the electrostatic force is computed in local Cartesian coordinates in Chapter 6, rendering the numerical computation of the membrane shape from this force less efficient than the computation of the shape from the mechanical force. Furthermore, the electrostatic force is defined on each leaflet of a bilayer membrane, whereas the mechanical force in Chapters 2-4 is computed on a sharp-interface surface. To account for these differences, we first assemble the electrostatic potential energy on a mid-plane of the membrane. This mid-plane corresponds to surface Γ on which the mechanical energy is computed. Then, we perform a change of coordinates on the electrostatic force given by equation (245) by a transfer matrix,

$$\frac{\delta G}{\delta \vec{a}} = \frac{\delta G}{\delta \vec{X}} \frac{\delta \vec{X}}{\delta \vec{a}}. \tag{449}$$

In the equation above, the variation of the electrostatic potential energy (245) is expressed as $\delta G/\delta \vec{X}$, emphasizing that the computation is performed locally. With the variation in terms of the surface harmonic coordinate system, Algorithm 4.1 can be extended to include the electrostatic force.

In Chapters 7-9, we model curvature-driven flows for lipid membranes by solving a phase field equation for the membrane shape and a diffusion equation for the flow of membrane constituents. Chapter 7 reviews and reproduces existing phase field models of vesicle membranes [28]. Then, Chapters 8 and 9 extend this framework to solve a curvature-driven diffusion equation on vesicle membranes in a novel way. The results are presented for curvature-driven diffusion on a fixed boundary; however, the mathematical framework is provided to compute curvature-driven diffusion on a moving boundary. Since the numerical methods for the membrane shape in Algorithm 7.1 and the numerical methods for the curvature-driven diffusion equations in Algorithm 8.1 consistently use Fourier spectral methods, the two models can be coupled using the techniques developed in Section 8.4.1. This will be our next project, and we expect very exciting results. We hope to capture the dynamic effects of curvature-driven diffusion on a moving interface, where the protein location contributes to the movement of the vesicle shape.

Other extensions to the curvature-driven model of Chapters 8 and 9 may also be made. We presented results for a single diffusive species, but the model allows for multiple diffusive species. The additional computational cost is linear with each additional species, since each additional diffusive species requires solving one additional diffusion equation. In addition, a spatially variable diffusion coefficient D may be introduced to our model. This addition should not pose a significant challenge, since the spatially dependent delta function is already handled. Finally, the electrostatic energy may be added to this model. To accomplish this, the dielectric permittivity should be defined as a continuous function of ϕ. We suggest the function

$$\varepsilon(\phi) = \begin{cases} 39 \cdot \left(1 - \tanh\left(\dfrac{\phi + 0.5}{\epsilon}\right)\right) + 2, & \phi \in [-1, 0], \\ 39 \cdot \left(1 + \tanh\left(\dfrac{\phi - 0.5}{\epsilon}\right)\right) + 2, & \phi \in [0, 1]. \end{cases} \tag{450}$$

This function has the following properties. In the solvent, when $\phi \approx \pm 1$, $\varepsilon(\phi) = 80$, but in the membrane, $\varepsilon(\phi)$ sharply drops as $-1 < \phi < 1$ so that in the middle of the membrane, $\varepsilon(0) = 2$. The head groups of the lipids are assumed to be positioned at $\phi = \pm 0.5$. Since $\tanh(-x) = -\tanh(x)$, the function is also continuous at the interface. A plot of (450) is shown in Figure 10.1 with $\epsilon = 0.01$. The electrostatic potential energy may be defined as

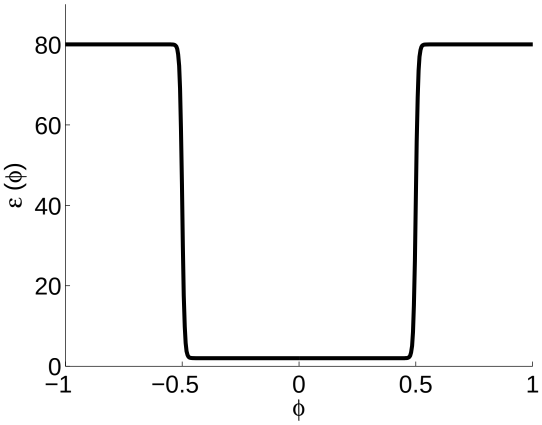

Figure 10.1: A plot of the dielectric permittivity as a function of ϕ, (450), with $\epsilon = 0.01$.

$$E_{\text{elec}} = \int_\Omega \left(-\frac{1}{2}\varepsilon|\nabla\Psi|^2 + \sum_{i=1}^{r} z_i^{\text{ion}} e \rho_i^{\text{ion}} \Psi + \left(z^{\text{pro}} \rho^{\text{pro}} + \sum_{l=1}^{m} z_l^{\text{lip}} \rho_l^{\text{lip}} \right) e\Psi \right) dx, \tag{451}$$

where ε is the dielectric permittivity, Ψ is the electrostatic potential, z_i^{ion} and z_l^{lip} are the valences of the ions and lipids respectively, and e is the elementary charge. The inclusion of the electrostatic potential energy will require the numerical solution of the Poisson equation for Ψ,

$$-\nabla \cdot (\varepsilon \nabla \Psi) = \sum_{i=1}^{r} \rho_i^{\text{ion}} q_i^{\text{ion}} + \sum_{l=1}^{m} \rho_l^{\text{lip}} q_l^{\text{lip}} + \rho^{\text{pro}} q^{\text{pro}}. \tag{452}$$

The diffusion (electrochemical) potentials should be updated as well with the additional energy. With these additions, electrostatic forces may be included to the diffuse-interface model.

BIBLIOGRAPHY

[1] David Adalsteinsson and James A Sethian. Transport and diffusion of material quantities on propagating interfaces via level set methods. *Journal of Computational Physics*, 185(1):271–288, 2003.

[2] David Andelman. Electrostatic properties of membranes: The Poisson–Boltzmann theory. *Handbook of Biological Physics*, 1:603–642, 1995.

[3] Bruno Antonny. Mechanisms of membrane curvature sensing. *Annual Review of Biochemistry*, 80(1):101–123, 2011. PMID: 21438688.

[4] Nathan A. Baker. Poisson-Boltzmann methods for biomolecular electrostatics. In Ludwig Brand and Michael L. Johnson, editors, *Numerical Computer Methods, Part D*, volume 383 of *Methods in Enzymology*, pages 94 – 118. Academic Press, 2004.

[5] Nathan A. Baker, Donald Bashford, and David A. Case. Implicit solvent electrostatics in biomolecular simulation. In *New Algorithms for Macromolecular Simulation*, volume 49 of *Lecture Notes in Computational Science and Engineering*, pages 263–295. Springer Berlin Heidelberg, 2006.

[6] Tobias Baumgart, Benjamin R Capraro, Chen Zhu, and Sovan L Das. Thermodynamics and mechanics of membrane curvature generation and sensing by proteins and lipids. *Annual review of physical chemistry*, 62:483, 2011.

[7] Tobias Baumgart, Samuel T. Hess, and Watt W. Webb. Imaging coexisting fluid domains in biomembrane models coupling curvature and line tension. *Nature*, 425:821–824, 08 2003.

[8] M. Bessis and R.I. Weed. *Living Blood Cells and Their Ultrastructure*. Springer, 1973.

[9] D.H. Boal. *Mechanics of the Cell*. Cambridge University Press, 2nd edition, 2012.

[10] Itamar Borukhov, David Andelman, and Henri Orland. Steric effects in electrolytes: A modified Poisson-Boltzmann equation. *Physical Review Letters*, 79:435–438, Jul 1997.

[11] Qin Cai, Xiang Ye, Jun Wang, and Ray Luo. Dielectric boundary force in numerical Poisson-Boltzmann methods: Theory and numerical strategies. *Chemical Physics Letters*, 514(4 - 6):368 – 373, 2011.

[12] K. M. Callenberg, N. R. Latorraca, and M. Grabe. Membrane bending is critical for the stability of voltage sensor segments in the membrane. *Journal of General Physiology*, 140(1):55–68, 2012.

[13] P.B. Canham. The minimum energy of bending as a possible explanation of the biconcave shape of the human red blood cell. *Journal of Theoretical Biology*, 26(1):61 – 81, 1970.

[14] R. Capovilla, J. Guven, and J.A. Santiago. Deformations of the geometry of lipid vesicles. *Journal of Physics A*, 36(23):6281, 2003.

[15] Jianwei Che, Joachim Dzubiella, Bo Li, and J. Andrew McCammon. Electrostatic free energy and its variations in implicit solvent models. *Journal of Physical Chemistry B*, 112(10):3058–3069, 2008.

[16] Christophe Chipot, MichaelL. Klein, and Mounir Tarek. Modeling lipid membranes. In Sidney Yip, editor, *Handbook of Materials Modeling*, pages 929–958. Springer Netherlands, 2005.

[17] P.G. Ciarlet. *Mathematical Elasticity: Three-Dimensional Elasticity*. Studies in Mathematics and Its Applications. North-Holland, 1994.

[18] Paul Concus and Gene H. Golub. Use of fast direct methods for the efficient numerical solution of nonseparable elliptic equations. *SIAM Journal on Numerical Analysis*, 10(6):pp. 1103–1120, 1973.

[19] Haosheng Cui, Edward Lyman, and Gregory A. Voth. Mechanism of membrane curvature sensing by amphipathic helix containing proteins. *Biophysical Journal*, 100(5):1271 – 1279, 2011.

[20] Malcolm E. Davis and J. Andrew McCammon. Electrostatics in biomolecular structure and dynamics. *Chemical Reviews*, 90(3):509–521, 1990.

[21] Klaus Deckelnick, Gerhard Dziuk, Charles M Elliott, and Claus-Justus Heine. An h-narrow band finite-element method for elliptic equations on implicit surfaces. *IMA Journal of Numerical Analysis*, 30(2):351–376, 2010.

[22] M.C. Delfour and J.P. Zolésio. *Shapes and Geometries: Metrics, Analysis, Differential Calculus, and Optimization.* Advances in Design and Control. SIAM, 2011.

[23] K. G. Van der Zee. *Goal-Adaptive Discretization of Fluid-Structure Interaction.* PhD thesis, Delft University of Technology, 2009.

[24] Markus Deserno. Fluid lipid membranes – a primer. `http://www.cmu.edu/biolphys/deserno/pdf/membrane_theory.pdf`.

[25] M.P. do Carmo. *Differential Geometry of Curves and Surfaces.* Pearson Education Canada, 1976.

[26] Q Du, C Liu, R Ryham, and X Wang. Modeling the spontaneous curvature effects in static cell membrane deformations by a phase field formulation. *Communications on Pure and Applied Analysis*, 4(3):537–548, 2005.

[27] Qiang Du, Chun Liu, and Xiaoqiang Wang. A phase field approach in the numerical study of the elastic bending energy for vesicle membranes. *Journal of Computational Physics*, 198(2):450 – 468, 2004.

[28] Qiang Du, Chun Liu, and Xiaoqiang Wang. Simulating the deformation of vesicle membranes under elastic bending energy in three dimensions. *Journal of Computational Physics*, 212(2):757 – 777, 2006.

[29] Gerhard Dziuk. Finite elements for the beltrami operator on arbitrary surfaces. In Stefan Hildebrandt and Rolf Leis, editors, *Partial Differential Equations and Calculus of Variations*, volume 1357 of *Lecture Notes in Mathematics*, pages 142–155. Springer Berlin Heidelberg, 1988.

[30] Gerhard Dziuk and Charles M Elliott. An eulerian approach to transport and diffusion on evolving implicit surfaces. *Computing and Visualization in Science*, 13(1):17–28, 2010.

[31] E.A. Evans. Bending resistance and chemically induced moments in membrane bilayers. *Biophysical Journal*, 14(12):923–931, 1974.

[32] Evan Evans and Yuan-Cheng Fung. Improved measurements of the erythrocyte geometry. *Microvascular Research*, 4(4):335 – 347, 1972.

[33] Evan. Evans and David. Needham. Physical properties of surfactant bilayer membranes: thermal transitions, elasticity, rigidity, cohesion and colloidal interactions. *Journal of Physical Chemistry*, 91(16):4219–4228, 1987.

[34] L.C. Evans. *Partial Differential Equations*. Graduate studies in mathematics. American Mathematical Society, 1998.

[35] J. Faraudo. Diffusion equation on curved surfaces. I. theory and application to biological membranes. *Journal of Chemical Physics*, 116:5831, 2002.

[36] Michael Feig and Charles L Brooks III. Recent advances in the development and application of implicit solvent models in biomolecule simulations. *Current Opinion in Structural Biology*, 14(2):217 – 224, 2004.

[37] Feng Feng and William S. Klug. Finite element modeling of lipid bilayer membranes. *Journal of Computational Physics*, 220(1):394 – 408, 2006.

[38] F. C. Frank. I. liquid crystals. on the theory of liquid crystals. *Discussions of the Faraday Society*, 25:19–28, 1958.

[39] Y.C. B. Fung and P. Tong. Theory of the sphering of red blood cells. *Biophysical Journal*, 8:175–198, 1968.

[40] G11-BioA-2011-12. Active transport. Wikispace. `http://g11-bioa-2011-12.wikispaces.com/(d)+Active+transport`.

[41] M. K. Gilson, M. E. Davis, B. A. Luty, and J. A. McCammon. Computation of electrostatic forces on solvated molecules using the Poisson-Boltzmann equation. *Journal of Physical Chemistry*, 97(14):3591–3600, 1993.

[42] Holger Gohlke and M. F. Thorpe. A natural coarse graining for simulating large biomolecular motion. *Biophysical Journal*, 91:2115–2120, 2006.

[43] John B Greer, Andrea L Bertozzi, and Guillermo Sapiro. Fourth order partial differential equations on general geometries. *Journal of Computational Physics*, 216(1):216–246, 2006.

[44] Baker R.F. Greer M.A. *Proceedings of the 7th International Congress of Electron Microscopy*, 3, 1970.

[45] Volkmar Heinrich, Bojan Božič, Saša Svetina, and Boštjan Žekš. Vesicle deformation by an axial load: From elongated shapes to tethered vesicles. *Biophysical Journal*, 76:2056–2071, 1999.

[46] Volkmar Heinrich, Saša Svetina, and Boštjan Žekš. Nonaxisymmetric vesicle shapes in a generalized bilayer-couple model and the transition between oblate and prolate axisymmetric shapes. *Physical Review E*, 48:3112–3123, Oct 1993.

[47] W. Helfrich et al. Elastic properties of lipid bilayers: theory and possible experiments. *Zeitschrift für Naturforschung C*, 28(11):693–703, 1973.

[48] Samuel T. Hess, Mukesh Kumar, Anil Verma, Jane Farrington, Anne Kenworthy, and Joshua Zimmerberg. Quantitative electron microscopy and fluorescence spectroscopy of the membrane distribution of influenza hemagglutinin. *Journal of Cell Biology*, 169(6):965–976, 2005.

[49] Edwin Hewitt and Robert E Hewitt. The Gibbs-Wilbraham phenomenon: an episode in Fourier analysis. *Archive for history of Exact Sciences*, 21(2):129–160, 1979.

[50] Wieland B. Huttner and Joshua Zimmerberg. Implications of lipid microdomains for membrane curvature, budding and fission: Commentary. *Current Opinion in Cell Biology*, 13:478–484, 2001.

[51] John David Jackson and John D Jackson. *Classical electrodynamics*, volume 3. Wiley New York etc., 1962.

[52] Khaled Khairy and Jonathon Howard. Minimum-energy vesicle and cell shapes calculated using spherical harmonics parameterization. *Soft Matter*, 7:2138–2143, 2011.

[53] George Khelashvili, Daniel Harries, and Harel Weinstein. Modeling membrane deformations and lipid demixing upon protein-membrane interaction: The BAR dimer adsorption. *Biophysics Journal*, 97(6):1626 – 1635, 2009.

[54] K. S. Kim, J. Neu, and G. Oster. Curvature-mediated interactions between membrane proteins. *Biophysical Journal*, 75:2274–2291, 1998.

[55] Vladimir Yu Kiselev, Marcin Leda, Alexey I Lobanov, Davide Marenduzzo, and Andrew B Goryachev. Lateral dynamics of charged lipids and peripheral proteins in spatially heterogeneous membranes: Comparison of continuous and monte carlo approaches. *Journal of Chemical Physics*, 135:155103, 2011.

[56] Veronika Kralj-Iglič and Aleš Iglič. A simple statistical mechanical approach to the free energy of the electric double layer including the excluded volume effect. *Journal de Physique II France*, 6(4):477–491, 1996.

[57] E. Kreyszig. *Differential Geometry*. Differential Geometry. Dover Publications, 1991.

[58] M. Krone, K. Bidmon, and T. Ertl. Interactive visualization of molecular surface dynamics. *Visualization and Computer Graphics, IEEE Transactions on*, 15(6):1391 –1398, Nov.-Dec. 2009.

[59] L.D. Landau, E.M. Lifshit͡s, and L.P. Pitaevskiĭ. *Electrodynamics of continuous media*. Course of theoretical physics. Butterworth-Heinemann, 1995.

[60] Hyun Geun Lee and Junseok Kim. Regularized Dirac delta functions for phase field models. *International Journal for Numerical Methods in Engineering*, 91(3):269–288, 2012.

[61] Bo Li. Minimization of electrostatic free energy and the PoissonBoltzmann equation for molecular solvation with implicit solvent. *SIAM Journal on Mathematical Analysis*, 40(6):2536–2566, 2009.

[62] Bo Li, Xiaoliang Cheng, and Zhengfang Zhou. Dielectric boundary force in molecular solvation with the Poisson-Boltzmann free energy: A shape derivative approach. *SIAM J. Appl. Math.*, 71:2093–2111, 2011.

[63] Chunming Li, Chenyang Xu, Changfeng Gui, and M.D. Fox. Level set evolution without re-initialization: a new variational formulation. In *IEEE Computer Society Conference on Computer Vision and Pattern Recognition, 2005. CVPR 2005.*, volume 1, pages 430–436 vol. 1, June 2005.

[64] Jung-Hsin Lin, Nathan A. Baker, and J. Andrew McCammon. Bridging implicit and explicit solvent approaches for membrane electrostatics. *Biophysical Journal*, 83(3):1374 – 1379, 2002.

[65] Erik Lindahl and Olle Edholm. Mesoscopic undulations and thickness fluctuations in lipid bilayers from molecular dynamics simulations. *Biophysical Journal*, 79(1):426 – 433, 2000.

[66] H. Lodish, A. Berk, C.A. Kaiser, M. Krieger, M.P. Scott, A. Bretscher, H. Ploegh, and P. Matsudaira. *Molecular Cell Biology*. W. H. Freeman, 2007.

[67] L. Lopez, I.M. Duck, and W.A. Hunt. On the shape of the erythrocyte. *Biophysical Journal*, 8(11):1228 – 1235, 1968.

[68] L. Ma and W. S. Klug. Viscous regularization and r-adaptive remeshing for finite element analysis of lipid membrane mechanics. *Journal of Computational Physics*, 227(11):5816–5835, 2008.

[69] D. Marsh. *Handbook of Lipid Bilayers, Second Edition*. Taylor & Francis, 2013.

[70] Harvey T McMahon and Jennifer L Gallop. Membrane curvature and mechanisms of dynamic cell membrane remodelling. *Nature*, 438(7068):590–596, 2005.

[71] Donald Allan McQuarrie. *Statistical thermodynamics*. HarperCollins Publishers, 1973.

[72] M. Mikucki and Y.C. Zhou. Fast algorithm for simulating lipid vesicle deformation I: Spherical harmonic approximation. *Journal of Computational Physics, under review.*

[73] M. Mikucki and Y.C. Zhou. Electrostatic forces on charged surfaces of bilayer lipid membranes. *SIAM Journal on Applied Mathematics*, 74(1):1–21, 2014.

[74] JR Murphy. *Journal of Laboratory and Clinical Medicine*, 65, 1965.

[75] D.L. Nelson, A.L. Lehninger, and M.M. Cox. *Lehninger Principles of Biochemistry*. Lehninger Principles of Biochemistry. W. H. Freeman, 2008.

[76] Philip Nelson. *Biological Physics: Energy, Information, Life*. W. H. Freeman, 2003.

[77] J. Nishiura. Phospholipid bilayers. Online Lectures. `http://academic.brooklyn.cuny.edu/biology/bio4fv/page/phosphb.htm`.

[78] Jorge Nocedal and Stephen J. Wright. *Numerical optimization.* Springer series in operations research and financial engineering. Springer, New York, NY, 2. ed. edition, 2006.

[79] Maxim A. Olshanskii and Danil Safin. A narrow-band unfitted finite element method for elliptic pdes posed on surfaces. Preprint.

[80] B. O'Neill. *Elementary Differential Geometry, Revised 2nd Edition.* Elementary Differential Geometry Series. Elsevier Science, 2006.

[81] S. Osher and R. Fedkiw. *Level Set Methods and Dynamic Implicit Surfaces*, volume 153 of *Applied Mathematical Sciences.* Springer, 2003.

[82] Daniel L. Parton, Jochen W. Klingelhoefer, and Mark S.P. Sansom. Aggregation of model membrane proteins, modulated by hydrophobic mismatch, membrane curvature, and protein class. *Biophysical Journal*, 101(3):691 – 699, 2011.

[83] Meenu N. Perera, Shang H. Lin, Yuri K. Peterson, Alicja Bielawska, Zdzislaw M. Szulc, Robert Bittman, and Marco Colombini. Bax and bcl-xl exert their regulation on different sites of the ceramide channel. *Biochemical Journal*, 445(1):81–91, 2012.

[84] ThomasR. Powers. Mechanics of lipid bilayer membranes. In Sidney Yip, editor, *Handbook of Materials Modeling*, pages 2631–2643. Springer Netherlands, 2005.

[85] Andreas Rätz and Axel Voigt. PDEs on surfaces—a diffuse interface approach. *Communications in Mathematical Sciences*, 4(3):575–590, 09 2006.

[86] W. Rawicz, K.C. Olbrich, T. McIntosh, D. Needham, and E. Evans. Effect of chain length and unsaturation on elasticity of lipid bilayers. *Biophysical Journal*, 79(1):328 – 339, 2000.

[87] Jeremy S. Rossman, Xianghong Jing, George P. Leser, Victoria Balannik, Lawrence H. Pinto, and Robert A. Lamb. Influenza virus M2 ion channel protein is necessary for filamentous virion formation. *Journal of Virology*, 84(10):5078–5088, 05 2010.

[88] Nathan W. Schmidt, Abhijit Mishra, Jun Wang, William F. DeGrado, and Gerard C. L. Wong. Influenza virus A M2 protein generates negative gaussian membrane curvature necessary for budding and scission. *Journal of the American Chemical Society*, 135(37):13710–13719, 2013.

[89] P. Seeman, D. Cheng, and G. H. Iles. Structure of membrane holes in osmotic and saponin hemolysis. *Journal of Cell Biology*, 56(2):519–527, 1973.

[90] Udo Seifert. Configurations of fluid membranes and vesicles. *Advances in Physics*, 46(1):13–137, 1997.

[91] Udo Seifert, Karin Berndl, and Reinhard Lipowsky. Shape transformations of vesicles: Phase diagram for spontaneous- curvature and bilayer-coupling models. *Physical Review A*, 44:1182–1202, Jul 1991.

[92] K.A. Sharp and B. Honig. Calculating total electrostatic energies with the nonlinear Poisson-Boltzmann equation. *Journal of Physical Chemistry*, 94(19):7684–7692, 1990.

[93] Jan W Slotboom. Computer-aided two-dimensional analysis of bipolar transistors. *Electron Devices, IEEE Transactions on*, 20(8):669–679, 1973.

[94] Peter Smereka. The numerical approximation of a delta function with application to level set methods. *Journal of Computational Physics*, 211(1):77–90, January 2006.

[95] I.S. Sokolnikoff. *Tensor analysis: theory and applications to geometry and mechanics of continua*. Applied mathematics series. Wiley, 1964.

[96] Jeanne C Stachowiak, Carl C Hayden, and Darryl Y Sasaki. Steric confinement of proteins on lipid membranes can drive curvature and tubulation. *Proceedings of the National Academy of Sciences*, 107(17):7781–7786, 2010.

[97] John Strain. Fast spectrally-accurate solution of variable-coefficient elliptic problems. *Proceedings of the American Mathematical Society*, 122(3):843–850, 1994.

[98] J.A. Stratton. *Electromagnetic theory*. International series in pure and applied physics. McGraw-Hill book company, inc., 1941.

[99] Shigeo Takamori, Matthew Holt, Katinka Stenius, Edward A. Lemke, Mads Grønborg, Dietmar Riedel, Henning Urlaub, Stephan Schenck, Britta Brügger, Philippe Ringler, Shirley A. Müller, Burkhard Rammner, Frauke Gräter, Jochen S. Hub, Bert L. De Groot, Gottfried Mieskes, Yoshinori Moriyama, Jürgen Klingauf, Helmut Grubmüller, John Heuser, Felix Wieland, and Reinhard Jahn. Molecular anatomy of a trafficking organelle. *Cell*, 127(4):831 – 846, 2006.

[100] Knut Erik Teigen, Peng Song, John Lowengrub, and Axel Voigt. A diffuse-interface method for two-phase flows with soluble surfactants. *Journal of Computational Physics*, 230(2):375 – 393, 2011.

[101] Ilan Tsafrir, Dror Sagi, Tamar Arzi, Marie-Alice Guedeau-Boudeville, Vidar Frette, Daniel Kandel, and Joel Stavans. Pearling instabilities of membrane tubes with anchored polymers. *Physical Review Letters*, 86:1138–1141, Feb 2001.

[102] Sarah L. Veatch and Sarah L. Keller. Separation of liquid phases in giant vesicles of ternary mixtures of phospholipids and cholesterol. *Biophysical Journal*, 85(5):3074 – 3083, 2003.

[103] Xiaoqiang Wang and Qiang Du. Modelling and simulations of multi-component lipid membranes and open membranes via diffuse interface approaches. *Journal of Mathematical Biology*, 56(3):347–371, 2008.

[104] Jian-Jun Xu and Hong-Kai Zhao. An Eulerian formulation for solving partial differential equations along a moving interface. *Journal of Scientific Computing*, 19(1-3):573–594, 2003.

[105] Naresh Yandrapalli, Delphine Muriaux, and Cyril Favard. Lipid domains in HIV-1 assembly. *Frontiers in Microbiology*, 5(220), 2014.

[106] H.D. Young, R.A. Freedman, and A.L. Ford. *Sears and Zemansky's University Physics*. Pearson/Addison Wesley, 2004.

[107] Ou-Yang Zhong-can and Wolfgang Helfrich. Bending energy of vesicle membranes: General expressions for the first, second, and third variation of the shape energy and applications to spheres and cylinders. *Physical Review A*, 39:5280–5288, May 1989.

[108] Y. C. Zhou. Electrodiffusion of lipids on membrane surfaces. *Journal of Chemical Physics*, 136(20):205103, 2012.

[109] J. Zimmerberg and M. M. Kozlov. How proteins produce cellular membrane curvature. *Nature Reviews Molecular Cell Biology*, 7(1):9–19, 2006.